LATERAL-LOAD RESPONSE OF A REINFORCED CONCRETE BRIDGE

WA-RD 305.2

Final Technical Report
August 1993

Washington State Department of Transportation

Washington State Transportation Commission
Transit, Research, and Intermodal Planning (TRIP) Division
in cooperation with the U.S. Department of Transportation
Federal Highway Administration

TECHNICAL REPORT STANDARD TITLE PAGE

1. REPORT NO.	2. GOVERNMENT ACCESSION NO.	3. RECIPIENT'S CATALOG NO.
WA-RD 305.2		

4. TITLE AND SUBTITLE	5. REPORT DATE
LATERAL-LOAD RESPONSE OF A REINFORCED CONCRETE BRIDGE	August 1993
	6. PERFORMING ORGANIZATION CODE
7. AUTHOR(S)	8. PERFORMING ORGANIZATION REPORT NO.
Marc O. Eberhard, Jeffrey A. MacLardy, M. Lee Marsh, Gaukur Hjartarson	
9. PERFORMING ORGANIZATION NAME AND ADDRESS	10. WORK UNIT NO.
Washington State Transportation Center (TRAC) University of Washington, JD-10 The University District Building, Suite 535; 1107 N.E. 45th St. Seattle, Washington 98105-4631	11. CONTRACT OR GRANT NO. GC8719, Task 37
12. SPONSORING AGENCY NAME AND ADDRESS	13. TYPE OF REPORT AND PERIOD COVERED
Washington State Department of Transportation Transportation Building, MS 7370 Olympia, Washington 98504-7370	Final Technical Report
	14. SPONSORING AGENCY CODE

15. SUPPLEMENTARY NOTES

This study was conducted in cooperation with the U.S. Department of Transportation, Federal Highway Administration.

16. ABSTRACT

This study was part of a Washington State Department of Transportation (WSDOT) program to assess the vulnerability of highway bridges built before 1984. Researchers applied slowly-varying transverse loads to a three-span, reinforced concrete bridge, including the superstructure, piers, and abutments. The purpose of the tests was to measure the transverse stiffness of the bridge and to estimate each support's contribution to stiffness. The researchers also evaluated analytical models by comparing the calculated and observed responses.

The bridge was extremely stiff and strong. In two cycles to a load equal to 45 percent of the bridge's weight, the maximum bridge displacement was 0.15 inch. During these cycles damage was minimal. At a load equal to 65 percent of the bridge's weight, the pier displacement was 0.30 inch. After the bridge had been excavated, the stiffness decreased to 15 percent of its initial stiffness. The stiffness further decreased to 8 percent of the initial stiffness after the superstructure had been isolated from the abutments.

The University of Washington (UW), California Department of Transportation (CALTRANS) and WSDOT models underestimated the stiffness of the bridge in its initial state. The UW model probably overestimated the resistance of the polystyrene at the abutments and underestimated the stiffness of the soil at the wingwalls. The CALTRANS model was too flexible because it neglected the resistance of the bearing pads and polystyrene. The WSDOT model was too flexible because it neglected the resistance of the bearing pads and polystyrene, and underestimated the soil stiffness.

The researchers concluded that (1) the tests can serve as a valuable benchmark against which to evaluate proposed seismic-evaluation procedures and models, (2) bridges that are similar to the test bridge are not highly vulnerable to transverse motions, (3) complex soil modeling is not justified if soil test data are not available, and (4) nonlinear analysis was necessary to reproduce the details of the observed response.

17. KEY WORDS	18. DISTRIBUTION STATEMENT
Bridge, earthquakes, reinforced concrete, tests, modeling, lateral loads	No restrictions. This document is available to the public through the National Technical Information Service, Springfield, VA 22616

19. SECURITY CLASSIF. (of this report)	20. SECURITY CLASSIF. (of this page)	21. NO. OF PAGES	22. PRICE
None	None	170	

Final Technical Report

Research Project GC8719, Task 37
Bridge Full Scale Seismic Test

LATERAL-LOAD RESPONSE OF A REINFORCED CONCRETE BRIDGE

by

Marc O. Eberhard
Assistant Professor of Civil Engineering
University of Washington

Jeffrey A. MacLardy
Research Assistant
University of Washington

M. Lee Marsh
Assistant Professor of Civil Engineering
Washington State University

Gaukur Hjartarson
Research Assistant
University of Washington

Washington State Transportation Center (TRAC)
University of Washington, JD-10
The University District Building
1107 N.E. 45th Street, Suite 535
Seattle, Washington 98105-4631

Washington State Department of Transportation
Technical Monitor
Ed Henley
Bridge and Structures Engineer

Prepared for

Washington State Transportation Commission
Department of Transportation
and in cooperation with
U.S. Department of Transportation
Federal Highway Administration

August 1993

DISCLAIMER

The contents of this report reflect the views of the authors, who are responsible for the facts and the accuracy of the data presented herein. The contents do not necessarily reflect the official views or policies of the Washington State Transportation Commission, Department of Transportation, or the Federal Highway Administration. This report does not constitute a standard, specification, or regulation.

TABLE OF CONTENTS

TABLE OF CONTENTS (Continued)

TABLE OF CONTENTS (Continued)

LIST OF FIGURES

LIST OF FIGURES (Continued)

LIST OF TABLES

SUMMARY

This study was part of a Washington State Department of Transportation (WSDOT) program to assess the vulnerability of multiple-span highway bridges built before 1984. A first series of static tests (Phase I) focused on the response of the entire bridge, including the superstructure, piers, and abutments. During Phase I, dynamic tests were also performed on the structure. A second series of static tests (Phase II) focused on the vulnerability of a pair of piers to large, transverse displacements. This report describes the Phase I static tests and the associated analysis.

WSDOT constructed the three-span, reinforced concrete bridge in 1966. Though the researchers applied transverse loads only to the two piers, the continuous superstructure transmitted these forces to both abutments. Each pier consisted of a crossbeam and two 3-foot diameter columns, which were supported on spread footings. Compacted fill surrounded the 25-foot high columns to a height of approximately 12 feet. Each abutment consisted of two wingwalls and a combination diaphragm/endwall, which was supported by elastomeric bearing pads and polystyrene. The bearing pads, polystyrene, and soil contributed to transverse resistance of the abutment. The soil resistance was expected to be large because the superstructure, endwall, and wingwalls were monolithic and heavily reinforced.

During Phase I, large, slowly-varying loads were applied in the transverse direction. The purpose of these tests was to measure the transverse stiffness of the bridge and to estimate each support's contribution to stiffness. During the initial tests, both the intermediate piers and the abutments provided resistance. The tests were repeated after researchers had excavated the soil at the abutments. The tests were repeated again after the researchers had isolated the superstructure from the abutments by replacing the bearing pads and polystyrene with a sandwich of hard plastic and polished, greased stainless steel.

The researchers measured the applied load, transverse displacements of the piers and abutments, and longitudinal displacements of the the bridge's four corners. They used 44

instruments to measure the relative rotations of critical beam and column cross sections. Additional instrumentation monitored footing translation and rotation for the west pier.

The bridge in its initial state was extremely stiff. In two cycles, at a load equal to 45 percent of the bridge's weight (550 kips, Test I), the maximum bridge displacement was 0.15 inch. For a clear column height of 25 feet, this displacement corresponded to a drift ratio of 0.05 percent. Displacements were recovered fully upon unloading. Damage in this test was limited to minor flexural cracking at the tops of the columns.

At a load equal to 65 percent of the bridge's weight (Cycle IIN1), the pier displacement corresponded to a drift ratio of 0.10 percent. At this load, the stiffness decreased abruptly. This decrease coincided with the formation of a 0.10-inch-wide crack in the northeast wingwall. For the three half-cycles of Test II, the secant stiffness of the pier-displacement response ranged from 25 percent to 50 percent of the initial stiffness. Upon unloading, deck deflection was fully recovered, but most of the abutment displacement was not recovered. In Test II, cracking increased at the columns' tops, but cracks were not visible at the columns' bases.

After the bridge had been excavated (Test EXC), the stiffness decreased to 15 percent of the initial stiffness (Cycle IS1). The stiffness decreased further to 8 percent of the initial stiffness after the superstructure had been isolated from the abutments (Test ISO). No new damage was observed during tests of the bridge in its excavated and isolated conditions.

The researchers checked the consistency of the records. The six measurements of transverse displacement were consistent with each other. The four longitudinal-displacement measurements were useful for calculating end rotations, but the measurements of longitudinal bridge translation had been greatly affected by temperature variations.

To better understand the lateral-load response of the bridge, the researchers created a series of nonlinear models for the initial, excavated, and isolated conditions (UW models). These models were developed on the basis of the structural plans and the measured material properties. The UW models were compared with the observed response and with finite-element models developed by the California Department of Transportation (CALTRANS) and WSDOT. The CALTRANS and

WSDOT analyses were more objective than the UW analyses because the engineers in those agencies were not aware of the measured response. The CALTRANS and WSDOT analyses were also more representative of standard practice because their engineers were not aware of the measured material properties.

The UW model provided a good fit to the measured response of the isolated piers (Test ISO). The CALTRANS and WSDOT models were approximately two-thirds as stiff as the measured response. The UW model overestimated the stiffness of the excavated bridge (Test EXC). CALTRANS and WSDOT did not analyze the bridge in the excavated condition.

The UW, CALTRANS, and WSDOT models underestimated the stiffness of the bridge in its initial state (Cycle IS1). The researchers found that the UW model probably overestimated the resistance of the polystyrene at the abutments and underestimated the stiffness of the soil at the wingwalls. The CALTRANS model was too flexible because it neglected the resistance of the bearing pads and polystyrene. The WSDOT model was too flexible because it neglected the resistance of the bearing pads and polystyrene, and underestimated the soil stiffness.

The researchers' acknowledgment of the tests' limitations influenced the recommendations. During the tests, a slowly varying, transverse load was applied to the bridge. Earthquake response involves higher loading rates as well as longitudinal, vertical, and torsional ground accelerations. Nevertheless, the researchers concluded that bridges similar to the test bridge are not highly vulnerable to transverse motions. They found it was necessary to include the effect of the polystyrene at the abutments to reproduce the measured response. They obtained concurrence with the observed behavior by combining soil tests with simple soil models. To reproduce the details of the observed response, it was necessary to perform nonlinear analysis.

CHAPTER 1
INTRODUCTION

1.1 CONTEXT

The tests and analyses described in this report were part of a Washington State Department of Transportation (WSDOT) program to assess the seismic vulnerability of multiple-span highway bridges built before 1984. A preliminary study of the Washington State bridge inventory identified 805 bridges that might require modifications to improve their response during strong earthquakes. (1) The study recommended that 87 bridges with in-span hinges, 165 with inadequate support lengths, and 123 supported on single-column piers be retrofitted within the next 20 years. The decision to retrofit the remaining 430 bridges, those supported on deficient multi-column piers, was postponed until further research could be performed. The goal of the tests and analyses described in this report was to improve the ability of bridge engineers to assess the seismic vulnerability of such bridges.

Though destructive vertical load tests (2) and small-displacement dynamic tests (3, 4) had been conducted before, destructive, lateral-load tests had not been performed on bridges. The unique opportunity to destructively test a bridge with typical multi-column bents arose when WSDOT decided to remove two bridges that spanned an abandoned railroad line near Moses Lake, Washington (Figure 1.1). WSDOT estimated that removing these obsolete bridges would cost less than maintaining them and replacing substandard railings. The south bridge was tested while interstate traffic was rerouted to the north bridge. Then both bridges were demolished.

1.2 SEISMIC VULNERABILITY OF PIERS

Detailing requirements for reinforced concrete piers have changed dramatically since the 1950s and 1960s, when much of the interstate system was constructed. In comparison with current requirements, common deficiencies in piers of that period include (1) bridge columns that have little confinement reinforcement, (2) reinforcing splices between the column reinforcement

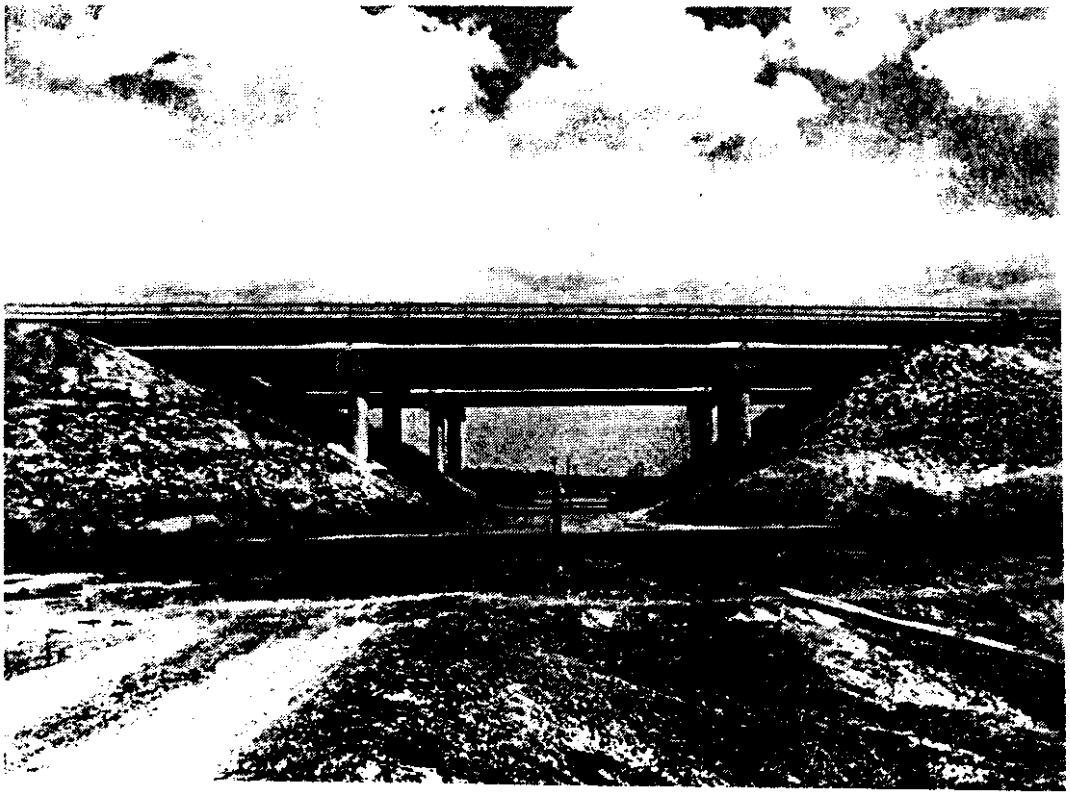

Figure 1.1. Photograph of Bridge

and footing dowels that are too short and are unconfined, and (3) a lack of top reinforcement in the footings. The bridge that was tested had all three of these detailing deficiencies.

Just because a bridge has details that do not satisfy current code requirements does not necessarily mean that the piers will be damaged during an earthquake. Retrofitting is unnecessary if the abutments and superstructure are stiff enough to limit displacements to a level below that which would cause damage to the piers. To decide whether the bridge is stiff enough to warrant leaving a brittle pier in service, an engineer needs reliable estimates of the stiffness of the abutments, superstructure, and piers. Preferably, such estimates should rely on models that have been calibrated to reproduce observed behavior. Phase I of the study, described in this report, provided one example of bridge response with which to calibrate analytical models.

In addition to needing reliable estimates of pier and abutment stiffnesses, an engineer needs estimates of the displacements likely to damage the piers. These estimates are particularly important for bridges whose abutments are ineffective at reducing the displacement demand for the piers. This lack of effectiveness is likely if (1) the abutments provide little resistance to transverse motion, (2) the piers are far from the abutments, or (3) the superstructure is flexible or discontinuous. For such bridges, the decision to retrofit relies on an assessment of the stiffness, strength, and toughness of the piers alone. Phase II, described by O'Donovan (5), focused on assessing the vulnerability of the two intermediate piers to large, transverse displacements. The two piers were similar to those found in many bridges on the interstate system.

1.3 OBJECTIVES

The objectives of the Phase I study were as follows:

1. to measure the stiffness and strength of the bridge to cyclic, transverse loads,
2. to estimate the contribution to resistance the abutments and piers provided,
3. to identify the members of the bridge most vulnerable to transverse loads,
4. to develop and calibrate analytical models that are consistent with the observed response, and
5. to make recommendations for modeling similar bridges.

1.4 SCOPE OF REPORT

This report describes the tests and analyses for Phase I only. During Phase I, large, slowly-varying loads were applied in the transverse direction of the three-span, reinforced concrete bridge. Initially, both the intermediate piers and the abutments provided resistance. The tests were repeated after the contribution of the soil had been eliminated by excavating the soil at the abutments. The tests were repeated once again after researchers had isolated the bridge from the abutments by replacing the bearing pads with low-friction pads. The loading history for Phase I is shown in the upper portion of Figure 1.2.

Concurrent with the static tests, four dynamic tests were performed on the structure, as shown in Figure 1.2. In the dynamic tests, small-displacement, harmonic response was induced with an eccentric mass shaker placed at midspan of the center span. The shaker was oriented such that the applied force was parallel to the skew. One objective of these tests was to measure changes in the small-displacement dynamic properties of the structure at two levels of damage and for varying restraint conditions at the abutments. A second objective was to compare the large-displacement static response measured during Phase I with the small-displacement dynamic response, which is easy to measure.

During Phase II, reported by O'Donovan (5), similar static tests were performed on the two piers but at larger displacements (lower portion of Figure 1.2) than had been imposed in Phase I. The objective of this second phase was to measure the stiffness, strength, and toughness of these typical piers.

Chapter 2 of this report describes the bridge and the measured material properties. The testing apparatus, instrumentation, data acquisition, and testing procedures are outlined in Chapter 3. The measured response during the Phase I tests is reported in Chapter 4, and the implications of the measured response are discussed in Chapter 5. In Chapter 6, a finite element model is described and calibrated to reproduce the observed response. Modeling recommendations are proposed on the basis of comparisons among the measured response, the calibrated model and finite element models developed by the WSDOT and the California Department of Transportation

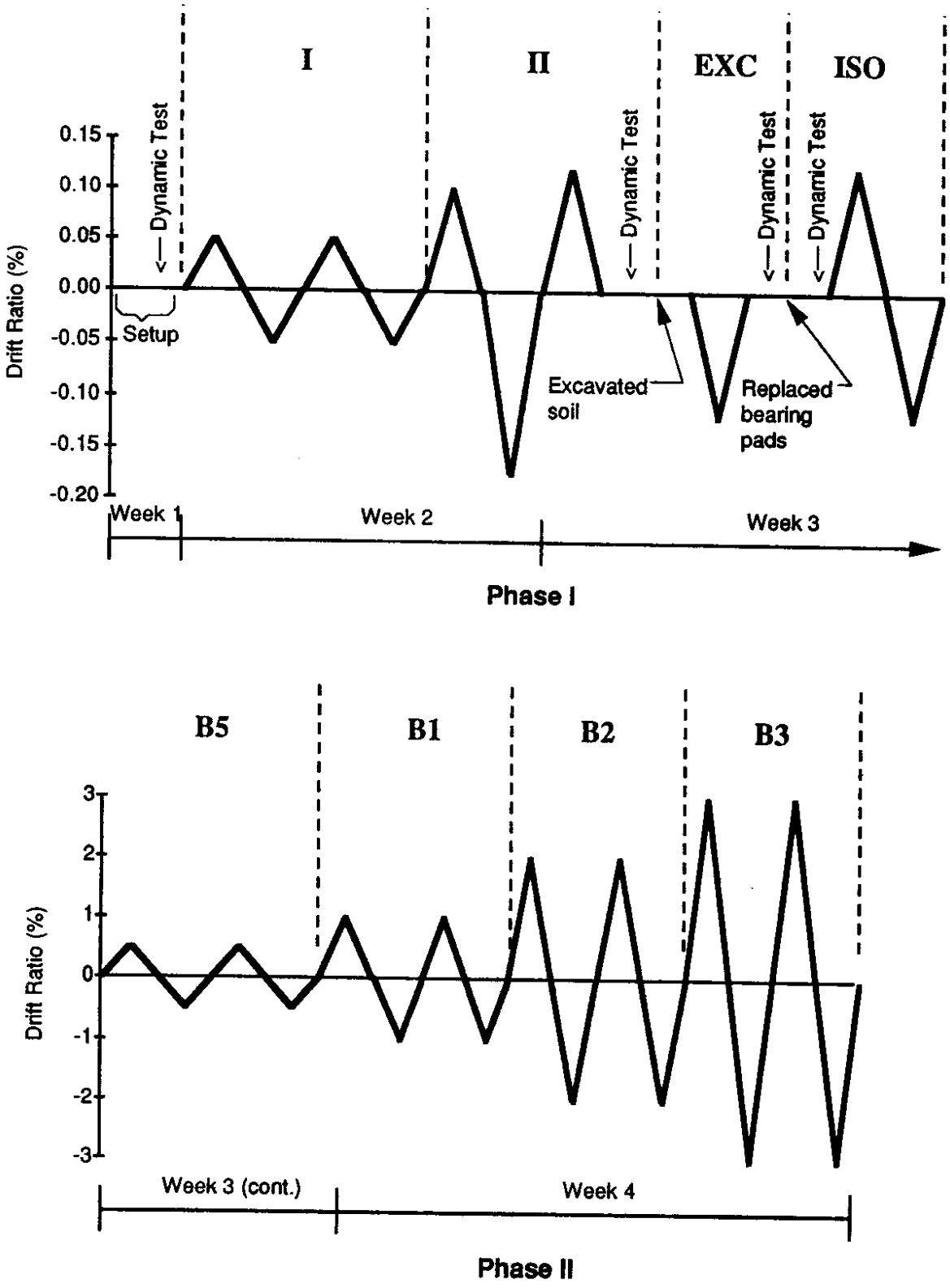

Figure 1.2. Loading History

(CALTRANS). Figure 1.3 provides an overview of the Phase I analysis. Chapter 7 lists recommendations, based on the results of Phase I, for evaluating the seismic vulnerability of bridges.

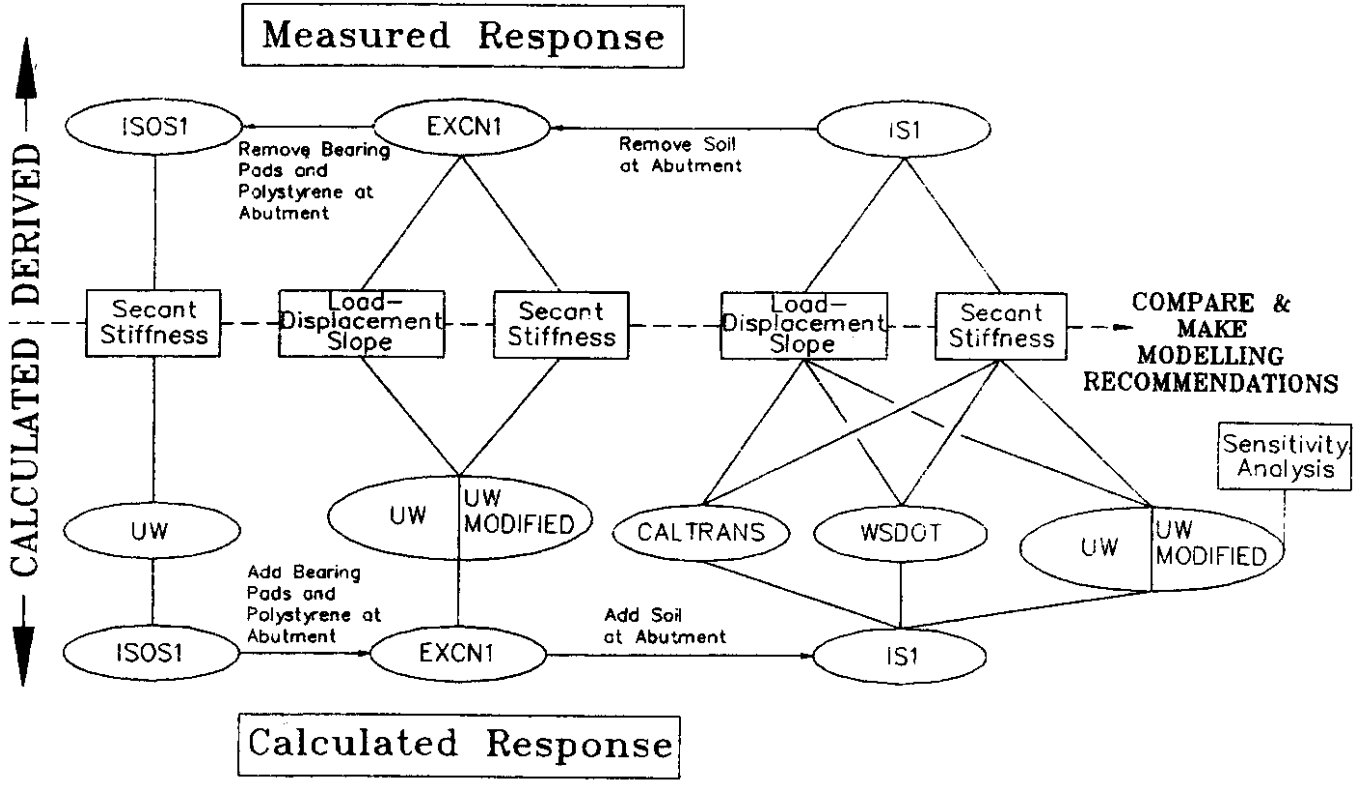

Figure 1.3. Phase I Analysis

CHAPTER 2

DESCRIPTION OF BRIDGE

The bridge that was tested (Figure 1.1) was located on Interstate 90, 13 miles east of the city of Moses Lake, Washington. It was one of a pair of reinforced concrete bridges constructed in 1966 to carry traffic across a railroad line. Before removing the obsolete bridges, WSDOT permitted destructive tests of the south bridge to be conducted while traffic was diverted onto the north bridge. Section 2.1 outlines the geometry and reinforcing details of the bridge. Subsequent sections report the material properties of the concrete (Section 2.2); reinforcing steel (Section 2.3); bearing pads and polystyrene (Section 2.4); and soil (Section 2.5).

2.1 GEOMETRY AND REINFORCING DETAILS

The researchers determined the geometry and reinforcing details of the bridge by reviewing the WSDOT structural drawings. Critical dimensions were verified in the field, and the locations of column reinforcement were confirmed with a pachometer.

Figure 2.1 shows the bridge in plan and elevation. The three-span, reinforced concrete bridge had two end spans of 41 feet each and a center span of 60 feet. The width of the bridge was nearly 40 feet, providing room for two 12-foot lanes, shoulders, and railings. The abutments and the intermediate piers (bents) were skewed by 12.8 degrees. The superstructure, abutments, and piers are described in the following paragraphs.

The lateral stiffness of the superstructure was provided mainly by a 6.5-in. thick, reinforced concrete slab, topped with 2 to 3 inches of asphalt. In the longitudinal direction, the slab was reinforced by #4 and #7 bars in the top and #5 bars in the bottom. The longitudinal reinforcement was continuous over the intermediate piers. Reinforcement in the transverse direction consisted of #5 bars, both top and bottom. The slab was supported by six, prestressed concrete I-girders, 3 feet 6 inches deep, spaced at 6 feet 10 inches on center.

The abutments were strong and stiff. The prestressed girders extended 2 inches into cast-in-place diaphragms at the abutments and piers. Four prestressing strands that extended into the

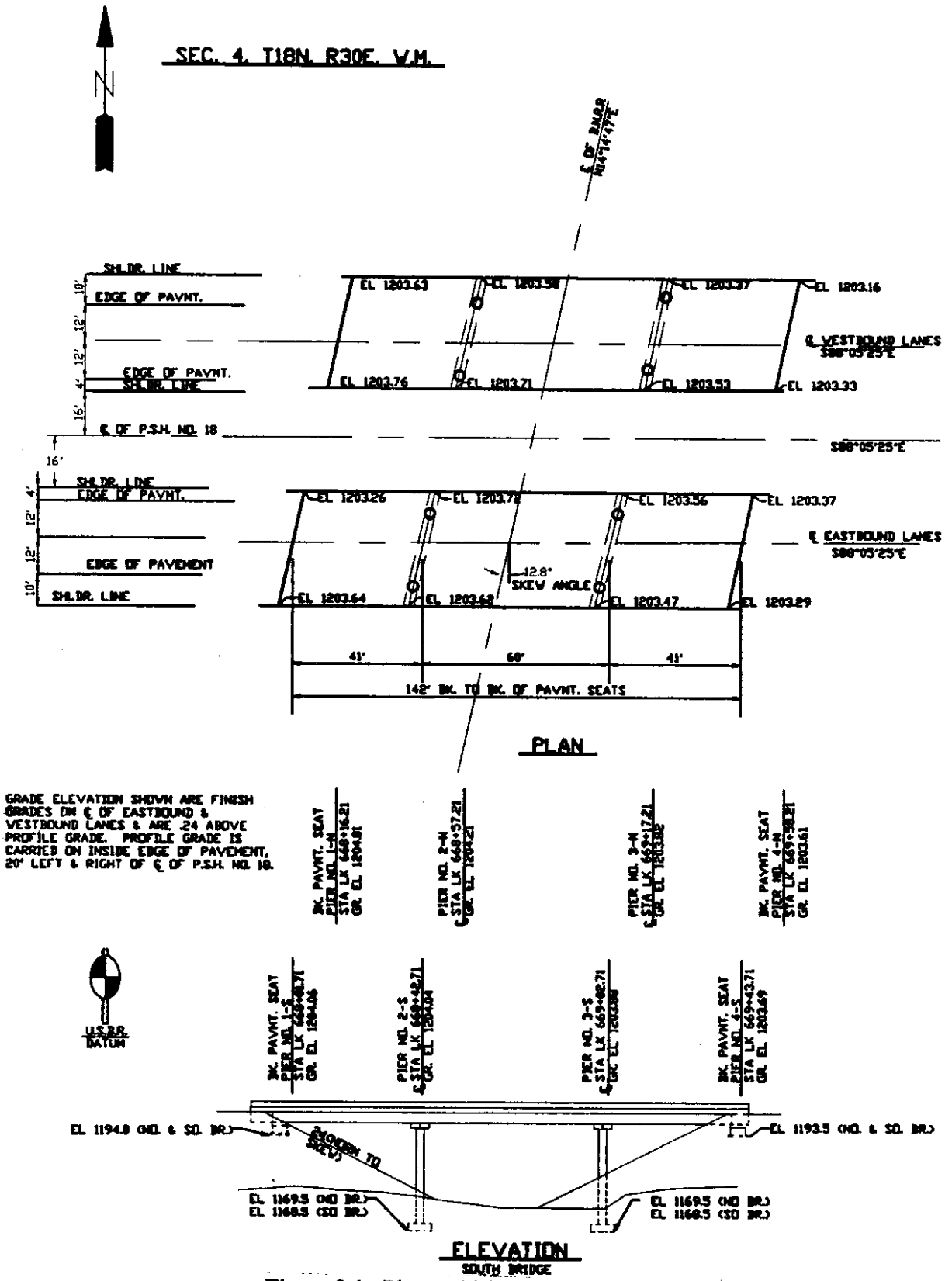

Figure 2.1. Plan and Elevation of Bridge

diaphragms and 1 5/8-inch shear keys provided some flexural and shear strength at the girder-diaphragm connection. The diaphragms at the abutments served also as endwalls, as shown in Figure 2.2. These 18-inch diaphragm/endwalls were cast monolithically with 12-in. thick, 4-foot deep wingwalls, which extended 7 feet parallel to the highway. The wingwalls were connected to the end diaphragms with ten #4 bars. Because of this combination of heavy reinforcement and monolithic construction, transverse forces were transmitted from the deck through the diaphragm into the wingwalls and then to the soil surrounding the wingwalls by passive soil pressure.

Each abutment diaphragm rested on six elastomeric bearing pads, measuring nominally 10 5/8 x 10 5/8 x 7/8 inches. A steel plate was embedded into the bottom of the diaphragms above each bearing pad. The pads were supported by a concrete pedestal that extended the length of the diaphragm/endwall. The gap between the pedestals and the abutment diaphragm was filled with polystyrene.

At the piers, 12-inch thick diaphragms were cast monolithically with the slab. These diaphragms were heavily reinforced to transfer forces from the deck and girders into the pier crossbeam. The crossbeam was monolithic with the 3-foot diameter columns, as shown in Figure 2.3. The interface between the diaphragm and the crossbeam was reinforced with #10 dowels. This connection was strong and stiff in the transverse direction.

The clear height of the columns was nearly 25 feet for all four columns. Longitudinal reinforcement consisted of eleven #9 bars. Transverse reinforcement consisted of #3 hoops, spaced at 12 inches; the hoops were closed with a 14-inch lap but had no hooks into the column core. Whereas the column longitudinal reinforcement extended into the crossbeam with no splice, the transfer of forces between the column and footing depended on the integrity of a 3-foot 4-inch lap splice (35 bar diameters). The columns stood on 9-foot 6-inch x 9-foot 6-inch x 2-foot concrete spread footings (Figure 2.1 and 2.3). The footings were reinforced only on the bottom with 14 #8 bars in each direction.

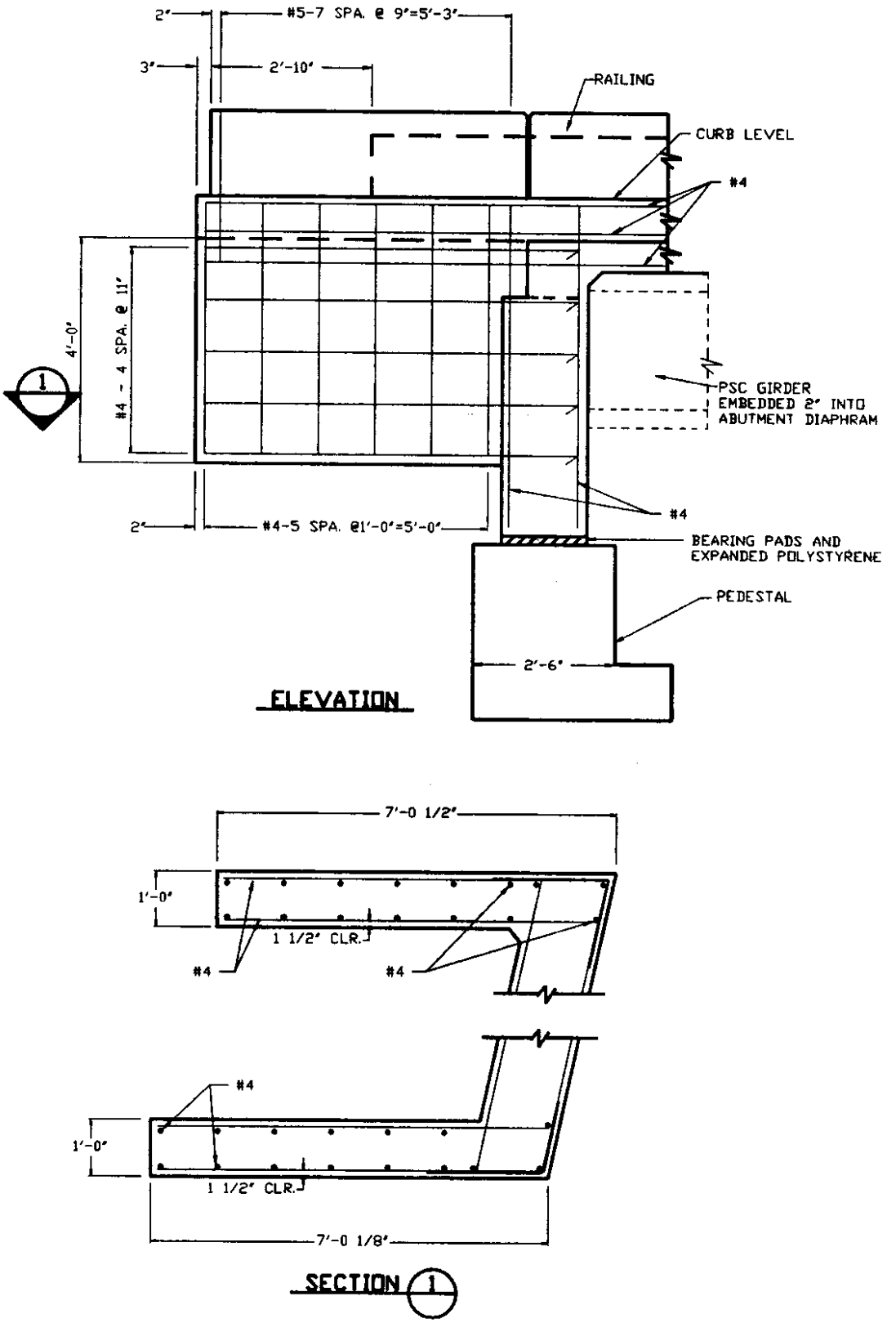

Figure 2.2. Abutment

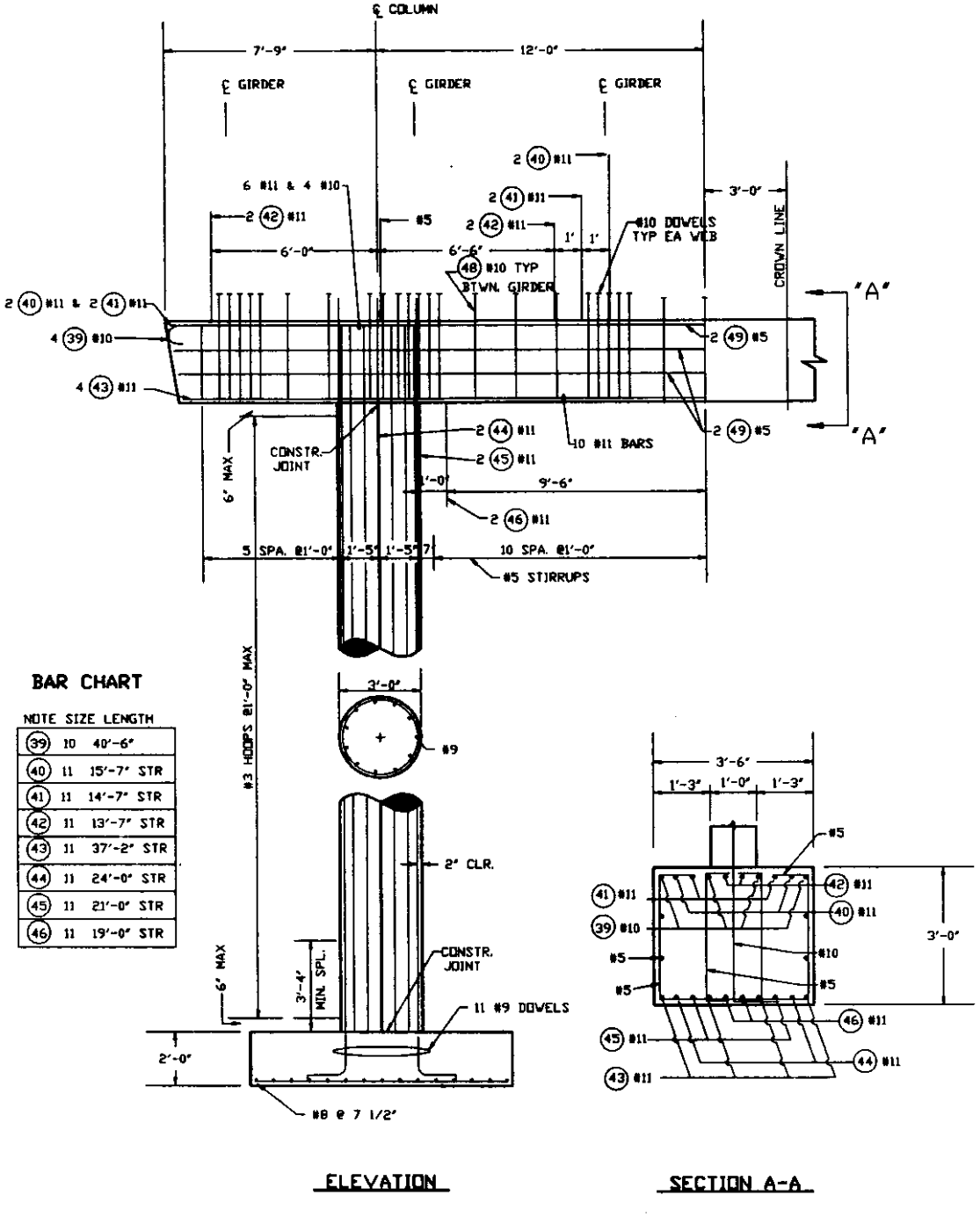

Figure 2.3. Pier

2.2 CONCRETE

With the exception of the prestressed girders, the bridge was constructed entirely of cast-in-place, reinforced concrete. The footings and abutments walls were constructed of WSDOT class B mix with a specified compressive strength at 28 days, f'_c, of 3,000 psi. (6) The remaining cast-in-place concrete was WSDOT class AX mix, which had a specified compressive strength of 4,000 psi. At the end of the tests, 12 concrete cores were taken from undamaged regions of the columns, and the cores were tested in accordance with ASTM Standards C31 and C39. (7) The measured compressive strength of the cores, f_c, was 6,400 +/- 300 psi, and the modulus of elasticity, E_c, was 4.7×10^3 ksi +/- 200 ksi. Hjartarson (8) gives a detailed description of class AX concrete and of the concrete core tests.

2.3 REINFORCING STEEL

After the field tests had been completed, two samples of longitudinal steel were removed from the midheight of the columns in a region with little cracking. The markings NW9N indicated that the steel bars had been produced by Northwest Steel Rolling Mills, Inc. with new billet steel. (9) The lack of a grade number indicated that the bars were GR 40. Following the procedure prescribed by ASTM A370-77 (7), the researchers determined that the steel had a modulus of elasticity of 29.5×10^3 ksi, a yield stress of 50.6 ksi, and a strength of 86.3 ksi.

2.4 BEARING PADS AND POLYSTYRENE

To model the bearing pads and polystyrene at the abutments, researchers measured their shear force-displacement behavior. Because this behavior varies with the level of axial load, axial force-displacement tests were conducted also.

The laboratory tests simulated field conditions as nearly as possible. In the field, the top surface of each bearing pad was in contact with a steel plate, which was embedded in the bottom of the end diaphragm. The bottom surface was in contact with the concrete pedestal. The expanded polystyrene was sandwiched between the two concrete surfaces, the bottom of the diaphragm and the top of the pedestal.

Axial Force-Displacement Relationships

The vertical force on the polystyrene and bearing pads was calculated by estimating the vertical reaction at the abutment and then distributing this reaction to the bearing pads and polystyrene according to their relative stiffness. The construction sequence determined the procedure by which the researchers estimated the abutment reaction. The simply-supported girders had been placed, and the slab had been cast, before the bent diaphragms had gained significant strength. Consequently, the vertical reaction caused by the dead load was calculated with the assumption that the spans were simply supported. The resulting calculated vertical load to each abutment was 180 kips.

Figure 2.4 shows the test set-up and the measured axial stress-strain relationship for the bearing pads. The measured response was approximated with a bilinear curve, in which the compressive elastic modulus for the bearing pads was 2,150 psi for strains less than 0.035 and 4,800 psi for larger strains. The measured initial elastic modulus was slightly larger than Gent (10) reported as typical. Gent reported that the initial elastic modulus for typical pads varied between 200 and 2,000 psi for International Rubber Hardnesses ranging from 40 to 80. The measured durometer hardness of the pads was 64 at room temperature, which corresponded well with the nominal hardness of 60.

Laboratory tests were performed on new samples of polystyrene because polystyrene from the bridge had not been recovered during the tests. Though the new material appeared similar in color and density to that used for the bridge, the engineering properties of the field and laboratory polystyrene may have differed. The lab set-up and the measured compressive stress-strain relationships for the polystyrene are shown in Figure 2.5. The stress-strain behavior varied little with the size of the sample and the roughness of the bearing surfaces. A good approximation for the compressive elastic modulus was 600 psi for strains less than 0.055 and 90 psi for larger strains.

If the contribution of the polystyrene were neglected, the calculated compressive force in each of the 6 bearing pads would be 30 kips, corresponding to an axial stress of 266 psi. This

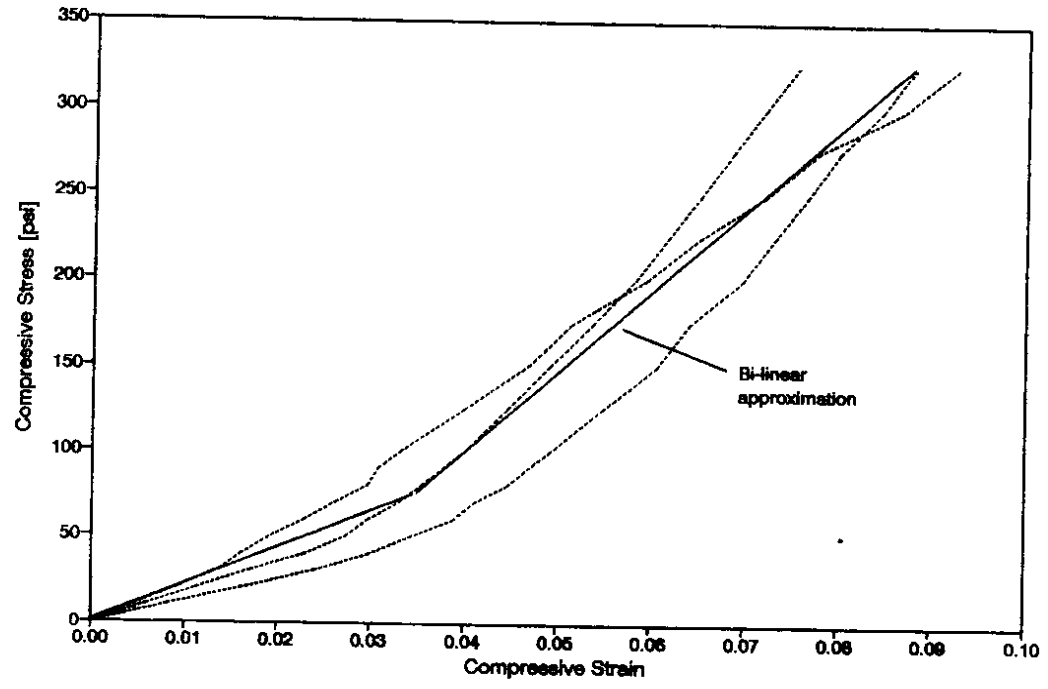

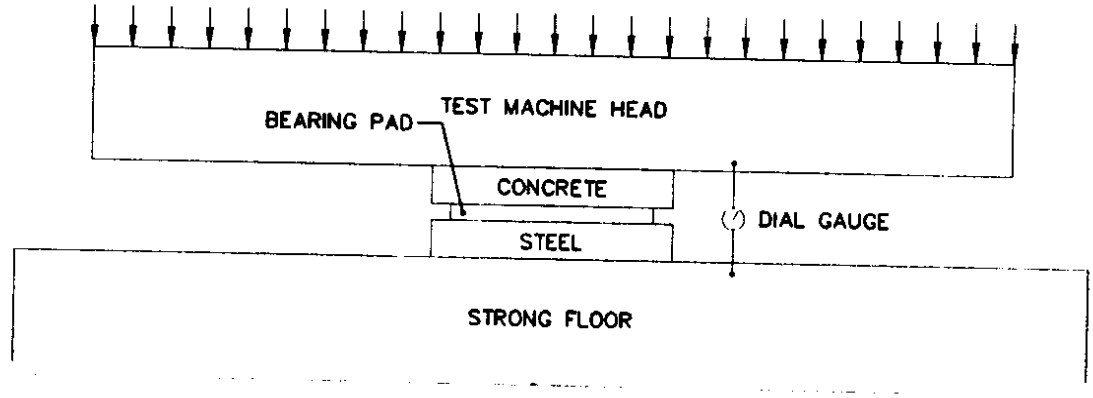

Figure 2.4. Axial Force-Displacement Behavior of Bearing Pads

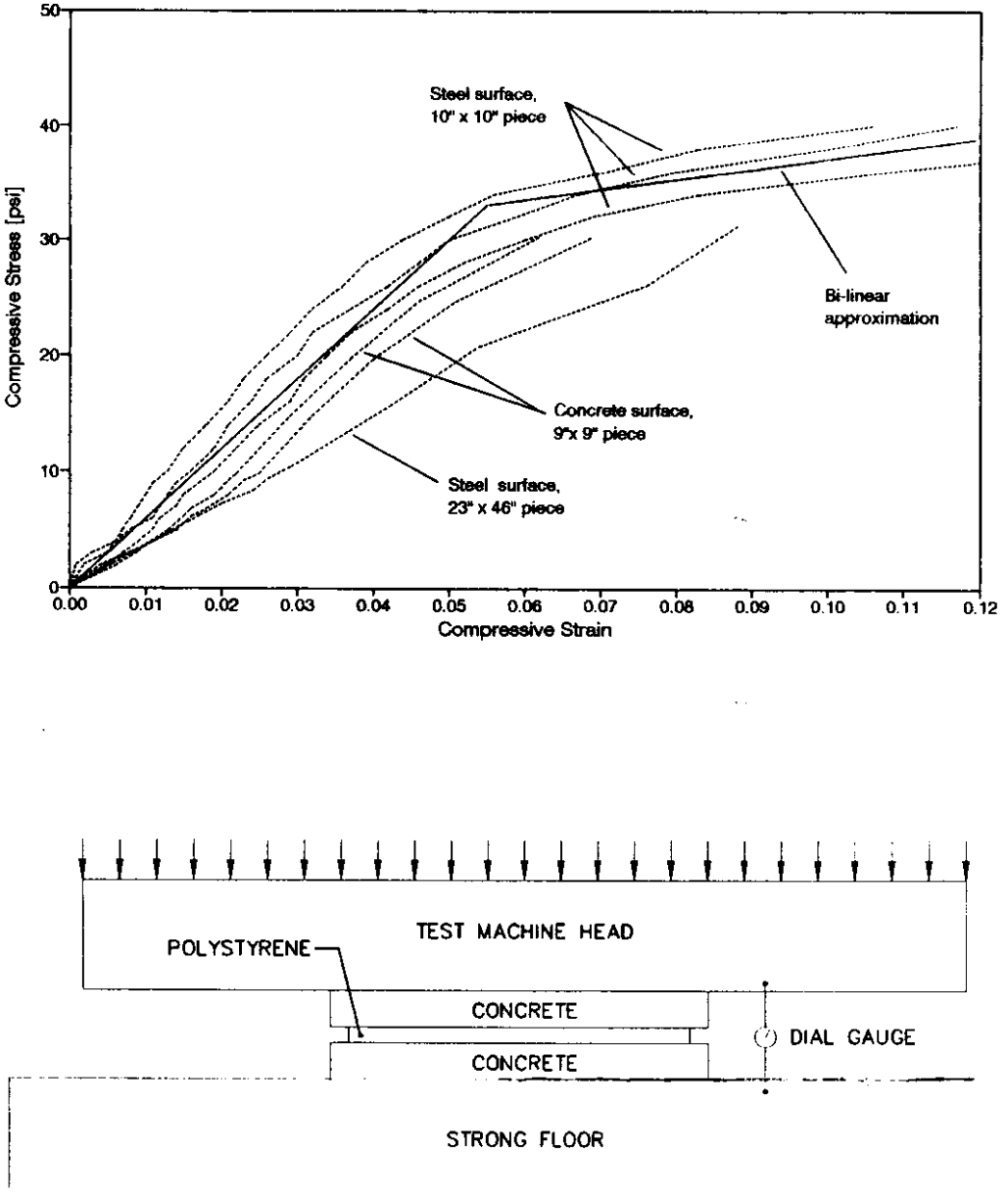

Figure 2.5. Axial Force-Displacement Behavior of Polystyrene

force would decrease to 7 kips (62 psi) if the 180-kip abutment reaction were distributed to the pads and polystyrene according to their relative stiffnesses. The force carried by the polystyrene was 138 kips, corresponding to a stress of 17 psi. Researchers neglected the effects of creep, temperature and possible deviations from the specified material thickness.

Shear Force-Displacement Relationships

Shear force-displacement behavior for the bearing pads was measured for axial loads of 5 and 27 kips with the test set-up shown in Figure 2.6. During a first series of tests, in which stress-strain behavior was measured, the maximum load was applied within a few minutes of the beginning of the test. Researchers performed a second series of tests at a slower rate of loading to determine the coefficient of friction. As shown in Figure 2.6, the shear modulus of the bearing pads was approximately 217 psi, corresponding to a pad shear stiffness of 28 kips/in. This stiffness varied little with changes in axial load. When the pad was subjected to an axial load of 5 kips, slip occurred at a shear force of 4 kips. If the coefficient of friction were assumed to be constant, the calculated shear force at slip would be 5.6 kips for an axial force of 7 kips.

Shear force-displacement relationships for polystyrene with compressive stresses of 15, 20 and 25 psi are shown in Figure 2.7. A good approximation of the shear modulus of the polystyrene was 460 psi. On the basis of additional tests at compressive stresses ranging from 15 to 25 psi, in which the shear force was increased slowly until slippage, the coefficient of friction was estimated to be 0.61. If the coefficient of friction remained constant, slip at a compressive stress of 17 psi would occur at a shear stress of approximately 10 psi.

2.3 SOIL

Site Conditions

As shown in Figure 2.1, compacted fill surrounded the lower 12 feet of the columns. Based on a 2 to 1 slope and a footing size of 9 feet 6 inches, the calculated soil depth at the ends of the footings was 14.4 feet on the uphill side of the footing and 9.6 feet on the downhill side. The soil at the columns consisted of dry, dense, silty sand with some rough cobbles near the surface. Generally, these cobbles ranged in size from $^1/_2$ to 3 inches, although a few were larger. An

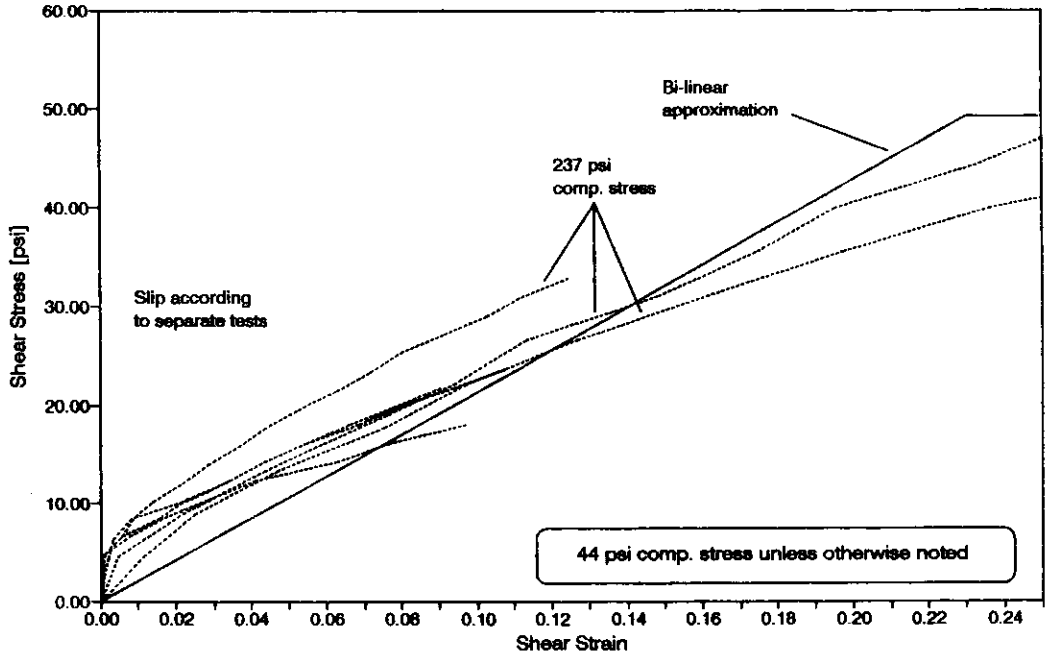

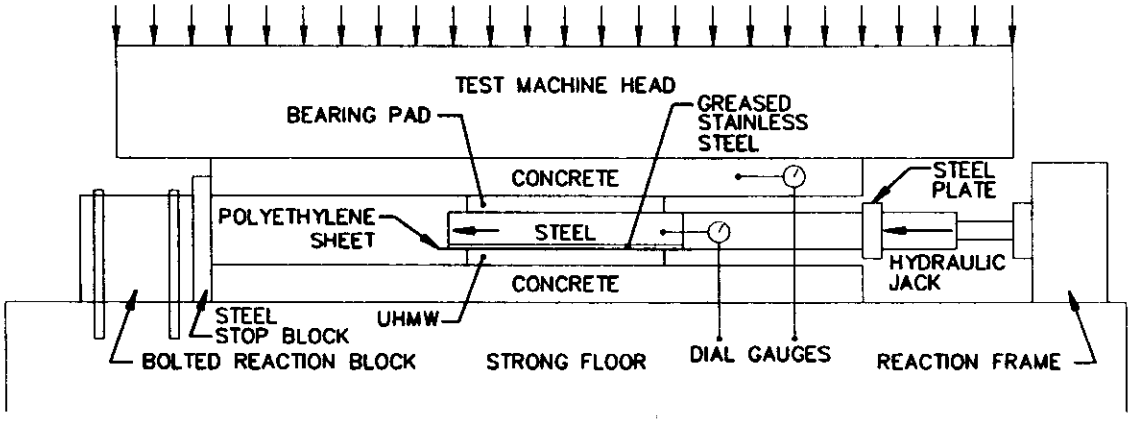

Figure 2.6. Shear Force-Displacement Behavior of Bearing Pads

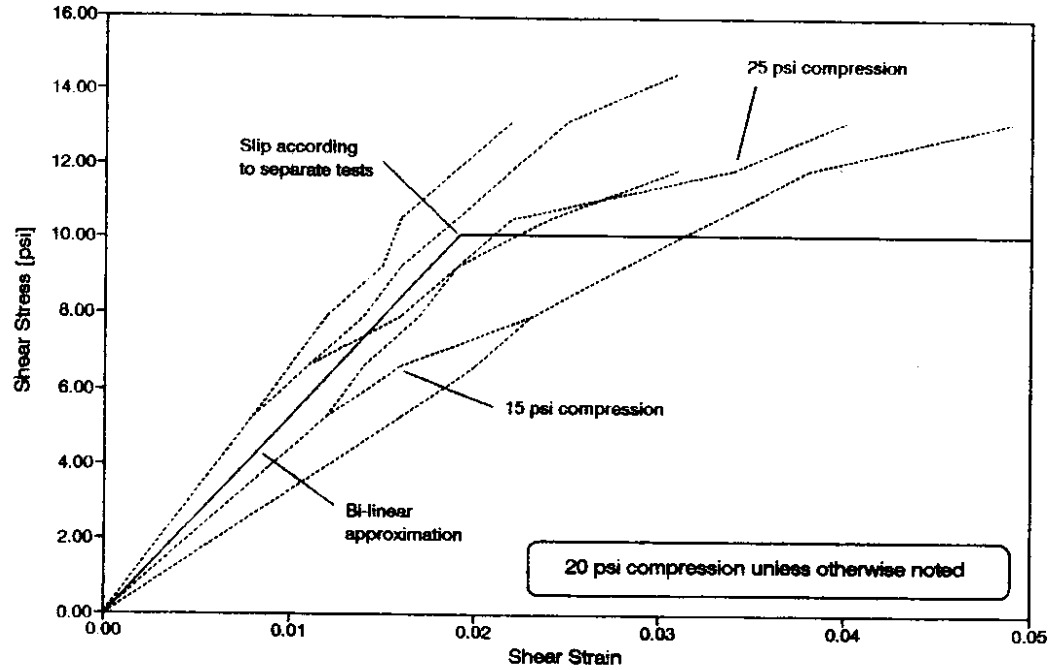

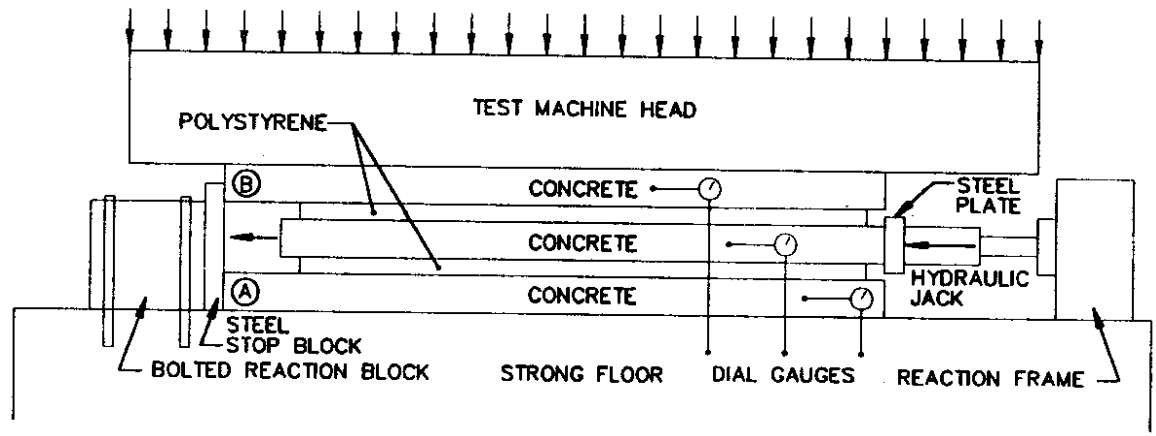

Figure 2.7. Shear Force-Displacement Behavior of Polystyrene

indication of the soil's cohesiveness is the fact that it stood vertically for several days in 12-foot deep trenches before the trenches were shored.

The soil at the abutment was also silty sand, but the soil had fewer rocks. The soil at the west abutment and north side of the east abutment was dry. The soil at the south end of the east abutment was moist because of a leak in a drainage pipe. The soil stood for 30 to 40 days at a steep slope, estimated at 60 to 70 degrees, in an 8-foot deep hole.

Measured Properties

Approximately one year after testing had been completed, researchers obtained undisturbed samples from the bridge site. The soil's engineering properties, as determined from laboratory tests, are summarized in Table 2.1. The soil consisted of 70 percent fine grains and 30 percent coarse grains. On the basis of the sieve analysis, a liquid limit of 24.2 and, a plasticity index of 3.5 percent, the soil was classified as a low-plasticity silt. Its designation is ML in the Uniform Soil Classification System.

The in-situ unit weight of the soil was 110 pcf, and its dry unit weight was 99 pcf. The corresponding moisture content of 11 percent was less than half of the liquid limit. Typical dry unit weights for silty sands range from 85 pcf to 125 pcf. (11) On the basis of the dry unit weight of 99 pcf, the soil at the site would be classified as having medium density.

Four undrained triaxial tests were performed at a confining pressure of 7 psi. This pressure would be expected to develop at a depth of approximately 9 feet. To determine the angle of internal friction, a fifth test was performed at a confining stress of 14 psi. The triaxial test results are shown in Figure 2.8.

The initial tangent modulus for the soil, E_S, was approximately 1,600 psi for a confining pressure of 7 psi. It was difficult to verify that the measured elastic modulus was reasonable because E_S varies greatly with confining pressure and density. Moreover, E_S is highly sensitive to sample disturbance. Terzaghi and Peck (12) state that the elastic modulus for loose sands can be approximated as 100 times the confining pressure (i.e., 700 psi). At this confining pressure, E_S

Table 2.1. Soil Properties

Item	Result
General Description	Medium-Dense, Silty Sand; low dry strength
USCS classification	ML, low plasticity silt
Sieve Analysis	Approximately 70% fines and 30% coarse grained
Color	Tan; uniform
Dilatancy	Medium to medium fast
Plastic Limit, PL	20.7
Liquid Limit, LL	24.2
Plasticity Index. PI	3.5
Undisturbed Samples:	
Unit Weight, In-Situ	110.1 pcf
Unit Weight, Dry	99.2 pcf
Void Ratio, e	0.67
Porosity, n	0.40
Water Content, In-Situ	11%
Degree of Saturation, S	43.8%
Standard Proctor Test:	
Unit Weight, Max. Dry	105.0 pcf
Unit Weight, at 95% Compact.	99.8 pcf
Unit Weight, at 95% Compact. &	111.0 pcf
Optimal Water Content	
Water Content, Optimal	17%
Undrained Triaxial Tests:	
Initial Tangent Compressive	
Elastic Modulus	1600 psi at 7 psi confining stress (average)
Strength	40 psi at 7 psi confining stress (average)
Strength	70 psi at 14 psi confining stress (average)

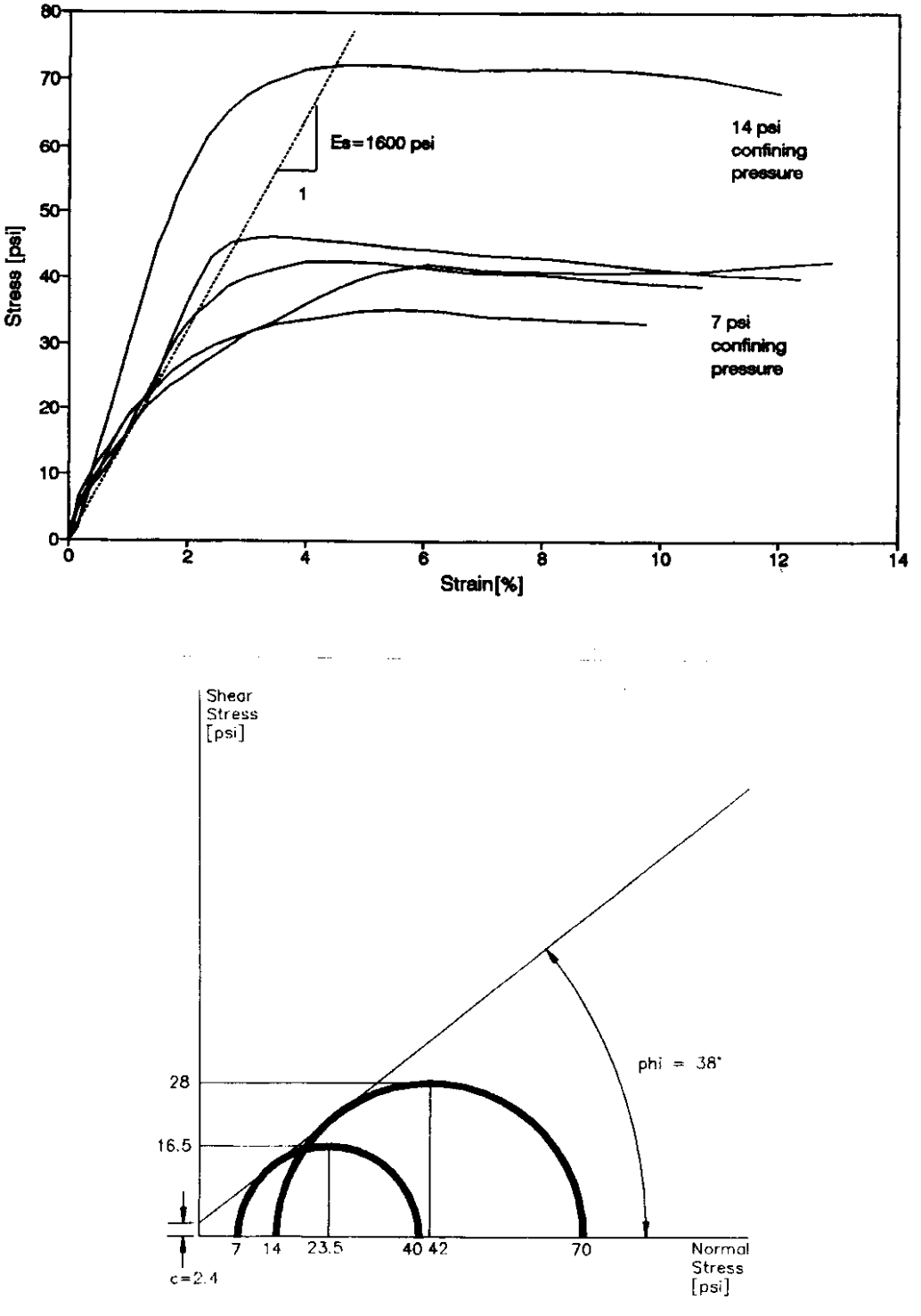

Figure 2.8. Triaxial Test Results

can be as large as 10,000 psi for a dense sand. On the basis of these rough approximations of the elastic modulus, the soil would be characterized as having low to medium density.

The measured angle of internal friction was 38 degrees. Typically, this angle ranges from 29 degrees for loose sands to 41 degrees for dense sands. (13) On the basis of the measured angle of internal friction, the soil would be classified as dense. The apparent discrepancy between the low value of the elastic modulus and the high angle of internal friction was probably attributable to sample disturbance. Sample disturbance was more likely to have affected the elastic modulus than the internal angle of friction because E_S is measured for small strains, whereas the internal angle of friction depends on larger strains.

CHAPTER 3

TEST PROGRAM

This chapter describes Phase I of the experimental program. After an overview of the tests in Section 3.1, subsequent sections report details of the loading system (Sec. 3.2), instrumentation (Sec. 3.3), data acquisition (Sec. 3.4) and test procedures (Sec. 3.5). O'Donovan (5) provides additional details of the design, construction, and operation of the test set-up.

3.1 OVERVIEW OF PHASE I TESTS

During Phase I, researchers imposed six cycles of transverse displacement on the bridge (Figure 1.2) by applying loads to the crossbeams of the intermediate bents (Figure 3.1). The magnitude of the load at each bent was controlled such that the displacements of the bents would be approximately equal. To measure the response of the bridge, 60 electro-mechanical instruments were installed. The measurements included pier and abutment displacements, as well as relative rotation of adjacent beam and column cross-sections.

The first cycle, Test P, was a preliminary test during which researchers checked the loading system and instrumentation without damaging the bridge. The bent displacement for this test was 0.06 inch which, for a clear column height of 25 feet, corresponded to a drift ratio of 0.2 percent. The following two cycles, denoted as Test I, had a target bent displacement of 0.15 inch, which corresponded to a drift ratio of 0.05 percent. During the third test (Test II), researchers applied the maximum load that could be applied safely with the loading system. This 800-kip force was equal to 65 percent of the superstructure's weight.

The final two tests, EXC and ISO, were conducted to determine the resistance provided by the soil and the bearing pads at the abutments. Test EXC was conducted after the soil behind the wingwalls and along the abutment endwall had been removed. After Test EXC, the abutment endwalls were lifted (Figure 3.2), and researchers replaced the bearing pads and expanded polystyrene with nylon blocks that rested on greased, polished, stainless-steel plates. The nylon block/steel plate combination was selected to minimize the abutment's resistance. The final cycle,

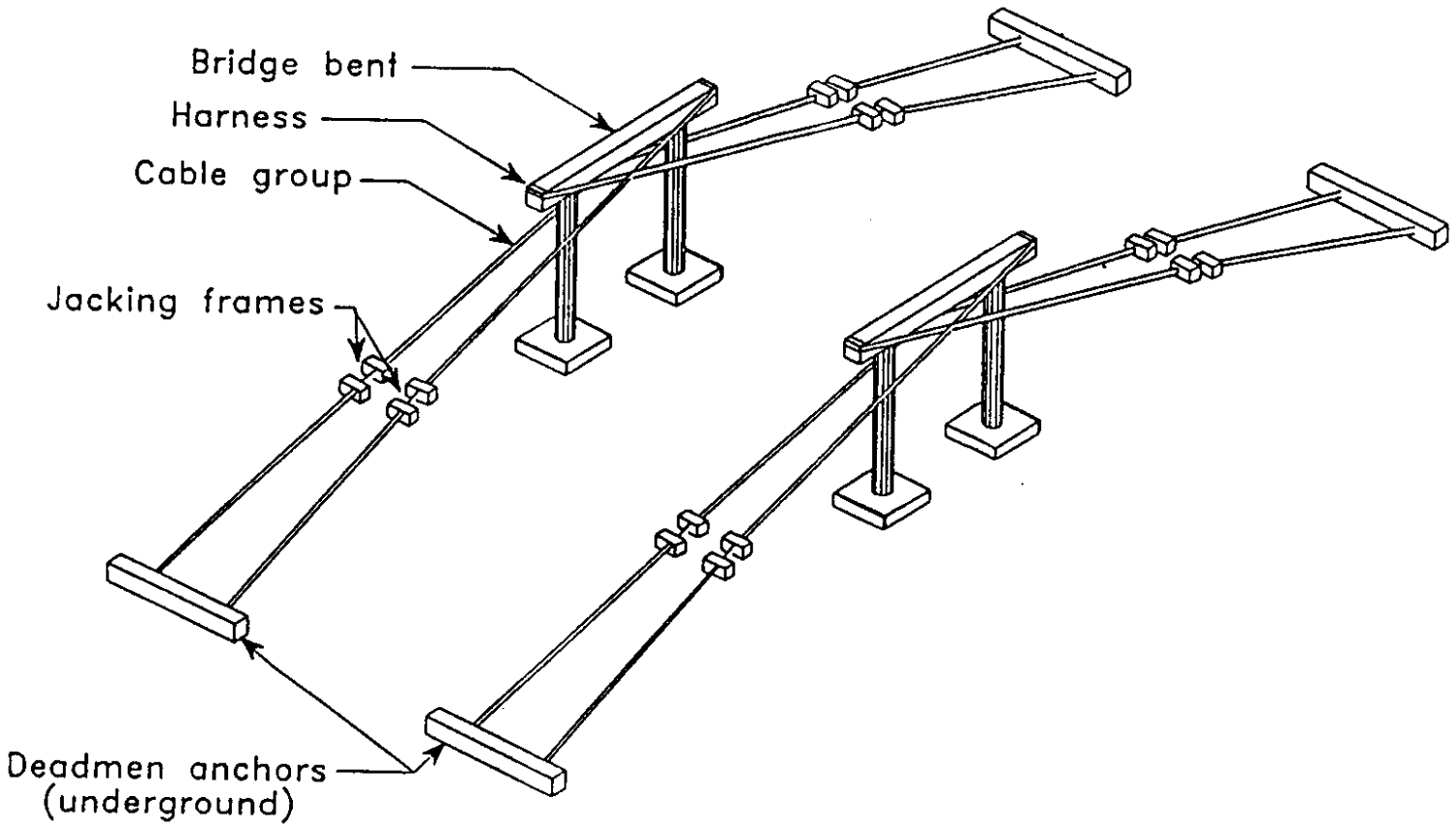

Figure 3.1. Loading System Schematic

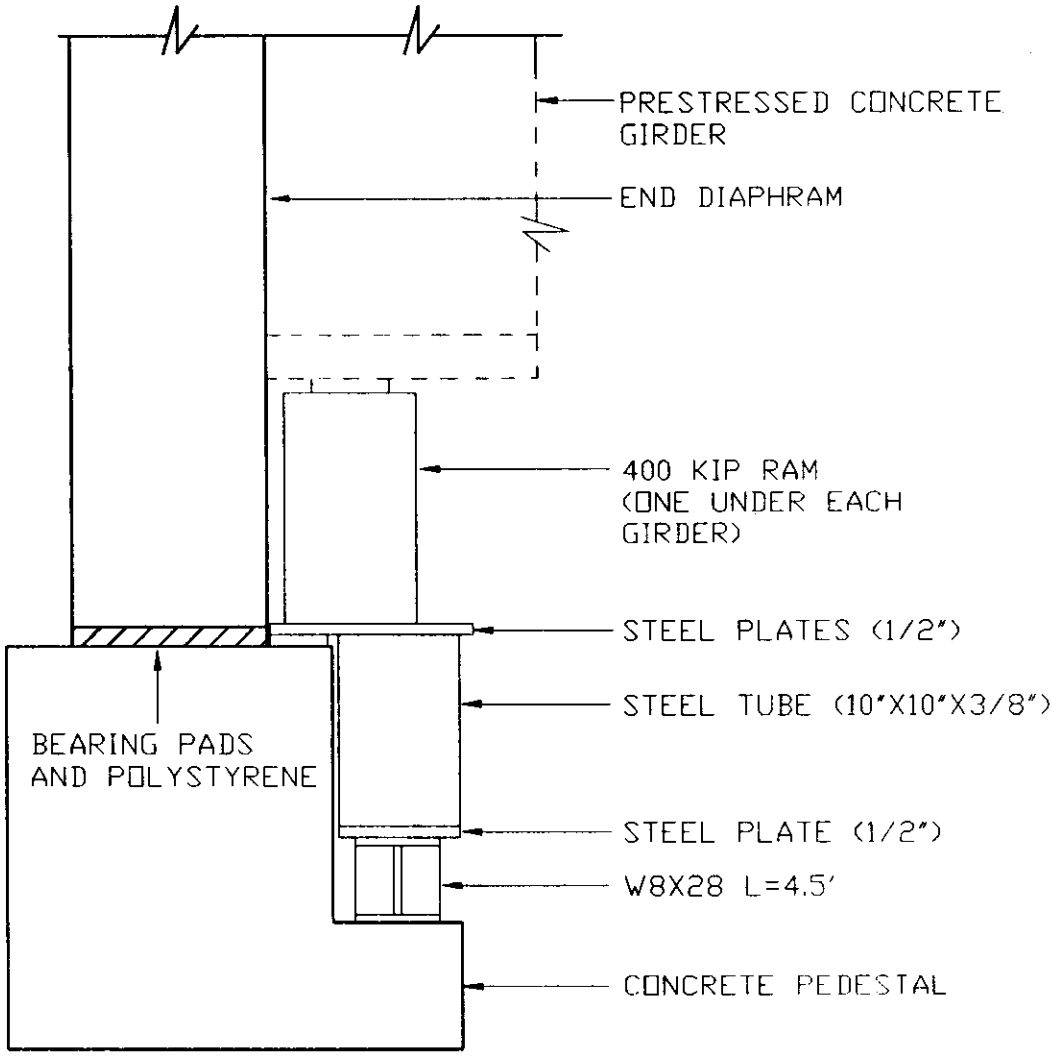

Figure 3.2 End-Span Lifting System

Test ISO, was conducted to measure the resistance of the bents. The stiffness of the soil and pads could be estimated by comparing the results of Tests EXC and ISO with the results of the previous tests.

3.2 LOADING SYSTEM

A critical constraint in designing the loading system was the 30-day period during which traffic on the south bridge could be rerouted to the north bridge. To maximize the time available to conduct the tests, the loading system and most of the instrumentation was installed before traffic was diverted.

The loading system consisted of four principal components: prestressing cables, harnesses, jacking frames and deadmen anchors, as shown in Figure 3.1. At each pier, a complete loading system was located on both sides of the bridge. In each system, sixteen, $^1/_2$-inch 270-ksi prestressing cables applied load to a pier. To distribute the load from the cables to the pier, a steel harness was installed on the ends of each crossbeam. Each set of cables was pulled by two hydraulic rams that were installed in a jacking frame located at ground level. Reactions were provided by a second set of prestressing cables that was anchored by a deadmen anchor (one for each loading system). In the horizontal plane, all components of the load train were aligned along the 12.8-degree skew of the bridge (Figure 2.1). In the vertical plane, components were aligned at an angle of 14 degrees below the horizontal, corresponding to a 4 to 1 slope.

Harnesses

A harness (Figure 3.3 and 3.4) was installed on the end of each crossbeam to transfer forces from the cables to the pier without crushing the crossbeam concrete. The cable forces were transferred to built-up sections (constructed of two C10 channels and 1-inch plates) by standard prestressing vises. The forces in the built-up sections were transferred through gusset plates to 1-inch bearing plates and then to the crossbeam. The gusset plates accommodated the difference in orientation between the flange of the built-up section and the crossbeam surface. To prevent the gusset plates from buckling, the space between them was filled with concrete.

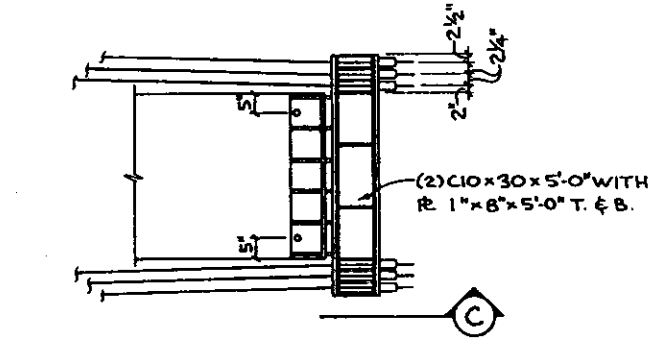

DETAIL 3

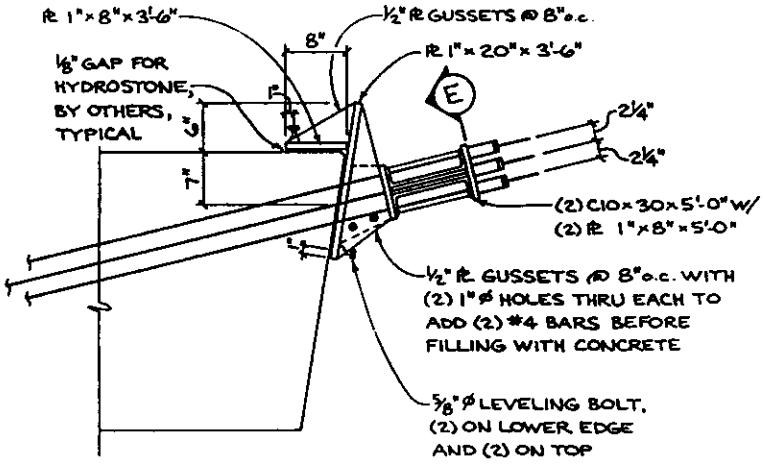

SECTION C

Figure 3.3. Harness Detail

Figure 3.4. Installation of Harness

Jacking Frames

Each 200-ton hydraulic ram was installed within a jacking frame (Figure 3.5 and 3.6). These frames transferred the forces from the solid rams to the prestressing cables. Also, they maintained load on the structure when the rams had reached the end of their 6-inch stroke and needed to be repositioned to continue loading.

Each hydraulic ram was mounted between two heavy wide flange sections. A W14x132 section transferred forces to prestressing cables that were attached to the bent harnesses. A W14x53 section transferred load to cables that were attached to the deadman. Extension of the ram placed the cables in tension. The ram's stability was provided by an assembly of tubular and channel sections and by each prestressing cable being threaded through both wide flange sections. The W14x132 section could move with respect to the W14x53 by sliding along a tubular section with little resistance.

Deadmen Anchors

A deadman anchor provided reactions to the applied loads in each of the four loading systems. Each deadman consisted of a 24-foot long W14x53 steel beam encased in 9 to 12 cubic yards of concrete (Figure 3.7 and 3.8). The deadmen were buried approximately 10 feet deep. On the south side of the bridge, where the water table was approximately 8 feet above the deadmen, an additional 10 feet of surcharge was added to increase their capacity.

Steel pipes were welded to the W14x53 to prevent bonding between the prestressing cables and the surrounding concrete. Reinforcing steel bars were welded to the steel beam to aid in positioning the beam at the proper angle when it was lowered below ground. Two-inch diameter holes, at 2-foot spacings, were made in the beam web to ensure that concrete would completely surround the beam. The cables were held in place with conventional prestressing vises.

3.3 INSTRUMENTATION

To monitor the applied load, the pressure in each hydraulic ram was measured. To monitor the bridge's response to the applied loads, sixty instruments were installed. These instruments can be categorized into the following groups:

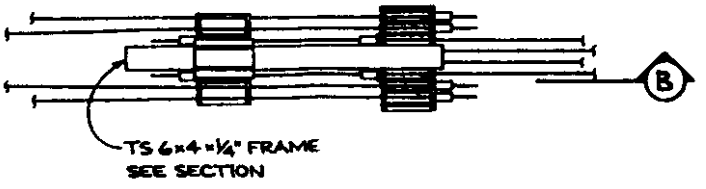

DETAIL (2)

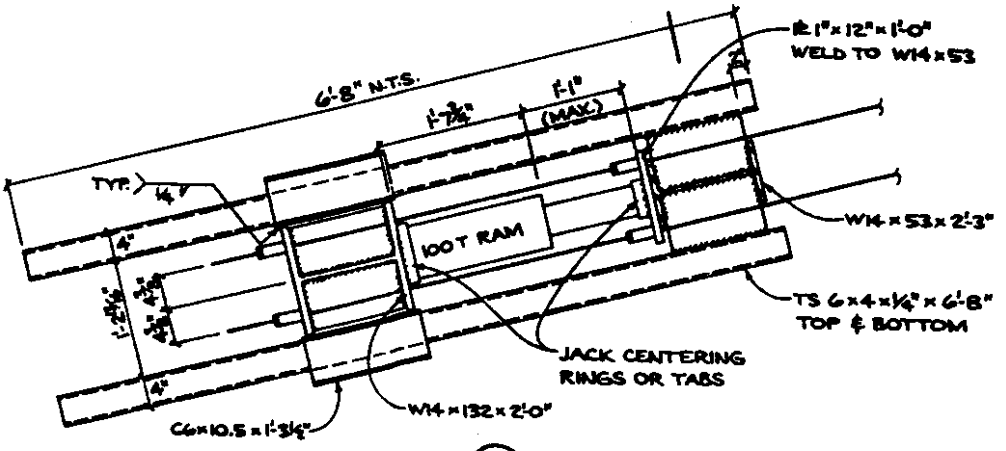

SECTION (B)

Figure 3.5. Jacking Frame Detail

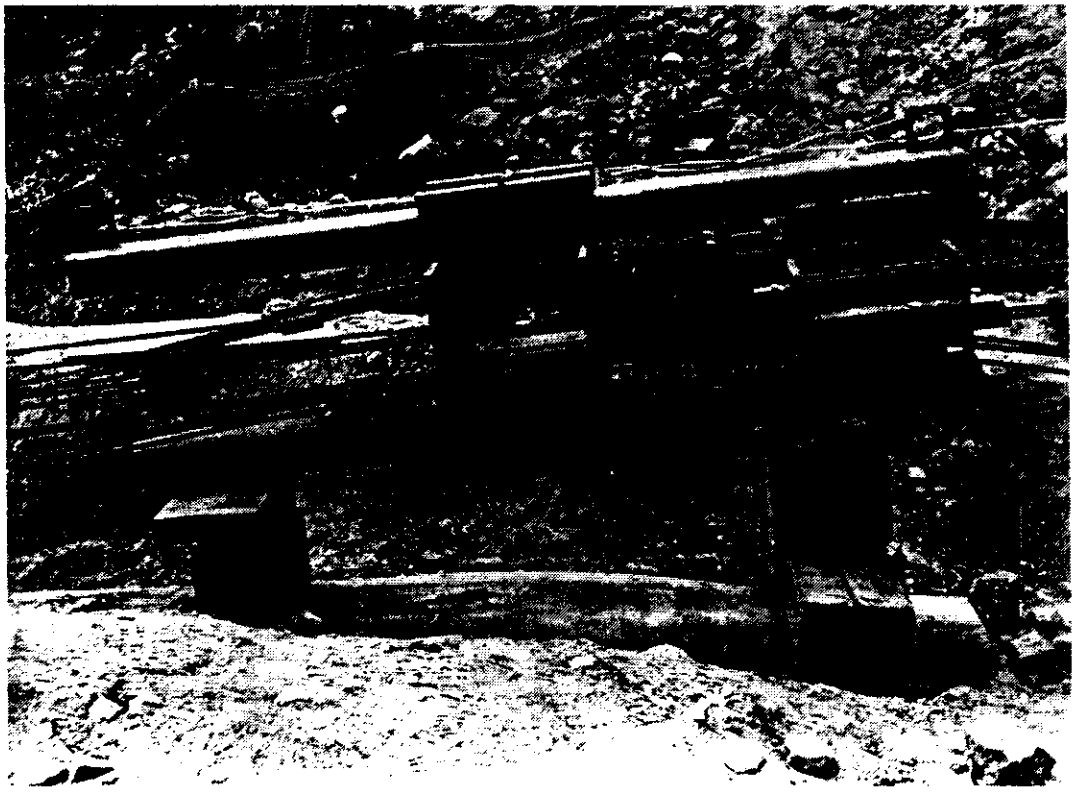

Figure 3.6. Photograph of Jacking Frame

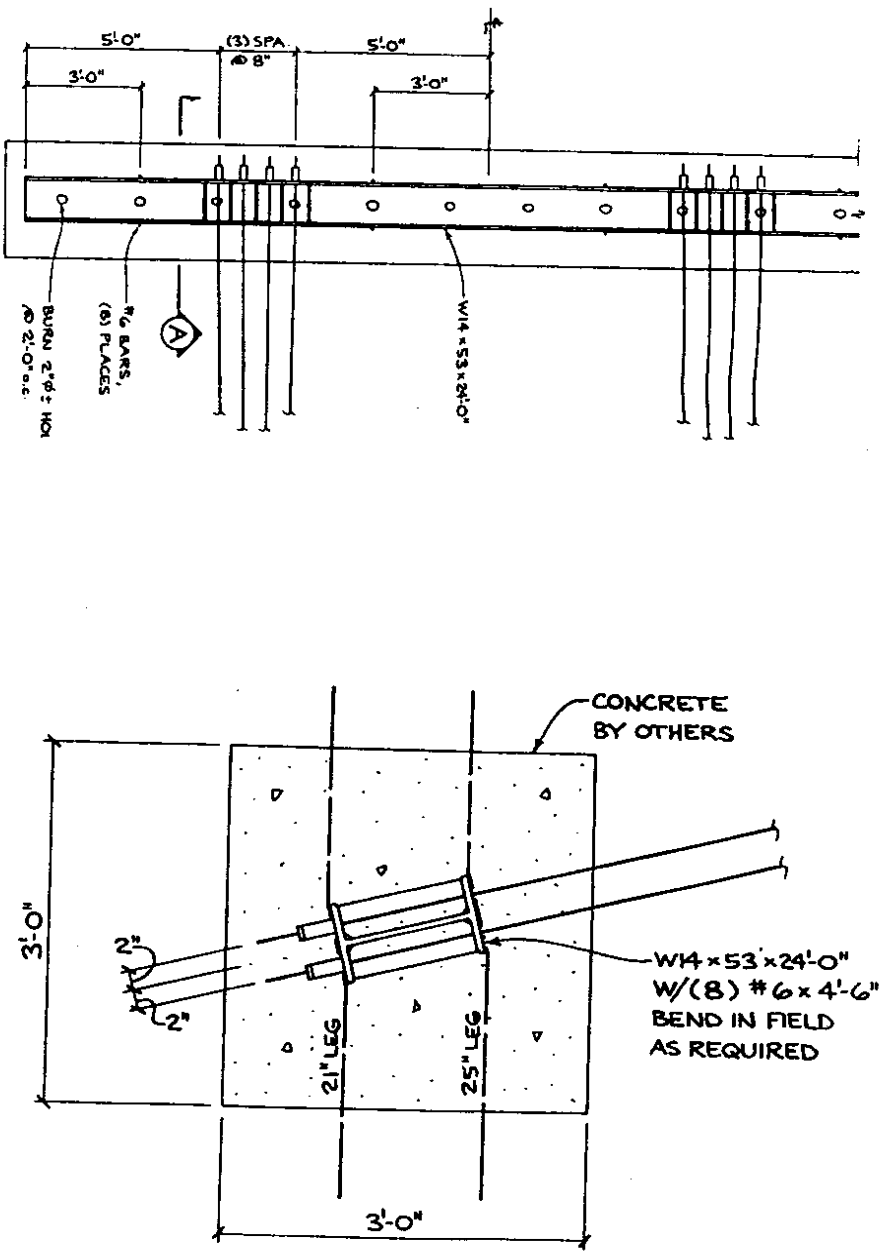

Figure 3.7. Deadman Detail

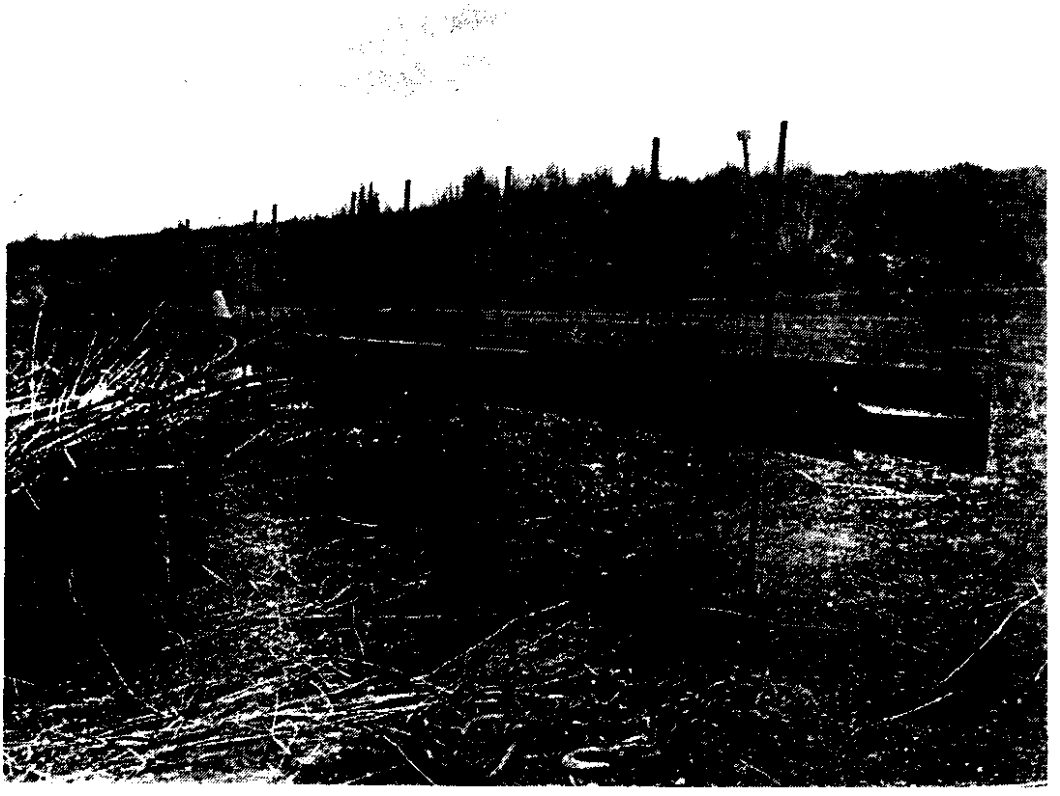

Figure 3.8. Photograph of Deadman

1. ten instruments that measured horizontal displacements of the superstructure (Fig. 3.9),
2. 44 instruments that measured the relative rotations of critical beam and column cross-sections (Figure 3.10), and
3. six instruments that monitored footing rotation and displacement (Fig. 3.10).

The location, designation, transducer type, and stroke for each instrument are listed in Table 3.1. The notation used to refer to the instruments is described in Appendix A. Each instrument group is discussed separately in the following subsections.

Horizontal Displacements of the Superstructure

Horizontal displacements of the deck were measured relative to timber posts located 15 to 25 feet from the bridge. As shown in Figure 3.9, transverse displacements along the skew were measured at each abutment and pier, whereas longitudinal displacements were measured at the abutments only. Two additional instruments monitored the relative displacement between the endwalls and pedestals.

Electro-mechanical transducers were used to measure the movement of a weight that was coupled to the bridge by a cable and pulley system. The details of one of these cable and pulley systems are shown in Figure 3.11. To protect the system from environmental effects, the instruments, weights, and pulleys were housed in plywood enclosures that were attached to the poles. The exposure of the two cable systems on the south side made them the most likely to be affected by weather conditions. Therefore, to provide additional protection for these two systems, plywood shelters were installed to shield the entire length of the cable from the sun and wind.

To minimize deflection and vibration of the reference poles, the 6 x 6-inch timbers were buried in the ground, encased in concrete, and guyed with steel angles. At the abutments, the 6-foot poles were embedded approximately 3 feet into the ground. At the bents, the 20-foot poles were embedded approximately 5 feet into the ground. Pulleys with internal bearings were used to minimize cable friction, thereby reducing cable elongation and motion of the reference pole. To verify the effectiveness of these measures, the researchers displaced each cable by a known amount

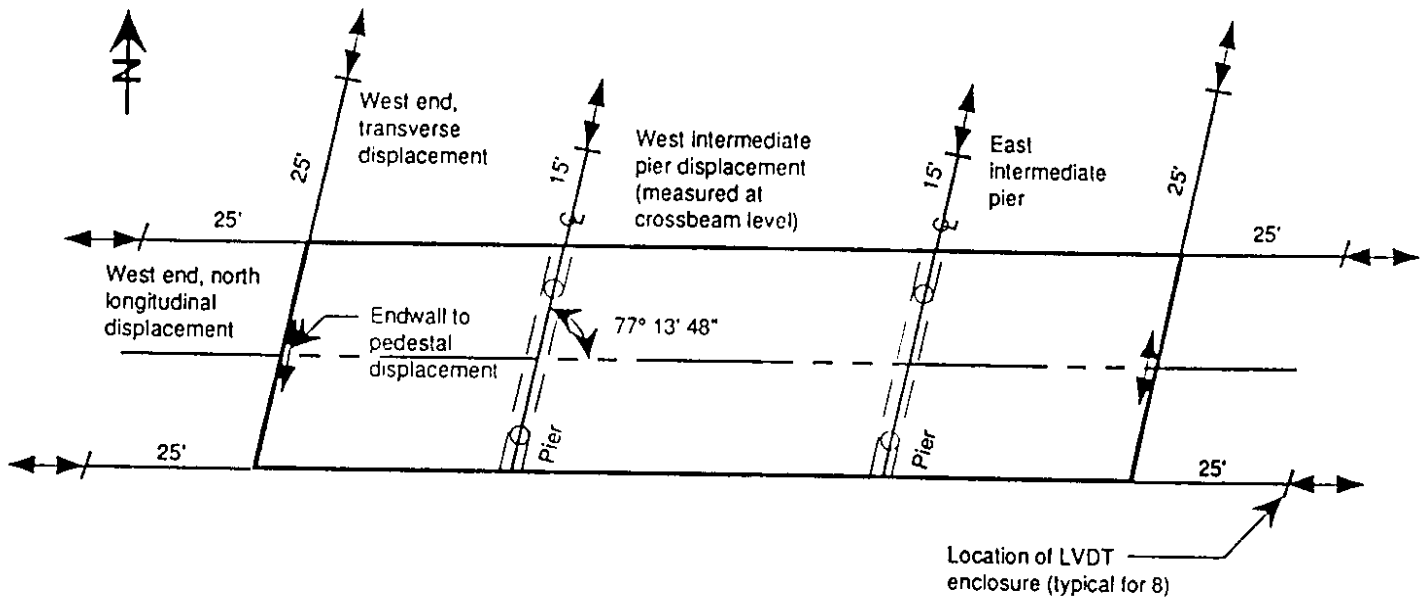

Figure 3.9. Deck Instrumentation Plan

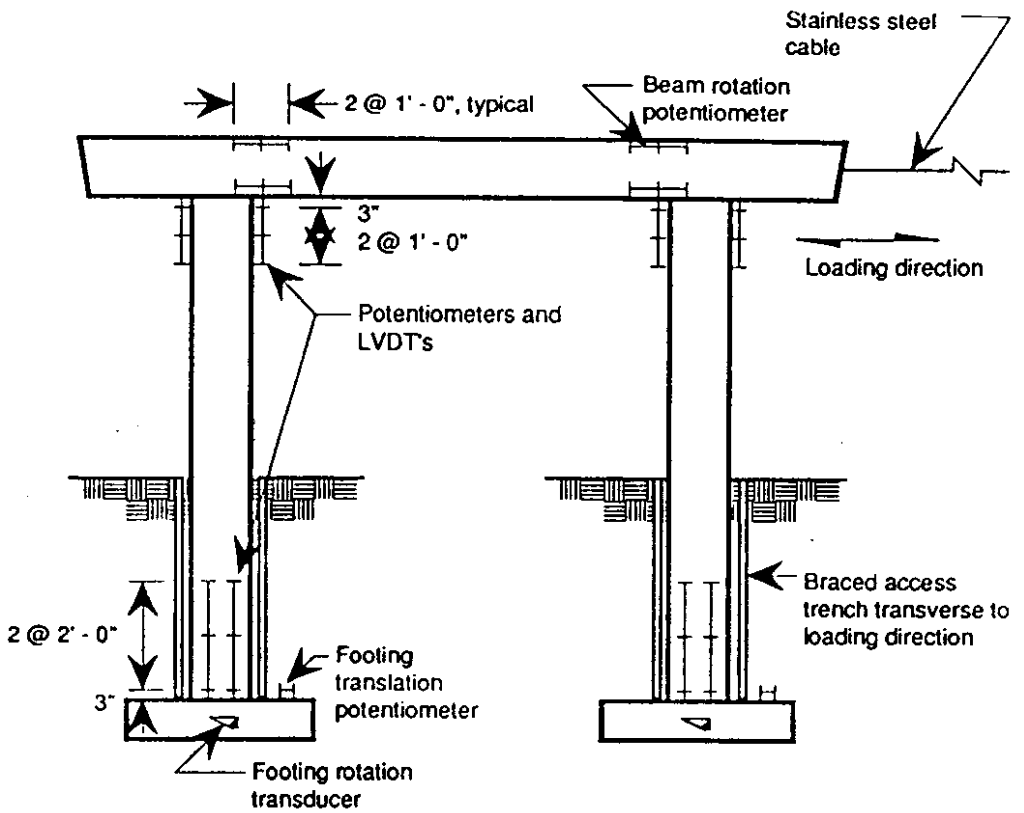

Figure 3.10. Pier Instrumentation Elevation

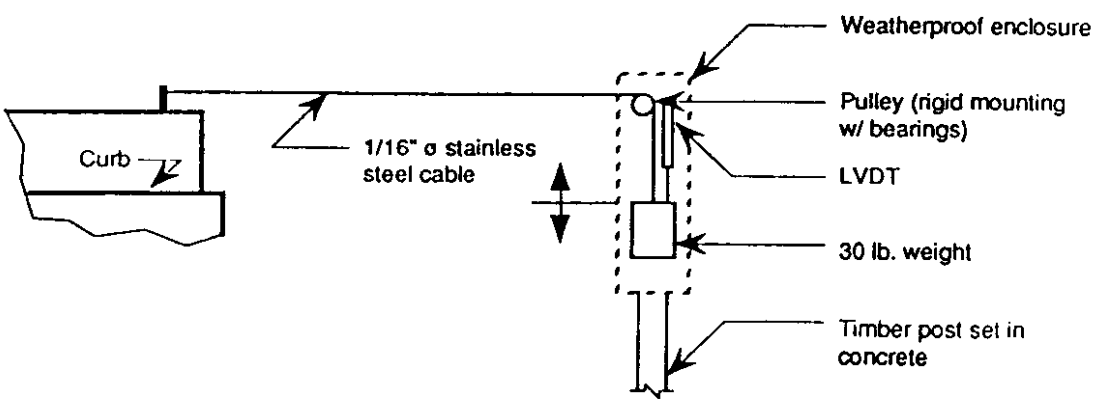

Figure 3.11. Detail of Cable and Pulley System

Table 3.1. Instrumentation Summary

Instrument Location	Instrument Name	Transducer Type	Transducer Manufact.	Stroke [inches]	Calibration Factor
West Bent	WB	Temposonics		12	0.6
East Bent	EB	Temposonics		12	0.6
Deck	WDNT	LVDT	Shaewitz	±3	0.1819
	EDNT	LVDT	Shaewitz	±3	0.1965
	WDNL	LVDT	Trans-Tek	±2	0.3259
	WDSL	LVDT	Shaewitz	±2	0.3113
	EDNL	LVDT	Shaewitz	±2	0.2992
	EDSL	LVDT	Shaewitz	±2	0.3134
	WD/AT	LVDT	Trans-Tek	±2	0.3242
	ED/AT	LVDT	Trans-Tek	±2	0.2940
West Bent	WNCT 1n	LVDT	Trans-Tek	±1	0.1349
North	WNCT 1s	LVDT	Trans-Tek	±1	0.1321
Column	WNCT 2n	Potentiometer	Waters	2	0.2108
Top	WNCT 2s	Potentiometer	Waters	2	0.2108
	WNCT 3n	LVDT	Trans-Tek	±1/2	0.1281
	WNCT 3s	LVDT	Trans-Tek	±1/2	0.1407
West Bent	WSCT 1n	LVDT	Trans-Tek	±1	0.1779
South	WSCT 1s	LVDT	Trans-Tek	±1	0.1327
Colum	WSCT 2n	Potentiometer	Waters	2	0.2108
Top	WSCT 2s	Potentiometer	Waters	2	0.2108
	WSCT 3n	LVDT	Trans-Tek	±1/2	0.1041
	WSCT 3s	LVDT	Trans-Tek	±1/2	0.1101
East Bent	ENCT 1n	Potentiometer	Waters	2	0.2108
North	ENCT 1s	Potentiometer	Waters	2	0.2108
Column	ENCT 2n	Potentiometer	Waters	2	0.2108
Top	ENCT 2s	Potentiometer	Waters	2	0.2108
East Bent	ESCT 1n	Potentiometer	Waters	2	0.2108
South	ESCT 1s	Potentiometer	Waters	2	0.2108
Column	ESCT 2n	Potentiometer	Waters	2	0.2108
Top	ESCT 2s	Potentiometer	Waters	2	0.2108

Table 3.1. Instrumentation Summary (continued)

Instrument Location	Instrument Name	Transducer Type	Transducer Manufact.	Stroke [inches]	Calibration Factor
West Bent	WNCB 1n	Potentiometer	Waters	2	0.2108
North	WNCB 1s	Potentiometer	Waters	2	0.2108
Column	WNCB 2n	Potentiometer	Waters	2	0.2108
Bottom	WNCB 2s	Potentiometer	Waters	2	0.2108
	WNCB 3n	Potentiometer	Waters	2	0.2108
	WNCB 3s	Potentiometer	Waters	2	0.2108
West Bent	WSCB 1n	Potentiometer	Waters	2	0.2108
South	WSCB 1s	Potentiometer	Waters	2	0.2108
Column	WSCB 2n	Potentiometer	Waters	2	0.2108
Bottom	WSCB 2s	Potentiometer	Waters	2	0.2108
	WSCB 3n	Potentiometer	Waters	2	0.2108
	WSCB 3s	Potentiometer	Waters	2	0.2108
West Bent	WNB 1t	LVDT	Trans-Tek	±1/2	0.0998
Crossbeam	WNB 2t	LVDT	Trans-Tek	±1/2	0.1006
North End	WNB 1b	LVDT	Trans-Tek	±1/2	0.0805
	WNB 2b	LVDT	Trans-Tek	±1/2	0.1108
West Bent	WSB 1t	LVDT	Trans-Tek	±1/2	0.1184
Crossbeam	WSB 2t	LVDT	Trans-Tek	±1/2	0.1136
South End	WSB 1b	LVDT	Trans-Tek	±1/2	0.0994
	WSB 2b	LVDT	Trans-Tek	±1/2	0.1014
East Bent	ENB 1t	Potentiometer	Waters	2	0.2108
Crossbeam	ENB 1b	Potentiometer	Waters	2	0.2108
	ESB 1t	Potentiometer	Waters	1	0.1054
	ESB 1b	Potentiometer	Waters	1	0.1054
North	WNCFT	Potentiometer	Waters	2	0.2108
Footing	WNCFR1,2	Clinometer	Lucas		9.474
South	WSCFT	Potentiometer	Waters	2	0.2108
Footing	WSCFR1,2	Clinometer	Lucas		9.474

at the bridge and compared this displacement with that recorded by the data-acquisition system. The two measurements nearly always agreed to within 0.001 inch, even under reversals of displacement direction.

Relative Rotations of Columns and Crossbeams

The majority of the instruments at the piers measured relative rotations of critical cross sections of the columns and beams. On the west pier, three instruments were installed on each side of the top and bottom of each column, as shown in Figure 3.10. The first pair of instruments measured rotation over the 2 inches nearest to the end of the columns; the second pair measured rotations over the next 12-inch segment; and the third pair monitored an additional 12-inch region. On the west bent, 3-foot trenches were excavated so that researchers could install instrumentation at the bottom of the columns, and so that they could monitor damage at the base of the columns. These trenches were oriented perpendicular to the direction of the applied load to minimize the effect of the excavation on the stiffness of the piers.

The east bent had less instrumentation than the west pier. Instruments were not placed at the base of the column, and an access trench was not excavated. Further, on this bent, only two pairs of instruments were placed at the top of each column, one measuring rotation over the first 2 inches, the other one measuring the next 24-inch segment.

To measure rotations of the crossbeams, instruments were placed on the underside and near the top of the crossbeams, close to the columns. On the west bent, researchers installed two pairs of instruments at each column, each measuring over a distance of 12 inches (Figure 3.10). On the east bent, one pair of instruments at each column measured displacements over a span of 24 inches.

The instruments on the columns and crossbeams were mounted on gimbal supports that were attached to $^3/_8$-in. diameter, all-thread rods epoxied into 6-inch deep holes. This set-up prevented relative rotations of the all-thread from damaging the LVDTs and potentiometers. The outermost 2 inches of the holes were drilled larger than the size of the rod to prevent the concrete cover spalling from affecting the measurements. To protect the instruments on the bents from dust, they were wrapped in plastic in a way that did not hinder motion of the instrument. The nominal

distance between each instrument and the column face was 4 inches; measured distances are listed in Table 3.2.

Footing Translation and Rotation

To measure the translational movement of the west footings, potentiometers were connected to the footing and to the end of a stiff cantilever. The other end of this cantilever was fixed by three pickets driven into soil approximately 8 feet from the edge of the footing. A dual axis clinometer with a resolution of 0.1 degrees was attached to the top of each footing to measure rotation. The clinometers were housed in a wooden box, and wrapped in a plastic bag, to protect them from falling debris and dust.

Corroborating Measurements

Additional instruments provided independent corroboration of the electronically acquired data.

To measure deformation of the deck, a $^1/_{16}$-inch steel wire was stretched between the ends of the bridge, and rulers were installed below the wire near the piers. By recording the movement of the wire relative to the rulers, the researchers independently measured deck deformation. Ruler readings were repeatable to within 0.01 inch when parallax was avoided. Dial gauge readings corroborated the electronic measurements of the weight movements in the instrument boxes. Dial gauges were read to the nearest 0.001 inch.

An electronic distance meter (EDM), precise to 0.01 feet, provided independent measurements of deck displacement. Reflectors were placed on the pier crossbeams, over the abutments, on the pier-displacement instrumentation poles and on the north bridge. The distance to each of these reflectors was measured several times during each loading cycle. The EDM's relatively crude precision limited the corroboration it provided for the initial cycles of displacement because the displacements were small.

Further documentation of the bridge's response was provided by photographs and by sketches of crack patterns. To permit reliable recording of crack locations, a 6-in. by 6-in. grid

Table 3.2. Distance from Column Face to Transducer

Instrument Location	Instrument Name	Distance From Top or Bottom of Col. [in.]	Distance From Face of Concr. [in.]
West Bent	WNCT 1n	2.75	4.13
North	WNCT 1s	2.78	3.97
Column	WNCT 2n	12.25	4.25
Top	WNCT 2s	12.13	4.47
	WNCT 3n	24.13	4.50
	WNCT 3s	24.38	4.75
West Bent	WSCT 1n	2.84	3.94
South	WSCT 1s	2.69	3.34
Colum	WSCT 2n	12.50	3.75
Top	WSCT 2s	12.63	3.31
	WSCT 3n	25.50	4.03
	WSCT 3s	24.25	3.28
East Bent	ENCT 1n	2.00	4.00
North	ENCT 1s	3.13	4.81
Column	ENCT 2n	25.00	4.28
Top	ENCT 2s	24.00	3.94
East Bent	ESCT 1n	1.94	4.41
South	ESCT 1s	1.72	4.41
Column	ESCT 2n	24.63	4.13
Top	ESCT 2s	24.25	4.28
West Bent	WNCB 1n	3.25	4.50
North	WNCB 1s	2.75	5.00
Column	WNCB 2n	24.50	5.38
Bottom	WNCB 2s	24.13	5.13
	WNCB 3n	48.00	5.75
	WNCB 3s	48.50	5.25
West Bent	WSCB 1n	2.63	4.06
South	WSCB 1s	2.09	3.91
Column	WSCB 2n	24.00	5.31
Bottom	WSCB 2s	23.88	4.63
	WSCB 3n	48.63	4.81
	WSCB 3s	48.38	4.34
West Bent	WNB 1t	N/A	3.75
Crossbeam	WNB 2t	N/A	3.88
North End	WNB 1b	N/A	3.75
	WNB 2b	N/A	4.25
West Bent	WSB 1t	N/A	3.94
Crossbeam	WSB 2t	N/A	4.00
South End	WSB 1b	N/A	3.88
	WSB 2b	N/A	3.75
East Bent	ENB 1t	N/A	5.00
Crossbeam	ENB 1b	N/A	4.38
	ESB 1t	N/A	4.50
	ESB 1b	N/A	4.28

was drawn at the top of each column; data sheets contained drawings of the columns with this grid. Other observations, including time and temperature, were recorded in detailed written and taped logs.

3.4 DATA ACQUISITION

The electronic instruments were connected to a data acquisition system located in a trailer near the bridge. The system included an IBM AT computer with a Metrabyte 12-bit data acquisition board (DAS-16F, analog/digital I/O expansion board) and four multiplexers (EXP-16A). The system was supported by LabTek Notebook software that produced datafiles compatible with spreadsheet programs.

The effect of temperature variations on the electric components was minimized by foregoing the use of signal amplifiers and filters, both of which can be sensitive to temperature. The instrumentation and cabling was shielded and grounded to minimize the disruptive effects of stray electrical fields. The data acquisition system occasionally caused severe problems; at times, readings from the system would become erratic. This behavior was carefully monitored, and the tests were interrupted when this erratic behavior was observed. After the tests had been completed, this problem was traced to faulty multiplexer microchips.

3.5 LOADING PROCEDURE

Before load was applied to the bridge, approximately 20 readings were taken from all the instruments. Inspection of these initial readings permitted the researchers to check the magnitude and stability of the initial voltages. At this time, all visible damage on the bridge was recorded.

The loading was increased in 16- to 21-kip increments. At each load increment, the rams were extended to a target pressure using two hydraulic pumps. The loads were selected so that the displacement of the bents would be approximately equal; therefore, pressures in each ram were not necessarily equal. Once the target pressure had been reached, all the channels were recorded by the data acquisition system. Pump pressure, air temperature, and time were also recorded.

At regular intervals, the structure was inspected thoroughly, crack patterns were sketched, observations were noted, and readings were taken from the dial gauges and deck rulers. This process was repeated until the maximum target displacement was reached. During unloading, fewer readings were taken than during loading. After unloading, the prestressing cables were loosened so that they would not carry load during the next half cycle.

CHAPTER 4

OBSERVED RESPONSE

This chapter describes the response of the bridge during Phase I (Tests P, I, II, EXC and ISO, Figure 1.2). After the data reduction procedures are summarized, the behavior of the bridge is documented in terms of response maxima, hysteretic response, and observed damage.

4.1 DATA REDUCTION

Calibration Factors

Before the tests, the hydraulic rams were calibrated to establish the conversion constant between pressure and applied force. This force was then adjusted to account for the inclination of the prestressing cables.

Calibration factors for all of the other instruments were measured in the laboratory before testing, corroborated in the field, and then checked again in the laboratory after testing. The laboratory and field calibration factors for the potentiometers and Temposonic transducers were nearly identical. Therefore, the calibration factors found in the laboratory before testing were used to convert voltage changes to displacements. In contrast, the laboratory and field calibration factors for the LVDTs differed significantly, so field calibration factors were used for these instruments. Table 3.1 lists the calibration factor for each instrument.

Data Purging

Seven of 458 measured points were eliminated from the database (Table 4.1) because they were inconsistent with adjacent points. The selection of points to be purged was facilitated by the fact that most of these readings differed by an order of magnitude from the measurements at adjacent points for all of the channels. The presence of seven erratic points was attributed to the transient instability of the multiplexers, discussed in Section 3.4.

In Phase I not all of the instruments recorded significant displacements. The 24 instruments located on the beams and at the bottoms of the columns measured movements that were less than 0.005 inch. The accuracy of such small measurements is questionable because

Table 4.1 Purged Data Points

Half Cycle	Data Point
IS2	19
IINI	36
ISON1	13
ISON1	14
ISON1	15
ISON1	22
ISON1	23

their magnitude is similar to that caused by environmental factors such as temperature. Furthermore, the voltage output for these instruments was often similar to the resolution of the analog-to-digital (A/D) converter. The four channels that monitored footing rotations also produced voltages near the resolution of the A/D converter.

Three other instruments were considered unreliable even though they measured more movement than 0.005 inch. Both instruments that measured footing translation were affected by falling rocks in most tests and, often, they were completely buried by soil that fell in the trenches. Also, the column instrument on the top of the north face of the southwest column (WSCT 1n) registered erratic voltages. The loose connection that was responsible for the erratic behavior was not repaired until the completion of Phase I.

Response histories for the remaining 29 channels are presented in Appendix A. The instrument that measured relative displacement between the west abutment and pedestal (WD/AT) produced erratic readings during Test ISO (Figure A.2).

Notation

Each half cycle was defined by the test name (P, I, II, EXC or ISO), the direction of applied load (S or N), and the number of times the bridge had been pulled in that direction during the test (1, 2 or 3). For example, "half-cycle IIS2" corresponded to the second pull to the south during Test II.

4.2 RESPONSE MAXIMA

The response histories presented in Appendix A are complete, but they are difficult to interpret because of the large number of data that must be assimilated. It is more convenient to characterize the response of the bridge in terms of response maxima.

For each half cycle, Figure 4.1 shows a plan view of the bridge and the deck displacements measured between the beginning of each half cycle and the time of maximum load. As shown in Figure 4.1, bent displacements were nearly equal, whereas abutment displacements often differed significantly. Typically, the east abutment (right-hand side of Figure 4.1) moved approximately twice as much as the west abutment, indicating that the bridge rotated in the counter-clockwise direction as the load increased. The measured motion of the abutments was corroborated by the two instruments that measured relative displacement between the abutment endwall and pedestal. These instruments consistently recorded relative displacements that were approximately 90 percent of the abutment displacement relative to the reference poles.

The longitudinal displacements shown in Figure 4.1 are more difficult to interpret. Longitudinal displacements included contributions from longitudinal translation, longitudinal expansion and contraction, rigid-body rotation, and bending of the deck. In addition, the longitudinal displacements included a component of transverse motion because the longitudinal instruments in the skewed bridge were not oriented perpendicular to the direction of transverse motion.

Interpretation of the displacements is easier if one describes deck motion in a coordinate system in which the various contributions to deck motion can be identified. Figure 4.2 shows such a system, in which the four transverse displacements (excluding the two channels that measured endwall/pedestal relative motion) were replaced with three coordinates. These coordinates were the following:

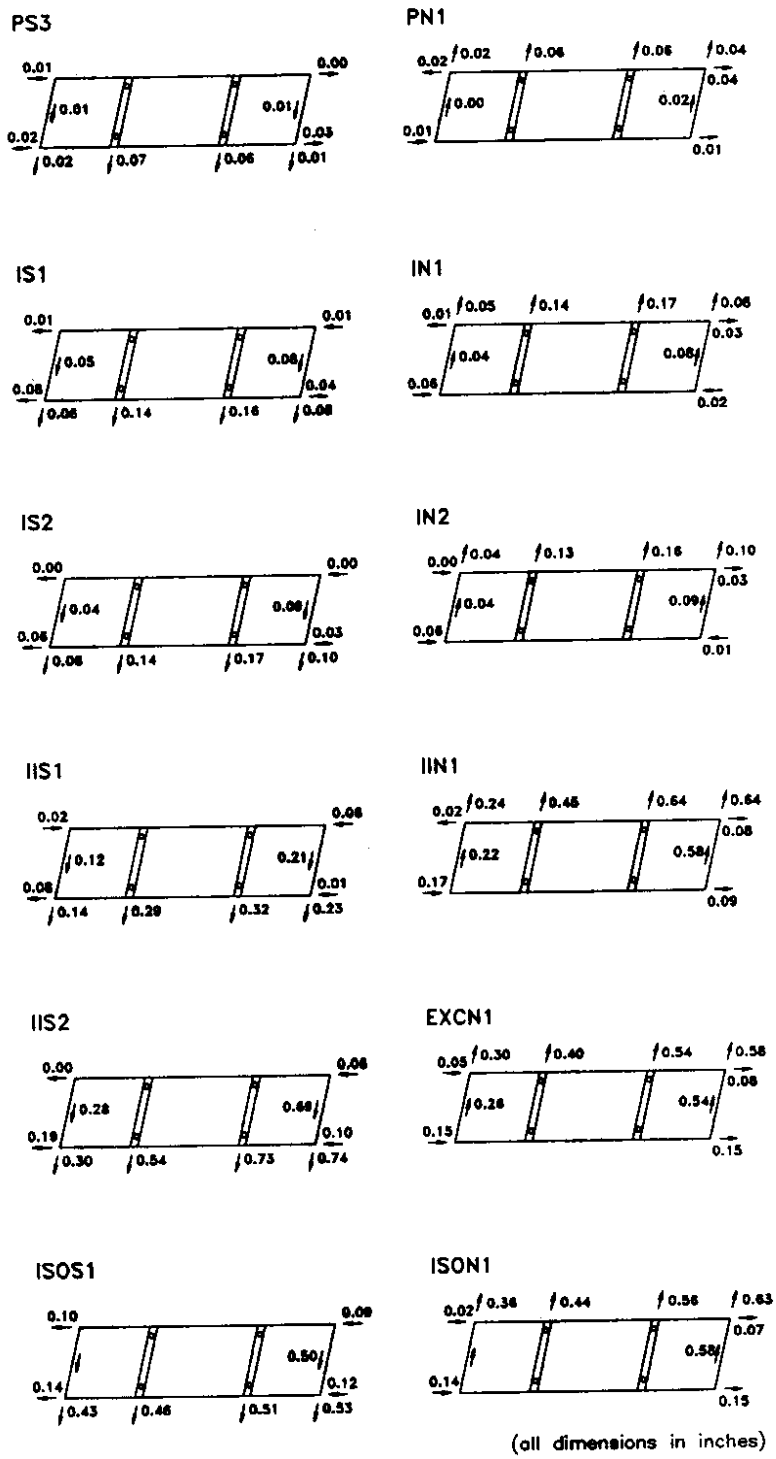

Figure 4.1. Measured Deck Displacements During Loading

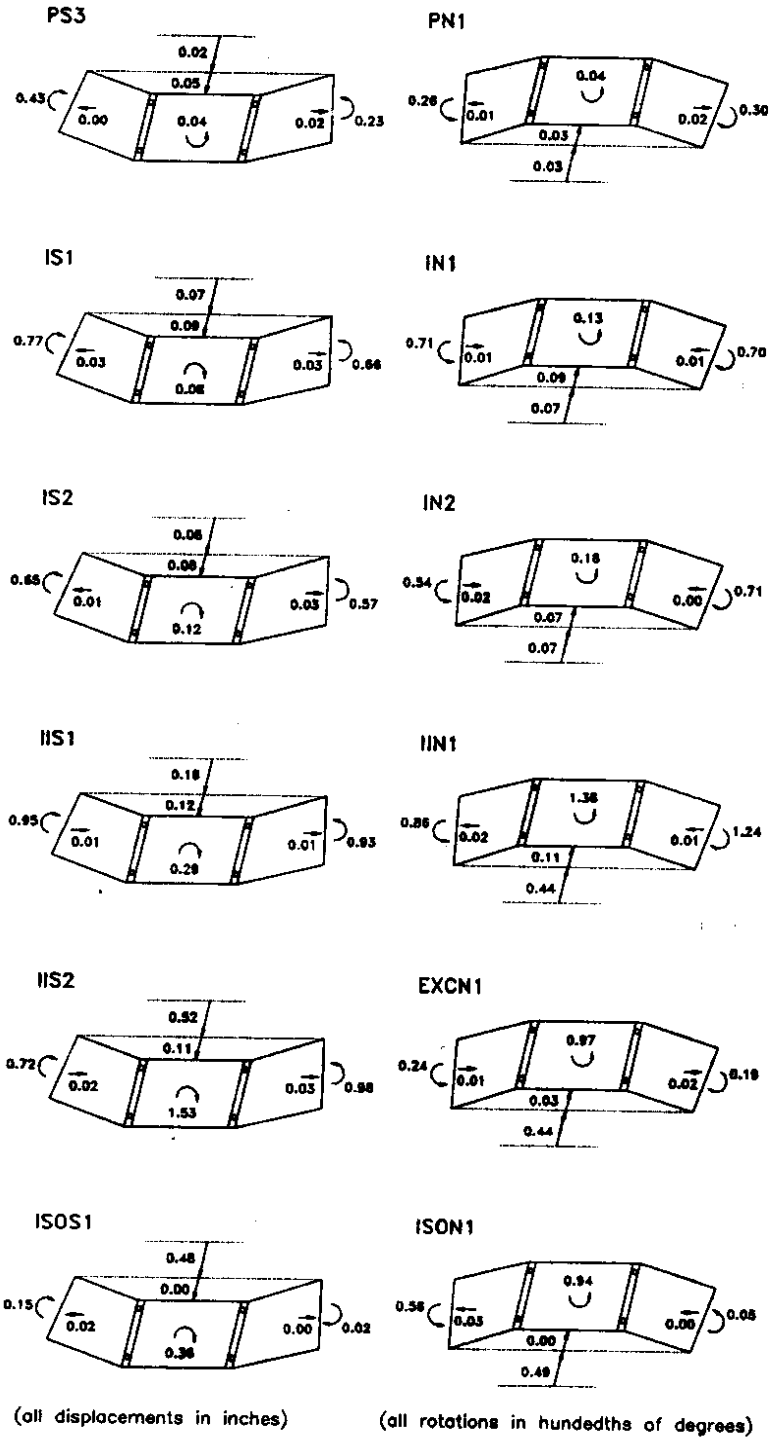

Figure 4.2. Derived Deck Displacements During Loading

- the average of the east and west abutment displacements,
- the rigid-body rotation of the bridge, calculated from the difference between the east and west abutment displacements (shown in Figure 4.2 in hundredths of degrees), and
- the deck deflection, in which the deck was considered to be a beam that spanned between abutments. Deck deflection was calculated as the difference between the average bent displacement and the average abutment displacement.

Little information was lost in the transformation from four to three transverse coordinates because the deck deflections at both bents were kept nearly equal throughout the tests.

Two sets of displacements and two sets of rotations were calculated from the longitudinal instrument records. First, the contribution of the transverse translation and rigid-body rotation was removed from the longitudinal records. Then, the four modified abutment displacements were replaced by two average translations and two rotations. The four additional coordinates were as follows:

- the end rotation of the east abutment (in hundredths of degrees),
- the end rotation of the west abutment (in hundredths of degrees),
- the longitudinal translation of the east abutment, and
- the longitudinal translation of the west abutment.

For loading of the bridge, these seven displacements are shown in Figure 4.2; for unloading, they are shown in Figure 4.3. Displacements are shown in inches.

Test P

During Test P, the loading apparatus and instrumentation were checked and modified. During half-cycle PS1, a 40-kip force was applied to the bridge, but no movement was measured and no damage was observed. In PS2, the applied load was doubled to 80 kips, and again, no movement was recorded and no damage was found. Because so little movement was recorded, the instrumentation was suspected of improper operation. Pulley friction was identified as causing significant precision reduction. To reduce the influence of friction, the pulleys were replaced with

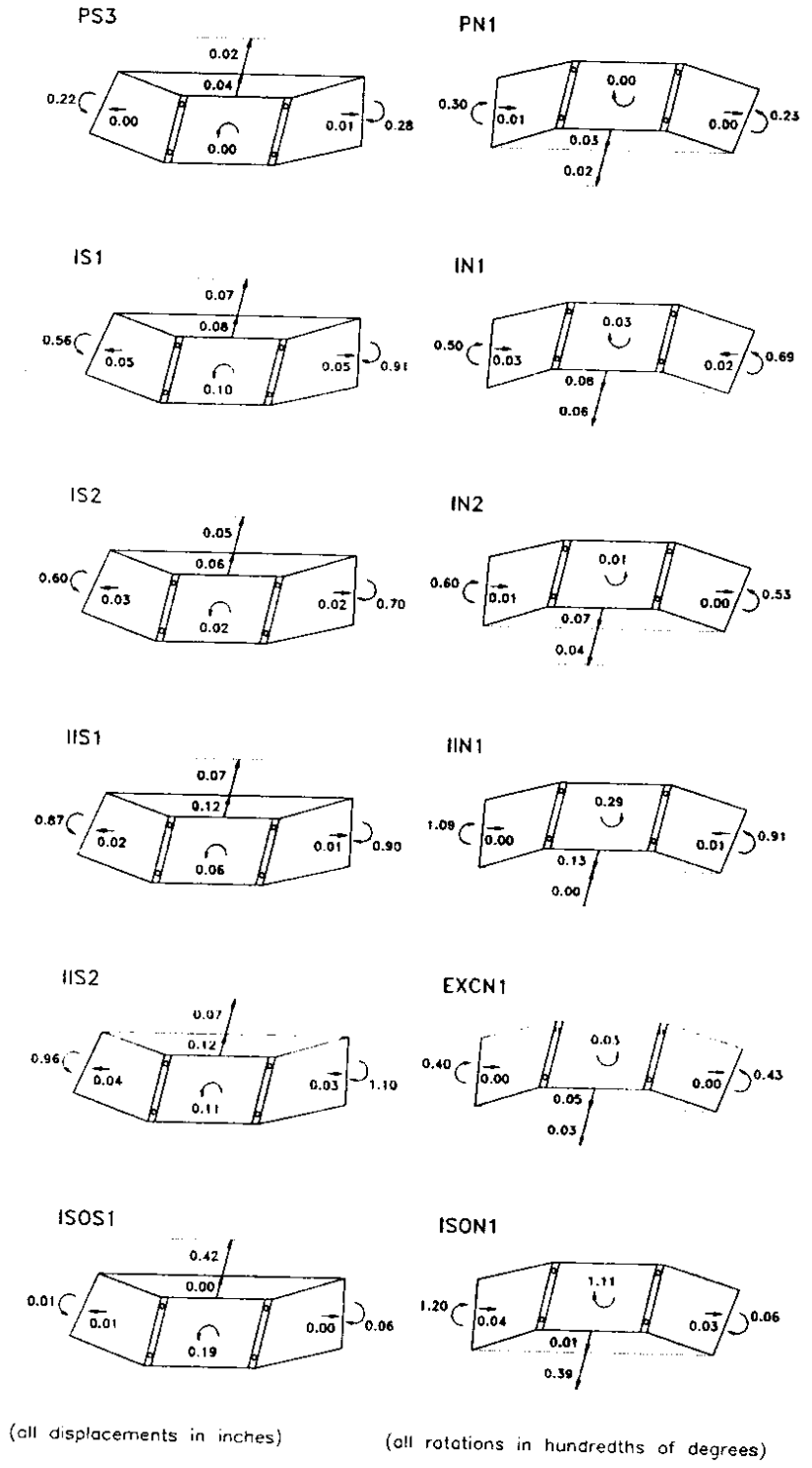

Figure 4.3. Derived Deck Displacements During Unloading

bearing-mounted pulleys, and the reference poles were stiffened. The accuracy of the modified instrument apparatus was established as approximately 0.001 inch.

Subsequently, the displacements measured during the last preliminary cycle (PS3 and PN1) were much more consistent than those that had been measured during PS1 and PS2. When subjected to an applied load of 300 kips, the bents displaced approximately 0.06 inch, corresponding to a drift ratio of 0.02 percent and a stiffness of 5,000 k/in. (Table 4.2). Approximately 30 to 50 percent of this displacement was attributable to abutment motion, and the remainder was attributable to deck deformation.

For loading (Figure 4.2) and unloading (Figure 4.3), rotations of the abutments were similar at the east and west ends of the bridge. Furthermore, these rotations were consistent with the direction of transverse displacement. The average rotation for loading and unloading of the east and west abutments was 0.0028 degrees. Longitudinal translation of the abutments was insignificant.

Test I

In Test I, the researchers imposed two full cycles of displacement to a drift ratio of 0.05 percent (0.15 inch). The average maximum applied load for the four cycles was equal to 550 kips. The corresponding stiffness of 3,700 k/in was approximately 75 percent of that measured during Test P. Approximately 45 percent of the bent displacement was attributable to motion of the abutments.

The east and west abutments rotated through nearly the same angle, averaging 0.0065 degrees for loading and unloading. The calculated longitudinal translations of the east and west abutments indicate that the bridge expanded during pulls to the south (i.e., IS1 and IS2) and contracted during pulls to the north (i.e., IN1 and IN2). This expansion and contraction occurred both during loading (Figure 4.2) and unloading (Figure 4.3).

Test II

During the three half cycles of Test II (IIS1, IIN1 and IIS2) the bridge was subjected to the maximum load, 770 kips, that could be applied safely by the load train. Half cycle IIS1 was the

Table 4.2. Phase I Response Maxima

Test Cycle	Data Point	Horizontal Force (kips)	Abutments		Bents			Deck		Abutment Disp. / Bent Disp. (%)
			Average Displacement (in.)	Recovered Displacement (%)	Average Displacement (in.)	Recovered Displacement (%)	Secant Stiffness (k/in.)	Deflection (in.)	Recovered Displacement (%)	
PS3	0	0								
	25	304	0.018		0.064		4720	0.047		28
	31	0	-0.016	88	-0.059	91	5191	-0.043	92	27
PN1	0	0								
	15	-302	-0.031		-0.060		5027	-0.029		52
	23	0	0.016	52	0.047	78	6442	0.031	106	34
IS1	0	0								
	29	618	0.069		0.154		4019	0.085		45
	45	0	-0.071	103	-0.152	99	4058	-0.082	96	46
IN1	0	0								
	30	-607	-0.066		-0.155		3912	-0.089		42
	36	0	0.062	95	0.144	92	4231	0.081	91	44
IS2	0	0								
	23	495	0.079		0.154		3221	0.075		51
	28	0	-0.053	67	-0.117	76	4227	-0.064	86	45
IN2	0	0								
	25	-534	-0.071		-0.145		3683	-0.074		49
	36	0	0.039	55	0.113	78	4736	0.074	99	35
IIS1	0	0								
	35	766	0.187		0.303		2528	0.116		62
	53	0	-0.070	37	-0.186	61	4120	-0.117	100	37
IIN1	0	0								
	34	-766	-0.437		-0.545		1406	-0.107		80
	48	0	-0.002	-0	0.132	24	5812	0.133	124	-1
IIS2	0	0								
	35	766	0.521		0.636		1205	0.114		82
	58	0	-0.072	14	-0.192	30	3993	-0.120	105	38
EXCN1	0	0								
	20	-348	-0.444		-0.469		743	-0.025		95
	34	0	0.032	7	0.079	17	4404	0.047	189	40
ISOS1	0	0								
	17	217	0.480		0.482		450	0.002		100
	26	0	-0.424	88	-0.426	88	508	-0.002	86	100
ISON1	0	0								
	17	-201	-0.493		-0.497		405	-0.003		99
	31	0	0.394	80	0.404	81	497	0.010	306	97

first cycle in which the bridge did not return to its initial position upon unloading (Figure 4.2 and 4.3). During this half cycle, the maximum measured bent displacement was 0.30 inch (0.10 percent drift ratio), of which 62 percent was attributable to abutment displacement (Table 4.2). Upon unloading, the deck deflection (0.12 inch) was fully recovered, but only 35 percent (0.07 out of 0.19 inch) of the abutment displacement was recovered.

The transverse bent displacements increased to 0.45 inch in half cycle IIN1; this represents a 50 percent increase over IIS1. As in IIS1, the transverse displacement was characterized by deck deformation, superimposed on abutment translation, and counter-clockwise, rigid-body rotation. The calculated rigid-body rotation for Cycle IIN1 differed greatly from that of previous cycles. As shown in Figure 4.2, the rotation (0.0136 degrees) was four and a half times that measured in the previous half cycle. As before, the deck deformation was recovered fully after the load had been removed, but the abutments did not return to their initial position. Cycle IIS2 was similar to IIN1.

The secant stiffnesses for Test II were smaller than those measured in previous tests. During half cycles IIS1, IIN1, IIS2, the loading secant stiffness was 2,500, 1,400 and 1,200 k/in., respectively, corresponding to 50, 28 and 24 percent of the initial stiffness. The unloading secant stiffnesses were larger than the loading stiffnesses, as would be expected for inelastic response.

During all three half cycles, maximum rotations were approximately 0.01 degrees for loading and unloading. The relationship between the direction of the applied load and the measured longitudinal abutment motion was no longer systematic, as it had been in Test I.

Test EXC

After removing the soil behind the wingwalls and along the endwall, the researchers subjected the bridge to one half cycle of displacement. A horizontal load of 350 kips produced abutment displacements that were similar to those of Test II. The deck deformation was reduced to 25 percent of that measured in Test II; this reduction is consistent with the reduced abutment stiffness. As in Test II, the deck deformation was fully recovered upon unloading (Table 4.2).

The secant stiffness for loading was 750 k/in., corresponding to 15 percent of the initial stiffness of 5,000 k/in. Abutment rotations were only one quarter of those measured in Test II.

Test ISO

After the bearing pads and polystyrene had been replaced with the isolation system (5), the deck moved essentially as a rigid body (Figure 4.2). As expected, deck deformation was negligible, as were most of the abutment rotations. The east abutment rotation of 0.0056 degrees recorded for ISON1 has not been explained. The secant stiffness for loading, 425 k/in., represented only 8.5 percent of the initial stiffness. Most of the bent and abutment displacements were recovered after the load had been removed from the bridge.

4.3 HYSTERETIC RESPONSE

Hysteresis curves were constructed by combining the force-displacement data measured during each half cycle. For most cycles it is reasonable to assume that the bridge did not move between tests. Therefore, the displacements measured during each half-cycle were added to those measured in previous cycles to yield the absolute position of each instrument.

The assumption that the bridge remained stationary between tests was violated twice, when the soil surrounding the abutments was excavated and when bridge was isolated from the abutments. The researchers observed movement, but unfortunately, they did not record the magnitude of this movement during these operations because the deck instrumentation had been removed to protect it from damage. Given that the absolute position of the bridge could not be determined with confidence, the initial displacements for cycles EXCN1 and ISOS1 were set to zero.

Figure 4.4 shows hysteresis curves for the horizontal component of applied force plotted against average bent displacement. The displacements that occurred during maximum load can be calculated by combining the loading and unloading displacements listed in Table 4.2. Similar hysteresis curves for average abutment displacement are displayed in Figure 4.5.

The hysteresis curves for average bent and abutment displacement are similar for all of the tests. During Tests P and I, energy dissipation was minimal, as reflected by the small area within

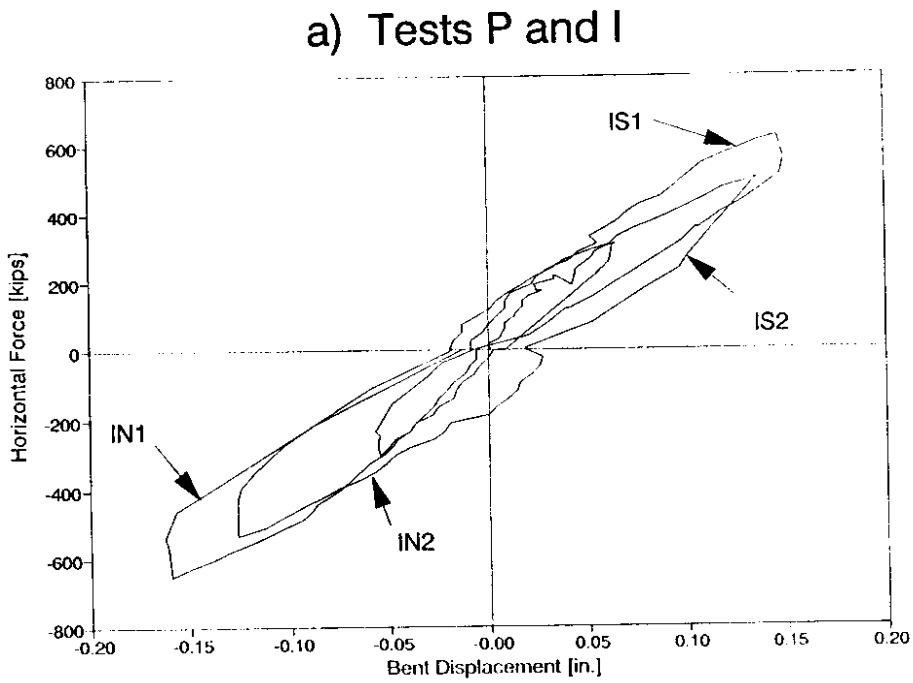

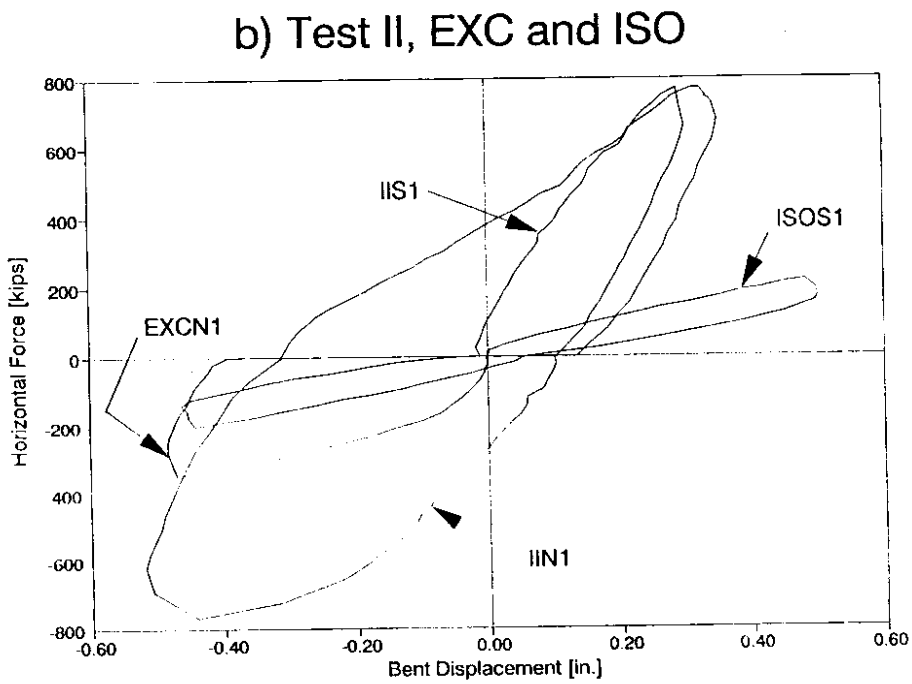

Figure 4.4. Hysteretic Response of Piers (Bents)

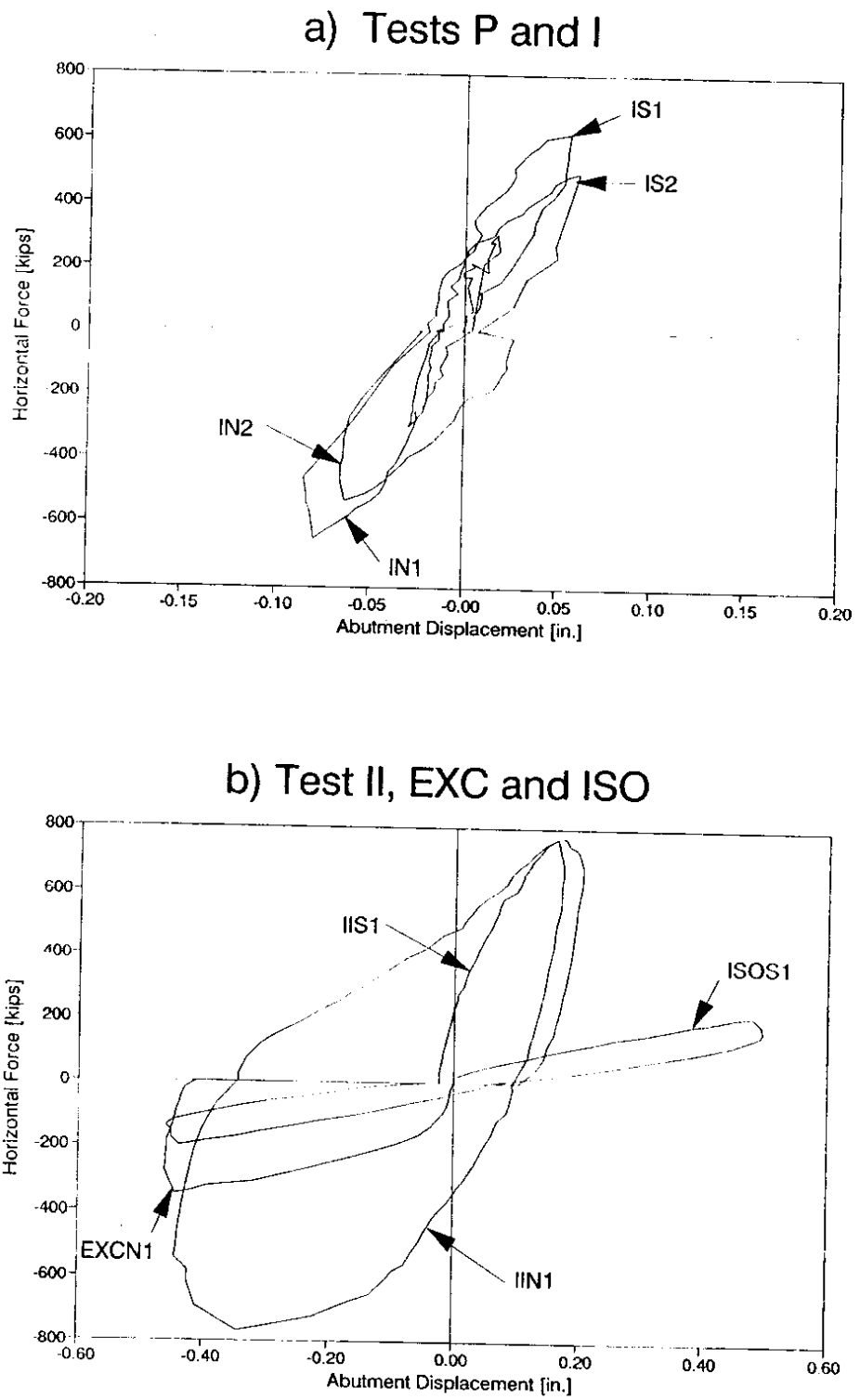

Figure 4.5. Hysteretic Response of Abutments

the hysteretic loops. The abutment curves were steeper than the bent curves; this was expected because bent displacement included both abutment displacement and deck deformation.

Energy dissipation was much greater in Test II and EXC than in previous tests. As noted in Section 4.2, deck deformation was fully recovered in all of the tests, whereas abutment displacement was not recovered fully. As a result, the abutment hysteresis loops in Tests II and EXC (Figure 4.5b) show less displacement recovery upon unloading than the hysteresis loops for bent displacement (Figure 4.4b). Energy dissipation in Test ISO was minimal.

4.4 OBSERVED DAMAGE

Condition of Bridge Before the Test

An inspection of the bridge verified that it had been built largely in accordance with the plans and that the bridge had deteriorated little during 30 years of service. The researchers found only minor cracks and occasional honeycombing.

All the columns had hairline cracks parallel to and directly over the longitudinal reinforcement. In addition, on the east bent, and in particular, on the southeast column, minor cracks were visible along the hoops. No cracks were observed at the bottom of the columns or on the footings.

The researchers found two types of cracks that might be attributable to applied loads. A small diagonal crack was found in the cantilever extension of the crossbeam that extended past the southwest column. This crack began directly below the exterior girder and extended towards the column at an angle of about 45 degrees with respect to the longitudinal axis of the crossbeam. Also, at the abutments, vertical cracks were found in the diaphragm under some of the girders. These cracks were consistent with tension resulting from the transfer of the girder shear into the diaphragm.

Minor honeycombing was found in one location in the diaphragm over the east bent, and at the bottom of the diaphragm on the east abutment. Patching was evident in many locations.

Test P

The researchers did not observe damage to the bents during this test, but they found small cracks in the wingwalls. During PS3, a hairline crack was found on the outside face of the southwest wingwall. During PN1, a hairline crack was found on the outside faces of both the northeast and northwest wingwalls. In all these cases, the cracks were so small that the researchers could not determine whether the cracks had existed before the tests, nor whether the cracks had grown during testing.

Test I

The first flexural crack in a column was found when researchers inspected the bridge shortly after they had applied the maximum load for cycle IS1. The 0.01-in. wide crack was located at the top of the south face of the southeast column. During the same inspection, researchers observed a small separation between the northwest wingwall and the surrounding soil.

After reversing the direction of applied load (IN1), the researchers found two flexural cracks on the north face of the southeast column. The smaller of the two cracks was located at the top of the column; the larger (approximately 0.01 in. wide) was located 12 inches below the crossbeam. A small flexural crack was also found at the top of the northeast column. Some extension of cracking was found on the northwest wingwall.

During the second cycle of Test I (IS2, IN2), no new cracks were found. Existing cracks opened on the column faces that were subjected to tension; these cracks then closed completely when the faces were in compression. A small gap was observed between the southeast wingwall and the soil.

Test II

During this test, the researchers subjected the bridge to the largest load that could be safely applied by the loading apparatus, 770 kips. During the first half cycle, IIS1, flexural cracks formed in the maximum moment regions on all of the columns. The largest crack, measuring 0.01 inch wide, was found on the south face of the southeast column. Cracks on the northeast and southeast

wingwalls opened up slightly more than in previous cycles. Gaps between the north sides of the wingwalls and the soil increased, some of which were as large as one eighth of an inch.

The amount of cracking and soil disturbance increased much more in cycle IIN1 than in previous cycles. Flexural cracks were observed at the tops of all the columns. These cracks, spaced approximately every 12 inches, were visible in the top 36 inches of the columns of the east bent. On the west bent columns, cracking was visible for the top 12 inches only. All but one of the column cracks were less than or equal to 0.01 inch in width. The exception was a 0.02-inch wide crack on the southeast column, located 12 inches below the crossbeam.

No cracks were visible at the bottom of any of the columns. The only manifestation of movement of the lower portion of the columns were small separations between the columns and the surrounding soil. On the southwest column, the separation was 0.10 inch at a height of 10 feet above the footing. This separation tapered to zero at a height of 4 feet above the footing.

The largest crack, measuring 0.10 inch, formed on the north face of the southeast wingwall (Figures 2.2 and 4.6). This crack formed abruptly during cycle IIN1 at the time of maximum load. A smaller, 0.02-inch crack was found on the north face of the northeast wingwall. Both of these wingwalls separated approximately half an inch from the surrounding soil. Less damage was apparent on the west abutment, though some soil separation was observed.

During the final cycle of Test II (IIS2), no new cracks were reported in the columns, but new cracks formed in the abutment wingwalls. At the east abutment, cracks formed on the south face of the wingwalls. The soil gap behind the wingwalls closed on the north faces and opened on the south faces to approximately 0.5 inch. At the west abutment, only minor cracking was observed, and the soil gaps were smaller than at the east abutment. This difference in gap size was consistent with the difference in abutment displacement (Section 4.2).

Figure 4.6. Crack in Southeast Wingwall After Half-Cycle IIN2.

Tests EXC and ISO

No further damage was observed during these tests. However, the east abutment endwall slipped approximately 0.4 inch with respect to the pedestal. The same cracks that had formed in previous tests opened in the columns to approximately the same widths as in cycle IIN1.

CHAPTER 5
DISCUSSION OF MEASURED RESPONSE

5.1 RELIABILITY OF MEASUREMENTS

Ideally, experimental results can be confirmed by repeating tests. Because such repetition was impossible in this study, the researchers investigated the reliability of the measurements by checking for consistency among the observations and by investigating the effects of temperature changes.

Consistency of Transverse Displacements

Differences between the east and west pier (bent) displacements were compared with differences between the east and west abutment displacements. Despite the researchers' efforts to impose equal displacements at the two bents, the east bent displaced slightly more than the west bent (Figure 4.1). This small difference was consistent with the observation that the east abutment moved more than the west abutment.

The deck deflection, calculated as the average pier displacement minus the average abutment displacement, varied linearly with the applied load (Figure 5.1). This linear relationship was consistent with a beam model of the bridge, in which loads are applied at two locations. The effect of nonlinearity in the pier resistance was small because the piers were undamaged and relatively flexible. Therefore, the transverse deck shear was approximately proportional to the applied load. In addition, the force-deflection relationship for the uncracked deck is likely to have remained linear.

As would be expected for an elastic component, residual deck deflections at the end of each test were insignificant. A nondimensional measure of residual displacement is the percentage of deck deflection that was recovered after the bridge had been unloaded. For the tests that preceded excavation, this recovery was on average 99.9 percent of the imposed deformation (Figure 5.1a, Table 4.2). The standard deviation for this ratio was 11 percent.

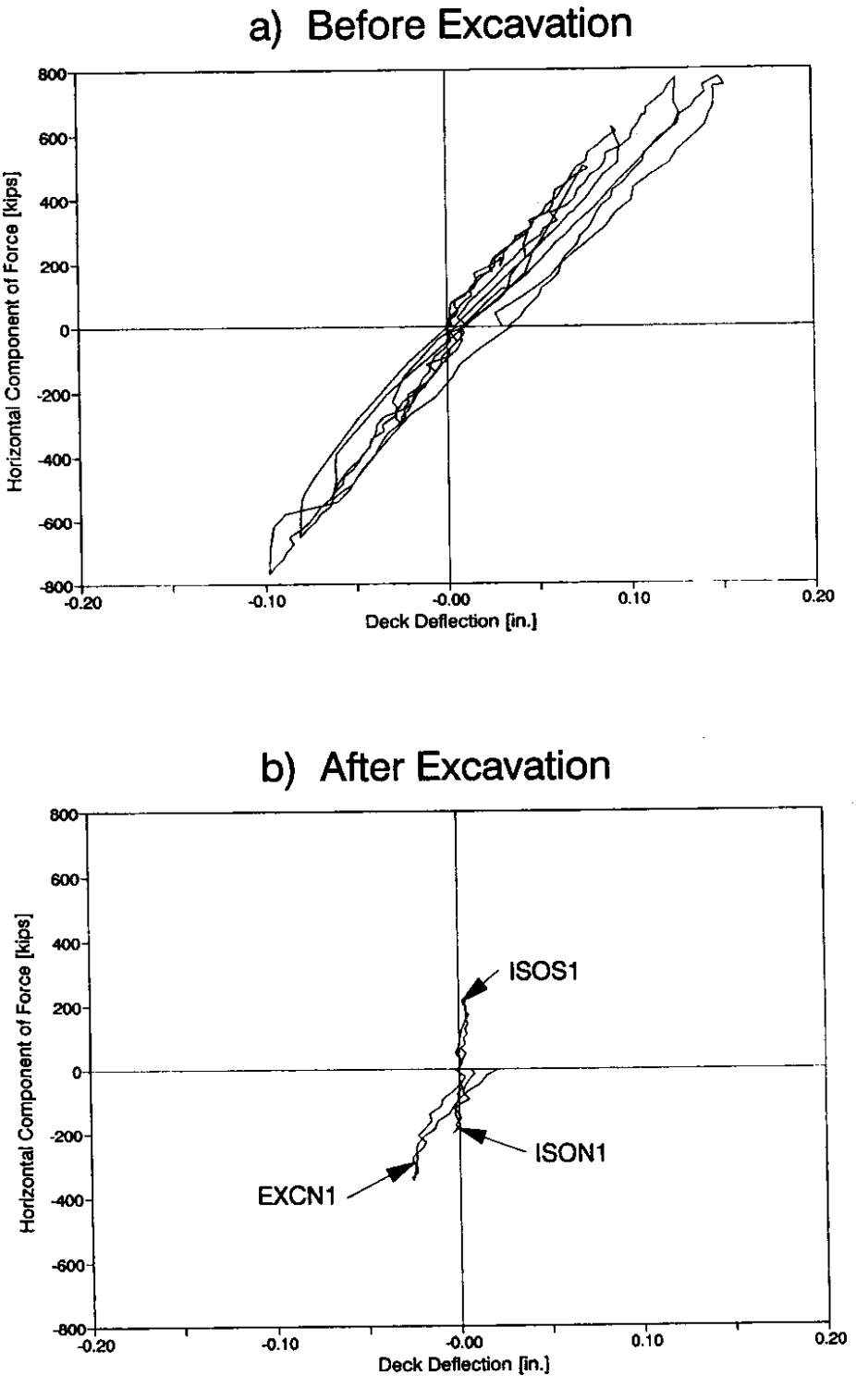

Figure 5.1. Deck Deflection

The relationship between the applied load and the deck deflection became steeper after excavation and isolation (Figure 5.1b). As expected, the deck deflection after excavation (Test EXC) was smaller than in previous tests because the excavation had reduced the abutment resistance. The deck deflection was negligible after isolation (Test ISO) because the abutment resistance was negligible.

The abutment displacements measured relative to the reference poles were consistent with those measured relative to the abutment pedestal (Figure 4.1). In Figure 5.2a, the two displacements are plotted for Tests P and I. The limited counter-clockwise hysteresis shown in the figure was consistent with small pedestal displacements in the direction of the applied load. For large displacements (Test II) and for the excavated and isolated bridges (Tests EXC and ISO), the relative displacements varied linearly with the absolute displacements (Figure 5.2b).

Consistency of Longitudinal Displacements

The longitudinal displacement records were manipulated more than the transverse displacement records. To compute the end-rotations and longitudinal translations shown in Figures 4.2 and 4.3, the researchers removed components of transverse translation and bridge rigid-body rotation. Therefore, the reliability of any one calculated end rotation or longitudinal translation was influenced by the errors in two measurements of abutment transverse motion and two measurements of longitudinal motion.

The east and west abutment rotations from Figures 4.2 and 4.3 are plotted in Figure 5.3. With the exception of Test ISO, the end rotations of the east and west abutments were nearly identical. The agreement between these two rotations suggests that the longitudinal instruments were reliable because the ordinates of Figure 5.3 were a linear combination of six displacement records. The discrepancy between the east and west ISO rotations remains unexplained.

Whereas longitudinal translation of the bridge was minimal, the longitudinal instruments repeatedly measured expansion and contraction of the bridge (Figure 4.2 and 4.3). The changes in length did not correlate well to the direction of transverse displacement. For example, the

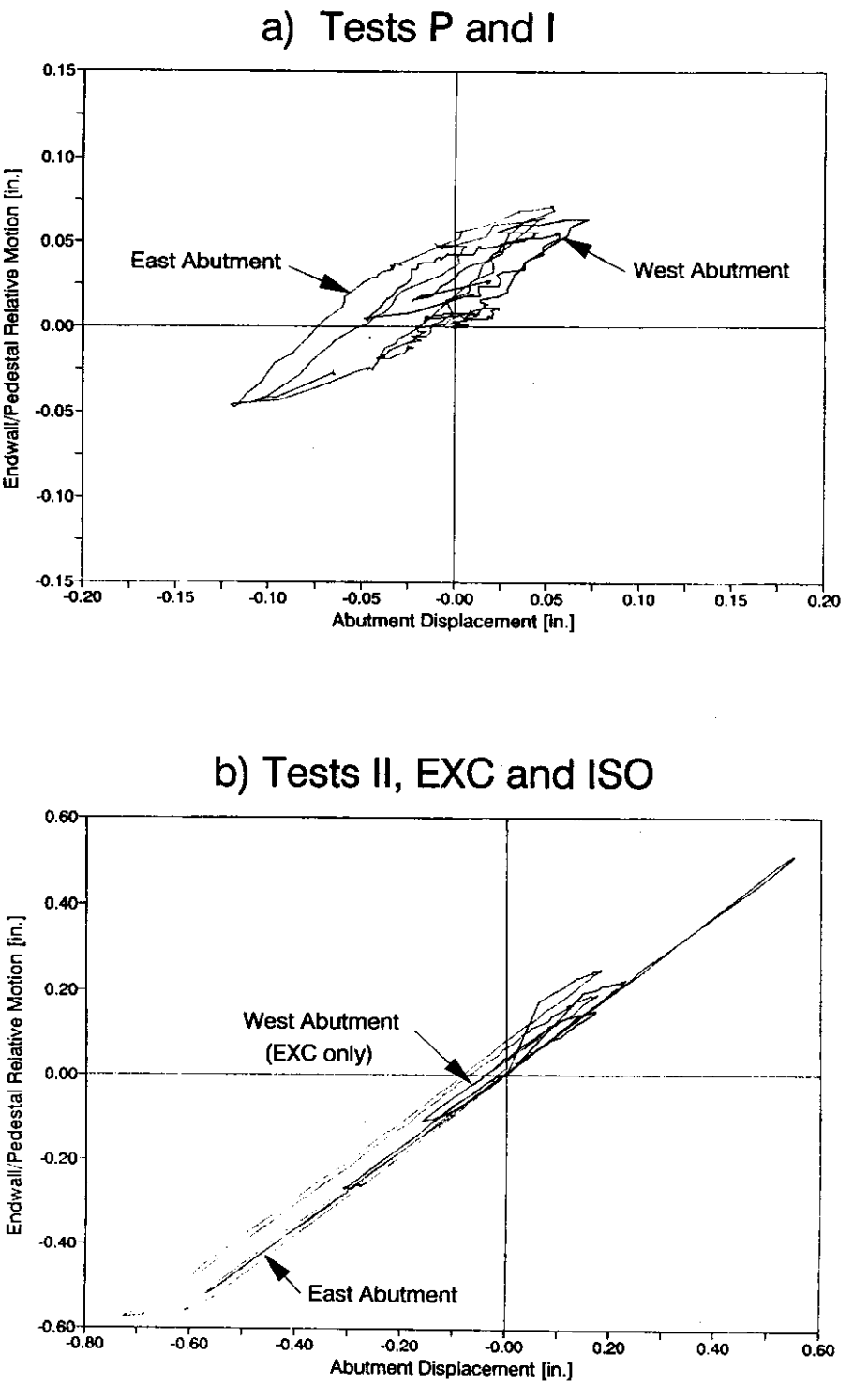

Figure 5.2. Absolute and Relative Displacement of Abutment Endwall

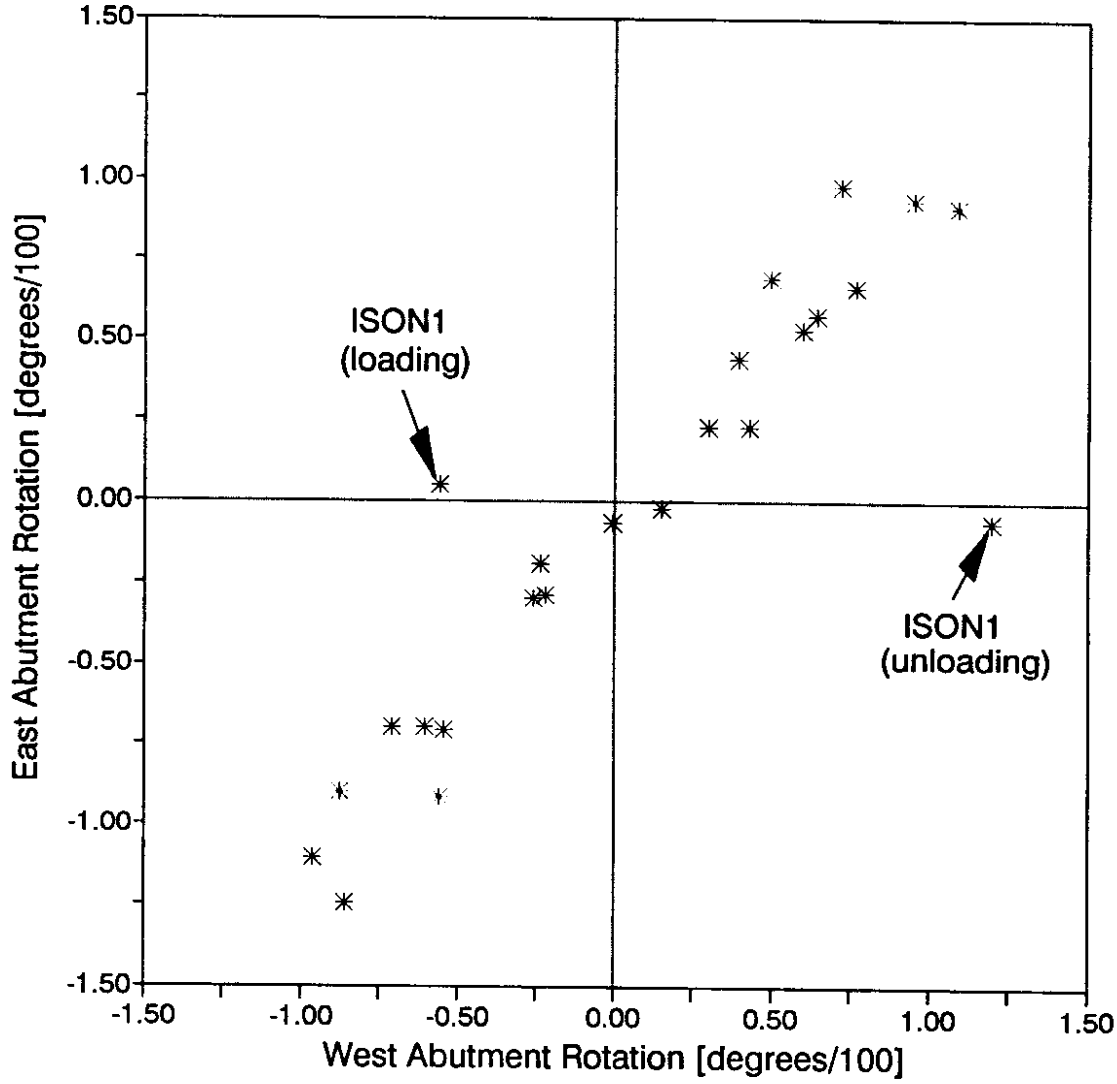

Figure 5.3. East and West Abutment Rotations

longitudinal instruments indicated that the bridge expanded by 0.06 inch during IS1 loading (Figure 4.2); during unloading, the bridge continued to expand (Figure 4.3).

It is likely that temperature effects dominated the longitudinal measurements. These effects would be expected to be greater in the longitudinal direction than the transverse direction because the bridge was 142 feet long, but only 40 feet wide. In addition, the endwall and pier diaphragms, which were sheltered from the direct sunlight, restrained transverse deck expansion. Because the researchers did not measure the deck temperature, they could not correlate it with the measured longitudinal expansion and contraction. Instead, the researchers correlated the expansion with the time of day, which is indirectly correlated to deck temperature. Favre (14) considered the temperature variation of a typical reinforced concrete deck during the summer. At a latitude similar to that of the test bridge, the deck temperature increases before 3 p.m. and decreases after 4 p.m. In Figure 5.4, changes in measured length (Figure 4.2 and 4.3) are plotted versus the number of test hours before 3 p.m. minus the number of hours after 4 p.m.

As shown in Figure 5.4, changes in deck length were roughly consistent with the length of time taken to perform the tests and the time of day. The correlation was not expected to be perfect because (1) calculated length changes included the errors of four independent instruments, (2) weather conditions varied, and (3) the effect of temperature on the stainless-steel wires and the instruments was different than the effect of temperature on the deck because these components have varying thermal properties. The influence of temperature is discussed further in the following subsection.

Temperature

Though no correction was made for the effects of temperature, the influence of temperature was investigated. The effect of temperature on the instruments is likely to have been small because, with the exception of cycle IN1, the air temperature measured at the data acquisition trailer did not vary more than 3° C during a half-cycle. It is unlikely that the temperature variation of the instruments significantly exceeded 3° C because the bent and abutment displacement instruments

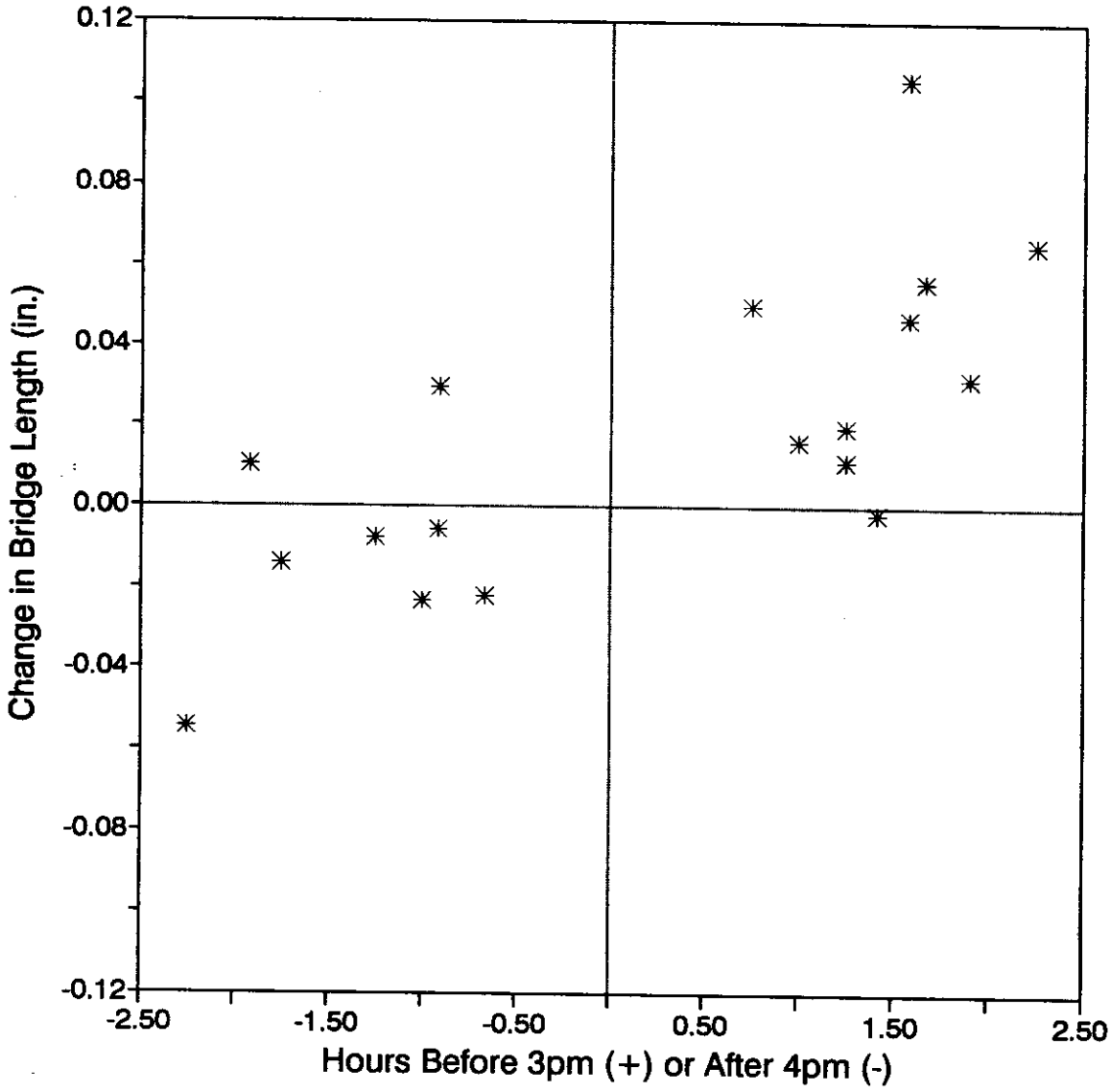

Figure 5.4. Longitudinal Expansion and Contraction

were enclosed in wooden shelters; the instrumentation on the bents was sheltered from direct sunlight by the bridge deck.

Temperature may have affected the stainless-steel cables that coupled the displacement instruments to the bridge (Figure 3.11). The coefficient of thermal expansion for stainless steel is approximately 16×10^{-6} per degree Celsius. (15) For the measured temperature variation of 3° C, the elongation of a 27-foot cable is 0.015 inch. Unfortunately, temperature changes in the stainless steel wires were not measured. They are likely to have differed from the changes in air temperature because they were exposed to wind and direct sunlight.

5.2 TORSIONAL RESPONSE

In every half cycle of Tests I, II and EXC, the east abutment displaced more than the west abutment. This difference caused the bridge to rotate in the clockwise direction when the bridge was pulled to the south (Figure 4.2). The bridge rotated in the counter-clockwise direction when the bridge was pulled to the north. Upon unloading, only a small fraction of the rotation was recovered (Figure 4.3).

Differences between the east and west bent stiffnesses were unlikely to cause significant torsional response. The concrete strength, concrete elastic modulus, and soil were similar for the two bents. The only obvious difference between the bents was that the researchers excavated trenches to place instrumentation at the base of the west-pier columns. If this excavation greatly reduced the stiffness of the west pier, the torsional response would have been in the opposite direction to that observed during the tests.

Even if there were a large difference in the pier stiffnesses, this difference would not lead to significant torsional response. The bents were relatively flexible and were located approximately 30 feet from the center of the bridge. Therefore, the torsional moment arising from differences in pier stiffnesses was small.

It is likely that differences in abutment resistance caused the torsional response. The abutments were much stiffer than the piers, and they were located 71 feet from the center of the

bridge. The abutment resistance was attributable to the resistance of bearing pads, polystyrene and soil.

It is unlikely that the soil at the east abutment was significantly more flexible than that at the west abutment. Such a difference in soil stiffness would be inconsistent with the observation that the east abutment wingwalls yielded before their counterparts at the west abutment. The hypothesis that differences in bearing pad and polystyrene resistance caused the observed torsion is supported by the behavior during unloading. Upon unloading, only a small fraction of the rotation was recovered. This suggests that the differences between the east and west abutment resistances were caused by a highly inelastic phenomenon. Slip of the abutment endwall with respect to the polystyrene is an example of such a phenomenon.

5.3 COLUMN CURVATURES

Relative rotations of adjacent beam and column cross-sections were measured at the base of both columns of the west pier, at the tops of all four columns, and for the beams (Figure 3.10). As discussed in Section 4.1, the instruments at the base of the columns and on the beams did not measure significant displacements. The response histories for the 19 instruments (instrument WSCT 1n malfunctioned) at the tops of the columns are presented in Figures A.17 to A.35. As shown in these figures, the measured displacements were small. Though most of the displacements were less than 0.01 inch, and therefore, of similar magnitude as the instrument resolution, the measurements varied consistently with the direction of applied load.

The response histories presented in Figures A.17 to A.35 are difficult to interpret. It is more convenient to present the data in terms of the average column curvature. The average column curvature, ϕ, was calculated as follows:

$$\phi = \frac{m_2 - m_1}{(D + d_1 + d_2)\, L} \qquad (5.1)$$

where m_1, m_2 = readings from instruments on each side of the column,
D = the diameter of the column (36 inches),
d_1, d_2 = distance of instruments from the columns (Table 3.2), and
L = the span of the instrument (Figure 3.10).

The average column curvature was calculated for three intervals on the northwest column but only for two locations on the other three columns.

Figure 5.5 shows the average curvature at the top of the columns for each half cycle at the time of maximum applied load. As expected, the curvature decreased rapidly as distance increased from the top of the columns. The measured curvature was largest on the southeast column. This measurement was consistent with the observation that the southeast column had the most cracks before the tests (Sec. 4.4).

The theoretical cracking moment and gross-section moment of inertia were calculated to be 5,700 in.-kips and 90,000 in^4, respectively (Sec. 6.1). Therefore, for an elastic modulus equal to 4.7×10^3 ksi (Sec. 2.2), the corresponding curvature is 1.3×10^{-5} rad/in. The curvature for the southeast column exceeded the theoretical cracking curvature in almost all of the cycles. The other three columns exceeded the cracking curvature during Test I. These measurements were consistent with the field observations.

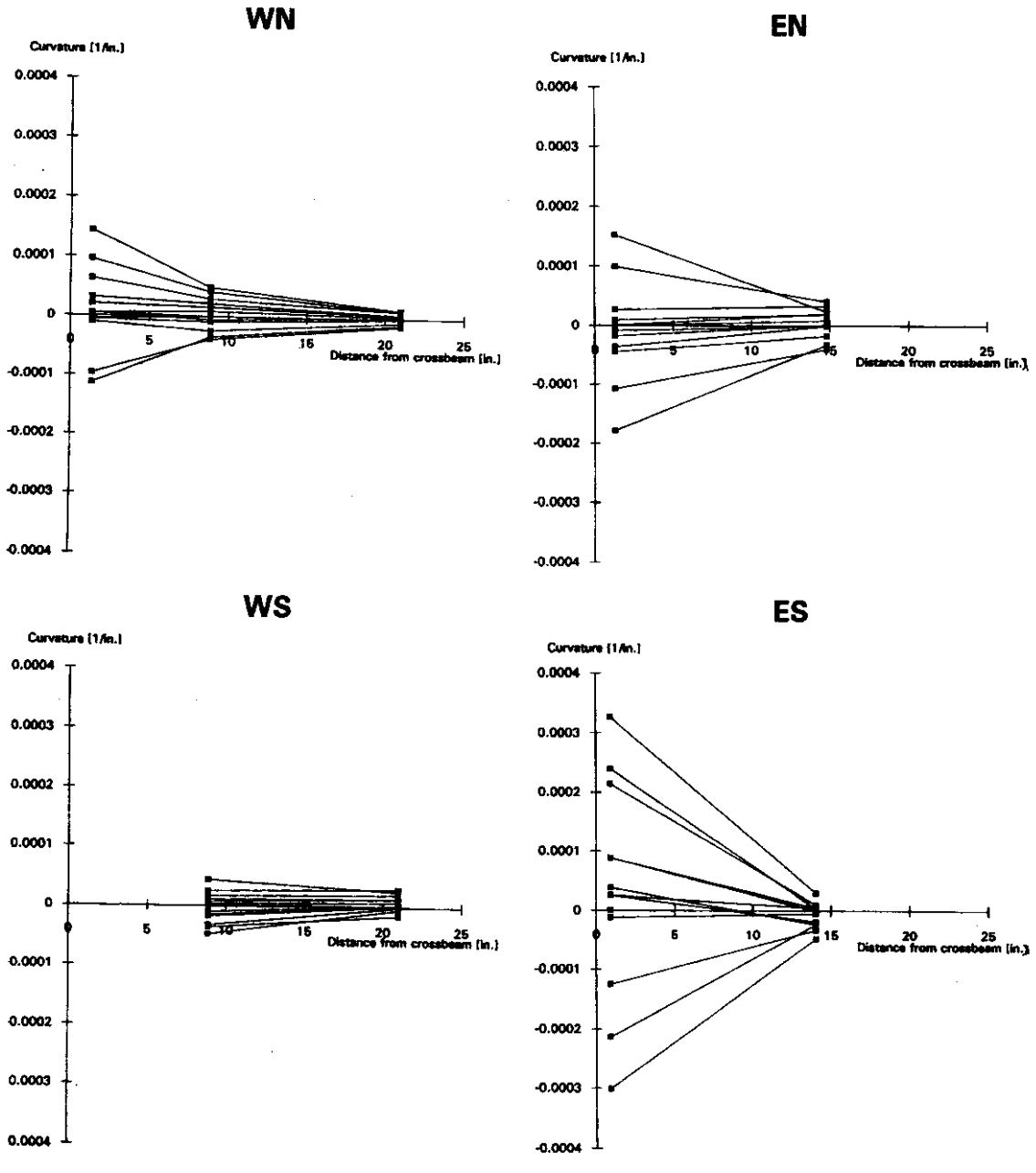

Figure 5.5. Column Curvatures

CHAPTER 6
ANALYSIS

An overview of the Phase I analyses was given in Figure 1.3. To better understand the lateral-load response of the bridge, the researchers created a series of nonlinear models for the initial, excavated, and isolated conditions. These models were compared with the observed response and with finite-element models developed by the California Department of Transportation (CALTRANS) and the Washington State Department of Transportation (WSDOT). These comparisons form the basis of the modeling recommendations proposed in Chapter 7.

Section 6.1 describes models that the researchers developed on the basis of the bridge plans and measured material properties ("UW models"). In developing the UW models, the researchers did not modify the material properties to fit the measured response. However, the objectivity of the analyses is questionable because the researchers who performed the analyses were aware of the measured response of the bridge.

CALTRANS (Section 6.2) and WSDOT (Section 6.3) calculated the load-displacement response of the test bridge under both the initial and isolated conditions. Their analyses were more objective and representative of standard practice than the UW analyses because the engineers from these agencies were not aware of the measured response. Further, to be consistent with standard practice, the engineers received only the information that would be commonly available to them, the structural plans.

The calculated pier and abutment displacements for half-cycles ISO, EXC and IS1 are compared with the measured response in Section 6.4. On the basis of these comparisons, the UW models for the excavated and initial conditions were calibrated to better reproduce measured response. The resulting calibrated models will be referred to as the "UW modified" models (Section 6.5).

To quantify the resistance that the piers and abutments provided, researchers derived secant stiffnesses for each structural component from the measured force-displacement response

(Section 6.6). These derived stiffnesses were obtained by calibrating a simple eight-degree-of-freedom model ("UW simplified Model") to reproduce observed response of the abutments and piers. The derived secant stiffnesses were compared with those of the UW, CALTRANS, WSDOT, and UW modified models.

A discussion of the differences among the UW, CALTRANS, WSDOT, UW modified, and UW simplified models is presented in Section 6.7. Section 6.8 presents a sensitivity analysis of the calculated response for the UW modified model.

6.1 DESCRIPTION OF UW MODEL

Model Overview

To perform nonlinear analysis, the researchers combined a series of linear SAP90 analyses. (16) A schematic of a typical finite-element model is shown in Figure 6.1, and an input file for the 3,164 degree-of-freedom model is given in Appendix B. Equal horizontal loads were applied along the skew to each pier crossbeam. A total of 278 beam elements modeled the girders; curb and railing; crossbeams; and columns. The columns were fixed at the footing level. A total of 444 four-node, shell elements modeled the bridge deck, end diaphragms, and wingwalls.

The step-by-step combination process was implemented by a BASIC computer program. At each step, the program extracted data from the SAP90 output file, modified the input data file, and performed another linear analysis. This procedure was repeated for a given load until the properties of the model were consistent with the component's nonlinear behavior. Between steps, the applied load was increased by 20 kips for the bridge under initial and excavated conditions. The step size was reduced to 10 kips for the bridge under isolated conditions. This step-by-step process continued until a target maximum applied load was reached or until a wingwall moment reached its flexural strength. The wingwall was the only reinforced concrete element that yielded in the analyses.

Initial properties of the reinforced concrete sections were calculated on the basis of gross sections and an elastic modulus of 4,600 ksi. The strength of the wingwall was calculated on the

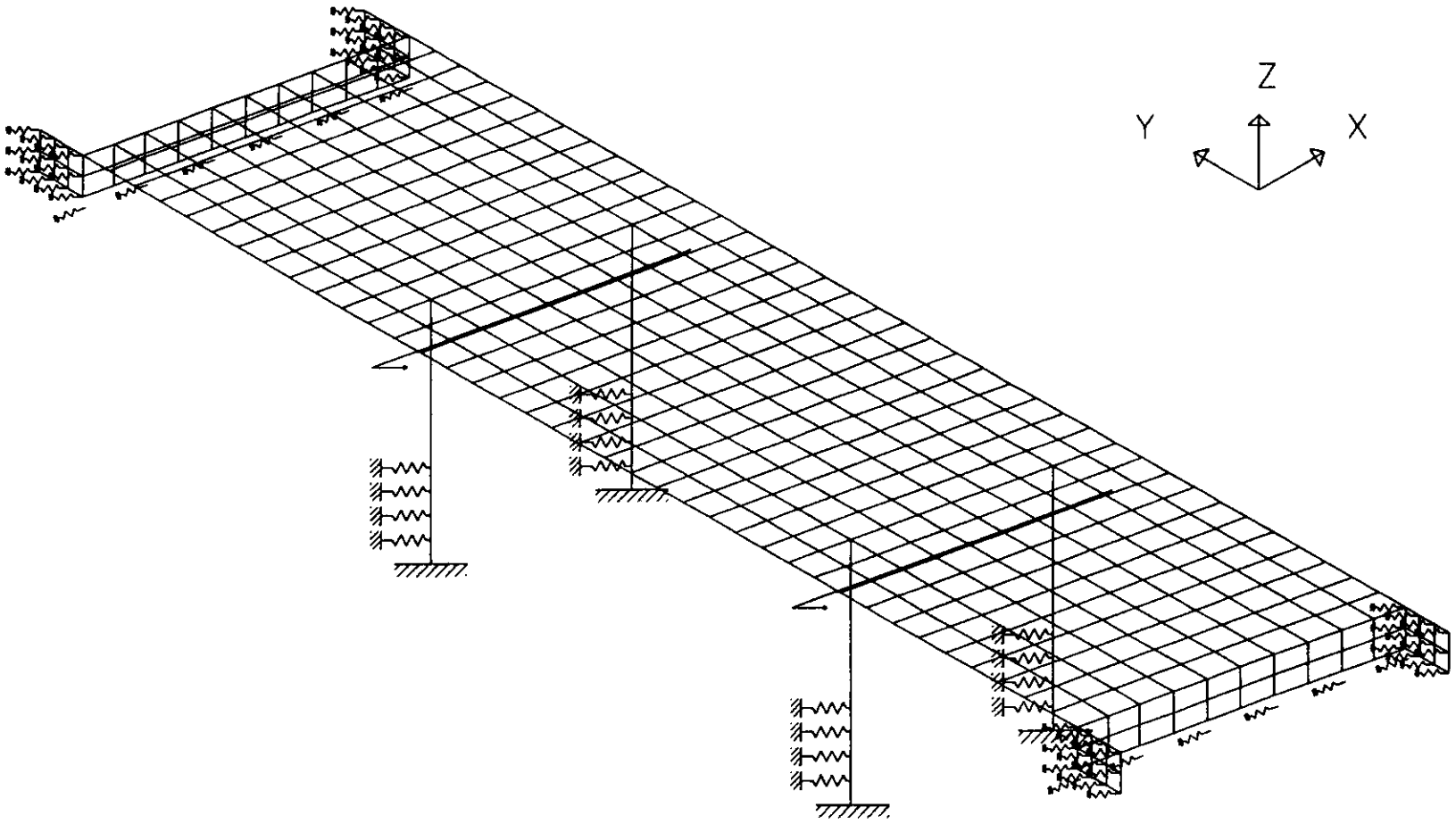

Figure 6.1. Schematic of UW Model

basis of the measured material properties of the concrete and steel. The unit weight of the concrete was assumed to be 150 pcf.

The analyses reflected the expected nonlinear behavior of the bearing pads, polystyrene, isolation system, columns, and wingwalls. Initial friction from the soil behind the abutment endwalls was modeled as perfectly plastic. Linear springs modeled soil compression behind the abutment endwalls, behind the wingwalls, and around the bottom half of the columns. The stiffness of the springs near the columns was the secant stiffness corresponding to the maximum pier displacement.

The assumed behavior of each model component is summarized in Table 6.1; the following subsections provide details of each model component.

Bearing Pads

Until the bearing pads reached the displacement at which slip occurred, they were modeled with linear springs distributed along the bottom of each end diaphragm. The total stiffness of these springs in each direction at an abutment was 167 kips/in. (Section 2.4). At a displacement of 0.206 inch, the springs were removed and replaced with a frictional force of 34 kips distributed along the bottom of each end diaphragm.

Polystyrene

The polystyrene was modeled similarly as the bearing pads. The total stiffness of the polystyrene at one abutment was 4,260 kips/in. (Section 2.4). At the displacement at which slip occurred (0.0196 inch), the springs were removed and replaced with a frictional force of 84 kips distributed along the bottom of each end diaphragm.

Isolation System

The isolation system was modeled for Cycle ISO. In the isolated bridge model, the abutments were fixed until either the transverse or longitudinal force at the abutment exceeded 9 kips. At this point, the restraint on the abutment was removed and a force of 9 kips simulated the friction.

Table 6.1. Assumed Component Behavior for UW Model

Item	Displacement		Force Experienced		Moment Experienced	Stiffness			Force to Add		Frictional Force		Comment
	y-dir.	x-dir.	y-dir.	x-dir.		ky	kx	I	y-dir.	x-dir.	y-dir.	x-dir.	
Column					<=5700			90000					Uncracked
					>5700			29500					Cracked
Soil Springs Around Column						See Table 6.2 for soil springs							
Polystyrene Springs Under Abutment	<=.0196					4260							
	>.0196					0					84		
		<=.0196					4260						
		>.0196					0					84	
Bearing Pad Springs Under Abutment (6 pads)	<=.2060					167							
	>.2060					0					34		
		<=.2060					167						
		>.2060					0					34	
Soil Springs Along Outside Abutment Wall			<=36			1x10^12 (Fixed)							1/2 spring at each abutment because soil does not resist tension
			>36			80							
				<=8			1x10^12 (Fixed)						
				>8			175						
Soil Friction Along Outside Abutment Wall			<=36								0 (Fixed)		
			>36								36		
				<=8								0 (Fixed)	
				>8								8	
Wingwall					<=1110			8200					Uncracked
					>1110			N/A					Flexural Strength
Soil Springs Behind Wingwall						90							

Notes:
All units in kips, inches, seconds
x-dir. is longitudinal direction; y-dir. is perpendicular to x-dir.

Columns

The column cracking moment was calculated to be 5,700 in.-kips with the MPHI moment-curvature program. (17) When the moment in a column element exceeded the cracking moment, the moment of inertia in that element was decreased from the calculated gross-section value of 90,000 $in.^4$ to the cracked value of 29,500 $in.^4$.

Wingwalls

It was assumed that a wingwall would first reach its capacity at the interface between the wingwall and the abutment diaphragm. The moment capacity of a wingwall was calculated to be 1,110 in.-kips. Wingwall properties were not modified until the moment at the wingwall-abutment diaphragm interface was equal to its flexural strength, at which point the analysis was stopped.

Soil

Soil Friction At Abutments. Soil friction along the outside of each abutment end diaphragm was modeled by restraining each node along the bottom of the end diaphragm until the abutment force reached the calculated soil resistance. When the frictional force in a direction was reached, the restraint was removed and replaced with a frictional force distributed along the bottom of the end diaphragm. Static friction between the soil and concrete was calculated with Equation 6.1:

$$f_{friction} = \mu_S N \qquad \textbf{(6.1)}$$

where $f_{friction}$ = frictional force
μ_s = static coefficient of friction between soil and concrete
N = normal force between soil and end diaphragm

The coefficient of friction between sand and concrete was estimated following a procedure proposed by Fang (18):

$$\delta = \phi - 5^o \qquad \textbf{(6.2)}$$

where, δ = dimensionless coefficient, and
ϕ = angle of internal friction for soil.

$$\mu_s = \tan(\delta) \qquad \textbf{(6.3)}$$

where, μ_s = static coefficient of friction between soil and concrete, and
δ = dimensionless coefficient.

For the measured internal angle of friction of 38 degrees, the static coefficient of friction between the soil and concrete was estimated to be 0.6. If it is assumed that the normal stress between the end diaphragm and soil varies linearly with depth, then the normal force, N, is the following:

$$N = K_o \gamma \frac{H^2}{2} L \qquad (6.4)$$

where, N = Normal force between soil and concrete,
K_o = coefficient of lateral earth pressure,
γ = in-situ unit weight of soil,
H = height of diaphragm, and
L = length of diaphragm.

The coefficient of earth pressure could vary between the coefficient of active earth pressure, K_a, and the coefficient of passive earth pressure, K_p.

$$K_a = \tan^2\left(45^0 - \frac{\phi}{2}\right) \qquad (6.5)$$

where, K_a = coefficient of active earth pressure, and
ϕ = angle of internal friction for soil.

$$K_p = \tan^2\left(45^0 + \frac{\phi}{2}\right) \qquad (6.6)$$

where, K_p = coefficient of passive earth pressure, and
ϕ = angle of internal friction for soil.

For the measured internal angle of friction of 38 degrees, K_a was calculated as 0.2 and K_p was calculated as 4.2. A coefficient of earth pressure of 1 was selected. For K_o equal to 1, the normal force between the soil and end diaphragm at an abutment was calculated with Equation 6.4 to be 60 kips. Therefore, the soil friction at an abutment was estimated to be 36 kips (Equation 6.1).

Soil Springs at Abutment. Springs modeled soil stiffness behind the wingwalls and perpendicular to each end diaphragm. Soil spring stiffnesses were calculated to be consistent with a

model recommended by Douglas and Davis (19) for geotechnical applications. They developed the solution for a vertically-oriented, thin, rigid, rectangular plate submerged in an elastic half-space. A horizontal load and moment are applied at the top of the plate. The dominant parameter in the solution was the initial tangent compressive modulus, E_S, of a soil. On the basis of the laboratory tests described in Section 2.5, this modulus was assumed to be 1,600 psi.

The effective horizontal stiffness of the soil was derived with Equations 6.7 and 6.8. A schematic of the plate model and a plot of coefficient used in estimating response is shown in Figure 6.2.

$$h = \frac{H}{E_S B} I_{hH} \qquad (6.7)$$

$$\frac{H}{h} = K_{horizontal} = \frac{E_S B}{I_{hH}} \qquad (6.8)$$

where, h = horizontal displacement at top of plate,
H = applied horizontal force at top of plate,
$K_{horizontal}$ = horizontal stiffness of plate in soil,
E_S = modulus of elasticity for soil,
B = width of plate,
D = height of plate, and
I_{hH} = influence coefficient from Figure 6.2.

The resulting calculated stiffness of 90 kips/in. was distributed to 9 springs at each wingwall. The stiffness of the soil behind each end diaphragm was calculated to be 376 kips/in. This stiffness was divided by a factor of two, because the soil acted only on the outside of the abutment wall, and because the tensile resistance of the soil was neglected.

Soil Springs At Base of Column. Four linear springs at 3-foot intervals simulated the soil resistance around the base of the columns. Stiffnesses were calculated following a p-y curve approach proposed by O'Neill and Murchison (13) for laterally-loaded piles in sands. A schematic of their model is shown in Figure 6.3. In the model, lateral load is applied at the top of the pile, and the top and bottom of the pile are free to rotate. Although the crossbeams and the footings provided some rotational resistance at the ends of the bridge columns, the model was implemented without modification. O'Neill and Murchison reasoned that their approach was still applicable to piles with end fixity.

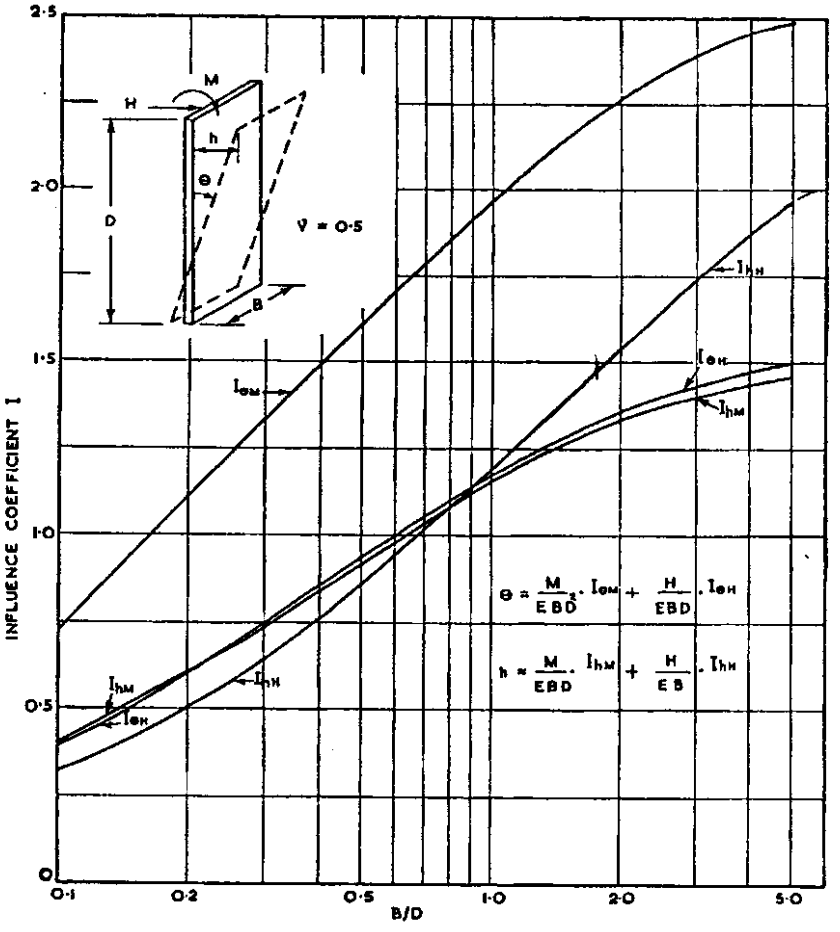

Figure 6.2. Influence Coefficients for Stiffness of Rigid Plate (19)

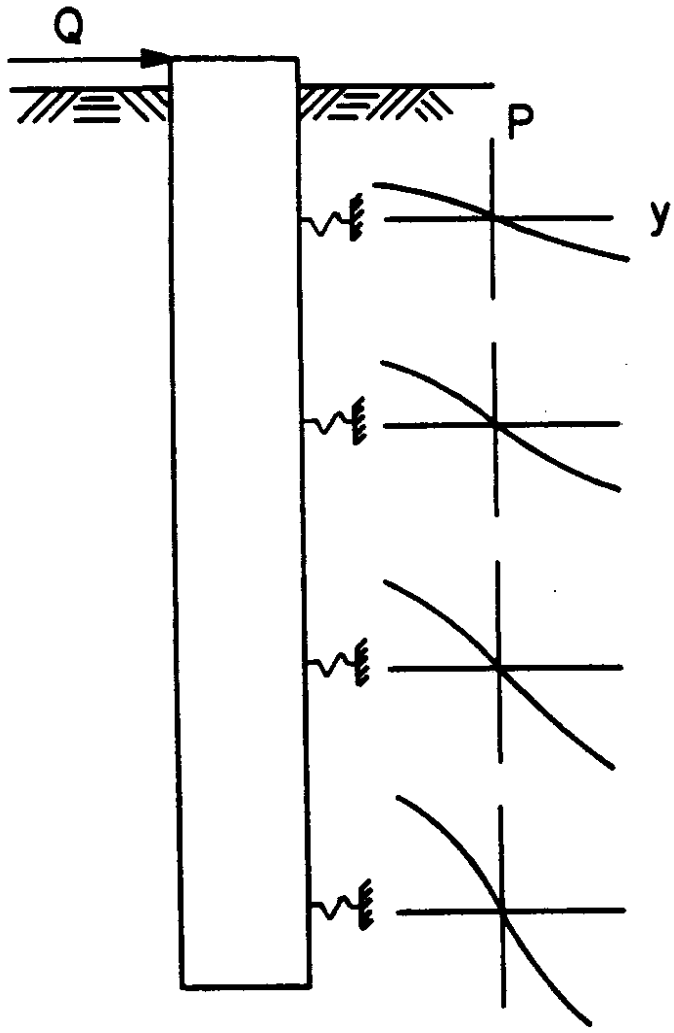

Figure 6.3. O'Neill and Murchison Model of Laterally-Loaded Pile (13)

The resistance of the soil, p, was a function of the depth below the ground surface, the displacement of the column at that depth, the ultimate soil resistance at that depth, and the internal angle of friction of the soil. The ultimate soil resistance was calculated using the lesser of Equation 6.9 for typical wedge failure and Equation 6.10 for failure in which the soil flows around the pile.

$$P_u = (C_1 z + C_2 D)\,\gamma' z \qquad (6.9)$$

$$P_u = C_3 D \gamma' z \qquad (6.10)$$

where, p_u = ultimate soil resistance [force/length of pile],
z = depth below ground surface,
D = diameter of pile,
γ' = effective unit weight of soil, and
C_1, C_2, C_3 = dimensionless coefficients that depend on the angle internal friction.

Wedge failure (Equation 6.9) controlled capacity for all the p-y curves developed to model the soil. Equation 6.11 was used to construct a p-y curve for each element along the column:

$$p = nAp_u \tanh\left[\left(\frac{k\,z}{Ap_u}\right) y\right] \qquad (6.11)$$

where, p = soil resistance [force/length of pile],
p_u = ultimate soil resistance [force/length of pile],
y = displacement of pile segment at depth z,
z = depth below ground surface,
k = coefficient from Figure 6.4,
A = 0.9 for cyclic loading, and
n = 1 for circular pile.

According to a correlation developed by O'Neill and Murchison, the relative density of the soil, D_r, was approximately 75 percent for the measured angle of internal friction. From Figure 6.4 and the estimate of D_r, the coefficient k was estimated to be 175 lb/in.^{3}. An example p-y curve for 6 feet below the ground surface is shown in Figure 6.5.

The stiffness of each soil spring was the secant stiffness of the p-y curve calculated at the maximum displacement during test half-cycles ISOS1, EXCN1, and IS1 (isolated, excavated, and initial conditions). The displacement at each element was estimated from a linear distribution of displacements between the top of the column and the footings. The maximum average bent

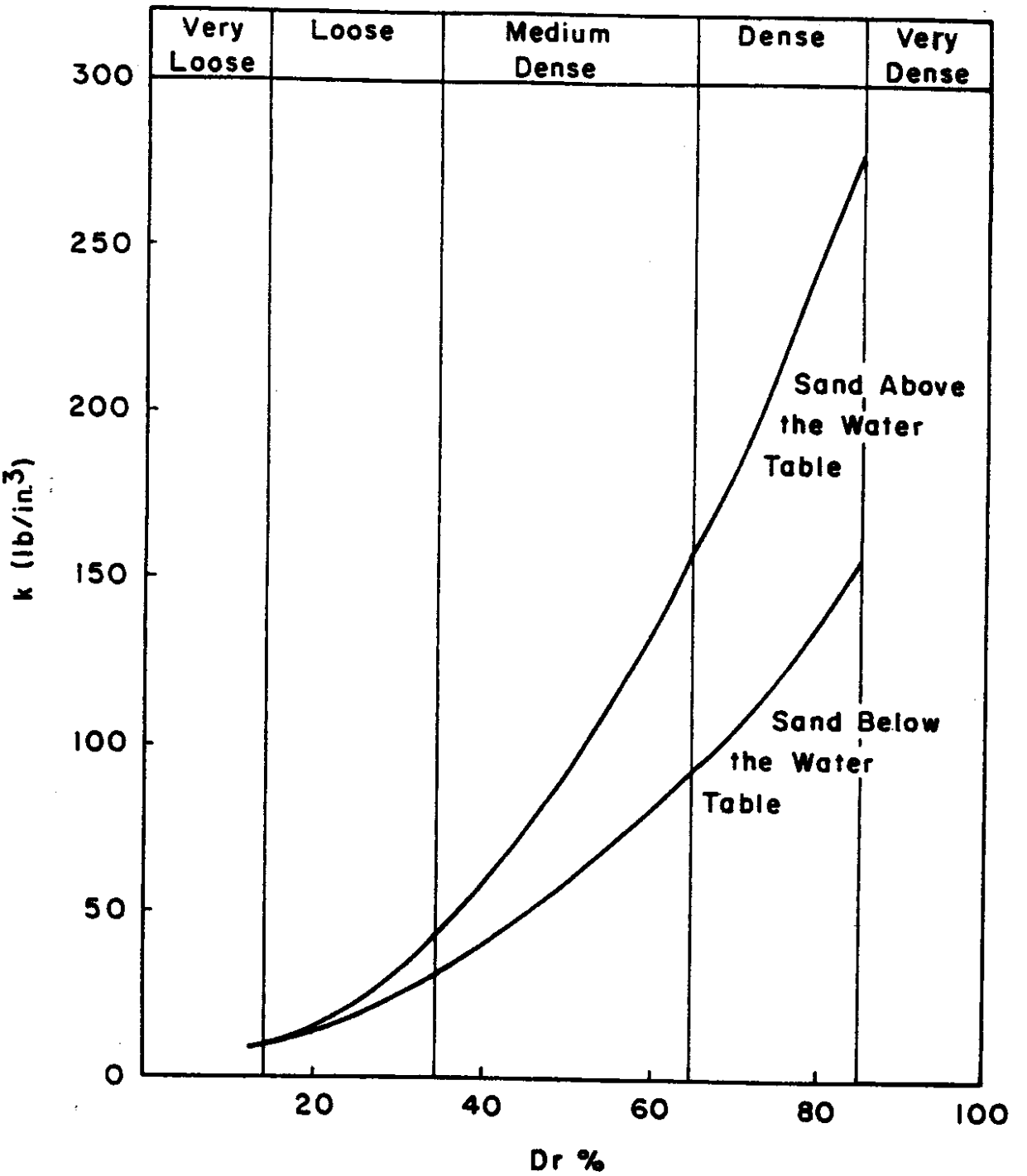

Figure 6.4. Variation of Coefficient k with Relative Density (13)

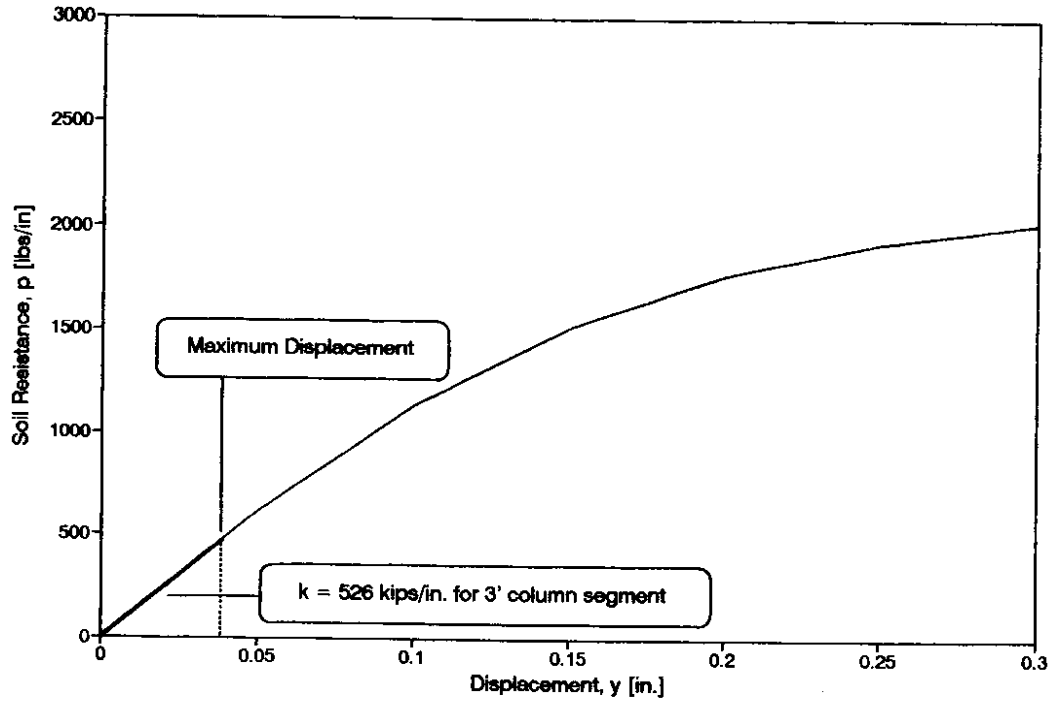

Figure 6.5. IS1 P-Y Relationship for 6 Feet Above Footing

Table 6.2. Soil Spring Secant Stiffnesses

Test Half-cycle	Height Above Footing [ft.]	Soil Spring Secant Stiffness [kips/in]
IS1	3	759
	6	526
	9	290
	12	66
EXCN1	3	750
	6	489
	9	220
	12	34
ISOS1	3	750
	6	487
	9	217
	12	34

Note:
Soil springs for 3' column segment

displacement for the test half-cycle was assumed at the top of the column, whereas zero displacement was assumed at the footing.

Table 6.2 lists the soil spring secant stiffnesses for the UW models. An example secant stiffness for the bridge under initial conditions and at maximum test half-cycle IS1 applied loading is shown in Figure 6.5. This secant stiffness of 526 kips/in. (also listed in Table 6.2) was calculated for a 3-foot column segment located 6 feet above the footing. This value was calculated by averaging calculated secant stiffnesses per unit column length from p-y curves at depths of 5 feet, 6 feet, and 7 feet and multiplying this value by the 3-foot column element length. The maximum IS1 displacement for the pier crossbeam was 0.154 inch. The corresponding displacements at which the secant stiffnesses were evaluated were 0.031 inch, 0.037 inch, 0.043 inch for 5 feet, 6 feet, and 7 feet above the footings, respectively.

Since soil spring stiffnesses were calculated as secant values from p-y curves at a particular displacement, the calculated load-displacement curves were consistent with the calculated p-y curves only at that displacement. For smaller displacements the springs would be expected to be too flexible.

6.2 DESCRIPTION OF CALTRANS MODEL

CALTRANS created a linear finite-element model of the bridge. Loads were applied along the skew to the bent crossbeams; reactions and displacements at the abutments and bents were recorded. The model was composed entirely of beam elements and linear springs. Model dimensions were determined from the bridge plans, and the abutment skew was modeled. Gross section properties were assumed.

The stiffness of the diaphragm over the bent crossbeam was neglected. The bent crossbeams were pinned to the superstructure for longitudinal movement of the bridge. The columns footings were fixed. The soil around the base of the columns was not modeled.

The end diaphragms were not modeled explicitly. The abutment nodes were free to rotate about a vertical axis and an axis parallel to the abutments, but the abutments were fixed against rotation about a horizontal axis perpendicular to the abutments. The abutments were fixed against

vertical displacement; transverse and longitudinal displacement were resisted by springs that modeled the resistance of the soil. The resistance of the bearing pads, polystyrene, and soil friction was neglected.

To model longitudinal resistance, CALTRANS assumed a soil stiffness of 200 kips/in. per foot of abutment. Because this value applies only to 8-foot high abutment walls, the stiffness was reduced to 168 kips/in. for the 5-foot, 8-inch abutment wall. CALTRANS calculated a total soil stiffness of 6,567 kips/in. at each abutment. This stiffness was halved because soil was present only on the outside of the abutment walls, and to neglect the tensile resistance of the soil. The resistance of the soil surrounding the wingwalls was modeled using the same soil stiffness constant of 200 kips/in. per foot that had been used for the end diaphragm. The wingwalls were modeled assuming that one wingwall was fully effective in resisting transverse loads, whereas the other wingwall was only 1/3 as effective. The stiffness of the soil around the wingwalls was calculated to be 708 kips/in. at each abutment.

6.3 DESCRIPTION OF WSDOT MODEL

WSDOT also created a linear finite-element model of the bridge. Loads were applied along the skew to the bent crossbeams; reactions and displacements at the abutments and piers were calculated. The WSDOT model was similar to the CALTRANS model in that it was composed entirely of beam elements and linear springs. Model dimensions were derived from the bridge plans. The abutment skew was not modeled. Gross-section properties were used in the WSDOT model.

The pier crossbeam and diaphragm were modeled as a single beam. The pier crossbeams were pinned to the superstructure for longitudinal translation of the bridge. Translational and rotational soil springs modeled the soil around the footings. Their stiffnesses were determined using empirical equations based on estimates of the shear modulus of the soil. The shear modulus, in turn, was a function of the shear wave velocity through the soil; the shear wave velocity was estimated using an empirical chart that related the shear wave velocity to Standard Penetration Tests

blow count numbers, N. WSDOT estimated blow count numbers for the soil from boring logs included in the bridge plans. The soil around the base of the columns was not modeled.

Each end diaphragm was modeled with one vertical beam element. The abutments were free to rotate about a vertical axis. The abutment was fixed against rotation about both horizontal axes. Vertical, transverse, and longitudinal translation was resisted by springs at the abutments. The springs modeled the resistance of the soil. The stiffness of the vertical spring was calculated to be 15,500 kips/in.; this stiffness was calculated following the same procedure that was used to estimate the stiffness of the vertical soil springs at the column footings.

To model transverse and longitudinal soil resistance at the abutments, a modulus of subgrade reaction of 230 lb/in.^{3} was assumed initially. Soil springs were formed on the basis of the area over which the soil resisted movement. WSDOT then analyzed the model subjected to a typical earthquake ground acceleration of 0.25 g to determine forces in the springs. When the calculated force in a soil spring exceeded 5 ksf, the spring stiffnesses was decreased until the 5 ksf criterion was met.

To model longitudinal resistance, a half spring of 3,660 kips/in. was used at each abutment because soil was present only on one side of the abutment wall, and the tensile resistance of the soil was neglected. Only one-third of a wingwall at each abutment was assumed to be effective. WSDOT modeled only one wingwall to account for the instability of the soil sloping away from the abutments; the contribution was reduced further to only one-third of a wingwall because of the flexibility of the wingwalls. The stiffness of the soil around the wingwalls was calculated to be 83 kips/in. at each abutment. The resistance provided by the bearing pads, polystyrene, and soil friction was neglected.

6.4 LOAD-DISPLACEMENT RESPONSE

Along with the measured load-displacement response for cycles ISOS1, EXCN1, and IS1, Figures 6.6 to 6.10 show the calculated response for the UW, CALTRANS, and WSDOT models. In these figures, the vertical axis is the horizontal component of the total applied load. In Figures 6.6, 6.7 and 6.9, the horizontal axis is the average displacement of the east and west bents

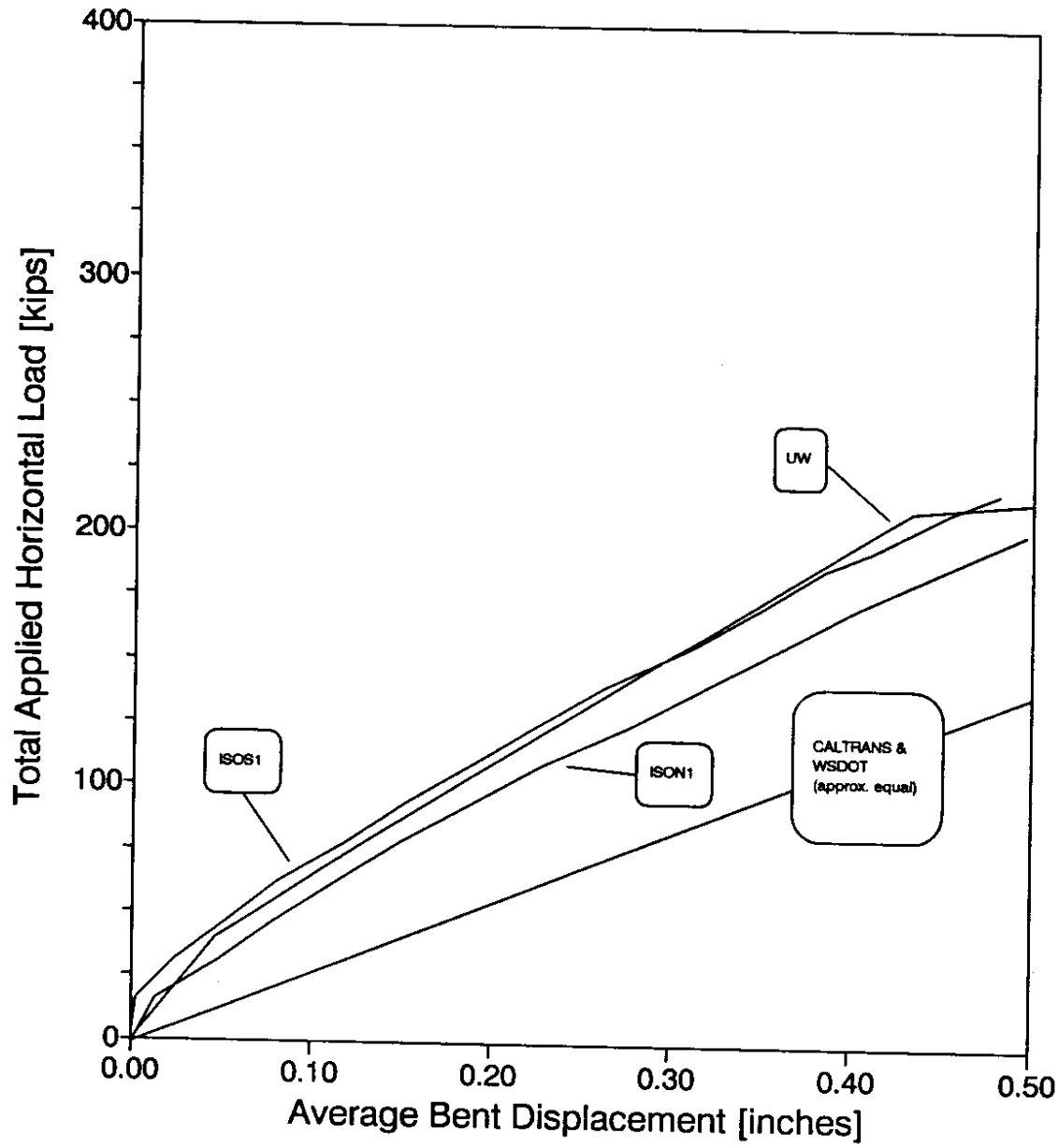

Figure 6.6. Average Bent Response for Isolated Bridge

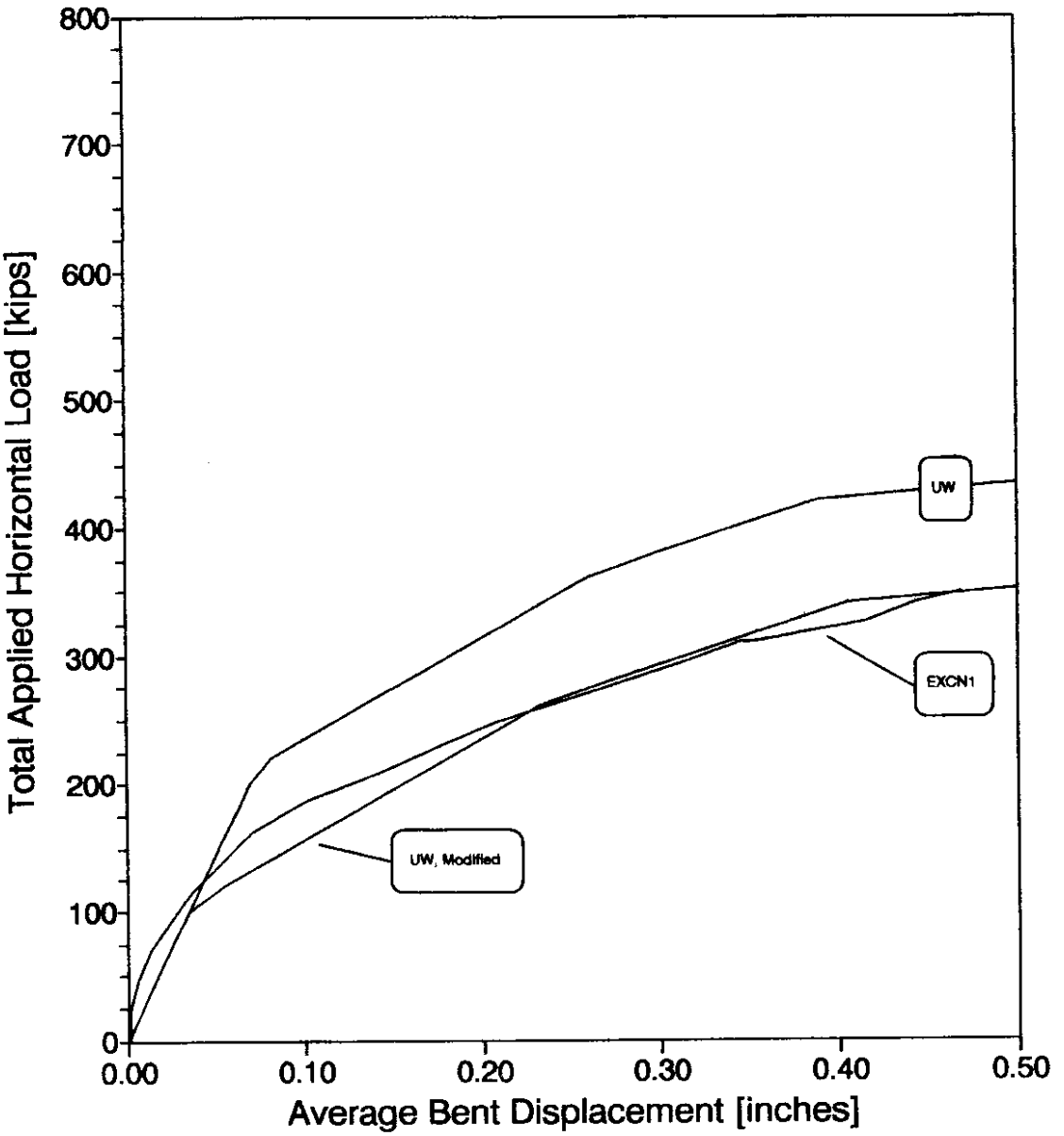

Figure 6.7. Average Bent Response for Excavated Bridge

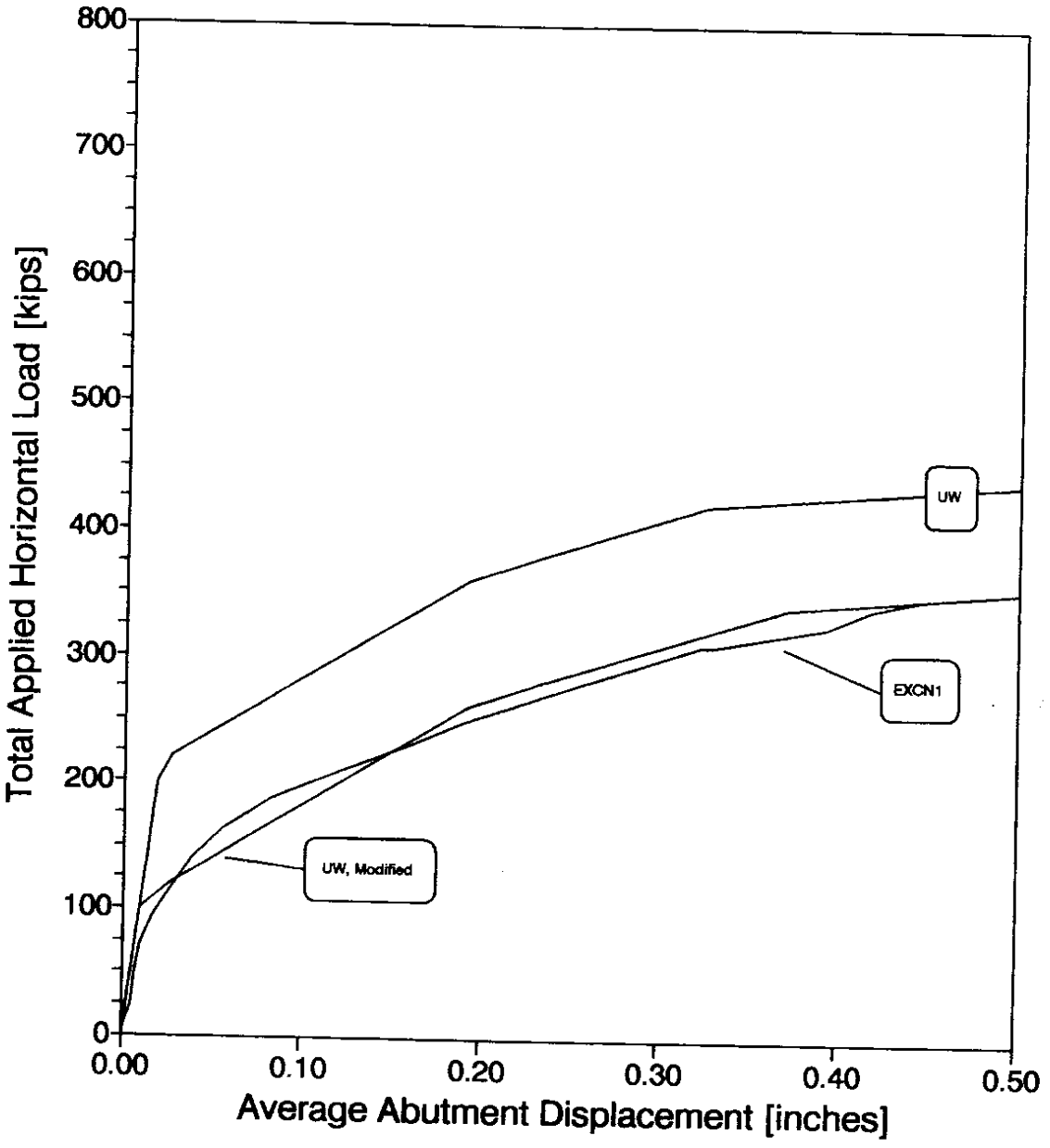

Figure 6.8. Average Abutment Response for Excavated Bridge

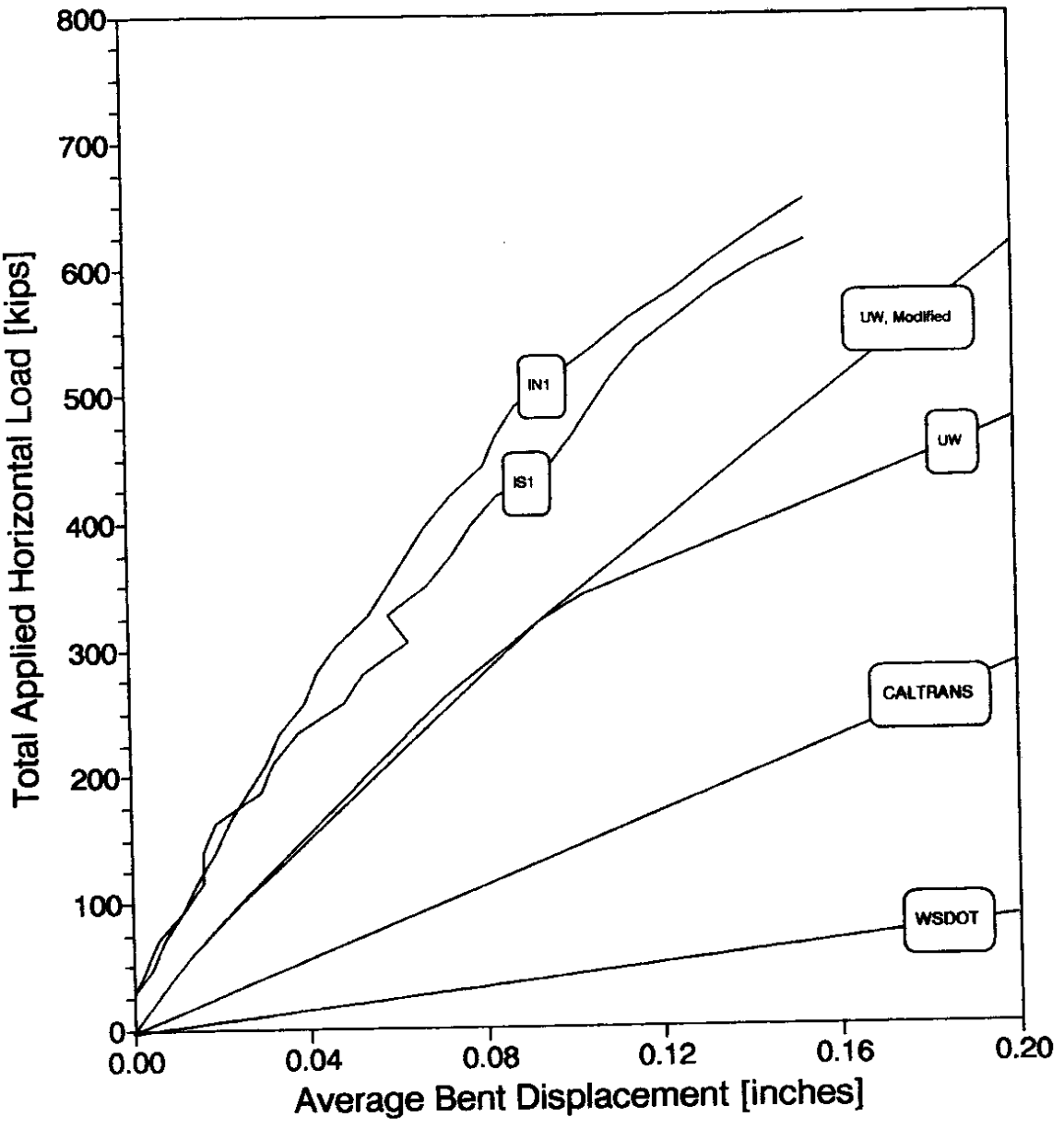

Figure 6.9. Average Bent Response for Bridge in its Initial State

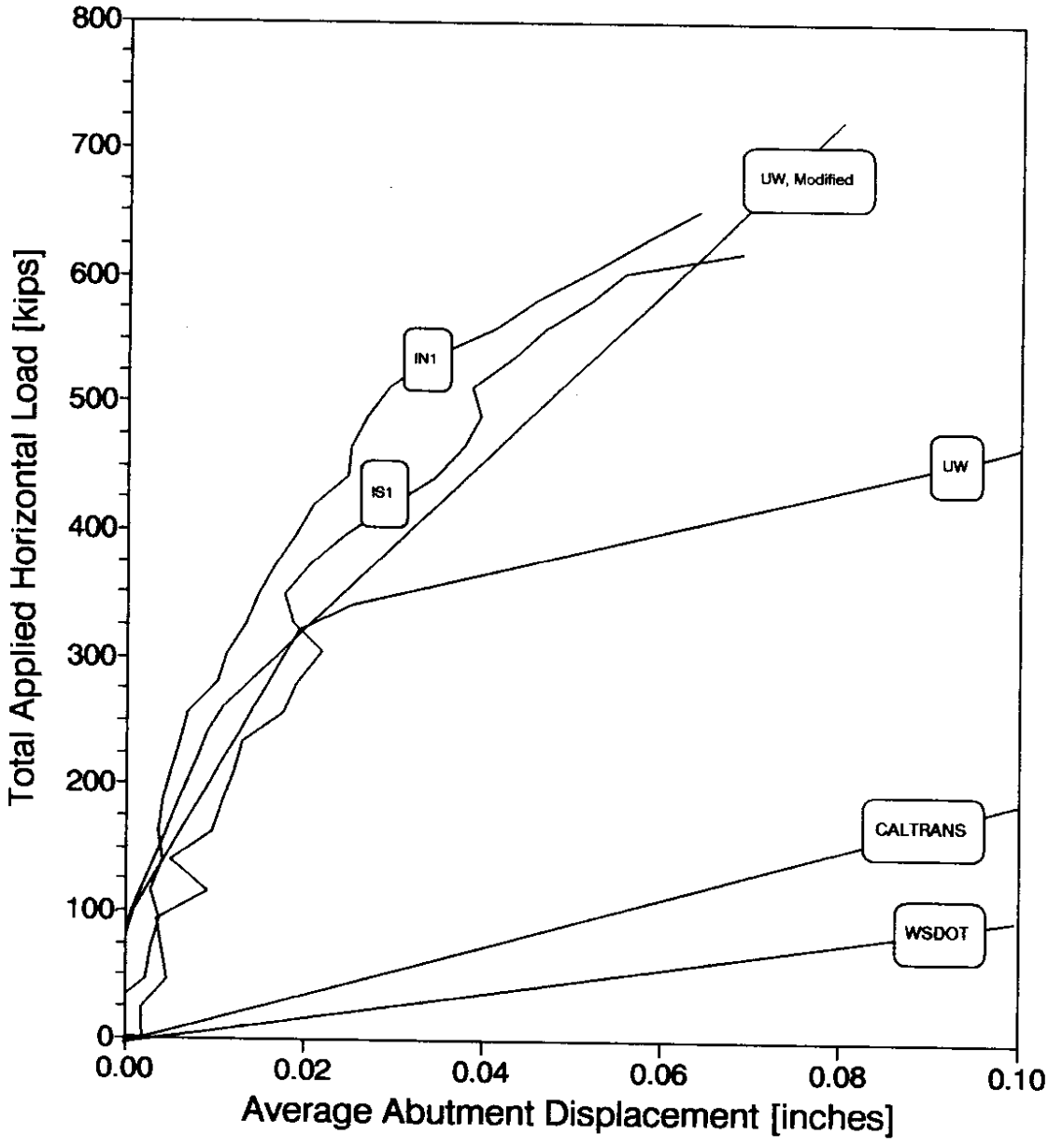

Figure 6.10. Average Abutment Response for Bridge in its Initial State

(i.e., piers). In Figures 6.8 and 6.10, the horizontal axis is the average displacement of the east and west abutments.

Isolated Conditions

The calculated response of the UW model provided a good fit to the measured response of the isolated piers (Figure 6.6). Abutment and pier average load-displacement slopes from the bridge models and measured response are listed in Table 6.3. These slopes were calculated at the maximum applied loads for cycles ISOS1, EXCN1, and IS1. For cycle ISOS1, the UW model load-displacement slope was 106 percent of the measured slope. The CALTRANS and WSDOT models predicted load-displacement slopes that were 65 and 68 percent, respectively, of the measured slope.

For the UW model of the isolated bridge, the top 3-foot column element was assumed cracked initially to be consistent with observed cracking. Additional cracking in the columns began at the bottom of the columns at an applied load of approximately 220 kips (Figure 6.6). This load was slightly greater than the 217-kip load that was applied in cycle ISOS1. No new cracking was reported in test cycle ISOS1.

Excavated Conditions

For the excavated bridge, the UW model was too stiff (Figure 6.7 and 6.8). The model indicated that the polystyrene slipped at a total applied load of approximately 200 to 220 kips. The observed reduction in slope of the measured response occurred at a lower load, in the range of 100 to 175 kips (Figure 6.7 and 6.8). The abutment and bent load-displacement slopes for EXCN1 were 253 and 194 percent, respectively, of the measured values (Table 6.3).

For the UW model of the excavated bridge, the top column element was assumed to be cracked initially to be consistent with observed cracking. No new damage was predicted by the model for loads below that applied in cycle EXCN1 (349 kips). In the field, no new damage was observed for this cycle.

Table 6.3. Average Load-Displacement Slopes

Bridge Environment & Bridge Test Cycle	Name of Model	Average Load-Displacement Slopes (LDS)		Maximum Bent Displacement
		Abutment	Bent	
Initial Bridge (IS1)	Measured	8956	4019	0.15
	Modified	9569 7%	3049 -24%	0.20 30%
	UW	2528 -72%	1668 -58%	0.37 140%
	CALTRANS	1818 -80%	1429 -64%	0.43 181%
	WSDOT	941 -89%	429 -89%	1.44 836%
Excavated Bridge (EXCN1)	Measured	784	742	0.47
	UW	1988 153%	1436 94%	0.24 -49%
	Modified	899 15%	823 11%	0.42 -10%
Isolated Bridge (ISOS1)	Measured (corrected for 18 kips friction)		420	0.47
	UW (corrected for 18 kips friction)		446 6%	0.45 -6%
	CALTRANS		274 -35%	0.73 53%
	WSDOT		284 -32%	0.70 48%

Notes:
All units in kips, inches, radians, seconds
The LDS's are at the maximum loading in the bridge test cycles
The percentage in each cell is the value as a percentage increase or decrease over the measured value

Initial Conditions

All of the analytical models underestimated the stiffness of the bridge in its initial state (Figure 6.9 and 6.10). The UW model predicted slip of the polystyrene at an applied load of approximately 320 kips. Though the model predicted a large reduction in stiffness at this load, no such reduction was observed in test IS1. The wingwalls failed during the bridge test at an applied horizontal load of approximately 760 kips in cycle IIN1. This load was comparable to the 700-kip load predicted by the UW model, but, the UW model was too flexible for loads greater than 330 kips. The load-displacement slopes of the UW, CALTRANS, and WSDOT models for cycle IS1 varied from 11 to 62 percent of the measured values.

The UW models were consistent with the cracking observed at the top of the columns. For the UW model of the bridge in its initial state, the columns were assumed to be uncracked initially. Column cracking was predicted at the top of the columns at an applied load of approximately 600 kips. Column cracking in the field was first observed at the top of the columns after cycle IS1, in which the maximum applied horizontal load was 620 kips.

The predicted cracking at the bottom of the columns was not identical to that observed in the field. In the model, the bottom of the columns cracked at an applied load of approximately 700 kips. At this point in the analysis, the top 3 feet and bottom 6 feet of the columns were cracked. In cycles IIS1, IIN1 and IIS2, the researchers observed cracking spread to the top 4 feet of the column and in a region 2 to 8 feet above the footings. In contrast to the model prediction, no cracks were visible at the bottom of the column.

6.5 CALIBRATION OF UW MODEL

In general, if an analytical model is complex, one can easily modify it to reproduce a few measured load-displacement relationships. However, the validity of such a calibration is difficult to establish, because several sets of modifications may result in similar calculated response. Fortunately, in developing the "UW modified" models, the calibration procedure was not arbitrary. The following goals guided the model calibration:

- The model should reproduce the measured load-displacement relationship for the isolated piers (Figure 6.6).
- For the excavated bridge, the model should reproduce the pier load-displacement relationship (Figure 6.7).
- For the excavated bridge, the model should reproduce the abutment load-displacement relationship (Figure 6.8).
- For the bridge in its initial state, the model should reproduce the pier load-displacement relationship (Figure 6.9).
- For the bridge in its initial state, the model should reproduce the abutment load-displacement relationship (Figure 6.10).
- The model should predict cracking at the top and bottom of the columns that is consistent with that observed in the test.
- The model should predict wingwall failure at a load and displacement that is consistent with that observed in the test.
- Only model parameters that have large uncertainty should be modified to reproduce response.

Isolated Conditions

The measured load-displacement response and the observed damage agreed well with those the UW model predicted. Therefore, the researchers did not modify the UW model of the isolated bridge.

Excavated Conditions

Whereas the UW model of the isolated bridge reproduced the observed behavior well, the excavated model was too stiff, particularly for small displacements. The resistance of the abutment bearing pads and polystyrene was the only difference between the UW models for the excavated and isolated conditions. Therefore, it is likely that the model overestimated the resistance the polystyrene and bearing pads provided. Of the two components, it most likely the polystyrene resistance was overestimated because the properties of the polystyrene were the most uncertain. As

mentioned in Section 2.4, laboratory tests were performed on polystyrene samples that were ordered from a manufacturer, not polystyrene from the bridge.

The UW model was modified by halving the coefficient of friction for the polystyrene. The calculated response from the UW modified model of the excavated bridge provided a good fit to the measured response throughout the load history (Figure 6.7 and 6.8). For this model, the polystyrene slipped at a total applied load of approximately 100 kips. The calculated abutment and bent load-displacement slopes were within 15 percent of the measured values (Table 6.3). As in the UW model, the top 3 feet in the UW modified model was assumed cracked initially. No new damage occurred in the model for the loads that were applied in half-cycle EXCN1. This behavior was consistent with the observed behavior.

Initial Conditions

For the bridge in its initial state, the UW models were too flexible, particularly for loads larger than 350 kips (Figure 6.9 and 6.10). The halving of the polystyrene friction (to fit the excavated bridge response) further reduced the stiffness of the model and, correspondingly increased the discrepancy between the measured and calculated responses. To match measured response, the stiffness of one or more components had to be increased.

The only differences between the UW bridge models for the excavated and initial conditions were the amount of pier column cracking (in cycle IS1, the columns were assumed to be uncracked initially) and the stiffness of the soil at the abutments. It was not reasonable to resolve the discrepancy by increasing the stiffness of the bents. The bent behavior was modeled successfully in cycle ISO. Further, the bent stiffness was too small to greatly affect the calculated response for the bridge in its initial state.

The amount of soil friction was not a good candidate for modification, either. Though soil friction is accompanied with great uncertainty, an increase in soil friction would primarily affect the calculated response for small applied loads. In contrast, the discrepancy was largest for large loads.

An underestimate of the stiffness of the soil behind the wingwalls and abutment was a more reasonable cause of the discrepancy in cycle IS1. The original UW model was based on Douglas

and Davis' (19) solution for a rigid plate that was free to rotate (Section 6.1). In the field, the wingwall and endwall rotation were restrained. Further, the model depended on the laboratory measurement of compressive modulus of the soil, E_S. As discussed in Section 2.5, the measured E_S was surprisingly low for a silty sand, with an internal angle of friction equal to 38 degrees. It is likely that soil disturbance resulted in a low value of E_S. To model the bridge without using E_S, the researchers followed recommendations proposed by Bowles. (20) For a medium-dense silty sand, Bowles suggested that a typical value for the modulus of subgrade reaction, k_S, is 175 lb/in.^{3} (20). This choice of k_S increased the stiffness of the soil at the wingwalls and endwalls by an order of magnitude from that of the UW model.

The calculated response from the UW modified model for the bridge in its initial state provided a good fit to measured response (Figure 6.9 and 6.10), particularly at the abutments. The model predicted slip of the polystyrene at an applied load of approximately 240 kips. Consistent with the observed response, there was not a great decrease in stiffness at this load. The UW modified model abutment load-displacement slopes were within 7 percent of the measured values (Table 6.3). The UW modified model bent load-displacement were within 25 percent of the measured slopes.

No column cracking occurred in the model, though minor column cracking was observed in the tests. The wingwalls reached their strength at an applied load of approximately 740 kips, which was nearly identical to the observed failure load of approximately 760 kips.

6.6 COMPONENT SECANT STIFFNESSES

UW Simplified Model

With a simple model of the bridge, the researchers derived component secant stiffnesses from the maximum applied loads and displacements. Table 6.4 lists the test half-cycles that were selected for analysis, along with the corresponding maximum applied loads and displacements. Figure 6.11 shows a plan view of the simple finite-element model.

Table 6.4. Calibration Data for UW Simplified Model

Test Cycle	Horizontal Load Applied to West Bent (y-comp.), Fy2	Horizontal Load Applied to East Bent (y-comp.), Fy3	West Abutment Rotation, theta1	East Abutment Rotation, theta4	West Abutment Displacement (y-comp.), y1	West Bent Displacement (y-comp.), y2	East Bent Displacement (y-comp.), y3	East Abutment Displacement (y-comp.), y4
IS1	300	302	1.48E-04	-1.01E-04	0.055	0.140	0.160	0.079
IIS1	374	374	2.17E-04	-1.12E-04	0.141	0.280	0.311	0.224
EXCN1	-170	-170	-2.10E-04	-1.36E-04	-0.295	-0.391	-0.523	-0.570
ISOS1	105	105	8.90E-05	6.58E-05	0.418	0.446	0.494	0.518

Notes:
All units in kips, inches, radians, and seconds
All displacements relative to position of bridge at beginning of test cycle (relative displacements)
South=positive displacement

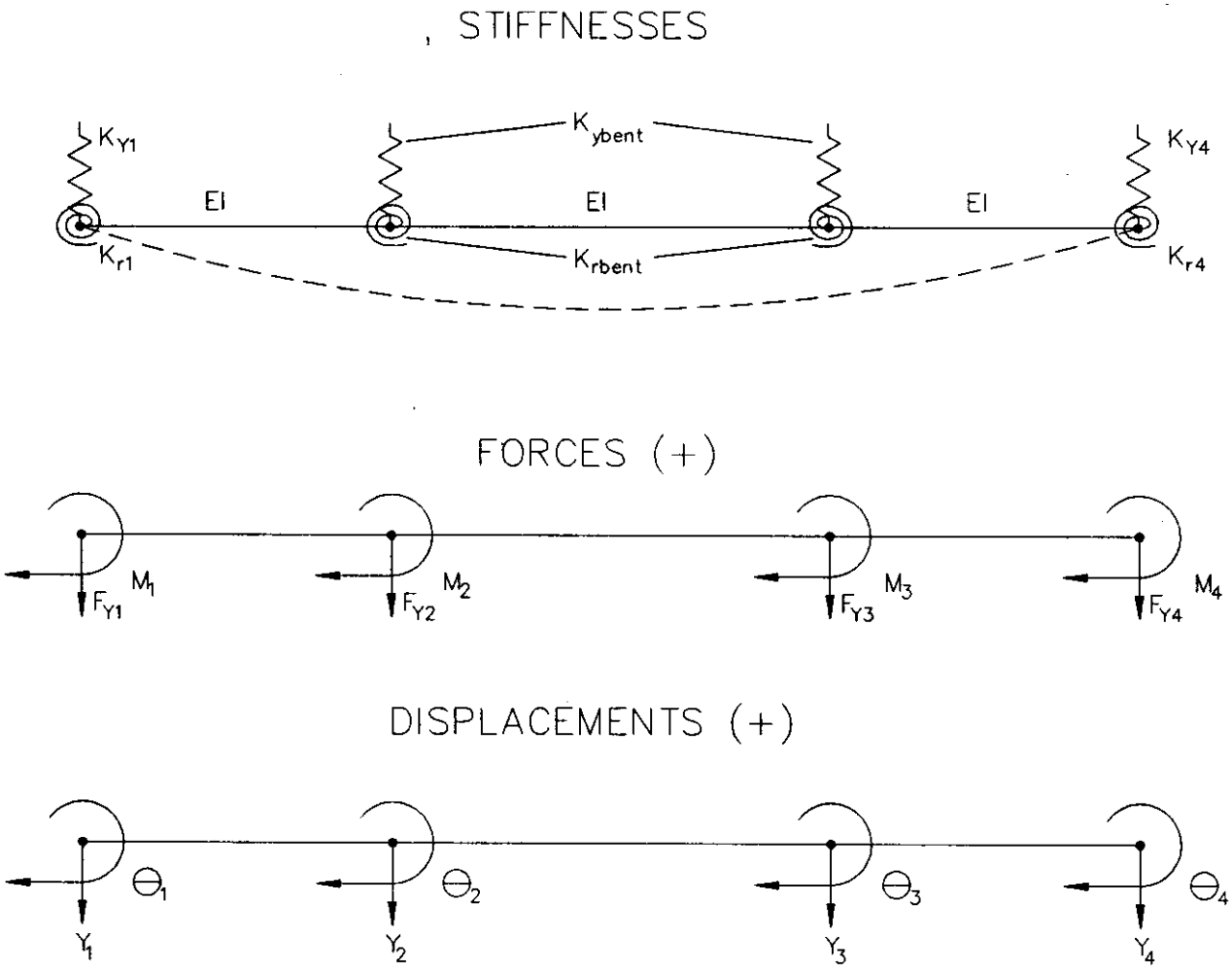

Figure 6.11. Schematic of UW Simplified Model

The eight degrees of freedom for the model consisted of a displacement and rotation at each of four nodes. The eight-by-eight global stiffness matrix for the model is given in Appendix C. Two of the applied forces, F1 and F4, and all of the applied moments, M1, M2, M3, and M4, were equal to zero in the bridge test. The model did not incorporate the skew in the bridge; therefore, the transverse applied loads and displacements used in the model were the components perpendicular to the longitudinal centerline of the bridge.

The rotations of the bents, θ_2 and θ_3, were not measured in the bridge tests. Therefore, these degrees of freedom were eliminated by matrix condensation, resulting in a six-by-six stiffness matrix. Initially, the seven unknown stiffnesses were the following: the flexural rigidity of the bridge spans (EI), transverse and rotational stiffnesses at each abutment (k_{y1}, k_{y4}, k_{r1}, k_{r4}), and translational and rotational bent stiffnesses (k_{ybent}, k_{rbent}). The number of unknown stiffnesses was reduced to six by assuming a value for k_{rbent}. The rotational stiffness of the bents, k_{rbent}, was estimated to be 2.40×10^7 kip-in./rad by assuming columns with uncracked sections, fixed ends, and no soil. Six unknown stiffnesses remained.

A trivial solution was found immediately by setting the superstructure flexural rigidity, EI, equal to zero. The solution is found by satisfying equilibrium at each node independently. To prevent convergence to this trivial solution, the bent stiffness was set equal to the average measured secant stiffness of the bents from test half-cycle ISOS1. Since only five unknown stiffnesses remained, an exact solution for a six-by-six system was not possible. The solution may be considered a "best fit" solution.

The model was nonlinear because of the matrix condensation. Automated searches for local minima often converged to unrealistic solutions. To find a solution that was physically meaningful, the unknown stiffnesses were adjusted manually in an interactive spreadsheet. As the values of stiffness were changed, the resulting displacements (given an applied loading) were compared with the measured displacements. The average calculated displacement of the bents was compared to the average measured displacement of the bents. This averaging was done because even a small

differential displacement between the bents due to measurement error would have induced a large twist in the bridge deck.

The stiffnesses were adjusted until the calculated displacements and rotations were within 1 percent of the measured displacements and rotations; at this point, the stiffnesses were recorded as the calculated stiffnesses for each trial. As an example of the fit achieved, the calculated displacements for IS1 are compared to the measured displacements in Figure 6.12. Theoretically, the nonlinearity of the system makes the uniqueness of the solution questionable. To investigate the stability and uniqueness of the solution, the spreadsheet iteration was started with several initial values for the stiffnesses. The iteration procedure always converged to the same solution.

Derived Secant Stiffnesses

Secant stiffnesses were calculated at the maximum applied load and displacement for test half-cycles ISOS1, EXCN1, IIS1, and IS1 (Table 6.5). The secant stiffness of the bents are derived in Trial 1. In Trial 2 (EXCN1 test half-cycle), the average measured abutment displacement and rotation were used at each abutment; the average measured bent displacement was used at each bent. This symmetric component of measured response was used because the bridge rotated a great amount during this test half-cycle. The actual measured displacements could not be matched by the model without the use of negative stiffnesses. In Trials 3 and 4, secant stiffnesses for test half-cycles IIS1 and IS1 were derived. Trials 5-9 were performed to determine the effects of varying k_{ybent}, k_{rbent} and G, the concrete shear modulus. In trial 9, G was estimated as one half of the elastic modulus.

The derived secant stiffnesses for the bridge under excavated conditions are given in Trial 2. The derived flexural rigidity, EI, of the bridge spans was 40 percent less than the value from the bridge under initial conditions (Trial 4). The derived abutment stiffnesses were approximately 4 percent of that calculated for the bridge under initial conditions (Trial 4). This was consistent with the loss of soil stiffness at the abutment for the bridge due to excavation.

Trials 5-8 (for test half-cycle IS1) revealed that doubling or eliminating the translational and rotational bent stiffnesses changed the derived stiffnesses by less than 13 percent. Trial 9 showed

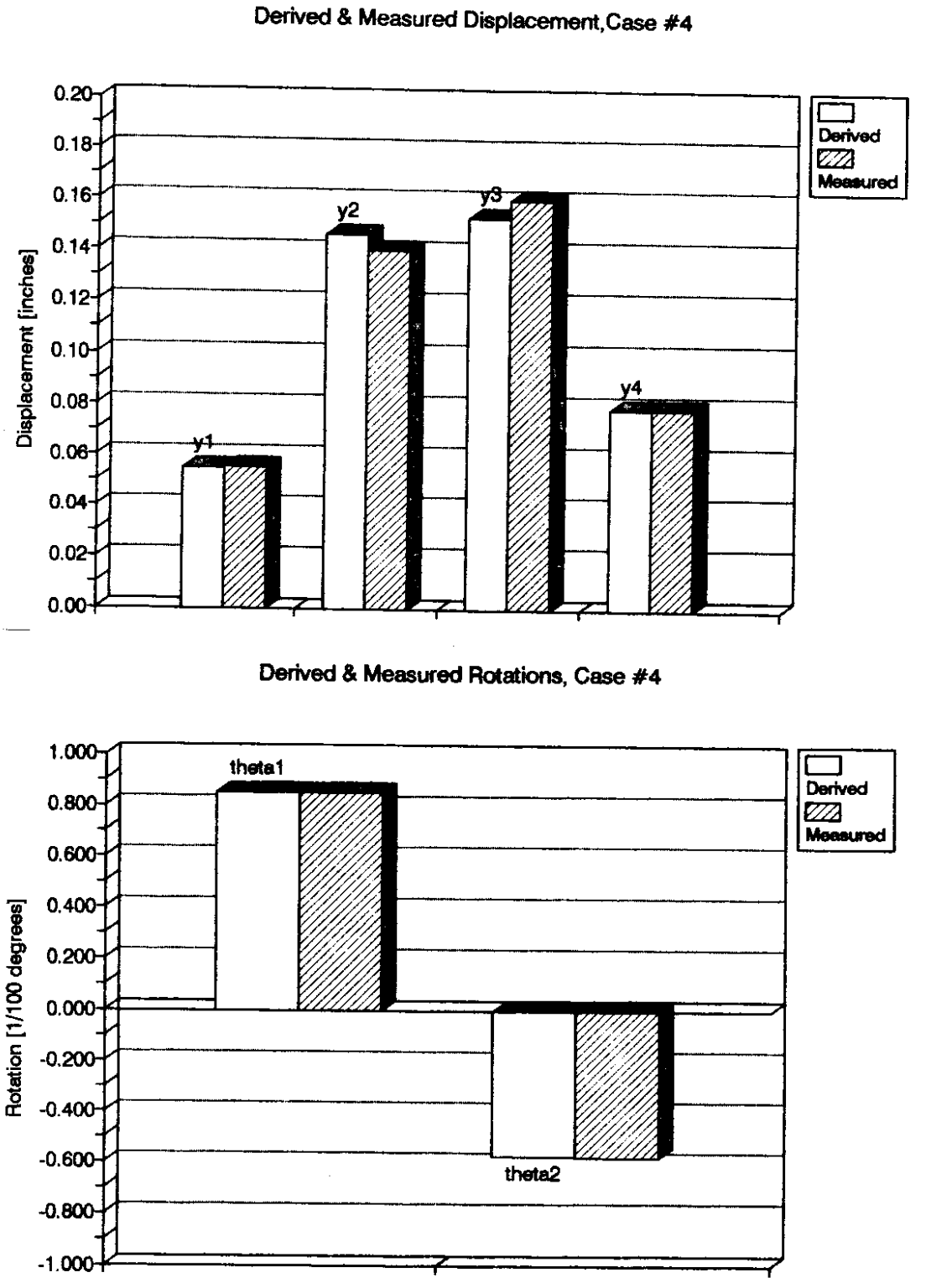

Figure 6.12. Comparison of Fitted and Measured Displacements for UW Simplified Model

Table 6.5. Derived Secant Stiffnesses for UW Simplified Model

			Derived Stiffnesses and EI					Assumed Stiffnesses and G		
Trial #	Bridge Test Cycle	Description of Trial	EI, Bridge Span	Ky1, West Abutment	Ky4, East Abutment	Kr1, West Abutment Rotation	Kr4, East Abutment Rotation	Kybent, Bent	Krbent, Bent Rotation	G, Bridge Span
1	ISOS1	Basic model; symmetric component of response	arbitrary	0	0	0.00E+00	0.00E+00	(Derived) 2.10E+02	0.00E+00	infinite
2	EXCN1	Basic model; symmetric component of response	9.00E+10 -40%	160 -97%	160 -95%	5.35E+08 20%	5.35E+08 -29%	210	2.40E+07	infinite
3	IIS1	Basic Model	1.20E+11 -20%	2230 -54%	1380 -61%	3.88E+08 -13%	7.62E+08 1%	210	2.40E+07	infinite
4	IS1	Basic model	1.50E+11	4800	3500	4.45E+08	7.55E+08	210	2.40E+07	infinite
5	IS1	Kybent=0	1.70E+11 13%	5350 11%	3950 13%	4.95E+08 11%	8.45E+08 12%	0	2.40E+07	infinite
6	IS1	2 X assumed Kybent	1.35E+11 -10%	4250 -11%	3100 -11%	3.95E+08 -11%	6.65E+08 -12%	420	2.40E+07	infinite
7	IS1	Kybent=0; Krbent=0	1.58E+11 5%	4750 -1%	3500 0%	4.45E+08 0%	7.65E+08 1%	210	0	infinite
8	IS1	2 X assumed Krbent	1.45E+11 -3%	4750 -1%	3500 0%	4.45E+08 0%	7.55E+08 0%	210	4.80E+07	infinite
9	IS1	G=E/2	2.70E+11 80%	4700 -2%	3550 1%	3.15E+08 -29%	6.20E+08 -18%	210	2.40E+07	2.30E+03
		Minimum (Trials 4-9):	1.35E+11	4250	3100	3.15E+08	6.20E+08			
		Maximum (Trials 4-9):	2.70E+11	5350	3950	4.95E+08	8.45E+08			
		Average (Trials 4-9):	1.71E+11	4767	3517	4.23E+08	7.34E+08			

Notes:
All units in kips, inches, seconds, and radians
Percentages in cells are percentage increases or decreases over those values in Trial #4

that, if the bent stiffness was fixed, incorporating the shear modulus, G, for the bridge spans into the model increased the derived bridge span flexural rigidity, EI, by 80 percent; changes in other stiffnesses were less than 30 percent.

Table 6.6 presents the sensitivity of the derived component secant stiffnesses to changes in measured displacement for the IS1 test half-cycle maximum applied loading (Trials 10-12). Derived stiffnesses changed less than approximately 27 percent for a 10 percent increase in the translations of the abutments and bents. Derived stiffnesses changed less than approximately 11 percent for a 10 percent increase in the rotation of the abutments.

Comparison of Secant Stiffnesses

The researchers computed the abutment and bent component secant stiffnesses for the UW simplified models (derived), UW models, UW modified models, CALTRANS, and WSDOT models. Table 6.7 lists these stiffnesses for the bridge under isolated, excavated, and initial conditions. For the isolated bridge, the bent secant stiffness of the UW model was equal to the derived value, whereas the stiffnesses from the CALTRANS and WSDOT models were just over 70 percent of the derived value.

Under excavated conditions, the bent secant stiffness of the UW model and UW modified model were nearly the same as the derived value from Trial 1. The derived abutment secant stiffness for the UW model was over three times the derived value, whereas the value from the UW modified model was 34 percent greater than the derived value.

For the bridge under initial conditions, the derived abutment secant stiffness and the abutment secant stiffness from the UW modified model were within 12 percent of each other, but the bent stiffness from the UW modified model was 176 percent of the value from Trial 1. Such a discrepancy was consistent with the fact that columns were not initially cracked for the UW modified model under initial conditions. In contrast, the columns were initially cracked in ISOS1, the cycle from which the bent secant stiffness was derived (Trial 1). The abutment secant stiffnesses from the UW, CALTRANS, and WSDOT models were less than 25 percent of the derived value. The bent secant stiffnesses of the CALTRANS and WSDOT models were less than

Table 6.6. Sensitivity Analyses for Derived Stiffnesses

			Derived Stiffnesses and EI					Assumed Stiffnesses and G		
Trial #	Bridge Test Cycle	Description of Trial	EI, Bridge Span	Ky1, West Abutment	Ky4, East Abutment	Kr1, West Abutment Rotation	Kr4, East Abutment Rotation	Kybent, Bent	Krbent, Bent Rotation	G, Bridge Span
10	IS1	Basic model; increase bent displacement by 10%	1.10E+11 -27%	4800 0%	3450 -1%	4.90E+08 10%	7.90E+08 5%	210	2.40E+07	infinite
11	IS1	Basic model; increase abutment displacement by 10%	1.80E+11 20%	4350 -9%	3200 -9%	4.20E+08 -6%	7.28E+08 -4%	210	2.40E+07	infinite
12	IS1	Basic model; increase abutment rotation by 10%	1.65E+11 10%	4750 -1%	3550 1%	3.70E+08 -17%	6.70E+08 -11%	210	2.40E+07	infinite

Notes:
All units in kips, inches, seconds, and radians
Percentages in cells are percentage increases or decreases over those values in Trial #4

Table 6.7. Comparison of Model Secant Stiffnesses

Bridge Environment & Bridge Test Cycle	Name of Model	Average Secant Stiffnesses	
		Abutment	Bent
Initial Bridge (IS1)	Derived	4150 (Trial #4)	210 (Trial #1)
	Modified	3637 -12%	369 76%
	UW	908 -78%	247 18%
	CALTRANS	708 -83%	137 -35%
	WSDOT	83 -98%	142 -32%
Excavated Bridge (EXCN1)	Derived	160 (Trial #2)	210 (Trial #1)
	Modified	215 34%	223 6%
	UW	685 328%	232 10%
Isolated Bridge (ISOS1)	Derived		210 (Trial #1)
	UW		223 6%
	CALTRANS		137 -35%
	WSDOT		142 -32%

Notes:
All units in kips, inches, radians, seconds
The secant stiffnesses are at the maximum loading in the bridge test cycles
The percentage in each cell is the value as a percentage increase or decrease over the derived value with the exception of the isolated bridge data set in which the percentage increase or decrease is over the derived value.

70 percent of the derived value. The bent secant stiffness from the UW model was 118 percent of the derived value from Trial 1.

6.7 COMPARISON OF MODELS

Important parameters from the UW, UW modified, CALTRANS, WSDOT, and UW simplified finite element bridge models are summarized in Table 6.8. Significant differences among the models include the abutment stiffness, bent stiffness, superstructure flexural rigidity, EI, and rotational resistance at the abutments.

It is likely that the UW model underestimated the abutment stiffness because the soil resistance was underestimated. CALTRANS underestimated the abutment stiffness because it did not model the polystyrene, bearing pads, and soil friction at the abutments. For cycle IS1, the abutment secant stiffness for the CALTRANS model was less than 25 percent of the abutment stiffness of the UW modified model. The WSDOT also neglected the resistance provided by the polystyrene, bearing pads and soil friction. In addition, the soil resistance of the WSDOT model was much less than in the UW, UW modified, and CALTRANS models. As a result, the abutment secant stiffness from the WSDOT model was less than 3 percent of the abutment secant stiffness from the UW modified model.

For test half-cycle IS1, the bent secant stiffness from the UW model was 67 percent of the bent secant stiffness of the UW modified model. This was attributable primarily to the decrease in column cracking in the UW modified model which, in turn, was attributable to greater abutment stiffness. Bent secant stiffnesses from the CALTRANS and WSDOT models were both approximately 60 percent of the bent secant stiffness from the UW modified model for a test half-cycle IS1 maximum applied loading.

The CALTRANS and WSDOT isolated models were too flexible primarily because the soil around the base of the columns was not modeled. Additional flexibility in the CALTRANS model could be attributed to the use of a modulus of elasticity of the column concrete that was approximately 80 percent of the measured value. Further, CALTRANS underestimated the moment of inertia about a horizontal axis of the bent crossbeam and diaphragm by neglecting the

Table 6.8. Summary of UW, UW Modified, CALTRANS and WSDOT Models

Item	UW	UW MODIFIED	CALTRANS	WSDOT	UW SIMPLIFIED
Abutment Transverse Stiffness:	908 kips/in. at IS1 max. ldg.	3,637 kips/in. at IS1 max. ldg.	708 kips/in.	83 kips/in.	4,200 kips/in. (from Trial 4, IS1)
Polystyrene	Yes	Yes	No	No	
Bearing pads	Yes	Yes	No	No	
Soil friction	Yes	Yes	No	No	
Soil resistance at wingwall	90 kips/in.	792 kips/in.	708 kips/in.	83 kips/in.	
Abutment Longitudinal Stiffness:	varies with load	varies with load	3,283 kips/in.	3,660 kips/in.	
Polystyrene	Yes	Yes	No	No	
Bearing pads at abutment	Yes	Yes	No	No	
Soil resistance	175 kips/in.	2,555 kips/in.	3,283 kips/in.	3,660 kips/in.	
Rotational soil resistance at abutment:	Yes	Yes	No	No	
Bent Transverse Stiffness:	247 kips/in. at IS1 max. ldg.	369 kips/in. at IS1 max. ldg.	137 kips/in.	142 kips/in.	210 kips/in.
Non-linear column behavior (cracking, etc.)	Yes	Yes	No	No	
Soil resistance around base of column	Yes	Yes	No	No	
Rotational soil resistance at column footing	Fixed	Fixed	Fixed	4.3x10^6 kip-in./deg.	
Translational soil resistance at column footing	Fixed	Fixed	Fixed	9,308 kips/in.	
Vertical soil resistance at column footing	Fixed	Fixed	Fixed	4,303 kips/in.	
Bridge Span:					
Concrete Modulus, Ec	4,600 ksi	4,600 ksi	3,600 ksi	4,400 ksi	
Moment of Inertia, I			9.6x10^7 in.^4	1.5 x 10^8 in.^4	
Flexural Rigidity, EI			3.5x10^11 kip-in.^2	6.5x10^11 kip-in.^2	1.5x10^11 kip-in.^2 (from Trial 4, IS1)
Column:					
Concrete Modulus, Ec	4,600 ksi	4,600 ksi	3,300 ksi	3,600 ksi	
Uncracked moment of Inertia, I	90,000 in.^4	90,000 in.^4	83,000 in.^4	83,000 in.^4	
Crossbeam:					
Concrete Modulus, Ec	4,600 ksi	4,600 ksi	3,300 ksi	3,600 ksi	
Moment of Inertia, I	infinite	infinite	164,000 in.^4	1,239,000 in.^4	

contribution from the diaphragm. Neglecting the bent diaphragm lead to more rotation at the top of a column which, in turn, added to the flexibility of the bent. Additional flexibility in the WSDOT model could be attributed to the use of soil springs at the footings that were too flexible. The measured bent secant stiffness used from the UW simplified model was approximately one half of the secant stiffness from the UW modified model for test half-cycle IS1.

The flexural rigidity of the superstructure, EI, could not be determined directly from the UW and UW modified models. For the WSDOT model, EI was nearly twice that of the CALTRANS model. The flexural rigidity of the bridge spans directly influenced the distribution of the applied load to the abutments and bents.

Rotational resistance at the abutments also directly affected the distribution of applied load. The UW, UW modified, and UW simplified models incorporated rotational resistance at the abutment, but the CALTRANS and WSDOT models did not.

6.8 SENSITIVITY ANALYSES

An analysis was performed for the UW modified model for the bridge in its initial state to determine the sensitivity of the calculated response to doubling of a single parameter All four of the selected parameters changed the stiffness of the abutments. The parameters doubled were the bearing pad stiffness, soil friction, polystyrene friction, and soil stiffness both at the wingwalls and longitudinally at the abutments.

The load-displacement responses for the abutments and bent for the four trials are shown in Figures 6.13 and 6.14 along with the unaltered UW modified model. Table 6.9 lists the load-displacement slopes of the abutments and bents for the UW modified model sensitivity analysis. At the abutments, doubling the stiffness of the bearing pads had little effect on the load displacement response. Doubling the polystyrene or doubling the soil friction had a similar effect. Both had the overall effect of raising the load-displacement curves by approximately 100 kips. Doubling the soil stiffness at the abutments had the greatest effect on the stiffness of the abutments. Almost no change in load-displacement response was calculated at the bents during the sensitivity analysis.

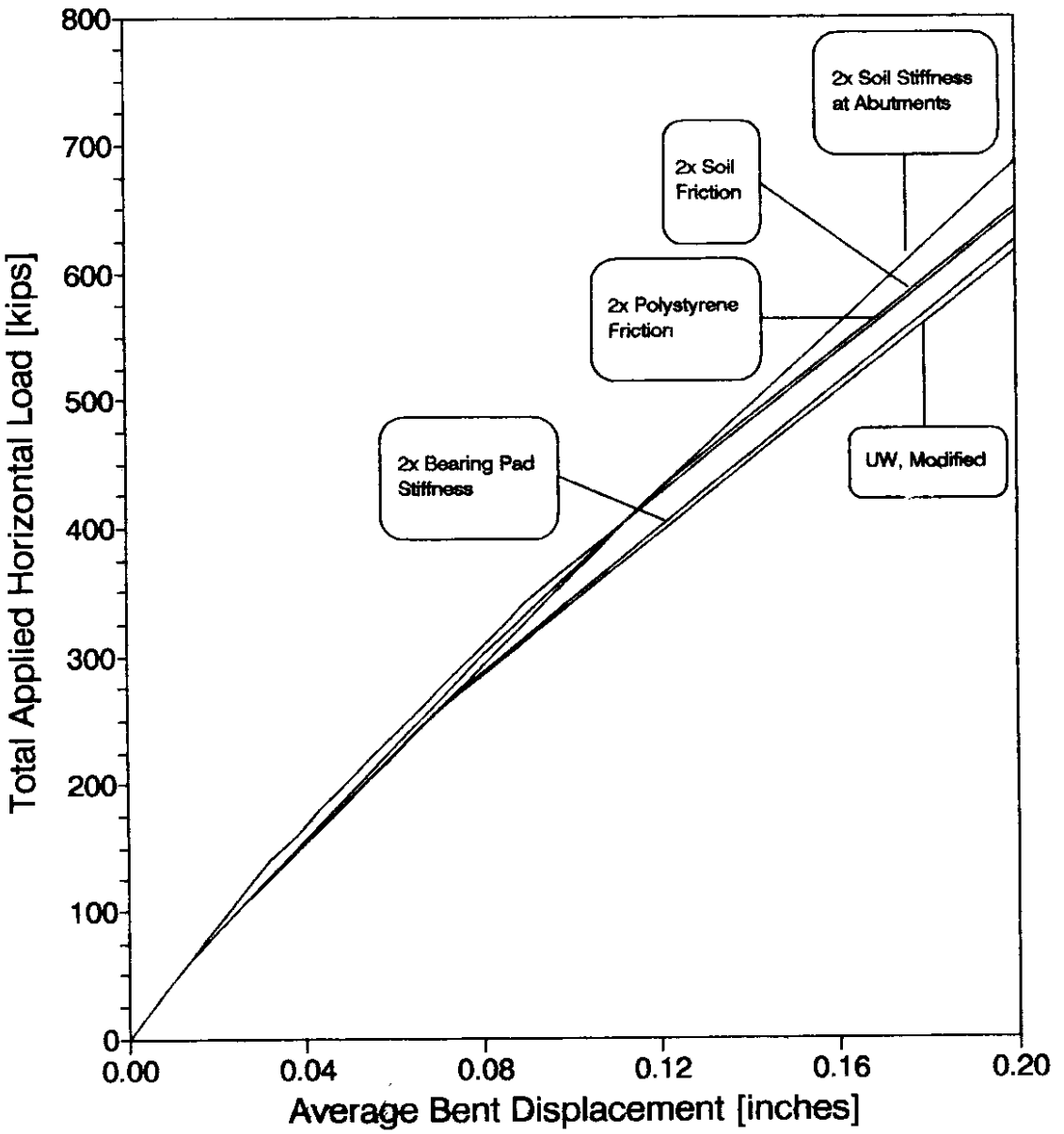

Figure 6.13. Sensitivity Analysis for UW Modified Model - Bent Response

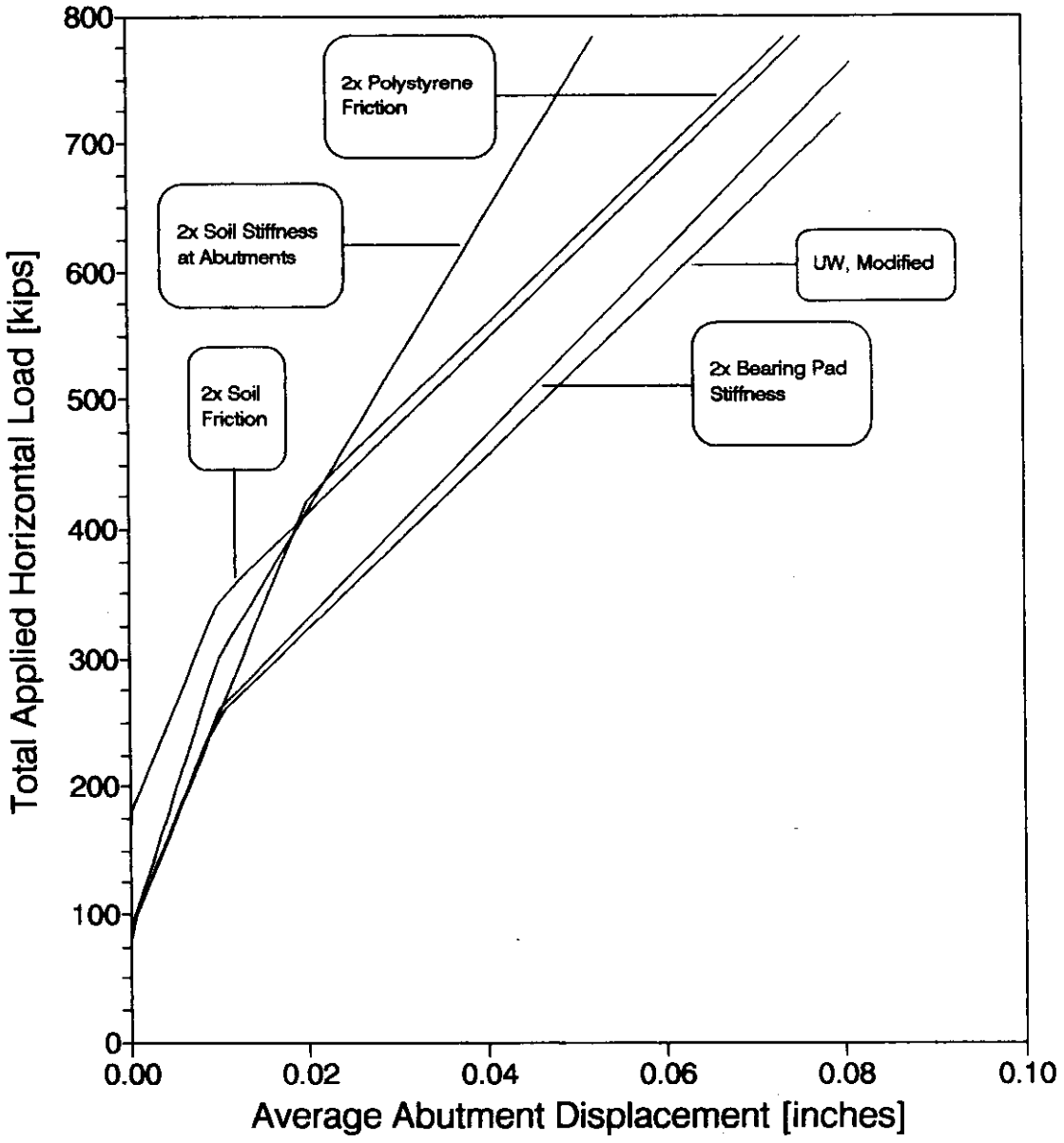

Figure 6.14. Sensitivity Analysis for UW Modified Model - Abutment Response

Table 6.9. Sensitivity Analyses for UW Modified Model

Name of Model	Average Load-Displacement Slopes (LDS)	
	Abutment	Bent
UW Modified	9569	3049
Double Soil Stiffness at Abutments	16366 71%	3455 13%
Double Polystyrene Friction	12515 31%	3274 7%
Double Bearing Pad Stiffness	10163 6%	3121 2%
Double Soil Friction	12078 26%	3250 7%

Notes:
All units in kips, inches, radians, seconds
The LDS's are at the maximum IS1 loading
The percentage in each cell is the value as a percentage increase or decrease over the modified value

CHAPTER 7

RECOMMENDATIONS

7.1 LIMITATIONS OF THE STUDY

Full-scale testing is a feasible means of obtaining data on the large-displacement behavior of a bridge. Such tests do not suffer from some of the constraints imposed by laboratory research, such as the difficulty of reproducing boundary conditions and component sizes. However, conclusions and recommendations on the implications of these tests and analyses should be tempered by the tests' limitations.

The lateral-load tests differed significantly from earthquakes. Earthquake motions are dynamic, whereas the tests performed were essentially static. Earthquake motions include longitudinal, vertical, and torsional components that were not modeled in the tests.

The measured response was not confirmed by repeating the tests with a second bridge. Therefore, the variability of the measured response was not determined. Furthermore, the extent to which the behavior of the test bridge can be confidently extrapolated and applied to other bridges depends on the similarity of the bridges. The continuous superstructure of this bridge coupled the displacements of the abutments and piers. Such coupling does not exist for many simply-supported bridges. The resistance provided by the polystyrene depends on the abutment configuration and is not present in many bridges. The resistance provided by the soil behind the wingwall will be mobilized only if an abutment is sufficiently strong and stiff to transfer the superstructure's transverse shear to the wingwalls. This resistance mechanism may not be present in all bridges. Additionally, the influence of the compacted fill surrounding the columns' bases will vary with the soil properties and embedment depth.

7.2 RECOMMENDATIONS DERIVED FROM THE MEASURED RESPONSE

Despite the limitations of the tests, some observations can be made independent of complex analysis.

The results of these tests should serve as a benchmark. Proposed seismic evaluation procedures should be consistent with the observed response. Proposed analytical models should be evaluated by comparing calculated and measured responses.

The combination of a continuous superstructure and the large abutment resistance made this bridge sufficiently stiff and strong to resist large transverse forces. The bridge's vulnerability to earthquakes can be estimated by considering the bridge as a single-degree-of-freedom system. At an applied load equal to 45 percent of its weight (Test I), damage was limited to minor column cracking. Assuming linear response and a dynamic amplification factor of 2.5, (21) this level of base shear corresponds to an effective peak acceleration of 0.2g. The wingwalls yielded at an applied load equal to 65 percent of the bridge weight (Test II). Therefore, allowing for a dynamic amplification factor of 2.5, the bridge could resist a ground motion of 0.25g with no inelastic demands. The ductile response observed after the wingwalls yielded suggests that the bridge would not have been seriously damaged by an earthquake with an effective peak acceleration of 0.4g.

Despite detailing deficiencies, the pier vulnerability was small for expected ground-motion intensities in western Washington state. Bridges that are similar to the test bridge should be assigned a low priority for retrofitting.

7.3 RECOMMENDATIONS DERIVED FROM ANALYSES

An engineer needs reliable estimates of abutment and superstructure stiffnesses to decide whether piers should be retrofitted. If one neglects components that provide substantial lateral resistance, such as the polystyrene in this case, the evaluation may be unnecessarily conservative. If such components are neglected, detailed modeling of the rest of the structure is not warranted.

For abutment configurations similar to those of the test bridge, the calculated abutment stiffness depends greatly on the estimated soil stiffness. When combined with simple soil tests, relatively simple soil models provided reasonable estimates of soil stiffness for the test bridge. In this study, soil stiffnesses for the wingwalls were calculated with a tabulated estimate of the modulus of subgrade reaction. The soil resistance along the columns was modeled by considering

the column to be a pile. Complex methods of modeling the soil resistance may not be justified if soils test data are not available.

Even for relatively low loads, some bridge components have nonlinear force-deflection relationships. Column cracking, bearing-pad resistance, polystyrene resistance, soil friction, and soil compression are examples of such nonlinear phenomena. The neglect of such phenomena can have profound effects on the predicted behavior, as evidenced by the range of estimated response predicted by the UW, CALTRANS, WSDOT, and UW modified models. Though the benefits of performing nonlinear analysis may not outweigh its costs, analysts should be aware of these nonlinear effects.

ACKNOWLEDGMENTS

The authors are grateful for the effort and support of many people and organizations. Captain O'Donovan, a graduate student at the University of Washington (UW) directed site construction activities. UW undergraduate students S. Clark, R. Mah, and C. Wang helped prepare and conduct the static tests. The loading system was fabricated by Concrete Technology Corporation under the direction of S. Moustafa and N. Peshtaz. The dynamic tests were performed by B. Hushmand and R. Relles from the California Institute of Technology, in cooperation with C. B. Crouse from Dames and Moore, Consulting Engineers. Professor D. McLean of Washington State University provided instrumentation to supplement the instrumentation available at the UW.

UW Professors S. Kramer and R. Holtz provided valuable advice on the geotechnical aspects of this project. Special thanks is given to H. Coffman of WSDOT, as well as J. Gates, T. Cartner, and G. Reyes-Gutierrez of CALTRANS for providing independent analyses of the bridge. This report was prepared with the assistance of UW graduate student S. Rodehaver, S. Ryter, and J. Strout; and TRAC staff members A. O'Brien, R. Porter, and D. Wright.

The project was funded primarily by the WSDOT and the Federal Highway Administration (FHWA). E. Henley served as the technical contact at the WSDOT Office of Bridges and Structures. R. Wang and C. Clark were supported by the National Science Foundation through the Research Experience for Undergraduates Program. Captain O'Donovan was supported by the U.S. Army Corps of Engineers, and G. Hjartarson was supported by the Valle Foundation at the University of Washington.

REFERENCES

1. George, O. and Henley, E.H. Jr., "Bridge Seismic Retrofit Program Recommendations," Washington State Department of Transportation Bridge and Structures Office, report, Olympia, Washington, 1991.

2. Plos, M., Gylltoft, K., and Cederwall, Krister, "Full Scale Shear Tests on Modern Highway Bridges," *Nordic Concrete Research.*, 1990.

3. Varney, R. and Galambos, C., "Field Dynamic Loading Studies of Highway Bridges in the U.S., 1948-1965," *Highway Research Record, No. 76*, Design - Bridges and Structures, pp. 285-305, 1965.

4. Crouse, C.B., Hushmand, B. and Marti, G.R., "Dynamic Soil-Structure Interaction of a Single-Span Bridge," *Earthquake Engineering and Structural Dynamics*, Vol. 15, pp. 711-729, 1987.

5. O'Donovan, T., Eberhard, M.O., Marsh, M.L., and MacLardy, J.A. "Lateral-Load Response of Two Reinforced Concrete Piers," Draft Technical Report, WA-RD 305.2, Washington State Department of Transportation, Olympia, Washington, September 1993.

6. "Standard Specifications for Road and Bridge Construction, "State of Washington Department of Highways, Olympia, Washington, 1964.

7. "1987 Annual Book of ASTM Standards, "American Society for Testing and Materials, Philadelphia, Pennsylvania, 1987.

8. Hjartarson, Gaukur, "A Study of the Behavior of a Highway Bridge Under Lateral Loading, Phase 1: Unaltered Conditions at the Abutments," Master's thesis, Department of Civil Engineering, University of Washington, Seattle, Washington, 1991.

9. "Manual of Standard Practice," Concrete Reinforcing Steel Institute, Schaumburg, Illinois, 1976.

10. Gent, A.N., "On the Relation Between Indentation Hardness and Young's Modulus," *Transactions of the Rubber Industry*, vol. 34, no. 2, 1958.

11. Kulhawy, F.H. and Mayne, P.W., *Manual for Estimating Soil Properties for Foundation Design*, Electric Power Research Power Institute, Final Report, EPRI EL-6800, Pleasant Hill, California, 1990.

12. Terzaghi, K. and Peck, R.B. *Soil Mechanics in Engineering Practice*, John Wiley and Sons, New York, 1967.

13. O'Neill, M.W. and Murchison, J.M., "An Evaluation of P-Y Relationships in Sands," American Petroleum Institute Report PRAC 82-41-1, 1983.

14. Favre, P., "Thermal Movements in The Casper Creek Bridge," Master's thesis, Department of Civil Engineering, University of Washington, Seattle, Washington, 1989.

APPENDIX A

RESPONSE HISTORIES

APPENDIX A

RESPONSE HISTORIES

This appendix presents response histories for the twenty-nine instruments (Section 4.1) that measured significant displacements during Phase I. In each figure, absolute displacement is plotted versus the total applied force. For transverse displacement of the bents and abutments, two plots are shown for each instrument, one for cycles PS3 through IN2 and one for cycles IIS1 through ISON1 (Fig. A.1 to A.12). For the other instruments, all cycles were plotted on the same graph (Fig. A.13 to A.35). The notation for each instrument is described here; the location and designation of each instrument are listed in Table 3.1.

The first letter of the name, E or W, designated whether the instrument was located on the East or West half of the bridge. For the instruments that measured horizontal displacement of the bridge, the second letter, B or D designated whether the instrument measured Bent or Deck displacement. The third letter, N, S, A varied according to whether the instrument was located on the North side, South side or whether it measured displacements with respect to the Abutment pedestal. The fourth letter, T or L, denoted the direction of measured motion, Transverse or Longitudinal.

For the instrumentation that measured column and beam rotation, the second letter, N or S, designated whether the instrument was located near the North or South column. The third letter was C or B according to whether the instrument measured Column or Beam rotation; the fourth letter, T or B, denoted that the instrument was installed at the Top or Bottom of a Column. The following number, 1, 2, or 3, indicated the location of the instrument with respect to the end of the column of beam. The number 1 was given to instruments nearest the end of the member and the number 3 was given to the instruments furthest from the end. The final letter, n or s, varied according to whether the instrument was mounted on the north or south face of the column.

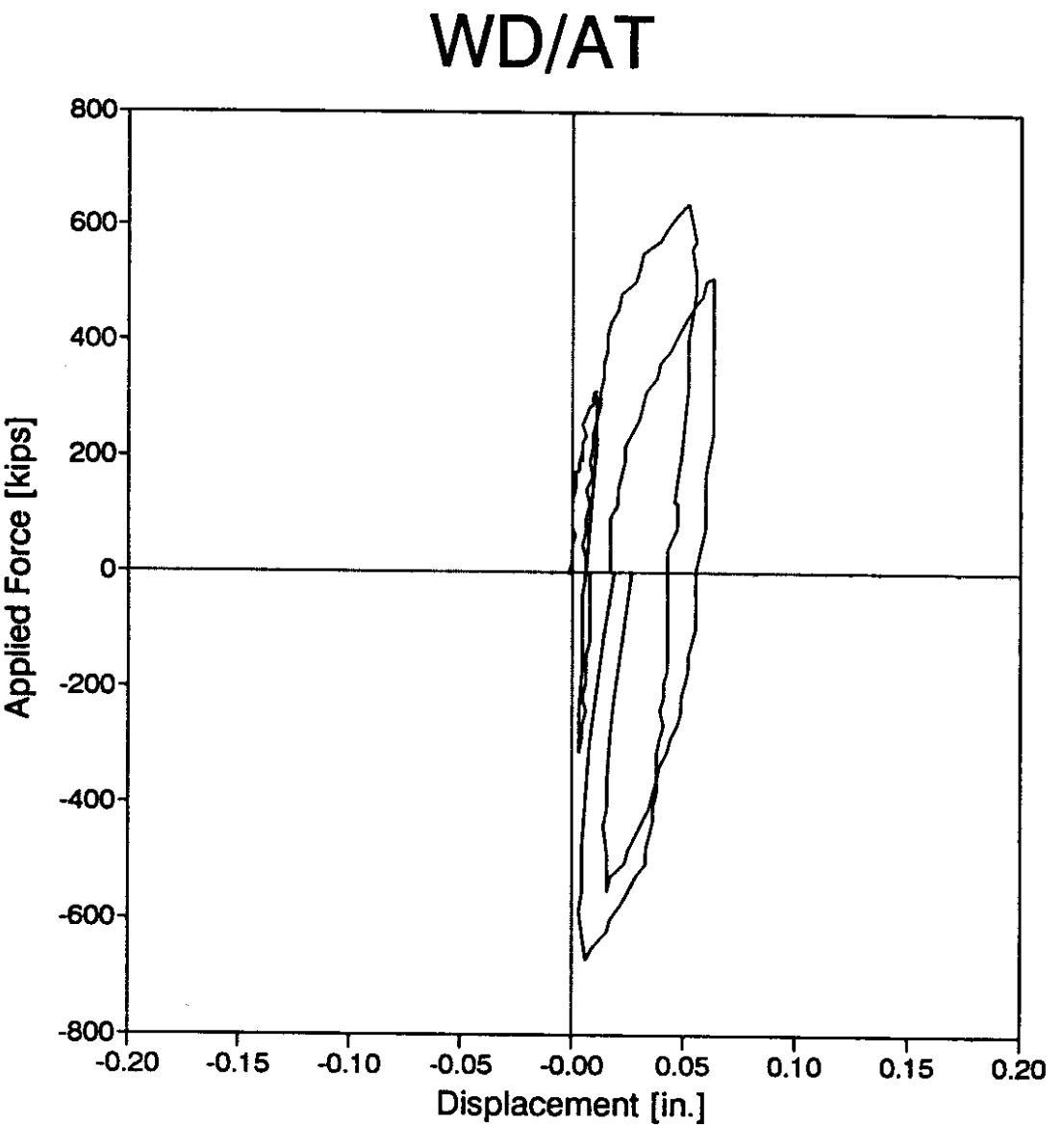

Figure A.1. Relative Displacement Between West Abutment Diaphragm and Pedestal - Tests P and I

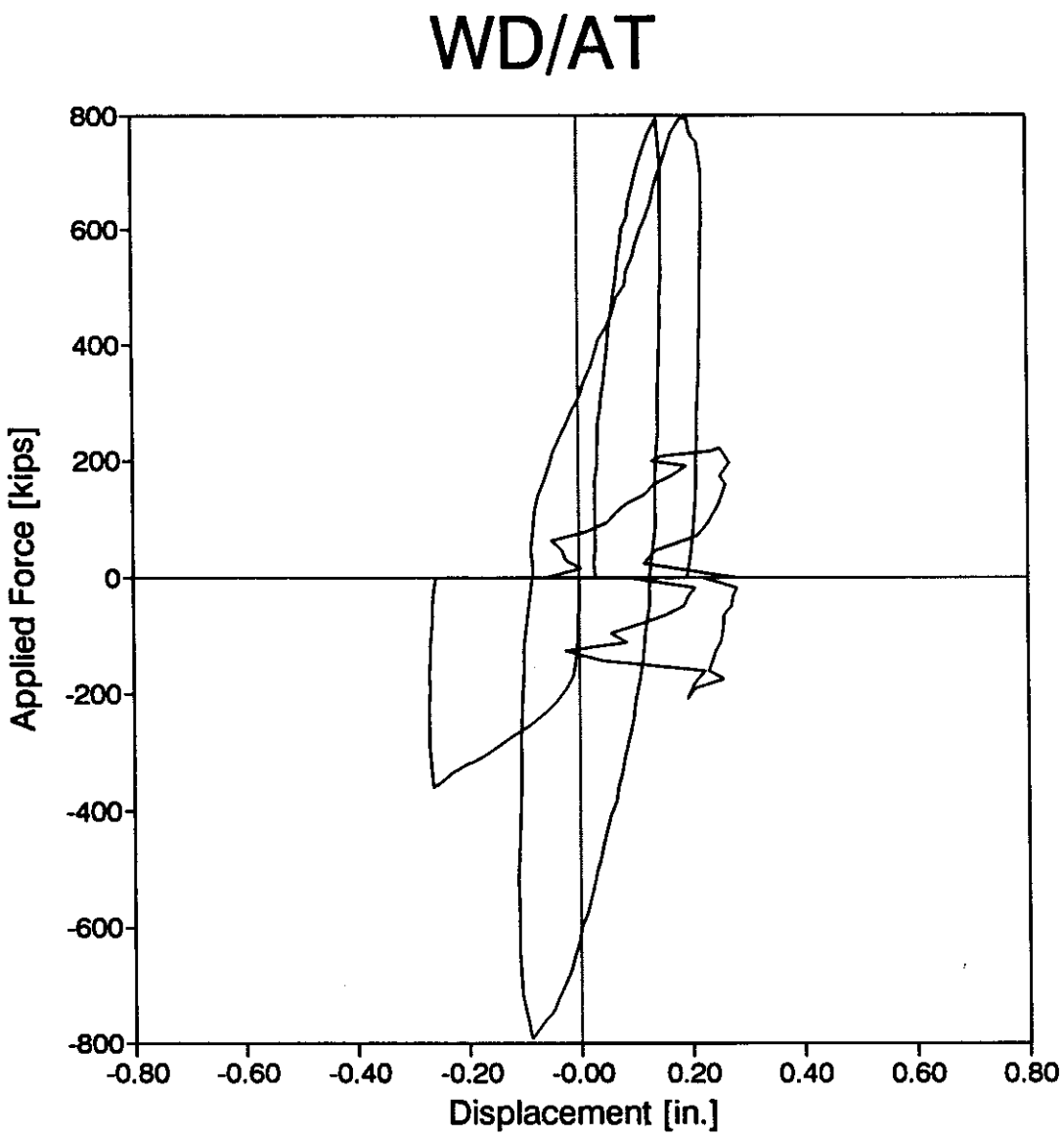

Figure A.2. Relative Displacement Between West Abutment Diaphragm and Pedestal - Tests II, EXC and ISO

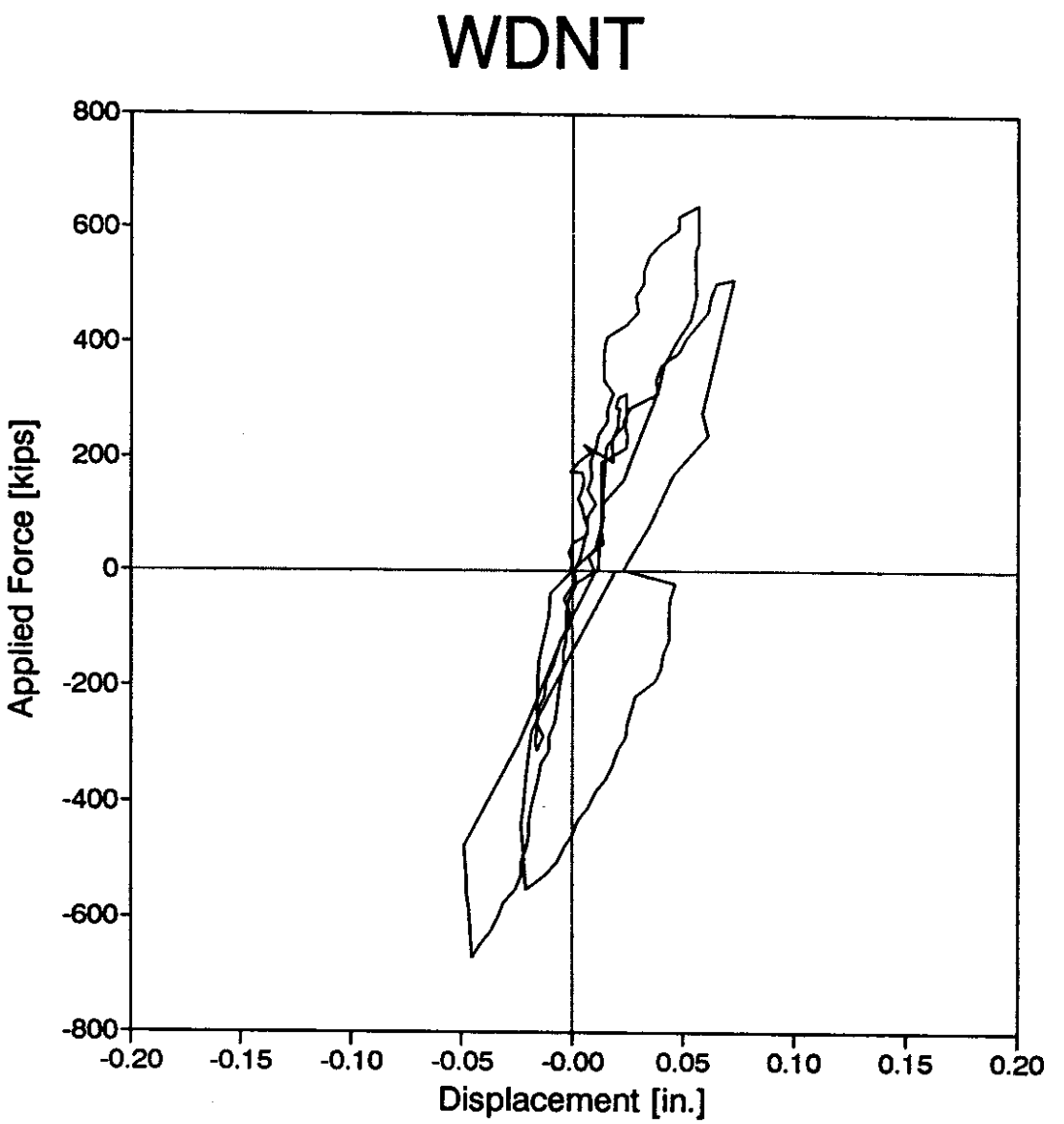

Figure A.3. West Abutment Transverse Displacement History - Tests P and I

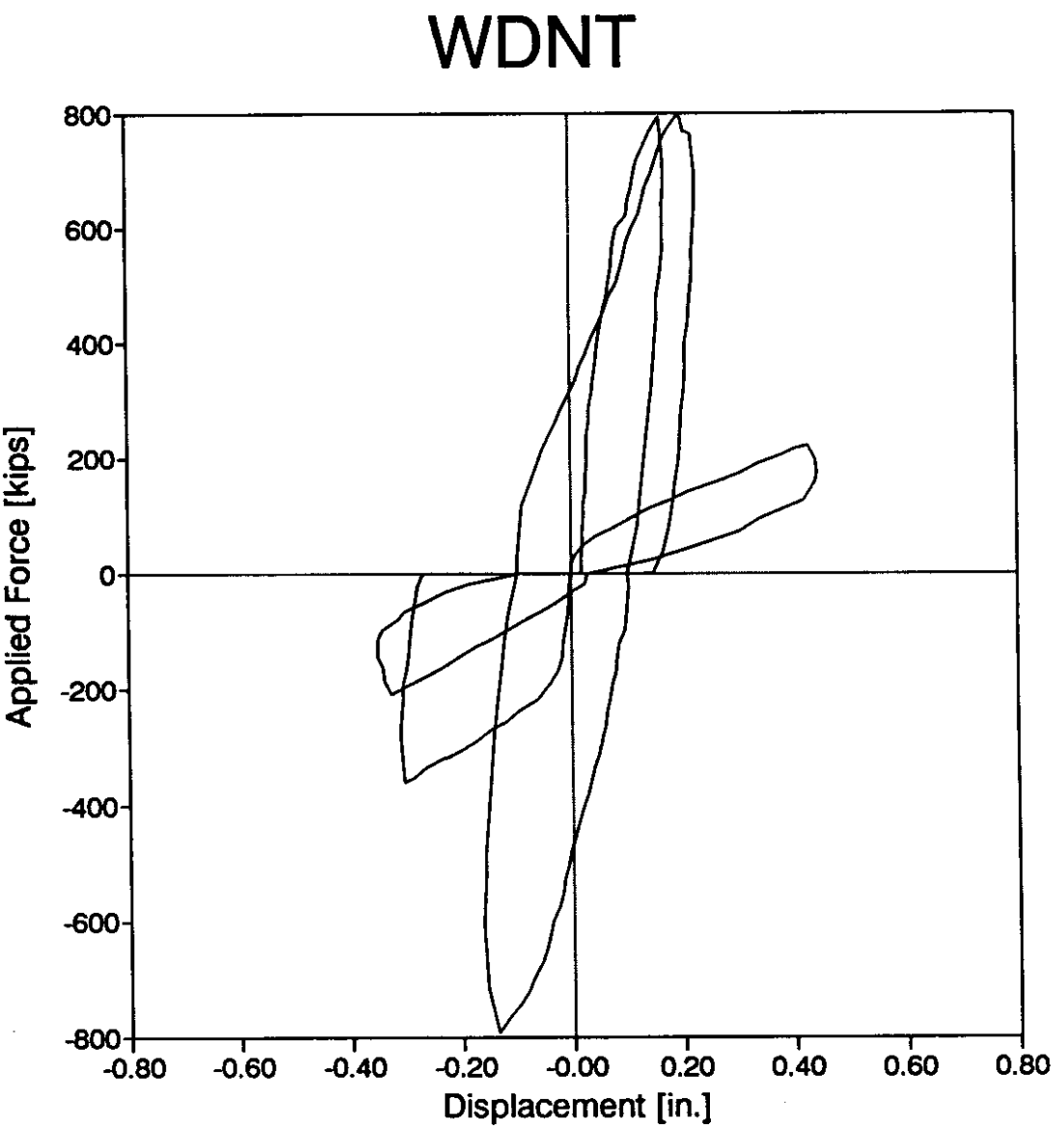

Figure A.4. West Abutment Transverse Displacement History - Tests II, EXC and ISO

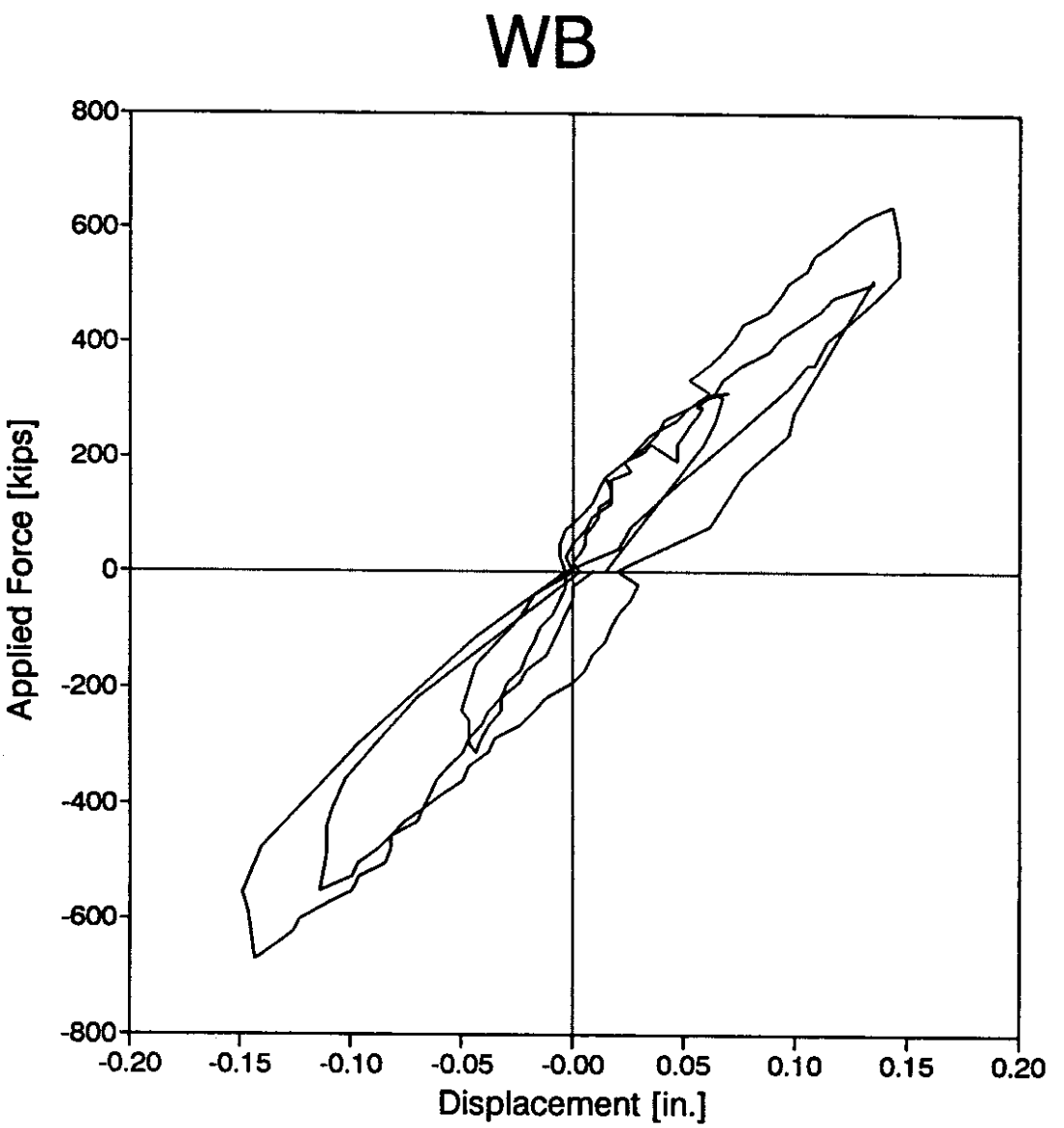

Figure A.5. West Bent Transverse Displacement History - Tests P and I

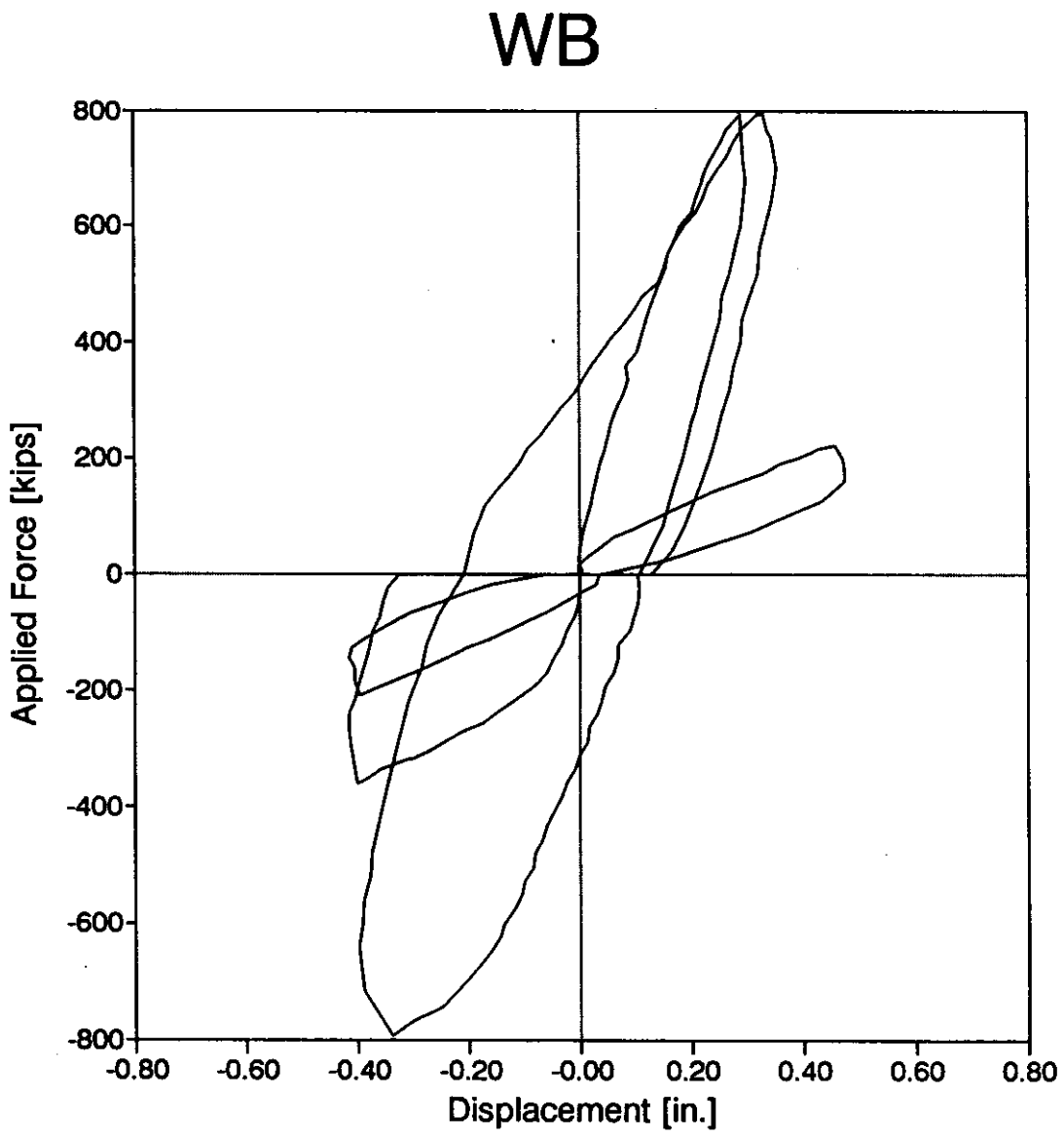

Figure A.6. West Bent Transverse Displacement History - Tests II, EXC and ISO

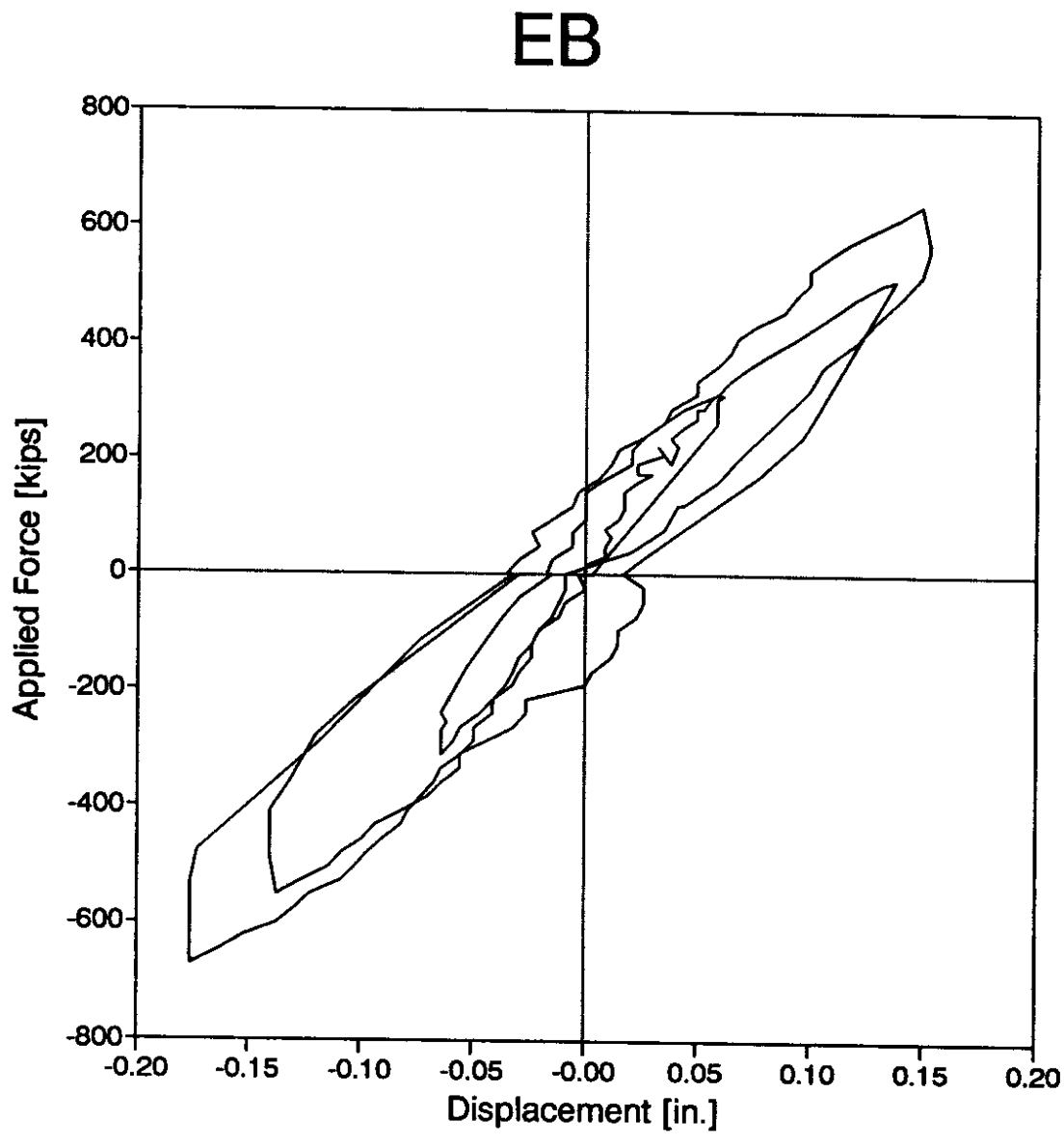

Figure A.7. East Bent Transverse Displacement History - Tests P and I

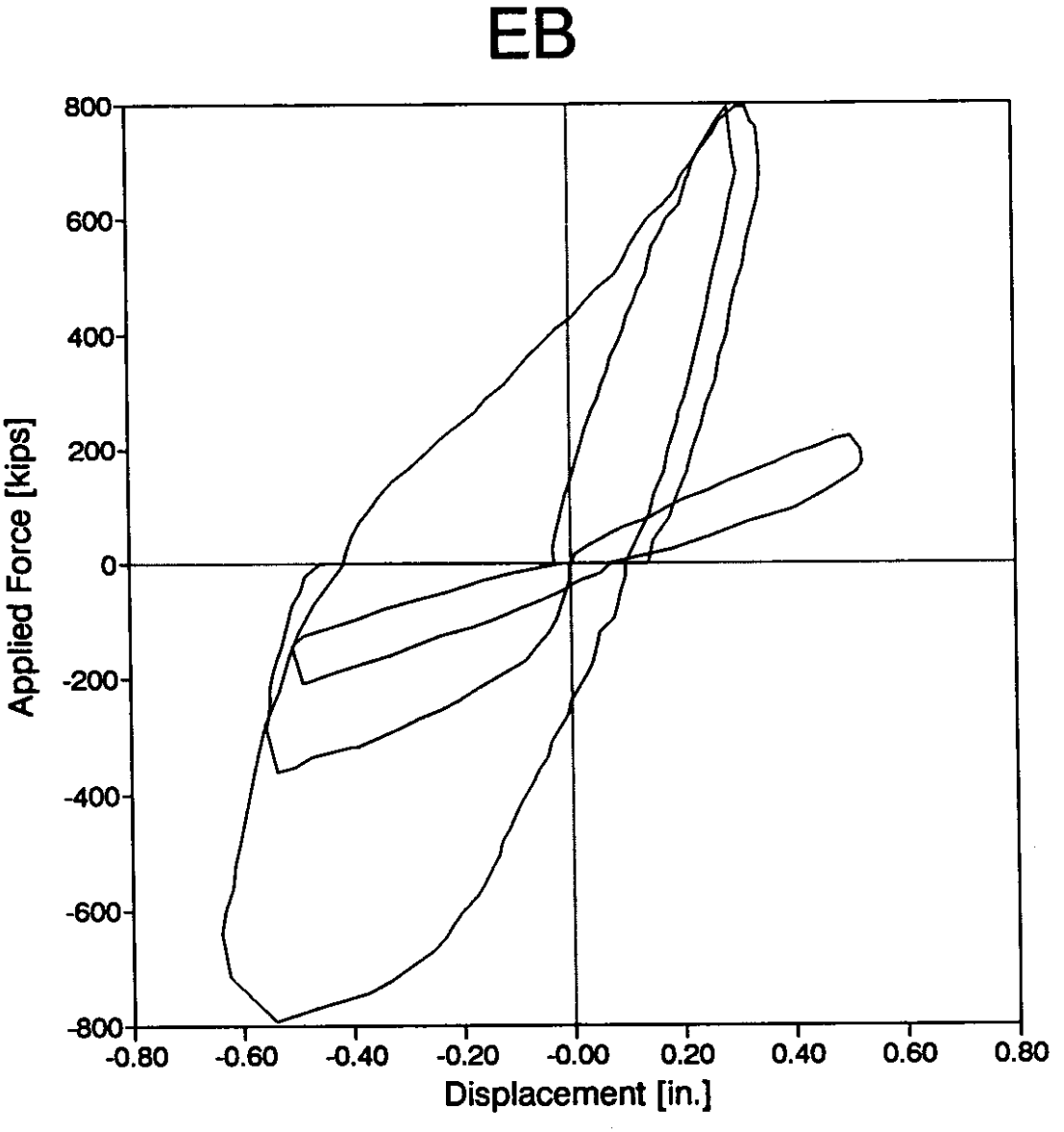

Figure A.8. East Bent Transverse Displacement History - Tests II, EXC and ISO

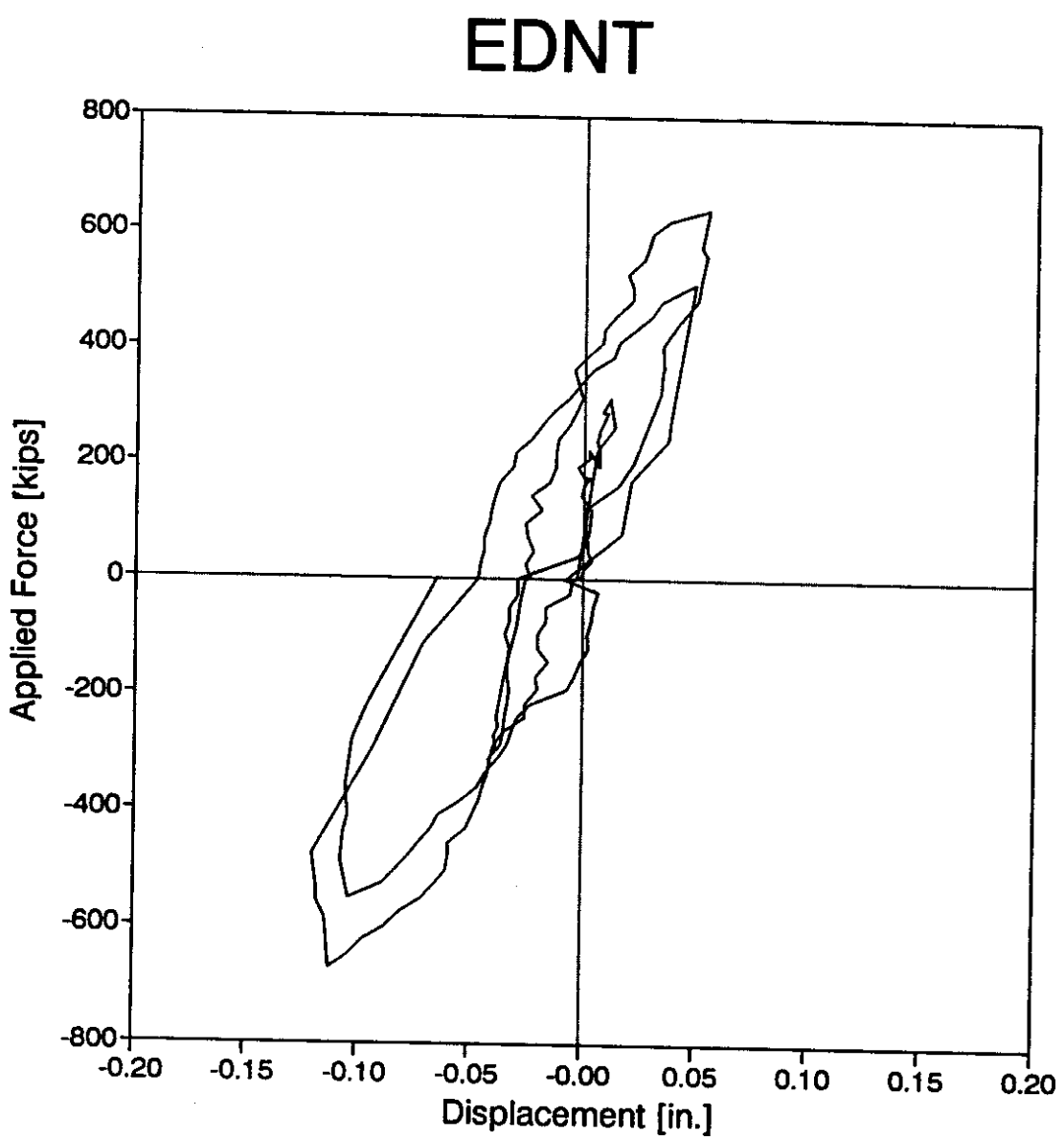

Figure A.9. East Abutment Transverse Displacement History - Tests P and I

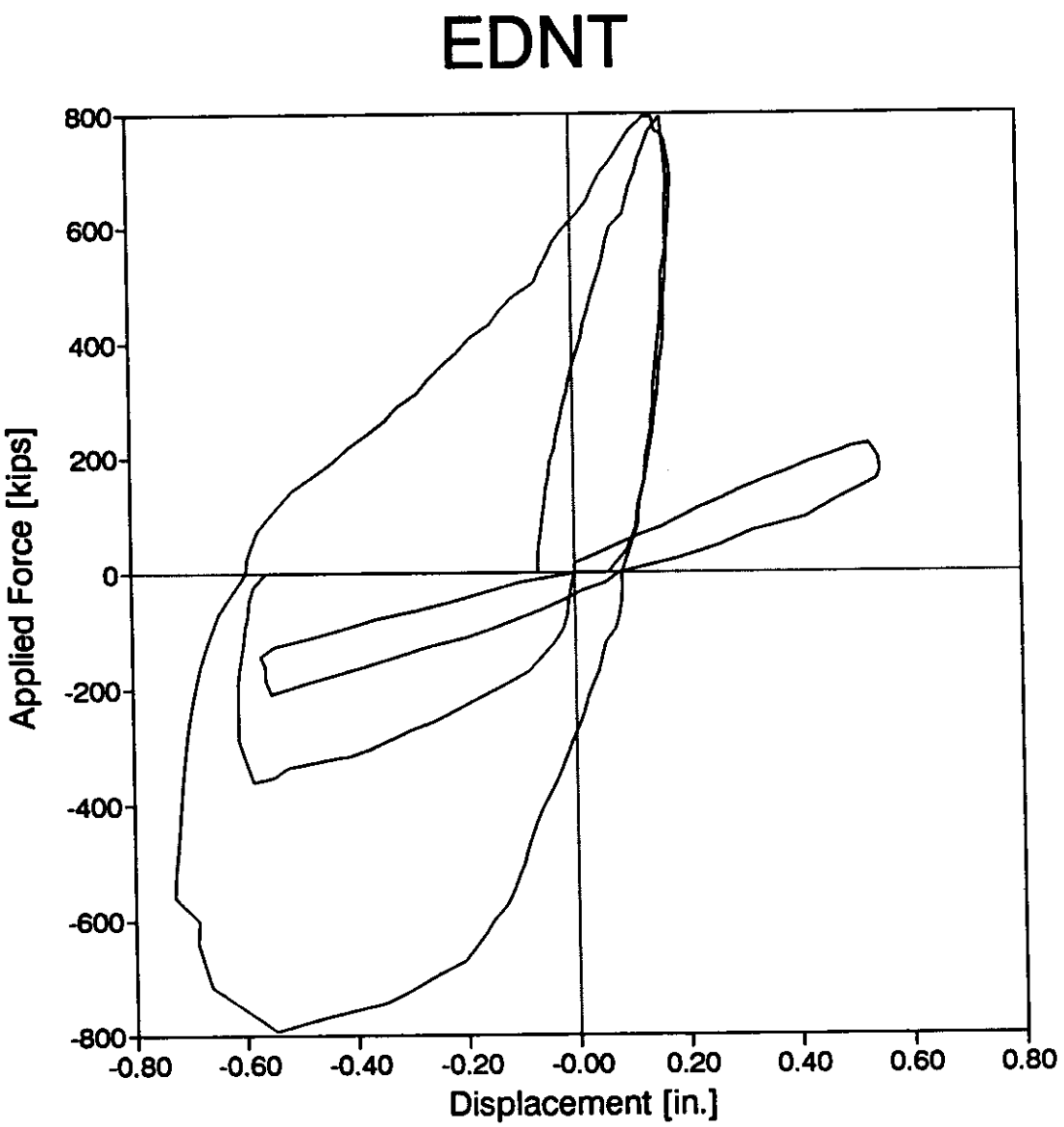

Figure A.10. East Abutment Transverse Displacement History - Tests II, EXC and ISO

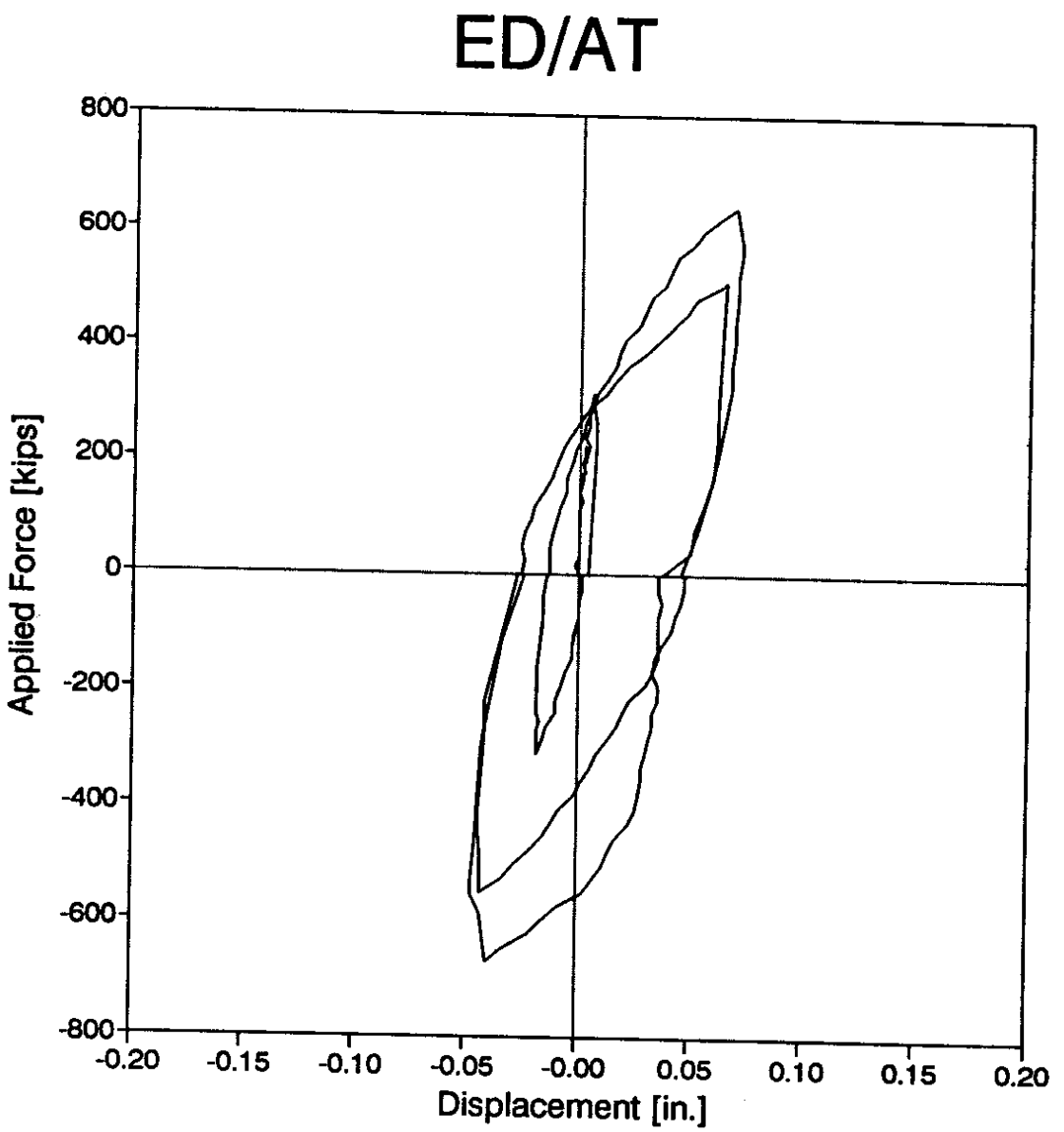

Figure A.11. Relative Displacement Between East Abutment Diaphragm and Pedestal - Tests P and I

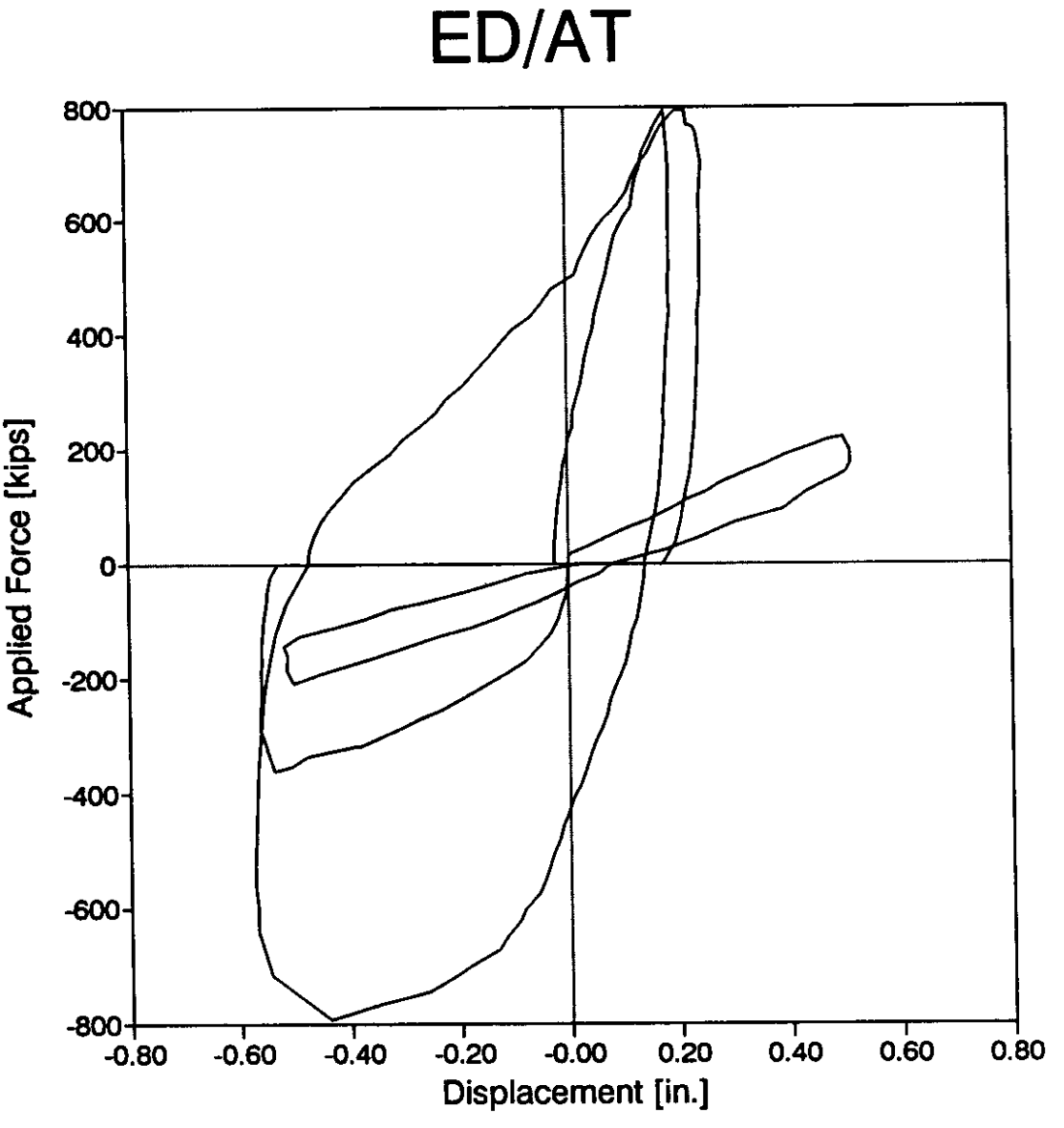

Figure A.12. Relative Displacement Between East Abutment Diaphragm and Pedestal - Tests II, EXC and ISO

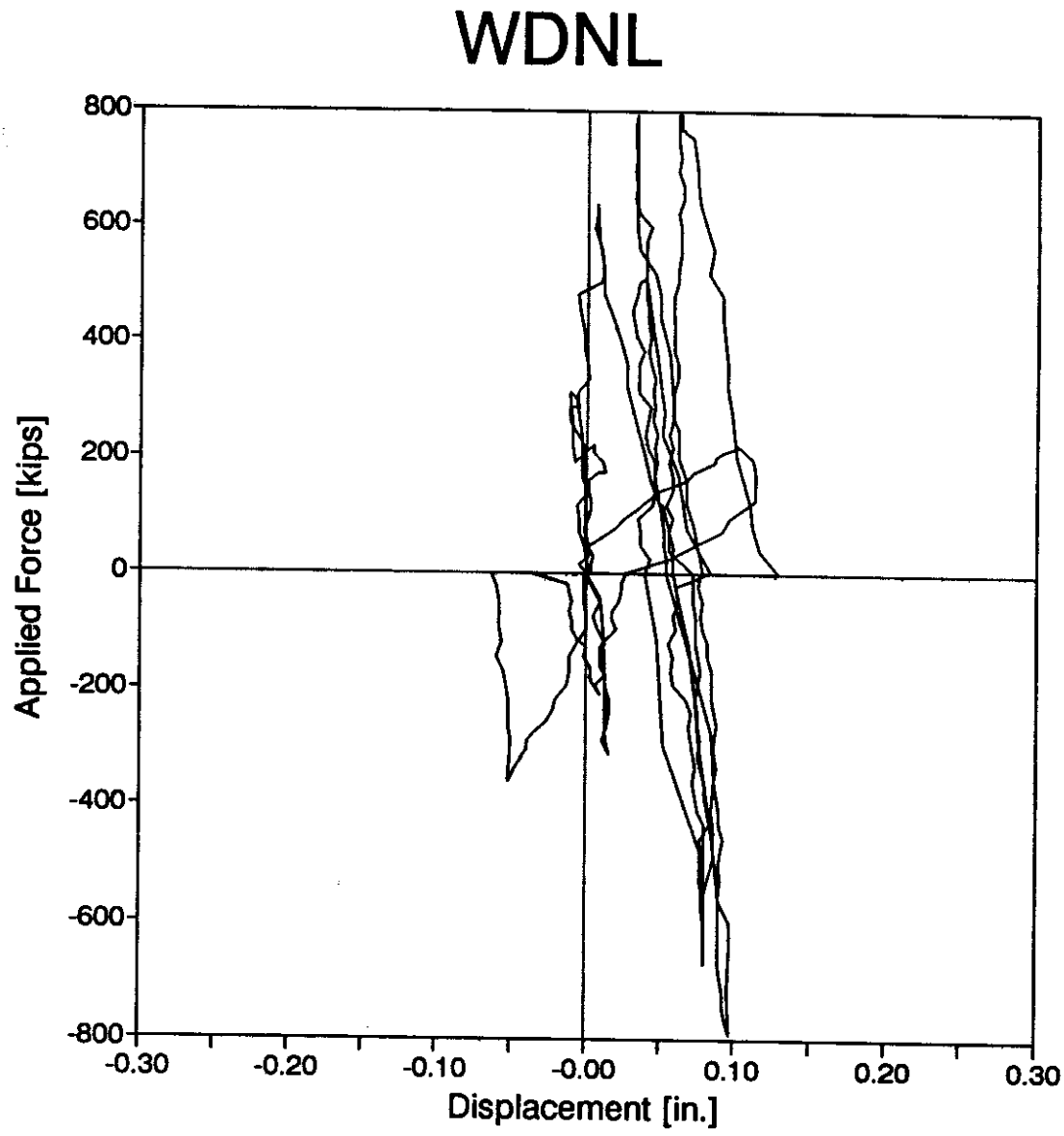

Figure A.13. Longitudinal Displacement of Northwest Corner

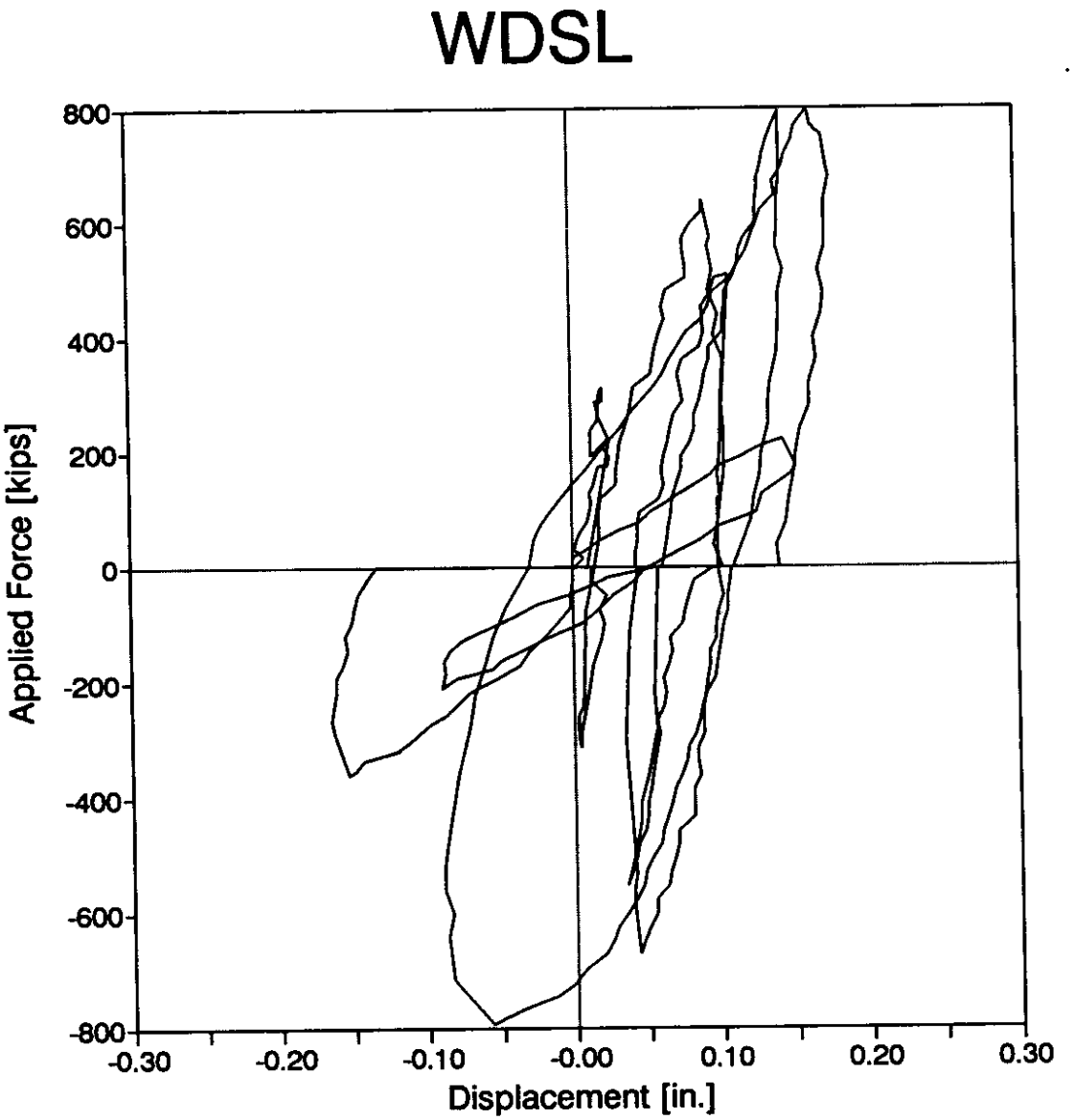

Figure A.14. Longitudinal Displacement of Southwest Corner

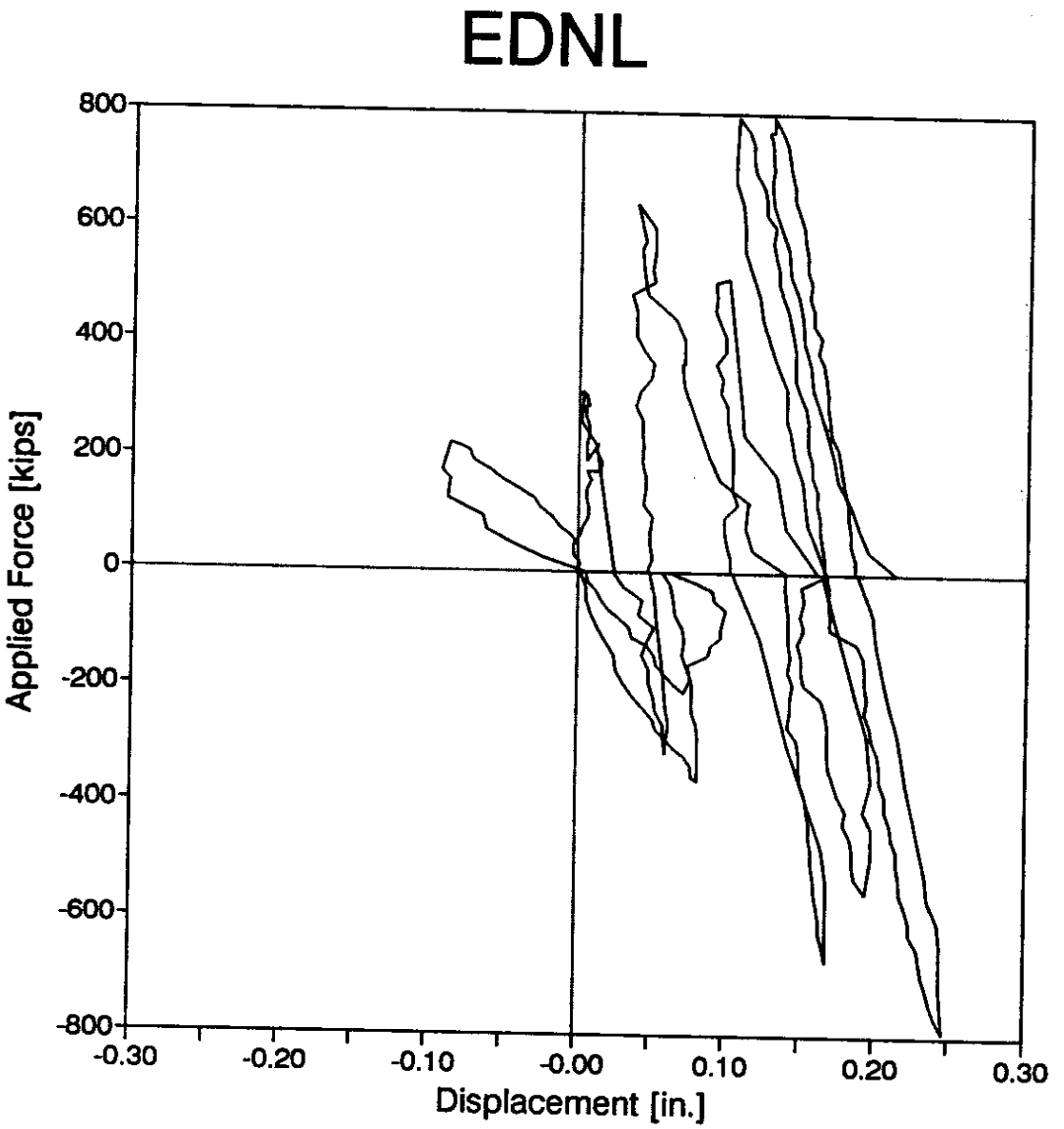

Figure A.15. Longitudinal Displacement of Northeast Corner

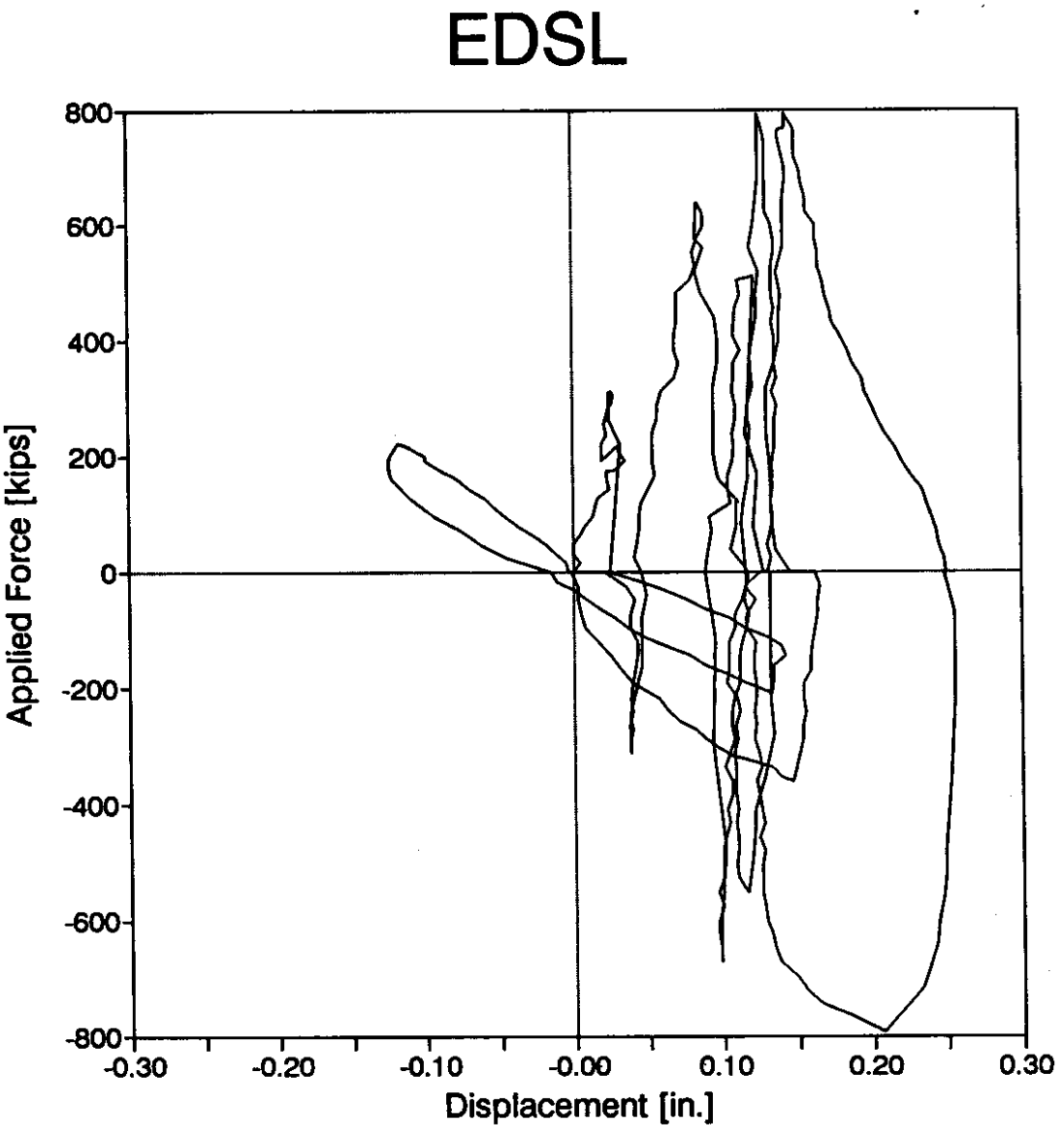

Figure A.16. Longitudinal Displacement of Southeast Corner

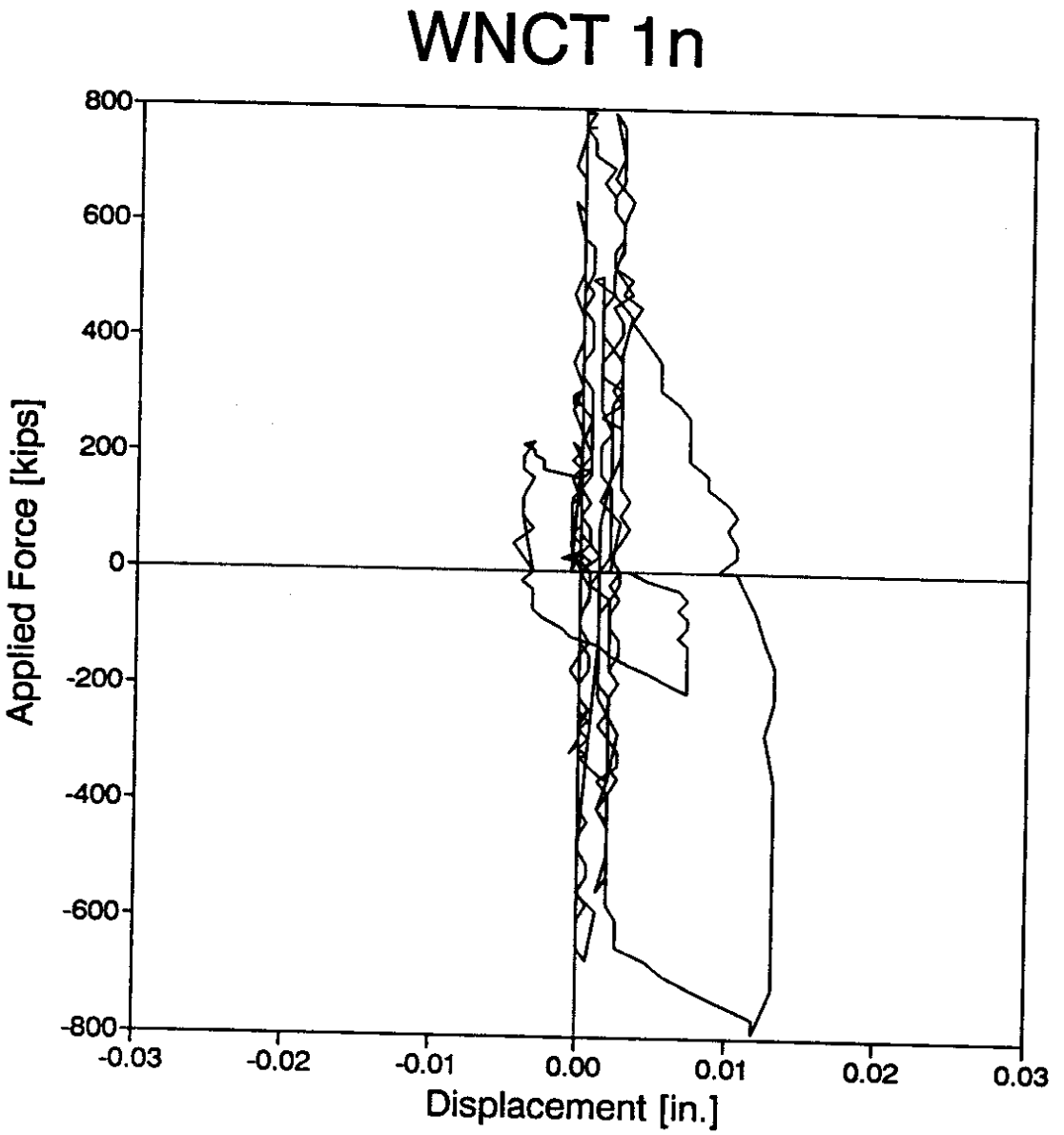

Figure A.17. Response History for WNCT 1n

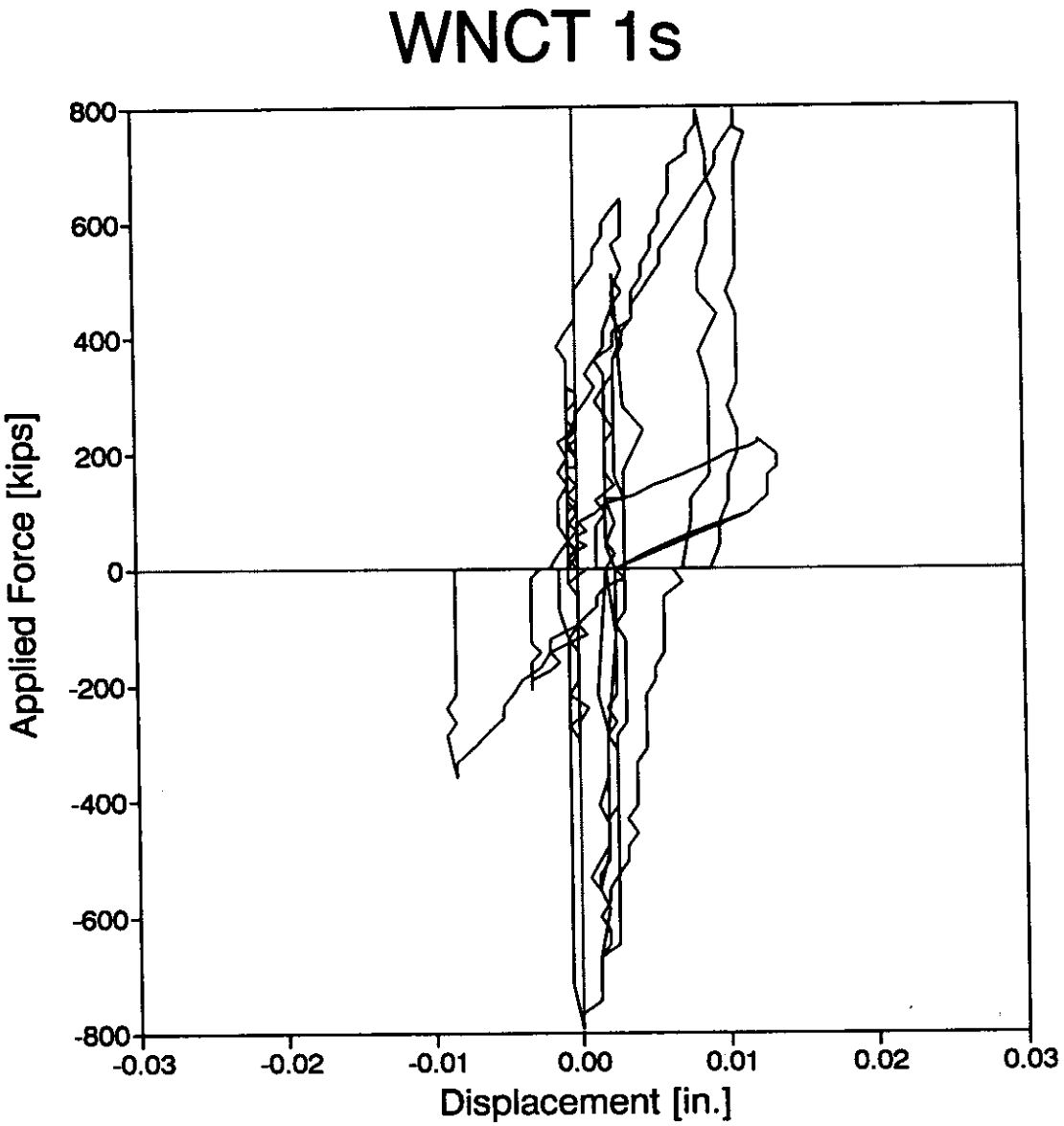

Figure A.18. Response History for WNCT 1s

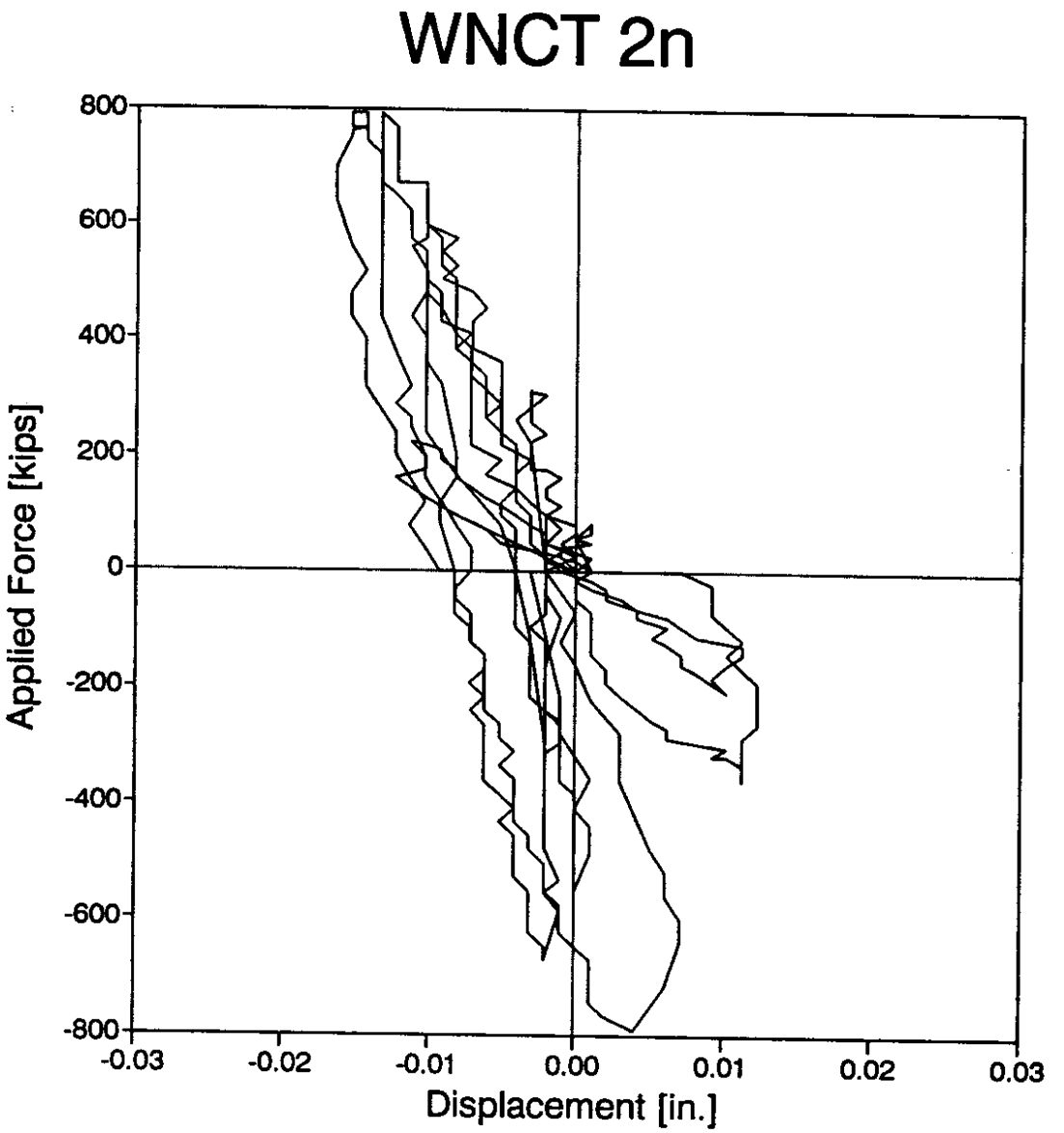

Figure A.19. Response History for WNCT 2n

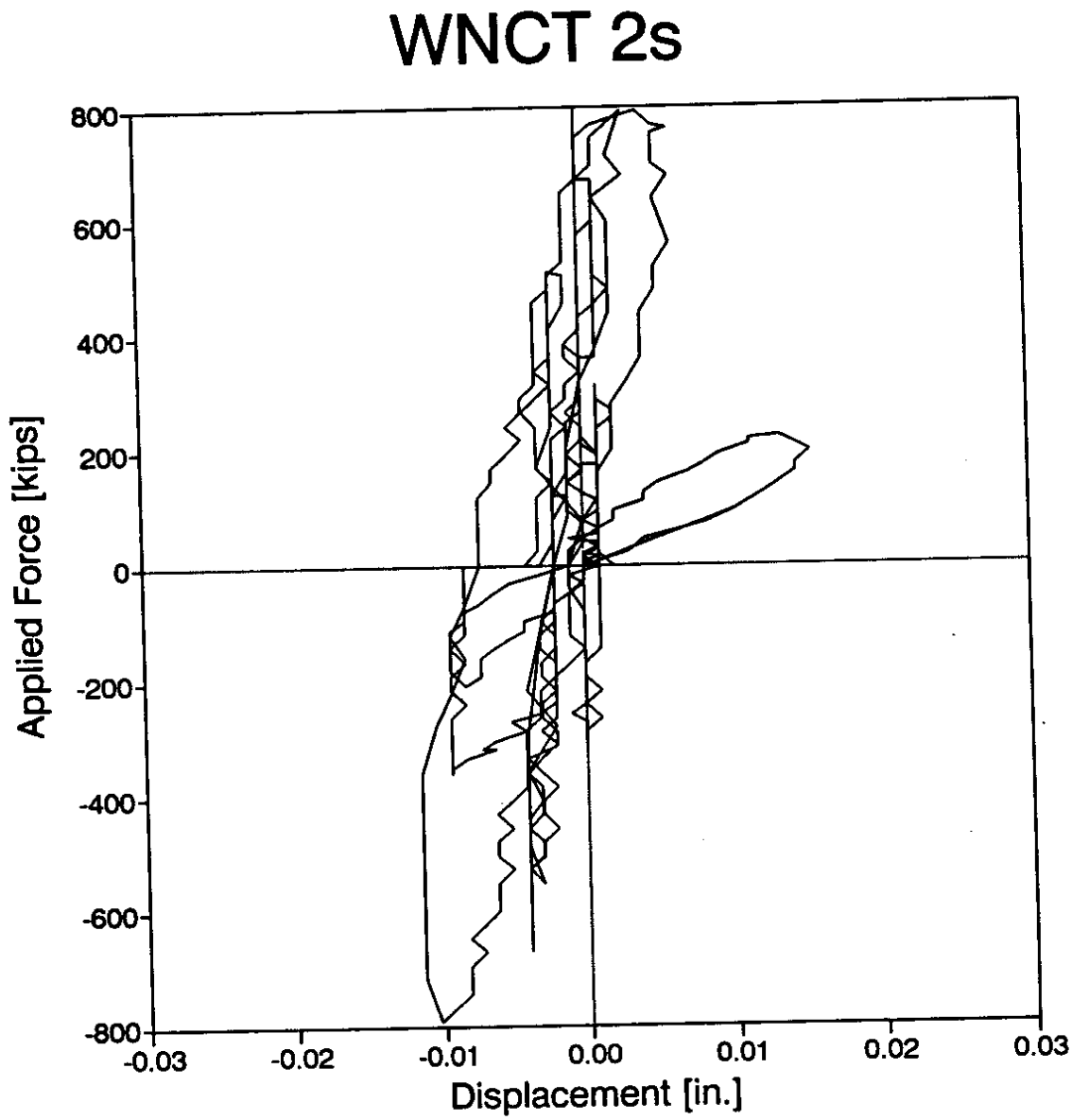

Figure A.20. Response History for WNCT 2s

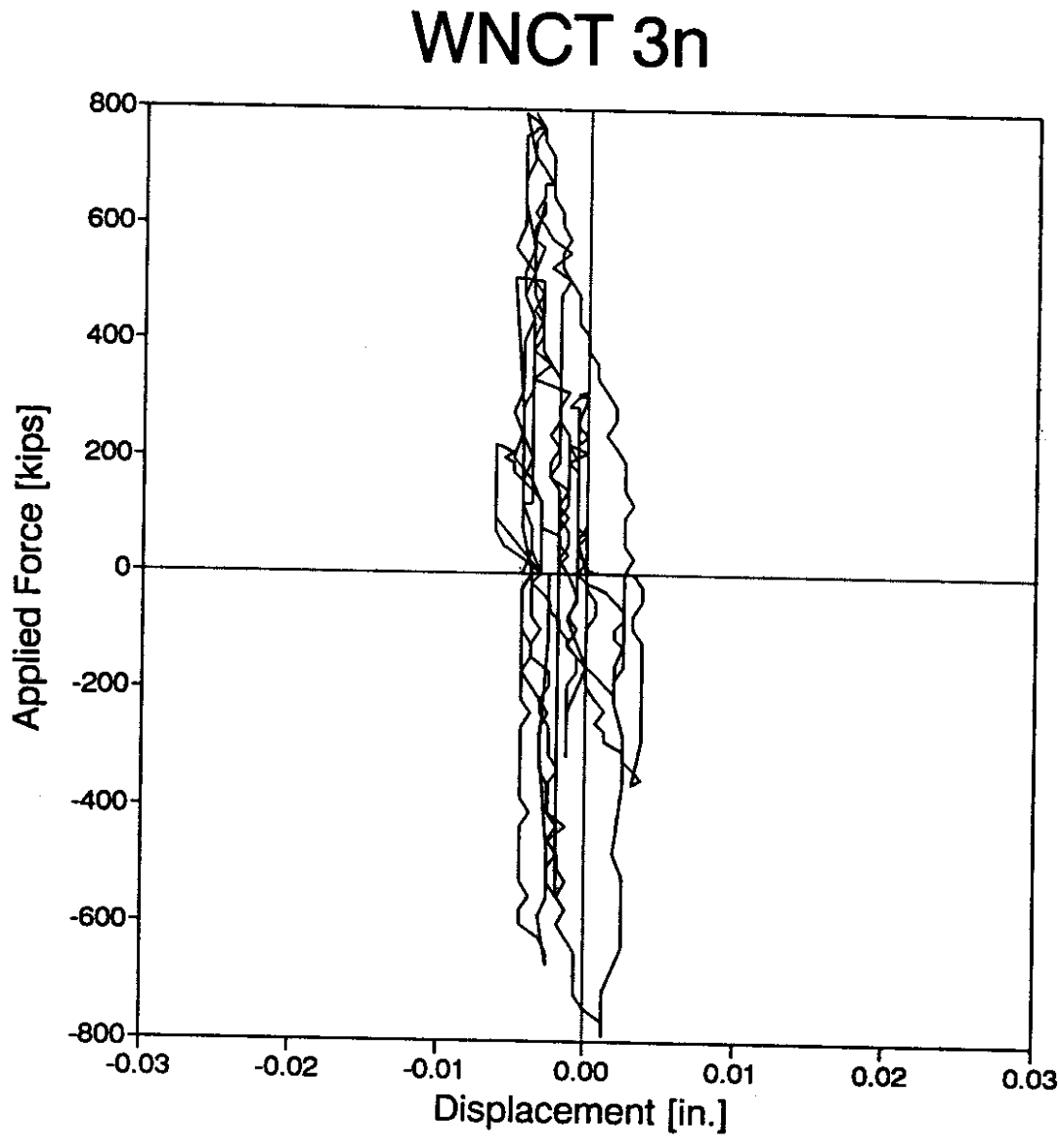

Figure A.21. Response History for WNCT 3n

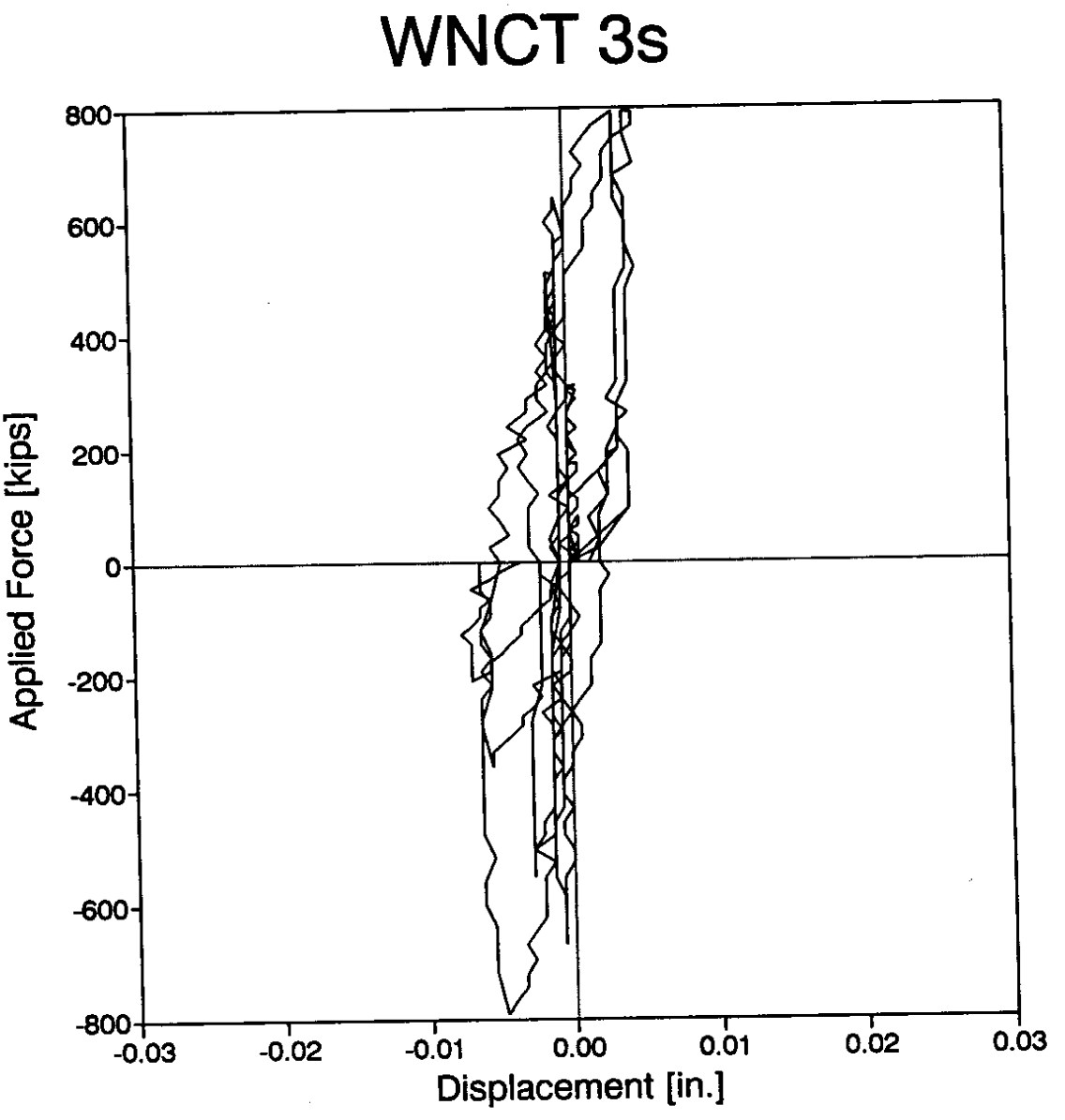

Figure A.22. Response History for WNCT 3s

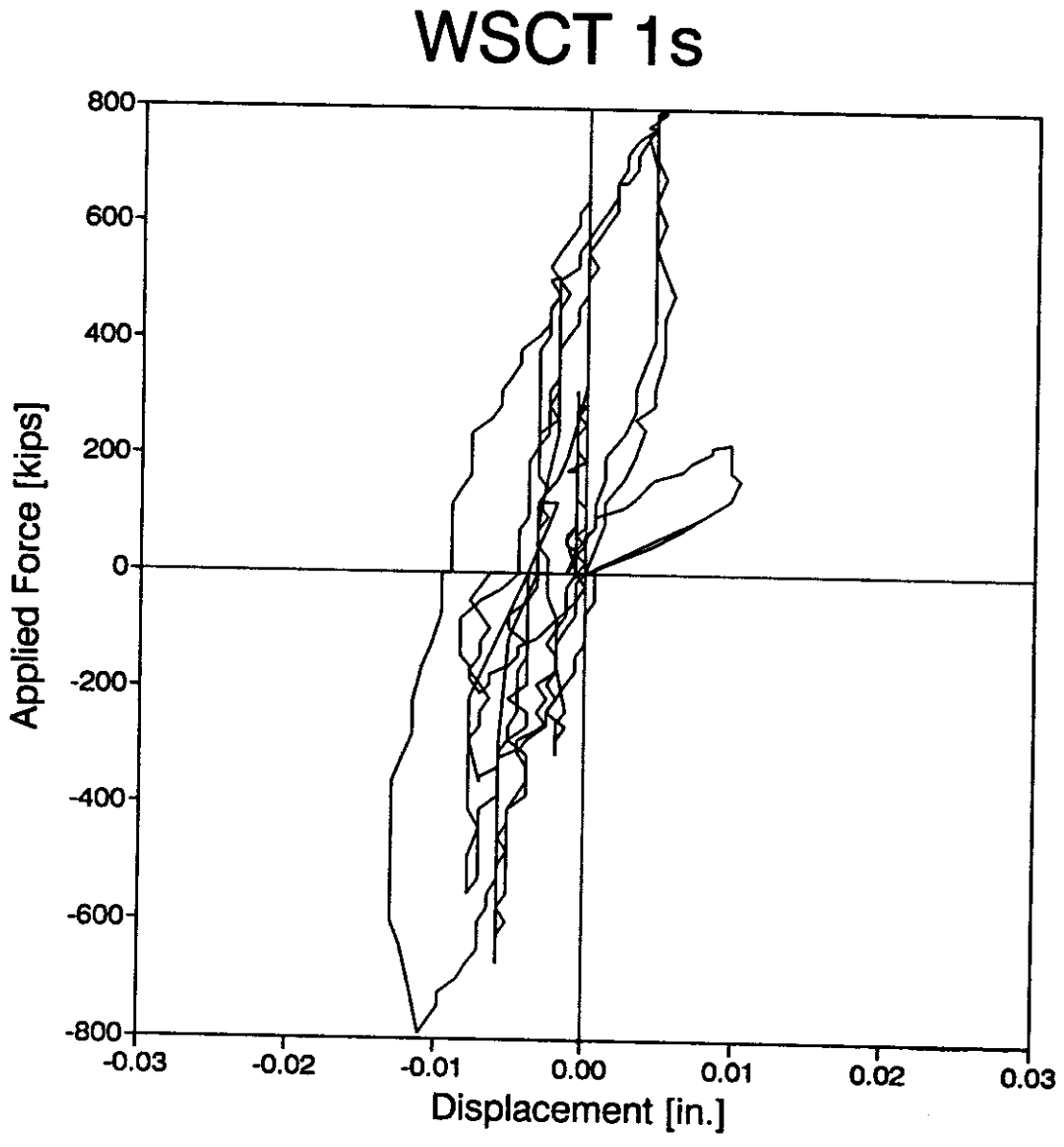

Figure A.23. Response History for WSCT 1s

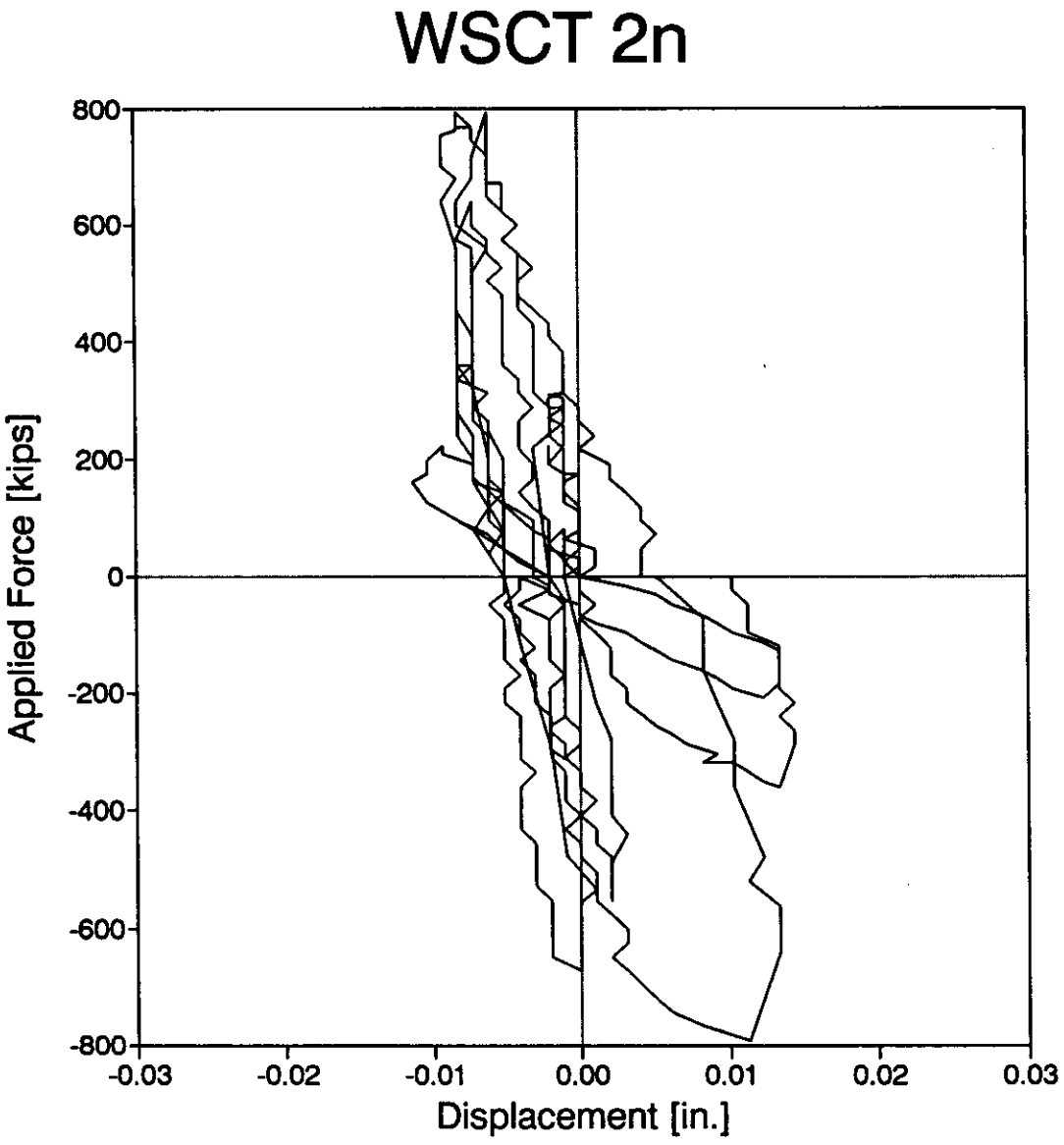

Figure A.24. Response History for WSCT 2n

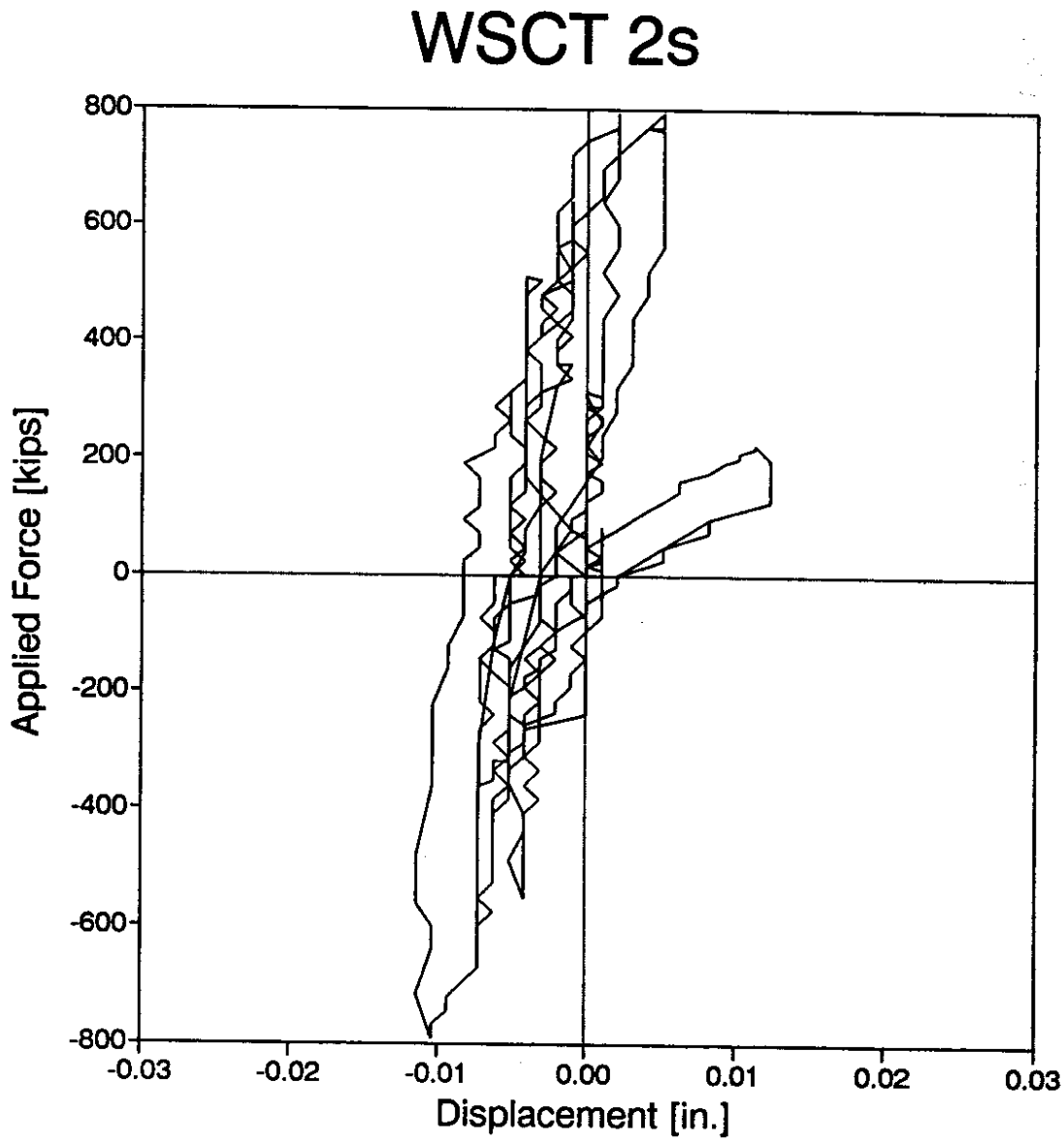

Figure A.25. Response History for WSCT 2s

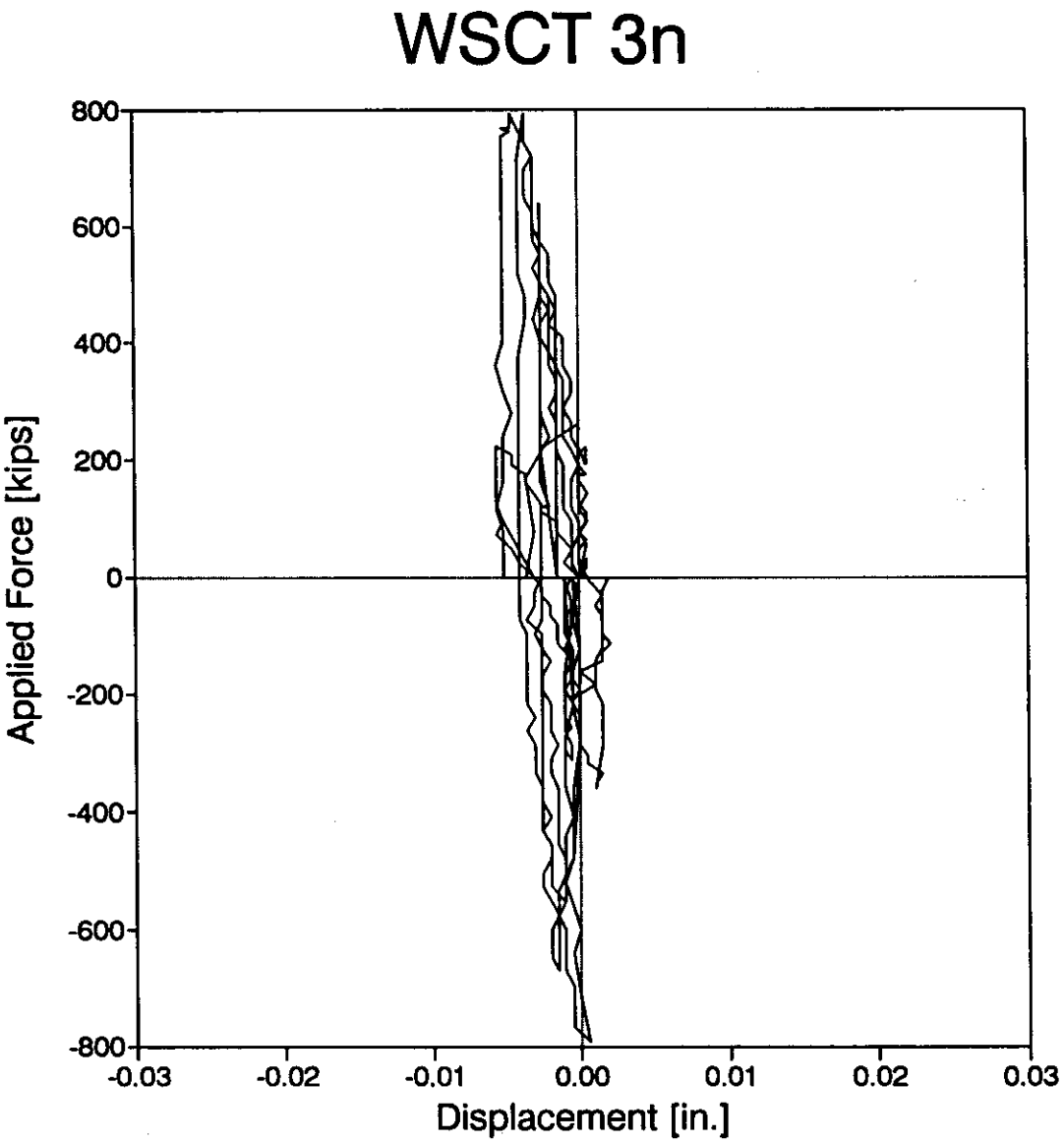

Figure A.26. Response History for WSCT 3n

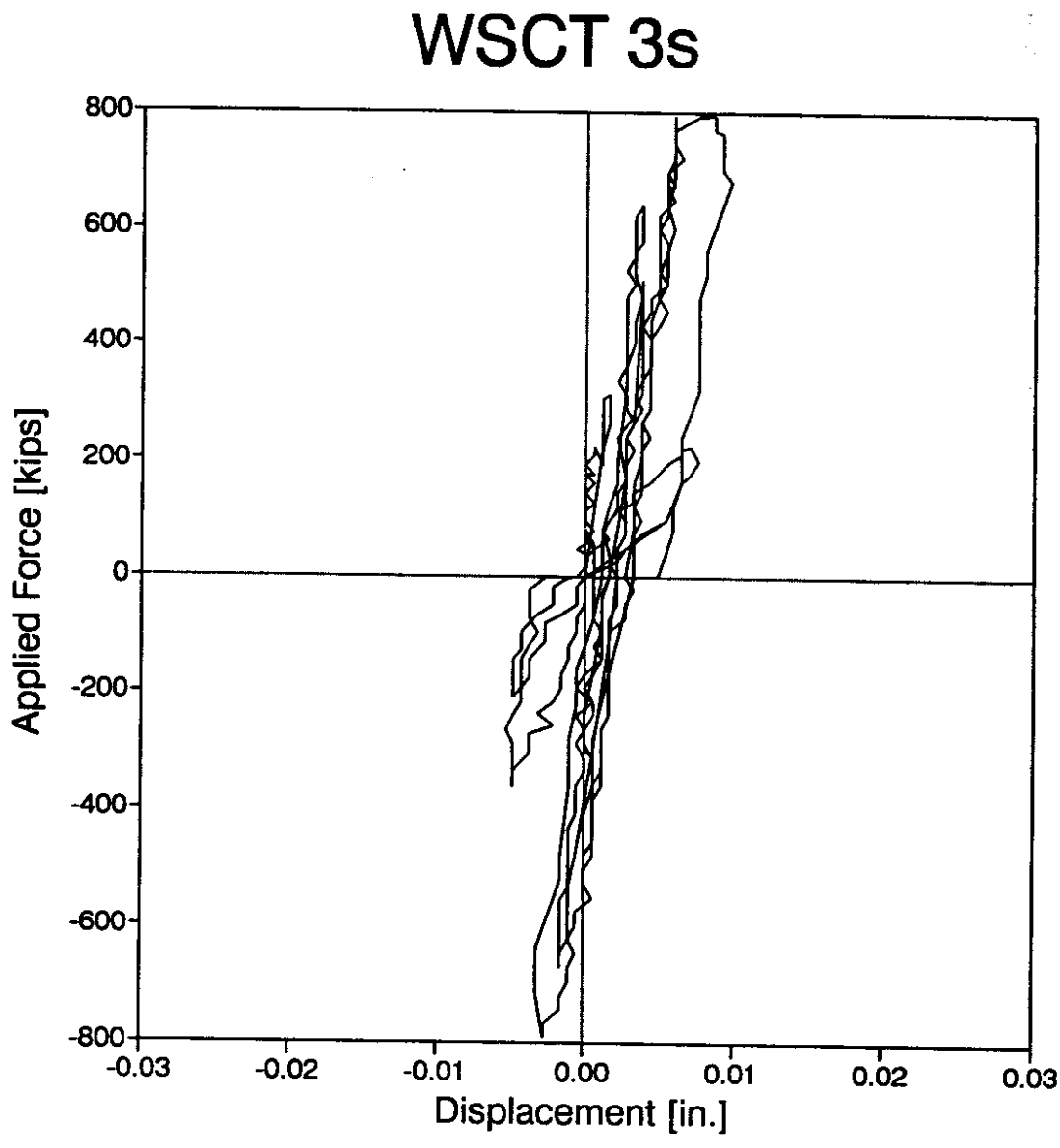

Figure A.27. Response History for WSCT 3s

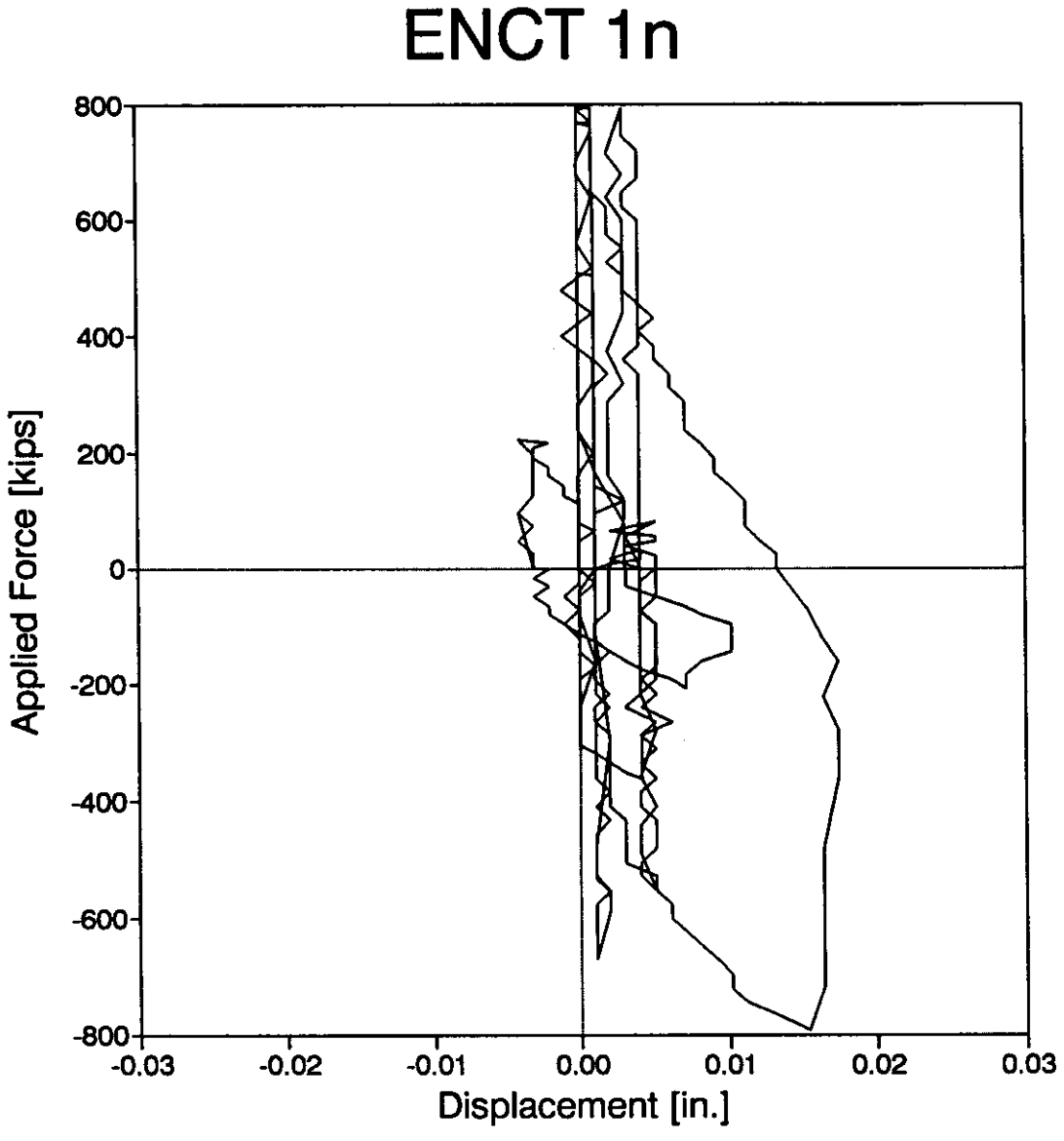

Figure A.28. Response History for ENCT 1n

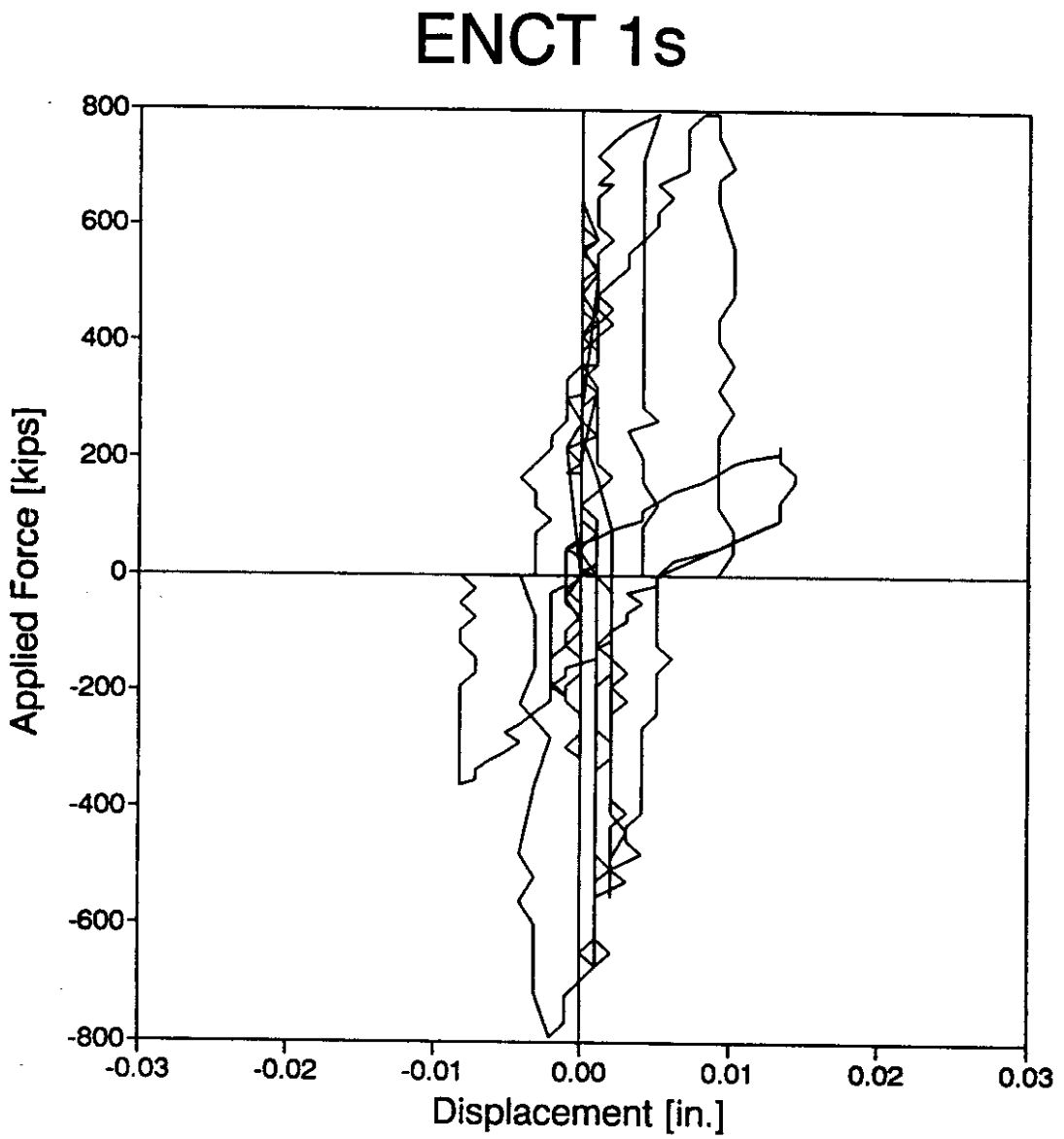

Figure A.29. Response History for ENCT 1s

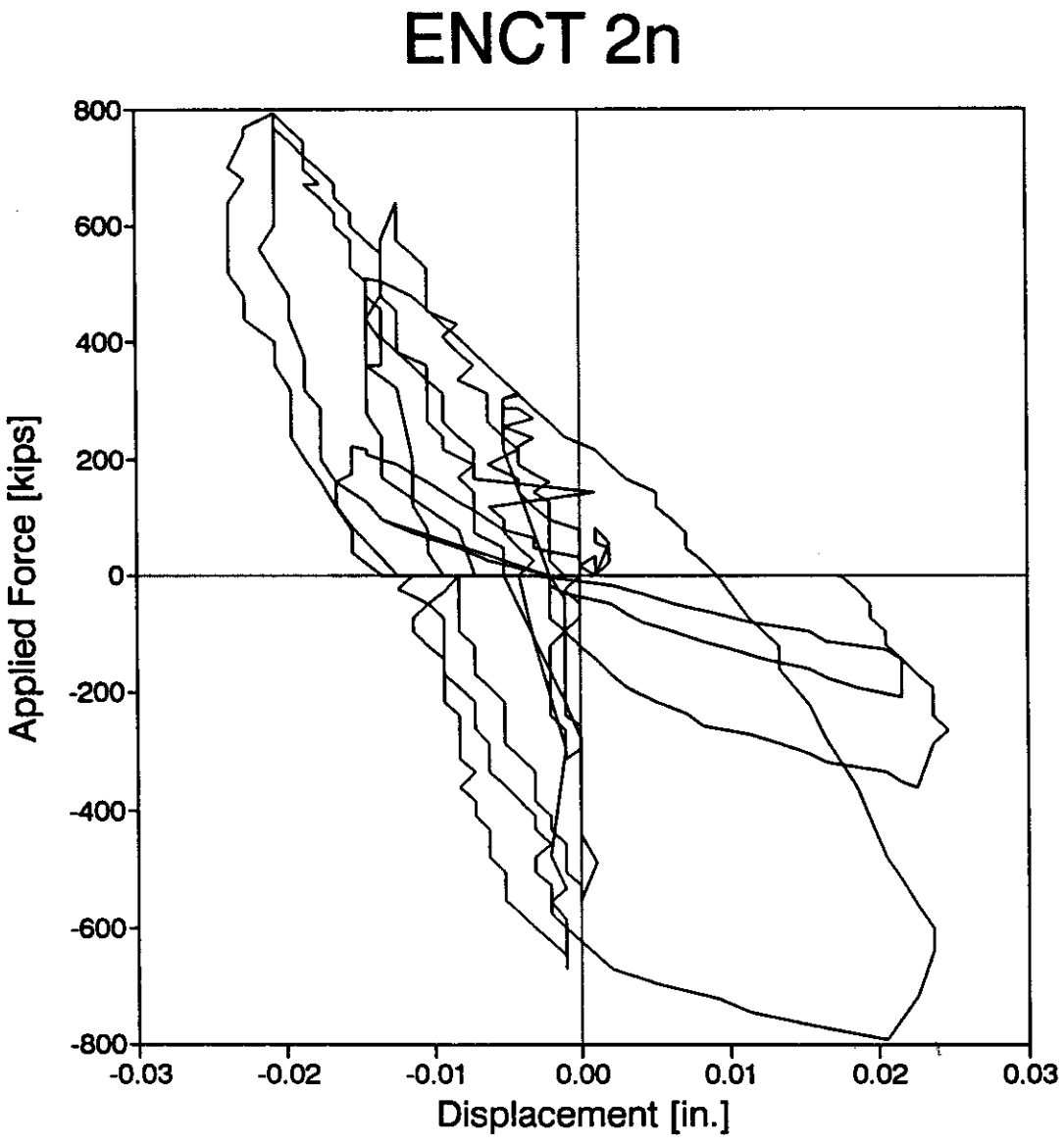

Figure A.30. Response History for ENCT 2n

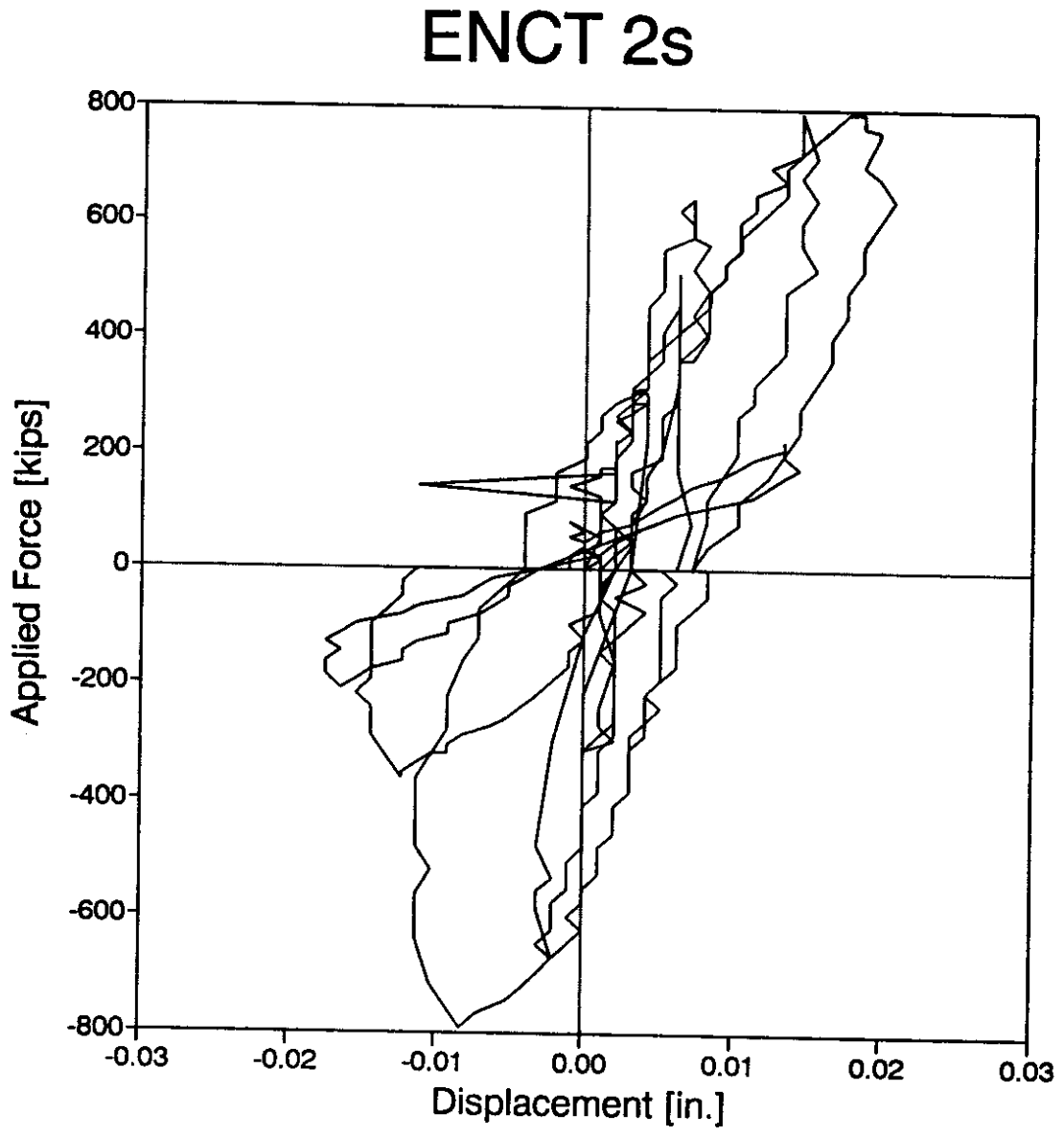

Figure A.31. Response History for ENCT 2s

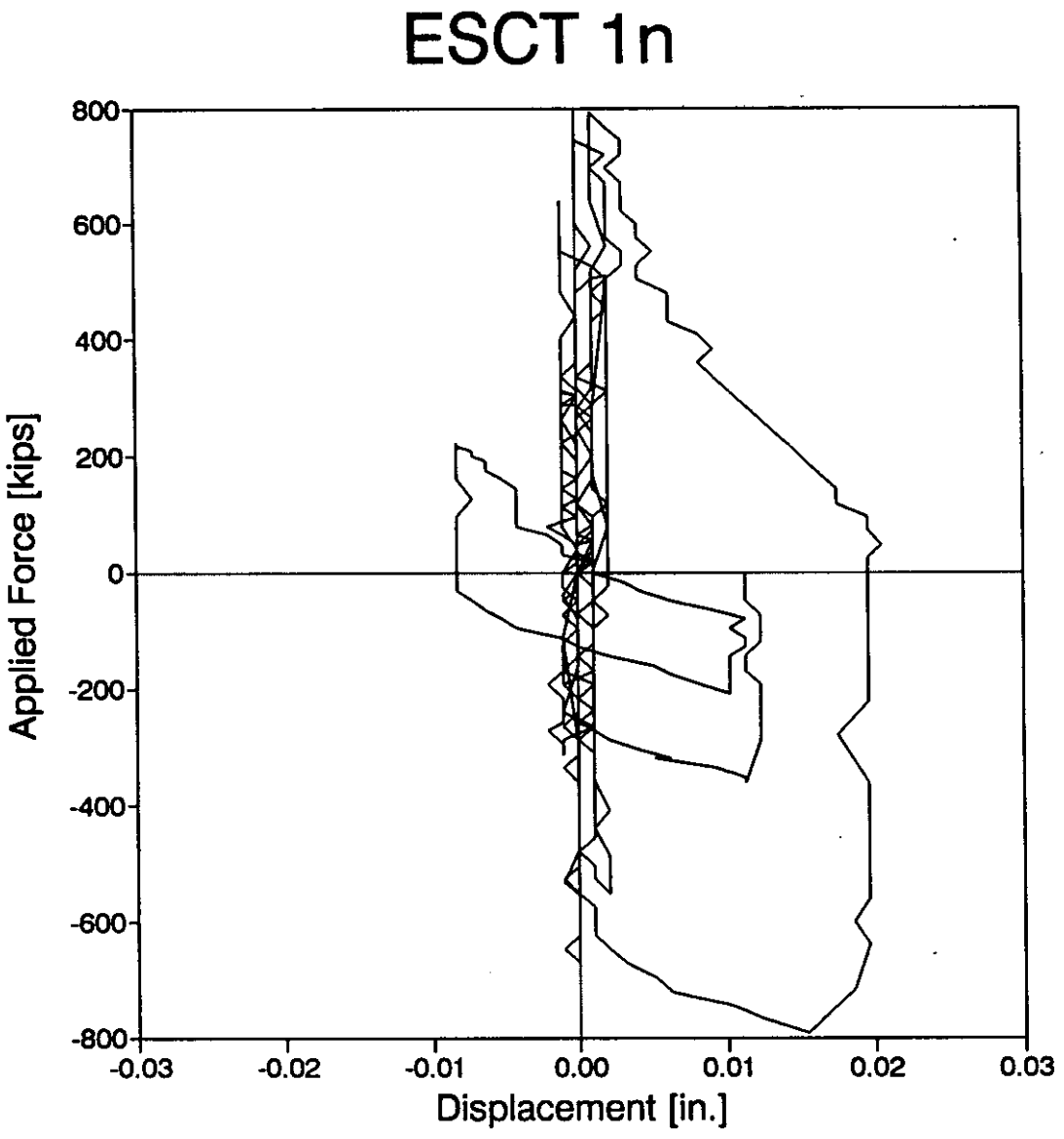

Figure A.32. Response History for ESCT 1n

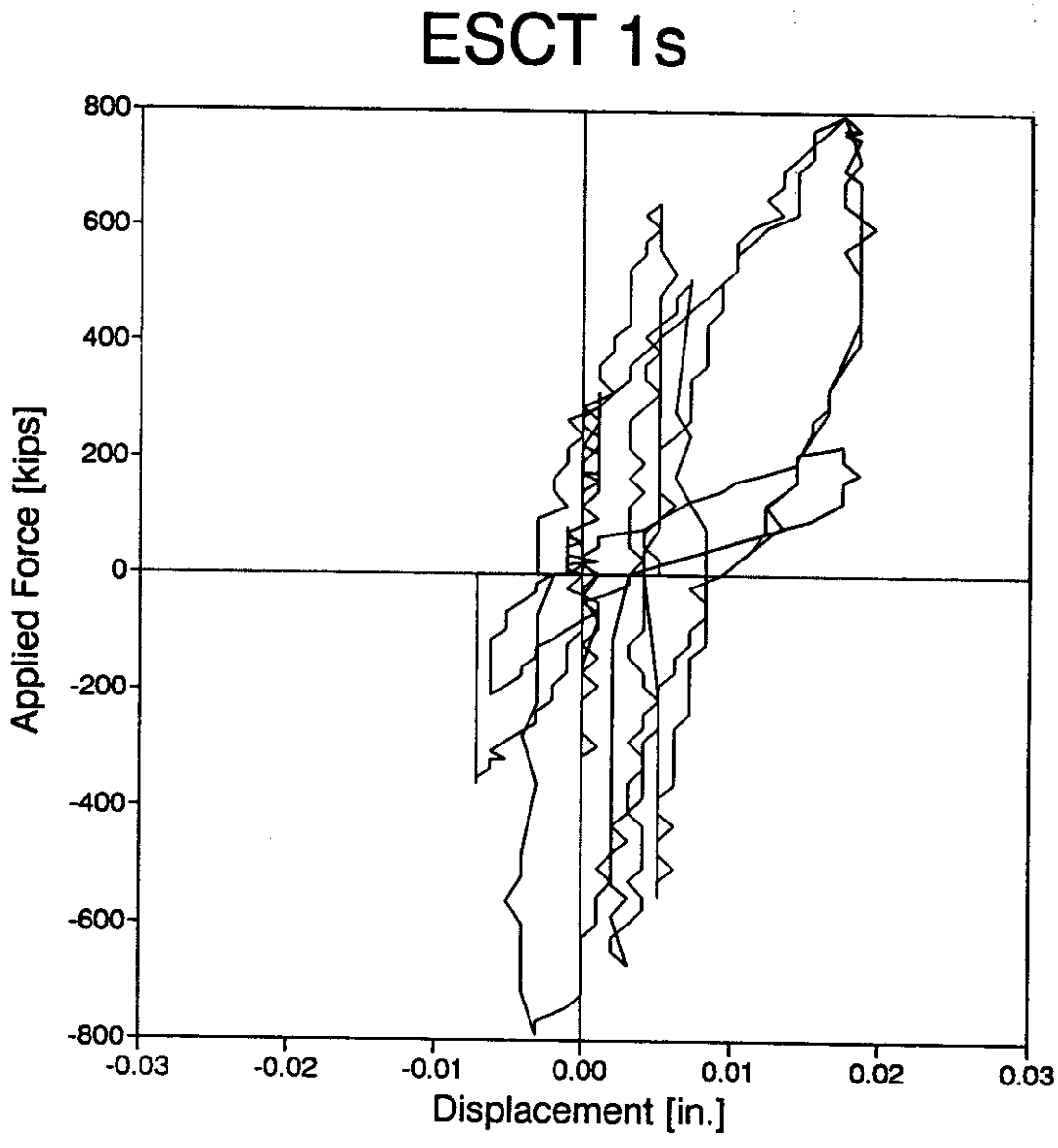

Figure A.33. Response History for ESCT 1s

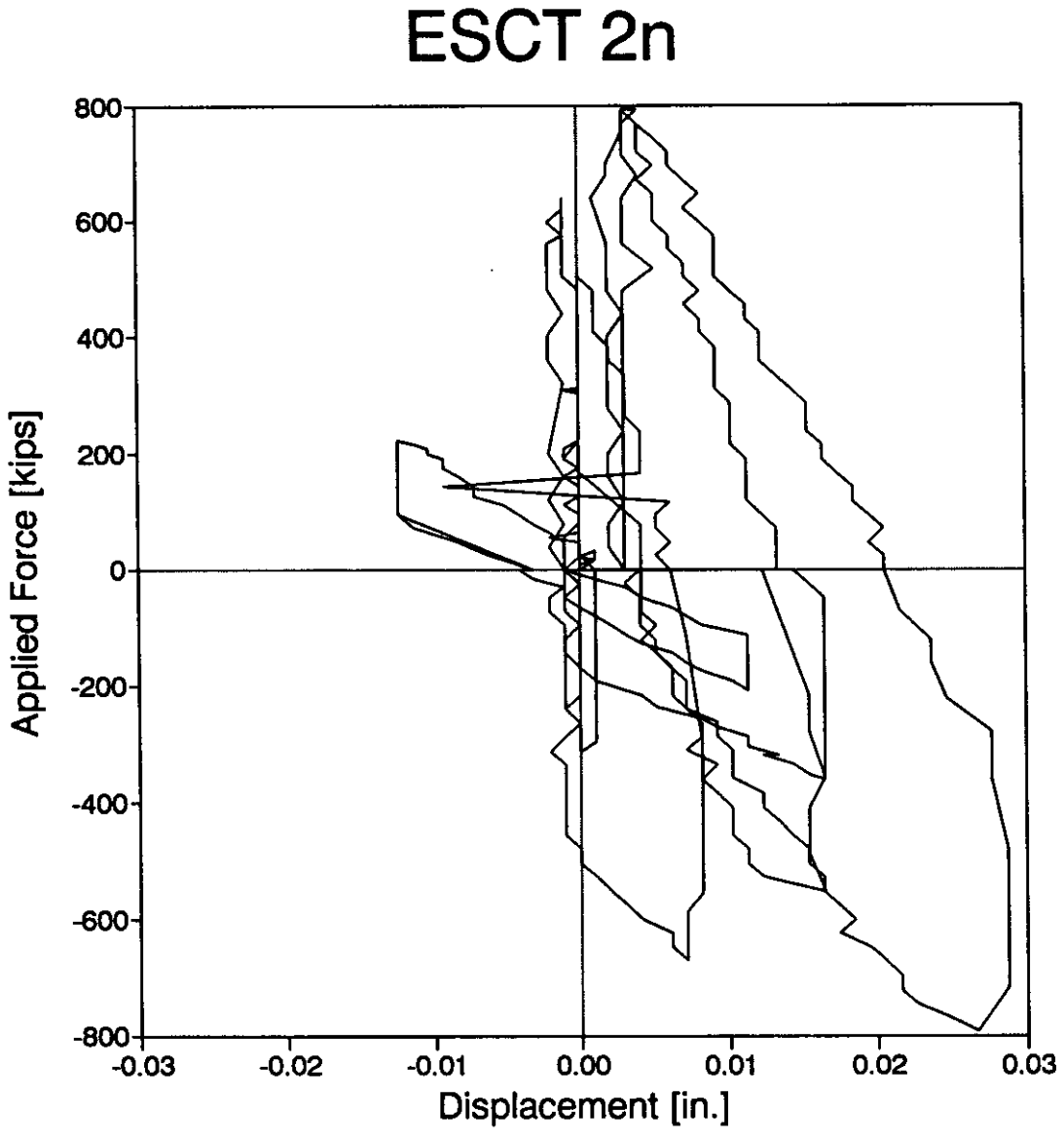

Figure A.34. Response History for ESCT 2n

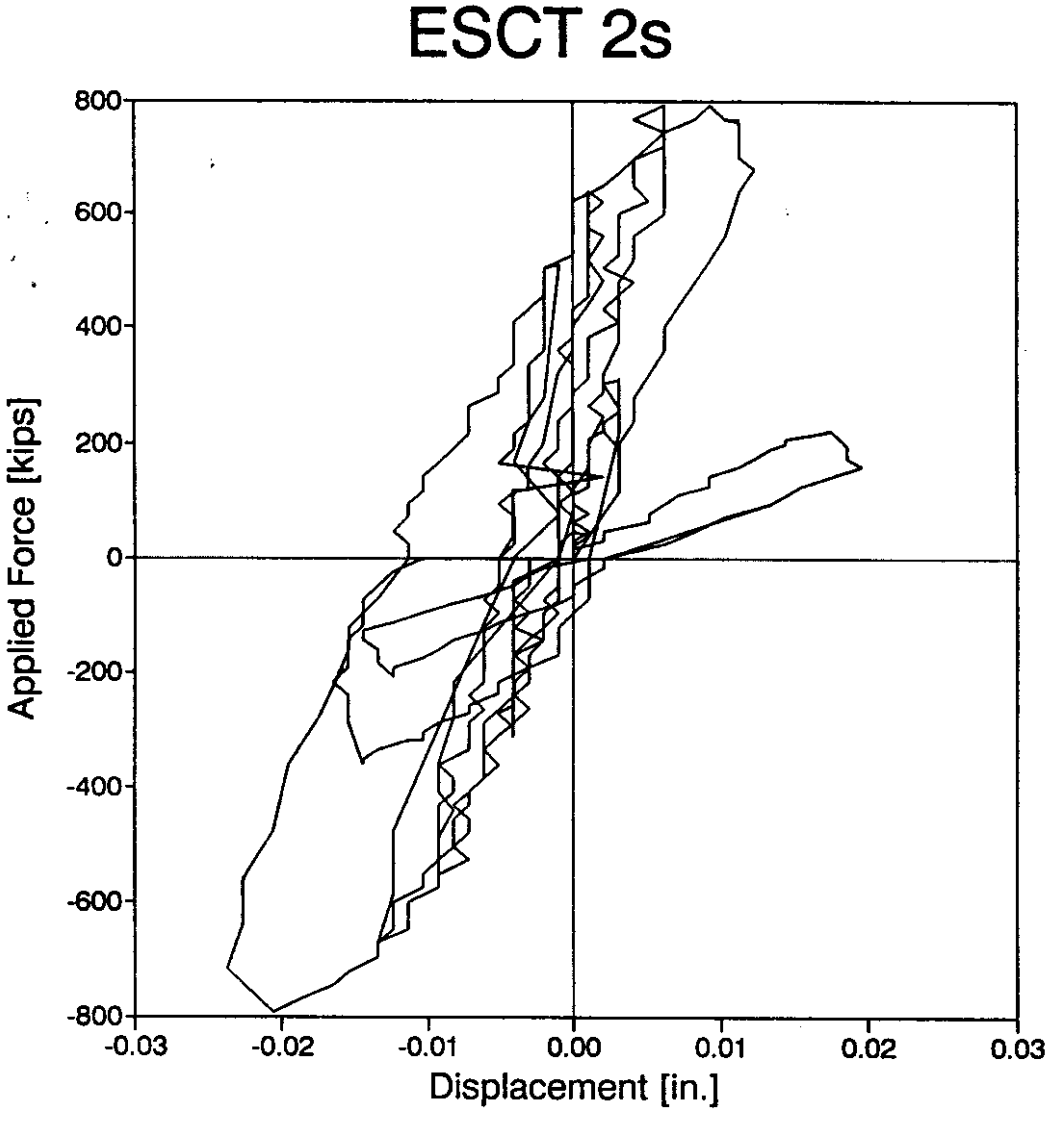

Figure A.35. Response History for ESCT 2s

APPENDIX B

TYPICAL SAP90 INPUT FILE FOR UW BRIDGE MODEL

APPENDIX B

TYPICAL SAP90 INPUT FILE FOR UW BRIDGE MODEL

(Input file corresponds to initial model for cycle Is1)

```
C  This is a finite element model of a reinforced concrete bridge
C  in Moses Lake, WA, that was tested in the summer of 1991.
C  The values of the parameters in this model are derived from concrete,
C  soils, bearing pad, and polystyrene laboratory tests.
C  The model was initially created by Gaukur Hjartarson and then later
C  corrected and modified by Jeffrey MacLardy and Stan Ryter.
C  If you need further information about this model, please contact
C  Marc Eberhard in the Civil Engineering Department at the University
C  of Washington.
C
C  Bridge has skew of 12.77 degrees=.0557 radians
C  Load was applied to each bent along skew at 14 degrees below horizontal
C
C  All units in inches, seconds, lbs., and radians

SYSTEM
L=1

JOINTS
C  COLUMNS
C  Bottom of northeast column
121  X=  368.2   Y=  511.8  Z=   0.0
C  Bottom of southeast column
101  X=   87.3   Y=  575.4  Z=   0.0
C  Top of southeast column
110  X=   87.3   Y=  575.4  Z=  324.0  G= 101,110,1
C  Top of northeast column
130  X=  368.2   Y=  511.8  Z=  324.0  G= 121,130,1
C  Bottom of southwest column
201  X=   87.3   Y= 1295.4  Z=   0.0
C  Top of southwest column
210  X=   87.3   Y= 1295.4  Z=  324.0  G= 201,210,1
C  Bottom of northwest column
221  X=  368.2   Y= 1231.8  Z=   0.0
C  Top of northwest column
230  X=  368.2   Y= 1231.8  Z=  324.0  G= 221,230,1
C
C  CROSSBEAMS
C  North end of east crossbeam
151  X=   5.4   Y=  594.0  Z=  324.0
C  South end of east crossbeam
152  X=  450.1   Y=  493.2  Z=  324.0
C  North end of west crossbeam
251  X=   5.4   Y= 1314.0  Z=  324.0
C  South end of east crossbeam
252  X=  450.1   Y= 1213.2  Z=  324.0
C
```

```
C  DECK
C  1001 is southeast corner
1001  X=   0.0   Y=  103.3  Z=  393.0
1003  X=  87.3   Y=   83.4  Z=  393.0
1004  X= 134.117 Y=   72.8  Z=  393.0
1009  X= 368.2   Y=   19.8  Z=  393.0
1010  X= 412.1   Y=    9.9  Z=  393.0
C  1011 is northeast corner
1011  X= 456.0   Y=    0.0  Z=  393.0
1067  X=   0.0   Y=  595.3  Z=  393.0
1069  X=  87.3   Y=  575.4  Z=  393.0 Q= 1001,1003,1067,1069,1,11
1070  X= 134.117 Y=  564.8  Z=  393.0
1075  X= 368.2   Y=  511.8  Z=  393.0 Q= 1004,1009,1070,1075,1,11
1076  X= 412.1   Y=  501.9  Z=  393.0
1077  X= 456.0   Y=  492.0  Z=  393.0 Q= 1010,1011,1076,1077,1,11
1177  X=   0.0   Y= 1315.3  Z=  393.0
1178  X=  43.65  Y= 1305.35 Z=  393.0 Q= 1067,1068,1177,1178,1,11
1179  X=  87.3   Y= 1295.4  Z=  393.0
1180  X= 134.117 Y= 1284.8  Z=  393.0 Q= 1069,1070,1179,1180,1,11
1181  X= 180.933 Y= 1274.2  Z=  393.0
1182  X= 227.750 Y= 1263.6  Z=  393.0 Q= 1071,1072,1181,1182,1,11
1183  X= 274.567 Y= 1253.0  Z=  393.0
1184  X= 321.383 Y= 1242.4  Z=  393.0 Q= 1073,1074,1183,1184,1,11
1185  X= 368.2   Y= 1231.8  Z=  393.0
1186  X= 412.1   Y= 1221.9  Z=  393.0 Q= 1075,1076,1185,1186,1,11
1187  X= 456.0   Y= 1212.0  Z=  393.0 G= 1077,1187,11
C  1243 is southwest corner
1243  X=   0.0   Y= 1807.3  Z=  393.0
1244  X=  43.65  Y= 1797.35 Z=  393.0 Q= 1177,1178,1243,1244,1,11
1245  X=  87.3   Y= 1787.4  Z=  393.0
1246  X= 134.117 Y= 1776.8  Z=  393.0 Q= 1179,1180,1245,1246,1,11
1247  X= 180.933 Y= 1766.2  Z=  393.0
1248  X= 227.75  Y= 1755.6  Z=  393.0 Q= 1181,1182,1247,1248,1,11
1249  X= 274.567 Y= 1745.0  Z=  393.0
1250  X= 321.383 Y= 1734.4  Z=  393.0 Q= 1183,1184,1249,1250,1,11
1251  X= 368.2   Y= 1723.8  Z=  393.0
1252  X= 412.1   Y= 1713.9  Z=  393.0 Q= 1185,1186,1251,1252,1,11
C  1253 is northwest corner
1253  X= 456.0   Y= 1704.0  Z=  393.0 G= 1187,1253,11
C
C  EAST END DIAPHRAGM
C   301 is bottom southeast corner
301  X=   0.0   Y=  103.3  Z=  331.8
303  X=  87.3   Y=   83.4  Z=  331.8  G= 301,303,1
309  X= 368.2   Y=   19.8  Z=  331.8  G= 303,309,1
311  X= 456.0   Y=    0.0  Z=  331.8  G= 309,311,1
321  X=   0.0   Y=  103.3  Z=  362.4
323  X=  87.3   Y=   83.4  Z=  362.4  G= 321,323,1
329  X= 368.2   Y=   19.8  Z=  362.4  G= 323,329,1
C  331 is bottom northeast corner
331  X= 456.0   Y=    0.0  Z=  362.4  G= 329,331,1
C
C  WEST END DIAPHRAGM
C  367 is bottom southwest corner
```

```
367  X=   0.0   Y= 1807.3  Z=  331.8
369  X=  87.3   Y= 1787.4  Z=  331.8  G= 367,369,1
375  X= 368.2   Y= 1723.8  Z=  331.8  G= 369,375,1
377  X= 456.0   Y= 1704.0  Z=  331.8  G= 375,377,1
387  X=   0.0   Y= 1807.3  Z=  362.4
389  X=  87.3   Y= 1787.4  Z=  362.4  G= 387,389,1
395  X= 368.2   Y= 1723.8  Z=  362.4  G= 389,395,1
C  397 is bottom northwest corner
397  X= 456.0   Y= 1704.0  Z=  362.4  G= 395,397,1
C
C  WINGWALLS
C  Southeast wingwall
401  X=   0.0   Y=  28.3  Z=  393.0
403  X=   0.0   Y=  28.3  Z=  331.8  G= 401,403,1
404  X=   0.0   Y=  65.8  Z=  393.0
406  X=   0.0   Y=  65.8  Z=  331.8  G= 404,406,1
C
C  Northeast wingwall
411  X= 456.0   Y= -75.0  Z=  393.0
413  X= 456.0   Y= -75.0  Z=  331.8  G= 411,413,1
414  X= 456.0   Y= -37.5  Z=  393.0
416  X= 456.0   Y= -37.5  Z=  331.8  G= 414,416,1
C
C  Southwest wingwall
421  X=   0.0   Y= 1882.3  Z=  393.0
423  X=   0.0   Y= 1882.3  Z=  331.8  G= 421,423,1
424  X=   0.0   Y= 1844.8  Z=  393.0
426  X=   0.0   Y= 1844.8  Z=  331.8  G= 424,426,1
C
C  Northwest wingwall
431  X= 456.0   Y= 1779.0  Z=  393.0
433  X= 456.0   Y= 1779.0  Z=  331.8  G= 431,433,1
434  X= 456.0   Y= 1741.5  Z=  393.0
436  X= 456.0   Y= 1741.5  Z=  331.8  G= 434,436,1

RESTRAINTS
C  Southeast and northeast column footing
101 121 20   R= 1,1,1,1,1,1
C  Southwest and northwest column footing
201 221 20   R= 1,1,1,1,1,1
C  East end diaphragm
301 311 1   R= 0,0,1,0,0,0
C  West end diaphragm
367 377 1   R= 0,0,1,0,0,0

SPRINGS
C  BEARING PAD SPRINGS
C  11 springs at bottom of east end diaphragm
301  311   1  K= 167000/11,167000/11
C  11 springs at bottom of west end diaphragm
367  377   1  K= 167000/11,167000/11
C
C  POLYSTYRENE SPRINGS
C  11 springs at bottom of east end diaphragm
```

```
301  311   1  K= 4260000/11,4260000/11
C  11 springs at bottom of west end diaphragm
367  377   1  K= 4260000/11,4260000/11
C
C  ABUTMENT SOIL SPRINGS XOR ISOLATION SYSTEM ABUTMENT RIGID SPRING
C  11 springs at bottom of east end diaphragm
301  311   1  K= 1E12/11,1E12/11
C  11 springs at bottom of west end diaphragm
367  377   1  K= 1E12/11,1E12/11
C
C  COLUMN SOIL SPRINGS
C  bottom soil spring
102  122  20  K= 759000,759000
202  222  20  K= 759000,759000
C  mid-bottom soil spring
103  123  20  K= 525000,525000
203  223  20  K= 525000,525000
C  mid-top soil spring
104  124  20  K= 290000,290000
204  224  20  K= 290000,290000
C  top soil spring
105  125  20  K= 67000,67000
205  225  20  K= 67000,67000
C
C  WINGWALL SOIL SPRINGS
C  9 soil springs at southeast wingwall
 401   406  1  K= 90000/9,0
1001         K= 90000/9,0
 301   321 20  K= 90000/9,0
C  9 soil springs at northeast wingwall
 411   416  1  K= 90000/9,0
1011         K= 90000/9,0
 311   331 20  K= 90000/9,0
C  9 soil springs at southwest wingwall
 421   426  1  K= 90000/9,0
1243         K= 90000/9,0
 367   387 20  K= 90000/9,0
C  9 soil springs at northwest wingwall
 431   436  1  K= 90000/9,0
1253         K= 90000/9,0
 377   397 20  K= 90000/9,0

FRAME
NM=7
C  Crossbeam
1    SH=R  T= 36,42  E= 4600000  W= 131.25 M= 131.25/32.17/12
C  Uncracked column (AS= .9 Pi r^2 from SAP90 manual)
2     A= 1017.9 J= 164900 I= 90000,90000 AS= 916,916 E= 4600000 W= 88.38 M=
88.38/32.17/12
C  Cracked column (AS= (cracked area/uncracked area)*(uncracked AS); estimated I22)
3     A= 188.5  J=  30537 I= 29500,29500 AS= 170,170 E= 4600000 W= 88.38 M=
88.38/32.17/12
C  Diaphragm over bent
4    A= 192 J= 0 I= 31536,9000000 E= 4600000  W= 144.84 M= 144.84/32.17/12
```

```
C  Girder
5    A= 332 J= 0 I= 2193014,5482 E= 4600000 W= 30.75 M= 30.75/32.17/12
C  Edge girder (area of girder is adjusted in order to make
C  the moment of inertia of the bridge in this model about its
C  centroidal z-axis equal to the moment of inertia of the actual bridge
C  about the centroidal z-axis.  This is necessary since the girder
C  placement in this model is not the same as the placement in the actual
C  bridge.  The area subtracted from each outside girder is 68 in^2.)
6    A= 264 J= 0 I= 2193014,5482 E= 4600000 W= 30.75 M= 30.75/32.17/12
C  Curb and railing
7    A= 412 J= 0 I= 27485,11546 E= 4600000  W= 35.76 M= 35.76/32.17/12
C
C  Southeast column
101 101 102 M= 2,2 LP= 2,0
102 102 103 M= 2,2 LP= 2,0
103 103 104 M= 2,2 LP= 2,0
104 104 105 M= 2,2 LP= 2,0
105 105 106 M= 2,2 LP= 2,0
106 106 107 M= 2,2 LP= 2,0
107 107 108 M= 2,2 LP= 2,0
108 108 109 M= 2,2 LP= 2,0
109 109 110 M= 2,2 LP= 2,0 RE= 0,18
C  Northeast column
121 121 122 M= 2,2 LP= 2,0
122 122 123 M= 2,2 LP= 2,0
123 123 124 M= 2,2 LP= 2,0
124 124 125 M= 2,2 LP= 2,0
125 125 126 M= 2,2 LP= 2,0
126 126 127 M= 2,2 LP= 2,0
127 127 128 M= 2,2 LP= 2,0
128 128 129 M= 2,2 LP= 2,0
129 129 130 M= 2,2 LP= 2,0 RE= 0,18
C  Southwest column
201 201 202 M= 2,2 LP= 2,0
202 202 203 M= 2,2 LP= 2,0
203 203 204 M= 2,2 LP= 2,0
204 204 205 M= 2,2 LP= 2,0
205 205 206 M= 2,2 LP= 2,0
206 206 207 M= 2,2 LP= 2,0
207 207 208 M= 2,2 LP= 2,0
208 208 209 M= 2,2 LP= 2,0
209 209 210 M= 2,2 LP= 2,0 RE= 0,18
C  Northwest column
221 221 222 M= 2,2 LP= 2,0
222 222 223 M= 2,2 LP= 2,0
223 223 224 M= 2,2 LP= 2,0
224 224 225 M= 2,2 LP= 2,0
225 225 226 M= 2,2 LP= 2,0
226 226 227 M= 2,2 LP= 2,0
227 227 228 M= 2,2 LP= 2,0
228 228 229 M= 2,2 LP= 2,0
229 229 230 M= 2,2 LP= 2,0 RE= 0,18
C  East crossbeam
151 151 110 M= 1,1 LP= 1,0 RE= 0,18
```

```
152 110 130 M= 1,1 LP= 1,0 RE= 18,18
153 130 152 M= 1,1 LP= 1,0 RE= 18,0
C  West crossbeam
251 251 210 M= 1,1 LP= 1,0 RE= 0,18
252 210 230 M= 1,1 LP= 1,0 RE= 18,18
253 230 252 M= 1,1 LP= 1,0 RE= 18,0
C  East bent diaphragm
161 110 1069 M= 4,4 LP= 1,0
162 130 1075 M= 4,4 LP= 1,0
C  West bent diaphragm
261 210 1179 M= 4,4 LP= 1,0
262 230 1185 M= 4,4 LP= 1,0
C  Prestressed girders (from south to north)
301 1001 1012  M= 6,6 LP= 3,0 G= 21,1,11,11
323 1003 1014  M= 5,5 LP= 3,0 G= 21,1,11,11
345 1005 1016  M= 5,5 LP= 3,0,G= 21,1,11,11
367 1007 1018  M= 5,5 LP= 3,0 G= 21,1,11,11
389 1009 1020  M= 5,5 LP= 3,0 G= 21,1,11,11
411 1011 1022  M= 6,6 LP= 3,0,G= 21,1,11,11
C  Curb and railing
500 1001 1012  M= 7,7 LP= 3,0 G= 21,1,11,11
600 1011 1022  M= 7,7 LP= 3,0,G= 21,1,11,11

SHELL
NM=1
1  E= 4700000  W= 0.08681 M= 0.08681/32.17/12
C
C  Deck
1001  JQ= 1001,1002,1012,1013  ETYPE= 0  M= 1  TH= 6.5,6.5  G= 10,22
C
C  East end diaphragm
301  JQ= 301, 302, 321, 322  ETYPE= 0  M= 1  TH= 18,18   G= 10,1
321  JQ= 321, 322,1001,1002  ETYPE= 0  M= 1  TH= 18,18   G= 10,1
C
C  West end diaphragm
367  JQ= 367, 368, 387, 388  ETYPE= 0  M= 1  TH= 18,18   G= 10,1
381  JQ= 387, 388,1243,1244  ETYPE= 0  M= 1  TH= 18,18   G= 10,1
C
C  Southeast wingwall
401  JQ= 401,404,402,405     ETYPE= 0  M= 1  TH= 12,12
402  JQ= 402,405,403,406     ETYPE= 0  M= 1  TH= 12,12
403  JQ= 404,1001,405,321    ETYPE= 0  M= 1  TH= 12,12
404  JQ= 405,321,406,301     ETYPE= 0  M= 1  TH= 12,12
C
C  Northeast wingwall
411  JQ= 411,414,412,415     ETYPE= 0  M= 1  TH= 12,12
412  JQ= 412,415,413,416     ETYPE= 0  M= 1  TH= 12,12
413  JQ= 414,1011,415,331    ETYPE= 0  M= 1  TH= 12,12
414  JQ= 415,331,416,311     ETYPE= 0  M= 1  TH= 12,12
C
C  Southwest wingwall
421  JQ= 421,424,422,425     ETYPE= 0  M= 1  TH= 12,12
422  JQ= 422,425,423,426     ETYPE= 0  M= 1  TH= 12,12
423  JQ= 424,1243,425,387    ETYPE= 0  M= 1  TH= 12,12
```

```
424 JQ= 425,387,426,367     ETYPE= 0 M= 1 TH= 12,12
C
C Northwest wingwall
431 JQ= 431,434,432,435     ETYPE= 0 M= 1 TH= 12,12
432 JQ= 432,435,433,436     ETYPE= 0 M= 1 TH= 12,12
433 JQ= 434,1253,435,397    ETYPE= 0 M= 1 TH= 12,12
434 JQ= 435,397,436,377     ETYPE= 0 M= 1 TH= 12,12

LOADS
C Load applied at east bent along skew
151 L= 1 F= 19505,-4421,0,0,0,0 : Fx,Fy,Fz,Mx,My,Mz
C Load applied at west bent along skew
251 L= 1 F= 19505,-4421,0,0,0,0 : Fx,Fy,Fz,Mx,My,Mz
C Soil friction applied along outside of east abutment wall
1001 1011 1 L= 1 F= 0,0,0,0,0,0
C Soil friction applied along outside of west abutment wall
1243 1253 1 L= 1 F= 0,0,0,0,0,0
C Force to add to east abutment to account for non-linear behavior
C of bearing pads at a given stage of loading (distributed over 11 nodes)
1001 1011 1 L= 1 F= 0,0,0,0,0,0
C Force to add to west abutment to account for non-linear behavior
C of bearing pads at a given stage of loading (distributed over 11 nodes)
1243 1253 1 L= 1 F= 0,0,0,0,0,0
C Force to add to east abutment to account for non-linear behavior
C of polystyrene at a given stage of loading (distributed over 11 nodes)
1001 1011 1 L= 1 F= 0,0,0,0,0,0
C Force to add to west abutment to account for non-linear behavior
C of polystyrene at a given stage of loading (distributed over 11 nodes)
1243 1253 1 L= 1 F= 0,0,0,0,0,0
C Force to add to east abutment to account for isolation system
1001 1011 1 L= 1 F= 0,0,0,0,0,0
C Force to add to west abutment to account for isolation system
1243 1253 1 L= 1 F= 0,0,0,0,0,0
C
```

APPENDIX C

STIFFNESS MATRIX FOR UW SIMPLIFIED MODEL

$$
\begin{Bmatrix} M_{\theta 1} \\ M_{\theta 2} \\ M_{\theta 3} \\ M_{\theta 4} \\ F_{y1} \\ F_{y2} \\ F_{y3} \\ F_{y4} \end{Bmatrix} =
\begin{bmatrix}
\frac{4EI_1}{L_1} + K_{r1} & \frac{2EI_1}{L_1} & 0 & 0 & \frac{6EI_1}{L_1^2} & -\frac{6EI_1}{L_1^2} & 0 & 0 \\
\frac{2EI_1}{L_1} & \frac{4EI_1}{L_1} + \frac{4EI_2}{L_2} & \frac{2EI_2}{L_2} & 0 & \frac{6EI_1}{L_1^2} & -\frac{6EI_1}{L_1^2} + \frac{6EI_2}{L_2^2} & -\frac{6EI_2}{L_2^2} & 0 \\
0 & \frac{2EI_2}{L_2} & \frac{4EI_2}{L_2} + \frac{4EI_3}{L_3} & \frac{2EI_3}{L_3} & 0 & \frac{6EI_2}{L_2^2} & -\frac{6EI_2}{L_2^2} + \frac{6EI_3}{L_3^2} & -\frac{6EI_3}{L_3^2} \\
0 & 0 & \frac{2EI_3}{L_3} & \frac{4EI_3}{L_3} + K_{r2} & 0 & 0 & \frac{6EI_3}{L_3^2} & -\frac{6EI_3}{L_3^2} \\
\frac{6EI_1}{L_1^2} & \frac{6EI_1}{L_1^2} & 0 & 0 & \frac{12EI_1}{L_1^3} + K_{y1} & -\frac{12EI_1}{L_1^3} & 0 & 0 \\
-\frac{6EI_1}{L_1^2} & -\frac{6EI_1}{L_1^2} + \frac{6EI_2}{L_2^2} & \frac{6EI_2}{L_2^2} & 0 & -\frac{12EI_1}{L_1^3} & \frac{12EI_1}{L_1^3} + \frac{12EI_2}{L_2^3} + K_{y2} & -\frac{12EI_2}{L_2^3} & 0 \\
0 & -\frac{6EI_2}{L_2^2} & -\frac{6EI_2}{L_2^2} + \frac{6EI_3}{L_3^2} & \frac{6EI_3}{L_3^2} & 0 & -\frac{12EI_2}{L_2^3} & \frac{12EI_2}{L_2^3} + \frac{12EI_3}{L_3^3} + K_{y3} & -\frac{12EI_3}{L_3^3} \\
0 & 0 & -\frac{6EI_3}{L_3^2} & -\frac{6EI_3}{L_3^2} & 0 & 0 & -\frac{12EI_3}{L_3^3} & \frac{12EI_3}{L_3^3} + K_{y4}
\end{bmatrix}
\begin{Bmatrix} \theta_1 \\ \theta_2 \\ \theta_3 \\ \theta_4 \\ y_1 \\ y_2 \\ y_3 \\ y_4 \end{Bmatrix}
$$

Figure C.1. UW Simplified Model Stiffness Matrix